Exploring additional mechanisms of cell injury by fluoropyrimidines in the treatment of cancer: an investigation of novel protide NUC-3373

Fiona Grace McKissock

A thesis submitted for the degree of PhD
at the
University of St Andrews

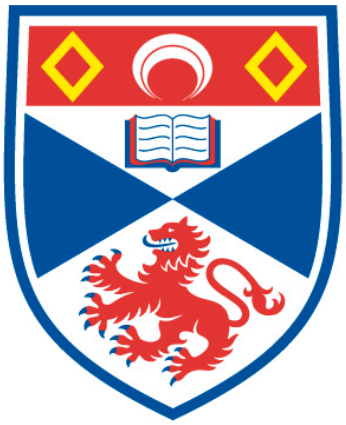

2019

Identifier to use to cite or link to this thesis:

DOI: https://doi.org/10.17630/10023-18785

Declarations

Candidate's declaration

I, Fiona Grace McKissock, do hereby certify that this thesis, submitted for the degree of PhD, which is approximately 35,000 words in length, has been written by me, and that it is the record of work carried out by me, or principally by myself in collaboration with others as acknowledged, and that it has not been submitted in any previous application for any degree.

I was admitted as a research student at the University of St Andrews in January 2016.

I received funding from an organisation or institution and have acknowledged the funder(s) in the full text of my thesis.

Date Signature of candidate

Supervisor's declaration

I hereby certify that the candidate has fulfilled the conditions of the Resolution and Regulations appropriate for the degree of PhD in the University of St Andrews and that the candidate is qualified to submit this thesis in application for that degree.

Date Signature of supervisor

Permission for publication

In submitting this thesis to the University of St Andrews we understand that we

are giving permission for it to be made available for use in accordance with the regulations of the University Library for the time being in force, subject to any copyright vested in the work not being affected thereby. We also understand, unless exempt by an award of an embargo as requested below, that the title and the abstract will be published, and that a copy of the work may be made and supplied to any bona fide library or research worker, that this thesis will be electronically accessible for personal or research use and that the library has the right to migrate this thesis into new electronic forms as required to ensure continued access to the thesis.

I, Fiona Grace McKissock, have obtained, or am in the process of obtaining, third-party copyright permissions that are required or have requested the appropriate embargo below.

The following is an agreed request by candidate and supervisor regarding the publication of this thesis:

Printed copy

Embargo on all of print copy for a period of 5 years on the following ground(s):

- Publication would preclude future publication

Supporting statement for printed embargo request

The data from this thesis is being used to produce a manuscript for future publication.

Electronic copy

Embargo on all of electronic copy for a period of 5 years on the following ground(s):

- Publication would preclude future publication

Supporting statement for electronic embargo request The data from this thesis are being used to produce a manuscript for furture publication.

Title and Abstract

- I require an embargo on the title and abstract but I understand that the title will be used in the graduation booklet.

Date Signature of candidate

Date Signature of supervisor

Underpinning Research Data or Digital Outputs

Candidate's declaration

I, Fiona Grace McKissock, hereby certify that no requirements to deposit original research data or digital outputs apply to this thesis and that, where appropriate, secondary data used have been referenced in the full text of my thesis.

Date Signature of candidate

Acknowledgements

First and foremost, I would like to thank my primary supervisor, David Harrison, who goes above and beyond for all his students. If not for his unwavering encouragement, support and kindness, I would not have completed this degree. Keep having those 'Harrison Hunches' and barbequing salmon!

None of this work would have been possible without the support of my family, particularly my father and sister. Thank you, Pater and Mel, for always believing in me, even when I don't.

I would also like to extend my appreciation to Peter Mullen for his assistance in the lab as well as his friendship. Peter's support and patience has been invaluable. I also extend thanks to Mary Wilson for mycoplasma testing and In Hwa Um for teaching me IHC. Furthermore, I thank all the undergraduate students who have worked on projects with me over the years.

The electron microscopy studies would not have been possible without my second supervisor, John Lucocq. Thank you, John, for your expertise and for sharing my excitement of rough ER proliferation mechanisms! Furthermore, I thank Fiona Murray at the Western General Hospital in Edinburgh for processing my samples.

A huge thank you is deserved by all of those in Lab 248 and indeed the rest of the medical school for their advice, smiles and banter! I am incredibly grateful for all of those in the Harrison group who cheer me up and are always willing to sing and dance in the lab, making the PhD roller-coaster a little smoother.

This work was supported by NuCana plc. I have great gratitude to NuCana plc, not only for funding this PhD, but for the continual support and opportunities working with them has provided. I am incredibly thankful for the work of the late Christopher McGuigan without whom ProTide technology, and therefore NUC-3373, would not exist.

This thesis is dedicated to the real heroes of cancer research; the brave patients who give up their final months of life to partake in clinical trials.

Abstract

5-Fluorouracil (5-FU) has been the backbone of chemotherapy for solid tumours such as colorectal cancer (CRC) for over 60 years. Despite advances in combinatorial treatments, most patients experience innate or acquired resistance to 5-FU as well as deleterious side effects. NUC-3373 is designed to overcome chemo-resistance by addition of a phosphoramidate moiety to the 5-FU molecule. Currently in Phase I clinical trials, NUC-3373 has a pharmacokinetic profile superior to 5-FU. The primary mode of action of both NUC-3373 and 5-FU is to inhibit thymidylate synthase (TS); resulting in a thymine-depleted state and impaired DNA replication and repair. In view of the current contradicting literature regarding the value of TS as a predictive biomarker for 5-FU, this study sought to elucidate the dynamics of TS in response to NUC-3373.

Two CRC cell lines were selected from a panel; one more sensitive (HCT116) and one less sensitive (SW480) to NUC-3373 treatment. TS protein expression and localisation were investigated by Western blot and immunocytochemistry. Endoplasmic reticulum (ER) stress was assessed on a biochemical level in addition to examining ultrastructure by Transmission Electron Microscopy (TEM).

Baseline TS was not predictive of response to NUC-3373 in cell lines. NUC-3373 treatment resulted in the formation of TS ternary complexes, a net increase in TS and a nuclear to cytoplasmic translocation of TS. NUC-3373 induced ER stress, detected by an upregulation of BiP protein and CHOP gene expression. Stereological assessment of TEM images found that, in response to NUC-3373, HCT116 cells undergo dilation of ER whereas in SW480 cells it proliferates.

These studies propose an additional mechanism of action for fluoropyrimidines that is independent of DNA damage. The ability of a cell to overcome ER stress may be a determinant of its resistance to fluoropyrimidines and a potential target for combination therapies.

Contents

List of Tables

List of Figures

List of Abbreviations

5-FU	5-Fluorouracil
AP	Apyrimidinic
APC	Adenomatous Polyposis Coli
APS	Ammonium persulfate
AQUA	Automated Quantitative Analysis
ATF4	Activation Transcription Factor 4
ATF6	Activation Transcription Factor 6
ATG5	Autophagy related 5
ATG7	Autophagy related 7
BCA	Bicinchoninic Acid
BER	Base excision repair
BiP	Immunoglobulin Binding Protein
BRAF	B-Raf proto-oncogene, serine/threonine kinase
CD91	Alpha-2-macroglobulin
cDNA	complementary Deoxyribonucleic acid
CH_2THF	Methylenetetrahydrofolate
CHOP	CCAAT-enhancer-binding protein homologous protein
CIMP	CpG island methylator phenotype
CIN	Chromosomal Instability
CK1α/ε	casein kinase 1 alpha/ε
CRC	Colorectal Cancer
CRT	Calreticulin
c-Src	Cellular proto-oncogene, non-receptor tyrosine kinase
C_t	Cycle threshold
CTC	Cycle threshold control
CTE	Cycle threshold experimental
DAB	3,3'-Diaminobenzidine
DAMP	Damage Associated Molecular Pattern
Dcp1a	Decapping mRNA protein 1a
DHFR	dihydrofolate
dhFU	dihydrofluorouracil
DMEM	Dulbecco's modified eagles medium
DMSO	dimethyl sulfoxide
DNA	Deoxyribonucleid acid
dNTP	deoxynucleotide
DPD	dihydropyrimidine dehydrogenase

Dsh	dishevelled
dTMP	deoxythymidine monophosphate
dTTP	deoxythymidine triphosphate
dUMP	deoxyuridine monophosphate
dUTP	deoxyuridine triphosphate
EC_{50}	Half maximal effective concentration
EDEM	ER degradation-enhancing alpha-mannosidase-like protein
EDTA	Ethylenediaminetetraacetic acid
EGFR	Epidermal Growth Factor Receptor
eIF2-α	eukaryotic initiation factor 2 alpha
eIF3	eukaryotic initiation factor 3
ELISA	Enzyme-Linked Immunosorbent Assay
ER	Endoplasmic Reticulum
ERdj4	Endoplasmic Reticulum DnaJ 4
ERp57	Endoplasmic reticulum resident protein 57
ERp60	Endoplasmic reticulum resident protein 60
FAP	Familial Adenomatous Polyposis
FBAL	alpha-fluoro-beta-alanine
FBS	Foetal Bovine Serum
FdUDP	Fluorodeoxyuridine diphosphate
FdUMP	Fluorodeoxyuridine monophosphate
FdUTP	Fluorodeoxyuridine triphosphate
FOBT	Faecal Occult Blood Test
FOLFIRI	5-Fluorouracil-Leucovorin-Irinotecan
FOLFOX	5-Fluorouracil-Leucovorin-Oxaliplatin
FOLFOXIRI	Fluorouracil-Leucovorin-Oxaliplatin-Irinotecan
Frz	Frizzled
FUDP	Fluorouridine diphosphate
FUDR	Fluorodeoxyuridine
FUMP	Fluorouridine monophosphate
FUTP	Fluorouridine triphosphate
GAPDH	Glyceraldehyde-3-Phosphate Dehydrogenase
GSK-3β	Glycogen synthase kinase 3 beta
HC	Housekeeping gene in Control samples
HE	Housekeeping gene in Experimental samples
HEDJ	Human ER-associated DNAJ
hENT1	human Equilibrative Nucleoside Transporter 1
HFS	Hand-Foot-Syndrome
HMGB1	High Mobility Group Box Protein 1
HMGB2	High Mobility Group Box Protein 2
HRP	Horse Radish Peroxidase
HSP70	Heat Shock Protein 70
HSP90	Heat Shock Protein 90
IBD	Inflammatory Bowel Disease
IC_{50}	Half maximal inhibitory concentration
ICC	Immunocytochemistry
ICD	Immunogenic Cell Death

IHC	Immunohistochemistry
IMM	Inner Mitochondrial Membrane
INF-γ	Interferon-gamma
IRE1	Inositol-requiring enzyme 1
ITH	Intratumoural Heterogeneity
KRAS	Kirsten rat sarcoma 2 viral oncogene homolog
LAMP1	Lysosomal Associated Membrane Protein 1
LC3	Light Chain 3
LD_{50}	Half maximal lethal dose
LEF	Lymphoid Enhancer Factor
LRP	Lipoprotein receptor-related protein
LSF	Late SV40 factor
LV	Leucovorin
MAM	Mitochondrial Associated Membrane
MMR	Mismatch Repair
mRNA	messenger Ribonucleic acid
MSI	Microsatellite Instable
MTD	Maximum Tolerated Dose
NF-κB	Nuclear Factor- kappa-B
NHS	National Health Service
OPRT	Orotate phosphoribosyltransferase
P2X7	P2X purinoceptor 7
p58IPK	DNAJ homolog subfamily C member 3
PBS	Phosphate Buffered Saline
PD-1	Programmed Death 1
PD-L1	Programmed Death Ligand 1
PERK	PRKR-like endoplasmic reticulum kinase
PIPES	Piperazine-N, N'-bis
PK	Pharmacokinetic
PS	Penicillin Streptomycin
PtdCho	Phosphatidylcholine
PtdEth	Phosphatidylethanolamine
PtdSer	Phosphatidylserine
PVDF	Polyvinylidene difluoride
RAMP-4	Ribosome-associated membrane protein 4
RAS	rat sarcoma 2 viral oncogene homolog
RDP2	Recommended dose for phase 2
RER	Rough Endoplasmic Reticulum
RIPA	Radioimmunoprecipitation assay
RNA	Ribonucleic acid
RR	Ribonucleotide reductase
RT	Reverse Transcription
RT-qPCR	Quantitative reverse transcription polymerase chain reaction
S1T	truncated variant of sarco/endoplasmic reticulum Ca2+ ATPase 1
SDS	Sodium dodecyl sulfate
SDS-PAGE	Sodium dodecyl sulfate-Polyacrylamide gel electrophoresis
SER	Smooth Endoplasmic Reticulum

SG	Stress Granule
SHMT1	Serine Hydroxymethyltransferase 1
siRNA	short interfering RNA
SP-1	site 1 protease
SP-2	site 2 protease
SRB	Sulforhodamine B
SUMO	Small Ubiquitin-like Modifier
SUR	Systematic Uniform Randomised Sampling
Sv	Surface density
TBS	Tris buffered saline
TC	Tested gene in Control samples
TCA	Trichloroacetic acid
TCF	T-cell Factor
TE	Tested gene in Experimental samples
TEM	Transmission Electron Microscopy
TEMED	Tetramethylethylenediamine
Tg	Thapsigargin
TK	Thymidine Kinase
TLR	Toll-like receptor
TMB	3,3',5,5'-Tetramethylbenzidine
TNM	Tumor Node Metastasis
TP	Thymidine Phosphorylase
TP53	Tumour protein 53
TS	Thymidylate synthase
Tu	Tunicamycin
TYMS	Thymidylate Synthetase
UK	Uridine kinase
UP	Uridine phosphorylase
uPAR	Urokinase-type plasminogen activator receptor
UPR	Unfolded Protein Response
UV	Ultraviolet
VEGF	Vascular endothelial growth factor
Vv	Volume density
Wnt	Wingless integrated
XBP1	X-box binding protein 1
ZO-1	Zonula occludens-1

Chapter 1

Introduction

1.1 5-Fluorouracil

The 1950s saw great advances in the knowledge of genetics and the structure of DNA, thanks to Watson, J. and Crick, F., (1953). The identification of the ability of cancer to replicate rapidly was to be its Achilles' heel, as drug development moved towards agents that could exploit this trait. In 1957, an experimental study by Heidelberger, C., *et al.*, (1957) described a new class of tumour inhibiting compounds; the fluorinated pyrimidines. 5-Fluorouracil (5-FU) has now been the backbone of chemotherapy regimens for various cancers, including head and neck, breast and colorectal cancer (CRC) for over 60 years.

1.1.1 Mechanism of Action

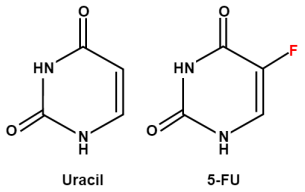

Figure 1.1: Similarity in the chemical structures of uracil and 5-FU.

5-FU, an analogue of the nucleoside uracil, possesses a fluorine atom at the C-5 position instead of hydrogen (Figure 1.1). Upon administration of 5-FU, 80% is degraded in the liver by dihydropyrimidine dehydrogenase (DPD) (Koopman, M., *et al.*, 2009), resulting in the formation of toxic metabolites such as α-fluoro-β-alanine (FBAL) shown in (Figure 1.2). The 20% of administered 5-FU that reaches cancer cells then must cross cell membranes, aided by the human equilibrative nucleoside transporter 1 (hENT1) transporter. A portion of 5-FU is then further degraded by intracellular DPD. The remaining 5-FU is then broken down to its active metabolites: fluorodeoxyuridine monophosphate (FdUMP), fluorodeoxyuridine triphosphate (FdUTP) and fluorouridine triphosphate (FUTP).

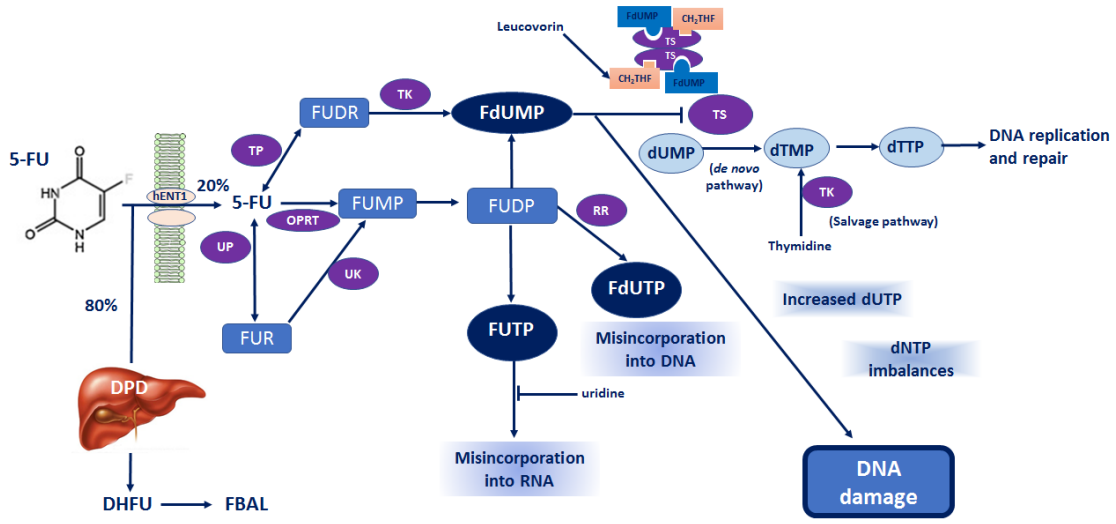

Figure 1.2: 5-FU mechanism of action. 80% of 5-FU is degraded by DPD before reaching cells. The 20% of 5-FU reaching cells is converted to its active metabolites; FdUMP,FdUTP and FUTP.

FUTP

Through the action of orotate phosphoribosyltransferase (OPRT), 5-FU is converted to fluorouridine monophosphate (FUMP). FUMP can also arise via conversion of 5-FU by uridine phosphorylase (UP) and uridine kinase (UK). Phosphorylation of FUMP results in fluorouridine diphosphate (FUDP) which can be further phosphorylated to form (FUTP) which is capable of mis-incorporation into RNA

in place of uracil. It has been reported that FUTP is more readily incorporated into RNA than uracil and that the toxicity of 5-FU is mainly dependent on this (Pettersen, H.S., *et al.*, 2011).

FdUTP

Alternatively, FUDP can be reduced by ribonucleotide reductase (RR) to fluorodeoxyuridine diphosphate (FdUDP). FdUDP can then be phosphorylated to form FdUTP which is capable of mis-incorporation into DNA in place of thymine.

FdUMP

Thymidine phosphorylase (TP) catalyses the phosphorylation of 5-FU to form fluorodeoxyuridine (FUDR) which is further phosphorylated by the action of thymidine kinase (TK) to form FdUMP. FdUMP targets the enzyme thymidylate synthase (TS) which is required to catalyse the *de novo* synthesis of deoxythymidine monophosphate (dTMP) from deoxyuridine monophosphate (dUMP). FdUMP forms a ternary complex with TS and a folate cofactor (CH_2THF), thus preventing dUMP binding. This inhibition of TS causes depletion of dTMP and therefore subsequent depletion of deoxythymidine triphosphate (dTTP). This has a two-pronged effect in that it abolishes thymine and therefore hinders DNA replication, as well as perturbing the deoxynucleotide (dNTP) pool balance along with elevating levels of deoxyuridine triphosphate (dUTP) which in turn further disrupts DNA synthesis and ultimately causes DNA damage (Yoshioka, A., *et al.*, 1987; Houghton, J.A., *et al.*, 1995).

DNA repair mechanisms

The cell has different mechanisms through which mis-incorporated nucleotides in DNA can be recognised and removed to repair DNA. One such pathway is Base

Excision Repair (BER) in which DNA glycosylase removes the inappropriate base, then the phosphodiester back bone is cleaved at the apyrimidinic (AP) site, allowing clean up of the 3' or 5' terminal end, finally allowing replacement of the excised nucleotide and sealing of the DNA (Wyatt, M., and Wilson, D., 2009). However, due to inhibition of TS by FdUMP, nucleotide pools are disturbed and further mis-incorporation can occur during the DNA resynthesis step of BER. This results in a futile cycle of attempted repair, and the introduction of DNA lesions by unpaired BER intermediates and eventually cell death. (Aherne, G., and Brown, S., 1999). Another mechanism by the cell to protect DNA integrity is mismatch repair (MMR). MMR recognises base:base mismatches in DNA and recruits exonucleases to degrade the daughter strand containing the mismatch then completes the repair through the action of polymerases and ligases. MMR can also signal to cell death machinery to trigger apoptosis where DNA damage is beyond repair. Loss of or mutations in genes involved in MMR can be tumorigenic and equip cancer with a tolerance to DNA damage and, as a result, resistance to some cytotoxic agents such as 5-FU (Meyers, M., *et al.*, 2005).

1.1.2 Modulation and Combination Therapy

5-FU may be administered as a single agent, but its efficacy is enhanced in the metastatic setting when combined with other agents.

Leucovorin

CH_2THF is a folate cofactor required to stabilise the ternary complex formed with TS and FdUMP. Leucovorin (LV) is a folate analogue which is transported into cells via reduced folate carriers and anabolised to CH_2THF which can then contribute to TS ternary complexes (Longley, D., *et al.*, 2003). CH_2THF is polyglutamated by folypolyglutamate synthetase, which increases its cellular retention and therefore enhances the stabilisation of the TS ternary complex (Dolnick, B.J., and Cheng,

Y.C., 1978; Radparvar, S., *et al.*, 1989). Leucovorin has been shown to positively modulate the cytotoxic action of 5-FU. A meta-analysis of 3300 patients found that those treated with 5-FU plus leucovorin had a 2-fold improved tumour response rate and a small but significant improvement in overall survival (median survival for 5-FU-LV was 11.7 months vs 10.5 months for 5-FU alone, P= 0.004) compared with those treated with 5-FU alone (Thirion, P., *et al.*, 2004). However, resistance is still experienced by many patients. It has been speculated that resistance to modulation of 5-FU by leucovorin may be due to reduced stability of ternary complexes caused by mutation(s) of TS (Lu, K., *et al.*, 1997; Spears, C.P., *et al.*, 1988; Omura, K., 2008).

Capecitabine

Capecitabine is an orally administered pro-drug of 5-FU. It requires conversion to 5-FU by the enzyme TP, of which higher levels are expressed in tumour cells than in healthy cells (Wagstaff, A.J., *et al.*, 2003). This makes it more targeted and therefore is indicated for use in metastatic colorectal cancer when single-agent fluoropyrimidine therapy is preferred (Walko, C.M., and Lindley, C., 2005). A randomised stage III clinical trial assessing oral capecitabine against intravenous 5-FU and leucovorin in the adjuvant treatment of stage III colon cancer found capecitabine to be of equivalent efficacy, but a significantly higher proportion of patients experienced grade 3 hand-foot syndrome when compared with those in the 5-FU/leucovorin arm (Twelves, C., *et al.*, 2005). It is also important to consider the issue of patient concordance with oral administration, with one study reporting a decrease in adherence with increasing cycles of therapy as measured by the Medication Adherence Report Scale (Timmers, L., *et al.*, 2016).

Oxaliplatin

The most common combination chemotherapy regimen is 'FOLFOX'; 5-FU, Leucovorin and Oxaliplatin. Oxaliplatin, a platinum-derived alkylating agent, exerts

its cytotoxic effect mainly through DNA damage in the form of DNA lesions, arrested DNA synthesis and inhibition of RNA synthesis (Alcindor, T., and Beauger, N., 2011). Compared to 5-FU alone, combination with Oxaliplatin has been found to increase median progression-free survival and response rate (50.7% vs. 22.3%) but not overall survival (de Gramont, A., *et al.*, 2000; Giacchetti, S., *et al.*, 2000). Synergism has been found when oxaliplatin and 5-FU are combined but the mechanism behind this is not fully elucidated. One explanation may be that oxaliplatin reduces the catabolism of 5-FU by DPD (Fischel, J., *et al.*, 2002).

Irinotecan

Irinotecan is a semi-synthetic pro-drug analog of camptothecin. It is converted to the active metabolite 'SW-38' by de-esterification in the liver (Kawato, Y., *et al.*, 1991). SW-38 acts by inhibiting topoisomerase I, the enzyme required for relaxing of DNA coils (Ma, M.K., and McLeod, H.L., 2003). The cleavable complex it forms collides with the replication fork during S-phase leading to DNA replication arrest and subsequent DNA fragmentation and apoptosis (Dancey, J., and Eisenhauer, E.A., 1996). There is evidence that patients with disease refractory to treatment with 5-FU and leucovorin have significant clinical benefit from the addition of irinotecan in the regimen termed 'FOLFIRI', with Douillard, J., *et al.* (2000) reporting an increased median overall survival of 17.4 months, compared to 14.1 months in those patients treated with 5-FU-LV (p=0·031).

Much uncertainty exists regarding the optimal first-line chemotherapy regimen for metastatic CRC. A triplet regimen of 5-FU, leucovorin, oxaliplatin and irinotecan 'FOLFOXIRI' has been shown to have superiority in tumour shrinkage, but the incidence of adverse events was much higher (Marques, R., *et al.*, 2017). When considering an appropriate line of therapy, it is vital for clinicians not only to consider the clinical benefit but also the 'fitness', quality of life and preferences of the patient.

Targeted Therapies

Targeted monoclonal antibody therapies have been developed to exploit traits of cancer which cause it to differ from healthy cells. Since many human malignancies express aberrantly high epidermal growth factor receptors (EGFR), targeted monoclonal antibody therapies such as cetuximab have been developed to blockade these receptors and treat cancer effectively without the cytotoxicity associated with other cancer treatments (Gullick, W., 1991; Herbst, R., and Shin, D., 2002). However, it is imperative to note that cetuximab has only been found to improve outcomes in those patients expressing the wild-type KRAS gene. Soeda, H., *et al.* (2014) reported that, in a study of patients with metastatic CRC treated with cetuximab in combination with irinotecan, response rate was 17.9% in KRAS wild type vs 0% in KRAS mutant subgroups. Bokemeyer, C., *et al.* (2012) pooled data from the CRYSTAL and OPUS randomised clinical trials which investigated the addition of cetuximab to first-line chemotherapy in metastatic CRC patients with wild-type KRAS. In a cohort of 845 patients, cetuximab was found to significantly improve median overall survival (23.5 vs 19.5 months in the cetuximab and non-cetuximab groups respectively, p=0.0062).

1.2 Resistance and Systemic Toxicity

Despite the advances in combination therapies and the development of targeted therapies, the majority of cancer patients experience either innate or acquired resistance to chemotherapy agents; this can be due to host factors as well as specific genetic or epigenetic alterations within cancer cells (Gottesman, M.M., *et al.*, 2002). In patients with CRC detected at a metastatic stage, chemotherapy resistance results in failure of treatment in over 90% of patients (Longley, D.B., and Johnston, P.G., 2005), posing a great burden on overall survival. The elucidation of the molecular mechanisms leading to drug resistance has been aided by advances in DNA microarray and proteomic technology as well as characterisation of the

signalling pathways integral to regulating tumour cell response to chemotherapy.

There are multiple stages at which the efficacy of anti-cancer drugs can be altered. Poor absorption, rapid metabolism or excretion of the drug can result in low serum levels. Particularly in elderly patients, tolerance to cytotoxic drugs may be low, resulting in the necessity to reduce dosage to below optimal levels which are no longer therapeutic. In addition, Steele, S.R.,*et al.*, (2014) identified that, in a cohort of 7948 CRC patients, 77% of those were aged between 50 and 79. An issue facing those in the older age demographic is the rise of polypharmacy, with Guthrie, B., *et al.*, (2015) reporting that individuals aged 60-64 years are in receipt of at least 5 different medications. This can lead to adverse interactions as well as iatrogenic effects.

Uptake of drugs into cancer cells can depend upon the transportation requirements of the drug and the expression of necessary transporters in the cell membrane. Once within the cell, many drugs require enzymatic activation to the active metabolite form which depends on the expression of intracellular enzymes.

1.2.1 Resistance mechanisms

Upon administration, 80% of administered 5-FU is degraded by DPD in the liver with DPD overexpression being related to poor patient outcomes (Koopman, M. *et al.*, 2009). 5-FU requires active uptake by the hENT1 to enter cells, as well as multistep conversion to the active metabolite FdUMP before it can target TS. Subsequently, low hENT1 expression is predictive of a poorer response to 5-FU (Tsujie, M., *et al.*, 2007). Once 5-FU is broken down to its active metabolites, the stability of the ternary complex is dependent on availability of CH_2THF as a cofactor, with its absence resulting in an unstable FdUMP binary complex and subsequent poor inhibition of TS. Leucovorin, described earlier, is administered concomitantly with 5-FU to modulate this action.

1.2.2 Systemic toxicity

There are many off-target effects associated with 5-FU, with systemic toxicity or adverse side effects being a major factor in cessation of therapy in patients. Hand-Foot-Syndrome (HFS) is a very common side-effect of 5-FU affecting 35% of those receiving a continuous infusion (Revollo, J.L., *et al.*, 2008). HFS is characterised by painful red lesions on the palms of the hands and the soles of the feet and can severely affect a patient's quality of life, with it being the leading cause of dose reduction, treatment interruption and even treatment cessation. The exact mechanism behind the development of HFS is not clear but there is strong evidence proposing that it is due to the degradation of 5-FU by DPD and further catabolism by β-ureidopropionase to form toxic FBAL (Yen-Revollo, J.L., *et al.*, 2008). Evidence to support this comes from reports of DPD-deficient patients treated with fluoropyrimidines who, whilst are at increased risk of severe toxicity, rarely experience HFS (Saif, M.W., and Diasio, R., 2006). The degradation of 5-FU by DPD has been reported to cause other adverse effects such as diarrhoea and neutropenia. A minority of patients experience cardiotoxicity, although the underlying mechanisms for this are poorly understood but are likely related to pre-existing disease of a cardiovascular aetiology (Polk, A., *et al.*, 2013).

1.3 Novel ProTide Drug NUC-3373

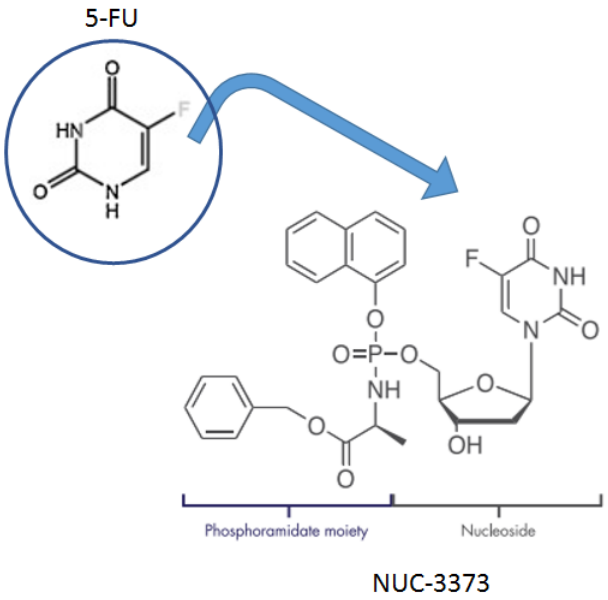

Figure 1.3: The chemical structure of NUC-3373.

NUC-3373, a novel pyrimidine nucleotide analogue produced by NuCana plc is the pre-activated form of anti-cancer metabolite FdUMP. ProTide technology, which employs the addition of a phosphoramidate moiety (Figure 1.3) to a parental nucleoside drug (McGuigan, C., *et al.*, 2011), is reported to overcome the resistance mechanisms faced by 5-FU. The addition of a phosphoramidate moiety allows NUC-3373 to bypass degradation by DPD in the liver, resulting in a higher level of drug reaching cells. Due to the addition of the phosphoramidate group, NUC-3373 can enter the cell independent of hENT1, with a study by Cavaliere, A., *et al.*, (2017) demonstrating that its cytostatic potency was maintained in hENT1-negative tumour cell lines. The phosphoramidate moiety is then cleaved to produce FdUMP which directly inhibits TS to induce apoptosis of tumour cells. By overcoming these resistance mechanisms, NUC-3373 can be administered in much lower doses than 5-FU, achieving superior results. NUC-3373 has now entered the clinic and has progressed to phase Ib study NuTide:302 which aims to determine its safety, efficacy and pharmacokinetics when combined with standard agents used in CRC

chemotherapy such as leucovorin, oxaliplatin and irinotecan (Evans, T.R., *et al.*, 2019). It is hoped that NUC-3373 possesses the potential to replace 5-FU as the backbone of colorectal cancer chemotherapy.

1.4 Colorectal Cancer

The colon is the terminal portion of the gastrointestinal tract and primarily functions to process contents received from the small intestine. These functions include storage, appropriate removal and secretion of water and electrolytes, compaction and eventual expulsion of faecal matter from the rectum through the anus (Bassotti, G., and Battaglia, E., 2015). Due to the rapid turnover rate of colonocytes, there is greater scope for mutations to occur that result in the development of carcinoma.

1.4.1 Epidemiology

Incidence and Mortality

Colorectal cancer (CRC) is the third leading cancer in both males and females and accounts for 12% of total cancer cases in the UK. 52-56% of cases are detected at later stages (stages III and IV), with 23-26% of patients having metastases at diagnosis. Prognosis has a very strong correlation to stage at diagnosis with the 5-year survival rate for cases detected at stage I (localised) being 90-100%, decreasing to less than 10% in those detected at stage IV. All of the aforementioned incidence and mortality statistics were acquired from Cancer Research UK (2016). These data highlight the need for early detection for successful outcomes.

Risk Factors

The majority of CRC cases are preventable, but some risk factors are non-modifiable, such as age, personal history of inflammatory bowel disease (IBD) and genetics. The

risk of developing CRC increases after the age of 40, rising sharply after 50, with 90% of cases being in individuals over 50 (Jemal, A., *et al.*, 2000). A history of adenomatous polyps (the precursor lesions of CRC) was found to increase the risk of developing CRC, in a study by de Jong, A.E., *et al.*, (2005). Boardman, L.A., *et al.*, (2007) established that the risk of developing CRC is increased by having a 1st degree relative with a history of adenomatous polyps or CRC, especially if that individual is a sibling. This could perhaps be due to either inherited genetics, a shared environment or indeed a combination of both. IBD such as Crohn's disease (CD) or Ulcerative Colitis (UC) present an 18- and 19-fold, respectively, increased risk of developing CRC, as found in a study by Gillen, C.D., *et al.*, (1994). 5-10% of CRC cases are hereditary as opposed to sporadic (Jackson-Thompson, J., *et al.*, 2006 as cited by Haggar, F., and Boushey, R.P., 2009).

Amongst modifiable risk factors for developing CRC, diet and lifestyle practices such as smoking and exercise (Botteri, E., *et al.*, 2008), have been found to have large influence. High intake of red and/or processed meat has been found to significantly increase the risk of CRC (Chan, D.S.M., *et al.*, 2011). Diets high in red meat, a source of nitrogenous residues, have been shown to increase levels of endogenously formed N-nitroso compounds reaching the colon, in a dose-dependent manner (Hughes, R., *et al.*, 2001). Some N-nitroso compounds are alkylating and induce GC-AT transitions at the second base of codon 12 or 13 within the Kirsten rat sarcoma 2 viral oncogene homolog (KRAS) gene, with these mutations ultimately resulting in the development of carcinomas. Additional nutritional factors such as high animal fat intake (Willett, W.C., *et al.*, 1990) and low dietary fibre intake (Aune, D., *et al.*, 2011) have been found to positively correlate with increased risk of CRC. In addition to these factors, excessive alcohol consumption has been found to increase risk of CRC, particularly in onset in younger individuals (Fedirko, V., *et al.*, 2011). This could be due to the carcinogenic effects of alcohol metabolites such as acetaldehyde, in addition to alcohol acting as a solvent to allow penetration of other carcinogenic molecules into cells (Haggar, F., and Boushey, R.P., 2009). All of the aforementioned nutritional factors have the capacity to significantly alter the gut

microbiome and lead to inflammatory processes and possible cancer, with dysbiosis more prevalent in the gut of individuals with CRC compared with healthy controls (Zackular, J.P., *et al.*, 2013). Dysbiosis favouring bacteria which produce hydrogen sulfide, such as *Fusobacterium*, *Desulfovibrio* and *Bilophila wadsworthia*, leads to DNA damage and chromosomal instability and subsequent CRC development (Attene-Ramos, M.S., *et al.*, 2006). These sulfidogenic bacteria have been found to correlate positively with diets high in fat and animal protein (Dahmus, J., *et al.*, 2018), further highlighting the impact of diet on the risk of CRC development.

1.4.2 Pathophysiology

CRC can be hereditary or sporadic, both with differing mechanisms of carcinogenesis. The inherited form accounts for 30% of all CRC cases, and comprises several well-characterised conditions including Lynch syndrome and Familial Adenomatous Polyposis (FAP). Lynch syndrome, accounting for 2-3% of all CRC cases (Roper, J., and Hung, K., 2013), can be differentiated from other inherited forms by microsatellite instability testing and the identification of germline mutations in DNA mismatch repair genes. This important distinction between Lynch syndrome and other CRCs determines the treatment and surveillance regimens of patients by clinicians (Shia, J., 2008). The majority (70%) of CRCs are sporadic, arising from somatic mutations not associated with a family history.

By the 1970s, it was becoming increasingly evident that adenomas were the precursors to colorectal adenocarcinomas (Roper, J., and Hung, K., 2013). This hypothesis was confirmed by Winawer, S.J., *et al.*, (1993) who, in their analysis of the National Polyp Study with reference to other published data, found that the incidence of CRC following colonoscopic polypectomy was significantly less than expected.

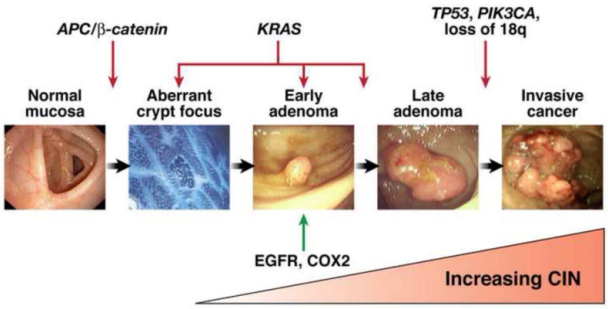

Figure 1.4: The chromosomal instability pathway. Accumulation of mutations leads to increasing CIN and consequently invasive cancer. Image from Pino, M., and Chung, D., 2010.

In 1990 Fearon, E., and Vogelstein, B., proposed a multi-step genetic model of colorectal carcinogenesis (see Figure 1.4), describing the multiple genetic changes required for progression of normal intestinal mucosa to adenomas and eventually to adenocarcinomas; the adenoma-carcinoma sequence. The initial step in this process is inactivation of the Adenomatous Polyposis Coli (APC) tumour suppressor gene, causing activation of the Wnt pathway. Evidence for APC inactivation being of importance in the earliest stages of adenoma formation came from sequence analysis of tumours, finding that APC mutations were present in 60% of CRC tumours and in 63% of adenomas. Furthermore, mutations were found in adenomas as small as 0.5 cm in diameter, with the frequency of mutation remaining constant as tumours progressed to malignant stages (Powell, S.M., *et al.*, 1992).

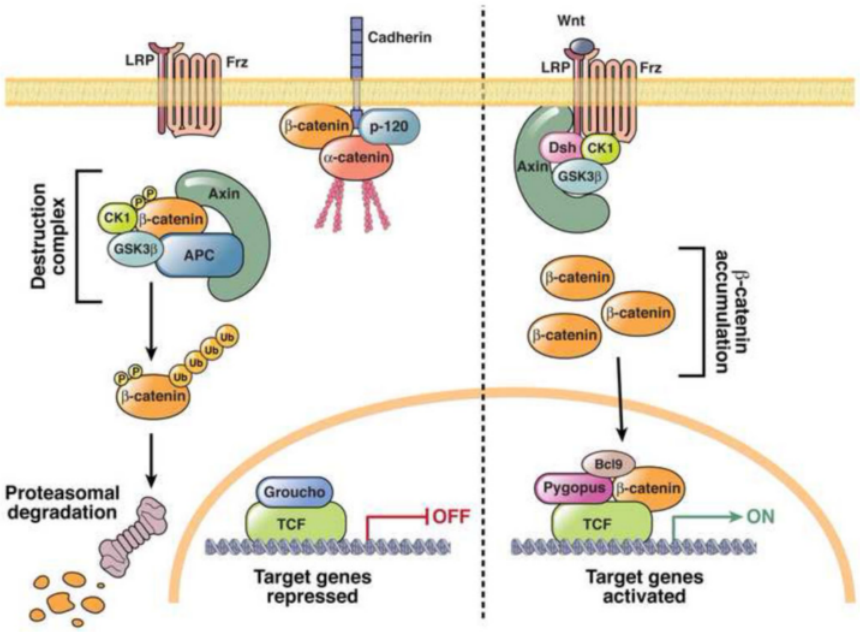

Figure 1.5: Activation of Wnt signalling causes β-catenin accumulation and transcription of target genes. Image from Roper, J., and Hung, K., 2013.

In the absence of Wnt signalling, a destruction complex formed by APC, glycogen synthase kinase-3β (GSK-3β) and casein kinase 1 alpha/ε (CK1alpha/ε) on an axin-conductin scaffold targets the proteasome-dependent degradation of cytoplasmic β-Catenin. However, when Wnt signalling is switched on, i.e. a Wnt ligand is present, this allows the receptors Frizzled (Frz) and co-receptor low-density lipoprotein receptor-related protein (LRP) to be occupied. This occupation triggers phosphorylation of the cytoplasmic tail of LRP by CK1 and GSK-3β along with recruitment of axin on phosphorylated LRP in a dishevelled (Dsh)-dependent manner. Phosphorylation of β-catenin is prevented, resulting in increased cytoplasmic levels of β-catenin to translocate to the nucleus. Subsequently, transcription of target genes related to tumour progression and metastasis, such as Zonula occludens-1 (ZO-1) and Urokinase-type plasminogen activator receptor (uPAR) (Mann, B., *et al.*, 1999) is initiated by displacement of Groucho and interaction of β-catenin with T-cell factor (TCF)/lymphoid enhancer (LEF) transcription factor family (Rubinfeld, B., *et al.*, 1996).

The progression to invasive carcinoma requires additional mutations; activation of proto-oncogenes such as KRAS (Fearon, B., and Vogelstein, A. 1990) and loss of anti-tumour genes such as TP53 (Jones, S., *et al.*, 2008). There are three main pathways of molecular pathogenesis of inherited and sporadic colorectal cancer; the chromosomal instability (CIN) pathway, the microsatellite instability (MSI) pathway and the CpG island methylator phenotype (CIMP) pathway (Colussi, D., *et al.*, 2013). The majority of CRCs develop via the CIN pathway, involving defects in chromosomal segregation, telomere stability, the DNA damage response as well as loss of heterozygosity (Pino, M.S., and Chung, D.C, 2010).

1.4.3 Intra-tumoural Heterogeneity

The 'Big Bang' model of CRC tumour growth (Sottoriva, A., *et al.*, 2015) suggests that the malignant potential of the tumour is determined early in its development. Since tumour growth is an evolutionary process with ancestral history recorded within tumour cell genomes, it is possible to gather information on the poorly characterised early growth phase by studying patterns of genomic intra-tumoural heterogeneity (ITH) in the final neoplasm. It has been proposed that the initial events in neoplastic transformation occurs through step-wise accumulation of driver alterations. So-called 'public' mutations are present in 100% of the tumour cells, with acquired 'private' mutations occurring as the tumour expands and often present in defined regions of the tumour. Only early-occurring private mutations have the ability to expand to a detectable size in tumours due to spatial constraints, limiting the selective forces that can drive tumour expansion. This model supports the stem cell model, in that malignancy is driven by a small number of self-renewing cells. This ITH poses problems for treatment, with potentially aggressive sub-clones remaining rare or possibly undetectable in the primary tumour, despite their relative survival advantage, resulting in resistance to treatment.

1.4.4 Diagnosis

In most countries with developed healthcare systems, screening programs are well established. The National Health Service (NHS) offers a two-yearly faecal occult blood test (FOBT) for men and women aged between 50-74 in Scotland and 60-74 in the rest of the UK. The sample is retrieved by the patient at home then sent for analysis. If results are found to be abnormal (presence of blood in sample), the individual will be offered a colonoscopy for further investigation, then any benign polyps removed (Cancer Research UK, 2016). A meta-analysis of randomised clinical trials (Mandel, J.S., *et al.*, 1993; Hardcastle, J.D., *et al.*, 1996; Kronborg, O., *et al.*, 1996; Hewitson, P., *et al.*, 2007) found that screening programs reduce mortality in CRC by 16% (NICE, 2014), most likely due to detection and removal of benign polyps, preventing progression to malignant lesions.

Staging

When malignant lesions are identified during colonoscopy, the resected specimen is subjected to pathological examination after which it is assigned a grade using TNM classification (Table 1.1). TNM provides more detail and precision than other systems such as Dukes staging, taking into account the depth of tumour penetration into the intestinal wall and adjacent structures (T), regional lymph node involvement (N) and the presence or absence of metastases (Egner, J.R., 2010). In addition to TNM staging, specimens are assigned a histologic grade. The grade relates to the differentiation of cells, with more poorly differentiated lesions indicating higher abnormality of cells and predicting more aggressive disease.

Primary Tumour (T)	
TX	Primary tumour cannot be assessed
T0	No evidence of primary tumour
Tis	Carcinoma *in situ.*: intraepithelial or invasion of lamina propria
T1	Tumour invades submucosa
T2	Tumour invades muscularis propria
T3	Tumour invades through the muscularis propria into the subserosa, or into a non-peritonealised pericolic or perirectal tissues
T4	Tumour directly invades other organs or structures and/or perforates visceral peritoneum
Regional lymph nodes (N)	
NX	Regional lymph nodes cannot be assessed
N0	No regional lymph node metastasis
N1	Metastasis in 1 to 3 regional lymph nodes
N2	Metastasis in 4 or more regional lymph nodes
Distant metastasis (M)	
MX	Distant metastasis cannot be assessed
M0	No distant metastasis
M1	Distant metastasis

Table 1.1: TNM identifiers. Adapted from Egner, J.R., 2010

TNM stage, histologic type and grade in addition to other factors such as residual disease after resection, serum carcinoembryonic antigen and cytokine levels, extramural venous invasion and submucosal vascular invasion by carcinomas can all be used to calculate a prognosis for disease progression or recovery. CRC diagnosed when metastatic has a very poor 5-year survival rate of 5-7% (Egner, J.R., 2010), with the most common sites of metastases being the lungs and liver (French, S.W., and DiSibio, G., 2008).

1.4.5 Treatment

The most common first line treatment for CRC, dependent on stage, is surgery. Whether this is local excision, resection and anastomosis, or colostomy, depends on the stage of the tumour. Localised lymph nodes are also removed and investigated for malignancy. Alongside surgery, adjuvant chemotherapy (common agents described

earlier) is usually administered to reduce the chance of local or systemic recurrence or alternatively given prior to surgery to shrink tumour margins (NICE, 2014).

1.4.6 Biomarkers

Biomarkers can be objectively measured and evaluated to inform treatment of patients and the most likely outcomes. Prognostic biomarkers are used to identify the likelihood of a clinical event, disease recurrence or progression in an individual, regardless of treatment received. Predictive biomarkers are used to identify the individuals who are likely or unlikely to respond to a specific treatment (Oldenhuis, C.N.A.M., *et al.*, 2008). A single biomarker can be both prognostic and predictive. In CRC, there are a variety of biomarkers based on the genetic signature of a tumour, such as MMR status, BRAF mutations or RAS mutational status, with much of the value of these markers depending on stage of disease (Zarkavelis, G., *et al.*, 2017). Molecular profiling platforms are available to guide clinicians on the most appropriate treatment based on biomarkers. One such intelligence platform, Caris, was evaluated by Carter, P., *et al* (2018). The Caris CODE database holds tumour molecular profile data for the solid tumours of 841 patients, alongside demographic information regarding any treatment patients had received before and after molecular profiling. The evaluation used the platform algorithm to determine the treatment recommended based on molecular profiling and compared this with the treatment received by the patient, classifying cases as 'matched' if the recommended treatment was the same as the actual treatment received, or 'unmatched' if it was not. Analysis of colorectal cancer patient tumours (n=95) found that matched cases had a significantly reduced mortality compared to unmatched cases (19% vs 49%, p=0.0022) and identified TS as a significant predictive biomarker. However, there was no detail for which drug TS was identified as a predictive biomarker. A caveat of this study is that the unmatched group had a higher proportion of tumours that were in advanced stages than the matched group, as well as the patient cohort being relatively small. Many studies have evaluated TS as a predictive biomarker of response to 5-FU, but the findings are very mixed, as will be described later. The

clinical utility of molecular profiling has potential to improve patient outcomes, however it must take a holistic approach and consider that acquisition of data derived from living subjects comes with the caveat of an infinite number of variables. These variables can be from co-morbidity, to patient adherence to treatment to the method of sample collection and may account for some of the contradictory findings of studies.

1.5 Aims and Objectives

Chemotherapy resistance remains a heavy burden in the treatment of metastatic CRC with 5-FU. ProTide NUC-3373 shows great promise in overcoming the resistance mechanisms of 5-FU but its mechanism of action and indeed that of the parental drug are not fully understood. This thesis will address the dynamic role of TS as well as the effects of its inhibition by FdUMP and establish its value as a predictive biomarker for response to NUC-3373 treatment. By elucidating further the mechanisms of action of NUC-3373, a rationale can be provided to inform drug targets or drug combinations which would be efficient in potentiating the effects of NUC-3373 thus enhancing treatment outcomes.

Chapter 2

Materials and Methods

2.1 Cell Culture

Throughout all cell culture, an aseptic technique was adopted. All reagents were warmed to 37^{o}C prior to use. All cell lines were cultured in Dulbecco's Modified Eagles Medium 'DMEM' 1x supplemented with 10% Foetal Bovine Serum 'FBS' and 1% Penicillin Streptomycin 'PS', all purchased from Gibco. Fully supplemented medium will henceforth be referred to as 'complete' medium. Cells were frozen in a freeze medium containing 10% dimethyl sulfoxide 'DMSO' (Sigma Aldrich) in FBS and stored in gaseous phase liquid nitrogen.

Cells were passaged when they reached 80% confluence by aspirating media, washing twice with Phosphate Buffered Saline 'PBS' then adding 6 mL Trypsin EDTA (Gibco) to detach cells from flask. Cells were centrifuged to a pellet at 280 g for 5 minutes then re-suspended in either fresh complete DMEM to be seeded for an experiment (see Table 2.1) or freeze medium as appropriate. Cells were not used beyond 5 passages of their original passage numbers. All cell lines were regularly tested for mycoplasma contamination (see Appendix for example).

Cell Line	Seeding density (cells/mL)
HT29	3,500
SK-CO-1	12,500
DLD-1	1,250
LoVo	7,500
HCT116	2,500
LS411N	5000
HCT116 p53-/-	1,250
SW480	7,500
SW620	12,500

Table 2.1: Cell line seeding densities

Cell densities were optimised prior to studies to achieve appropriate confluence for each assay. A haemocytometer was used to count cells prior to dilution to the desired density.

2.2 Drug Treatments

NUC-3373, supplied as powder by NuCana plc, was diluted in DMSO (warmed to 37^{o}C) to a stock concentration of 40 mM and stored at -20^{o}C in aliquots. 5-FU (Sigma Aldrich) supplied as powder was diluted to 10 mM and stored in aliquots at -20^{o}C. NUC-3373 and 5-FU were diluted in complete DMEM to a working concentration of 10 μM unless otherwise stated.

Thapsigargin (Sigma Aldrich, UK) supplied as powder was diluted in DMSO to a concentration of 1 mM and stored at -20^{o}C. Tunicamycin (Sigma Aldrich, UK) supplied as powder was diluted to 5 mg/mL and stored at -20^{o}C. Thapsigargin and tunicamycin were diluted to working concentrations of 1 μM and 5 μg/mL respectively in complete DMEM and incubated with cells for 5 hours prior to fixation or lysis.

Thymidine (Sigma Aldrich, UK) supplied as powder was prepared to a stock concentration of 50 μg/mL by gently heating in sterile tissue culture grade dH_2O

then passing through a sterile filter. Thymidine was used immediately after preparation by diluting in complete DMEM to a working concentration of 8 μg/mL.

2.3 Antibodies

Primary antibodies used are described in Table 2.2. Secondary antibodies used were as follows:

For Immunocytochemistry (ICC) applications

All primary antibodies raised in rabbits were paired with Goat anti-Rabbit Alexa-Fluor 488 secondary antibody (Invitrogen), except for Dcp1a, which is conjugated to Alexa-Fluor 594. All primary antibodies raised in mice were paired with Goat anti-Mouse Alexa-Fluor 594 antibody (Invitrogen). Secondary antibodies were prepared to a concentration of 1:1000 in the same serum used to dilute the primary antibody. Hoechst (Invitrogen) was used as a nuclear stain in all ICC experiments, diluted to a concentration of 1:10,000 in PBS.

For Western Blot applications

All primary antibodies raised in rabbits were paired with Donkey-anti-Rabbit IRDye 800CW (Licor) secondary antibody. Those raised in rats were paired with Goat anti-Rat IRDye 800CW (Licor). Those raised in mice were paired with Donkey-anti-Mouse IRDye 680RD (Licor). All secondary antibodies were diluted to a concentration of 1:10,000 in the same diluent used for the primary antibody but with the addition of sodium dodecyl sulfate (SDS) to a concentration of 1:10,000.

Antigen	**Host species**	**Purchased From**	**Ref**	**Application**	**Dilution**	**Diluent**
Thymidylate Synthase	Rabbit	Abcam	ab108995	Western blot	1:1000	PBS/Licor Blocking Buffer
				ICC	1:100	10% goat serum in PBS
β-actin	Mouse	Cell Signalling	cs3700s	Western blot	1:2000	PBS/Licor Blocking Buffer
LAMP1	Mouse	gift from Lucocq group	n/a	ICC	1:200	2% FBS in PBS
BiP	Rabbit	Cell Signalling	cs	Western blot	1:1000	TBS/Licor Blokcing Buffer
HMGB1	Rabbit	Abcam	ab18256	ICC	1:100	10 % goat serum in PBS
TS-5FU	Rat	Merck-Millipore	MABE370	Western blot	1:2000	PBS/Licor Blocking Buffer
Phospho-eIF2α	Rabbit	Cell Signalling	cs9721	Western blot	1:1000	TBS/Licor Blocking Buffer
GLG1	Rabbit	Novus Biologicals	NBP19036	ICC	1:200	10% goat serum in PBS
DCP1a	Rabbit	Abcam	ab17092	ICC	1:100	10% goat serum in PBS
ATF6	Mouse	Novus Biologicals	NBP140256	Western blot	1:300	TBS/Licor Blocking Buffer
Calreticulin	Rabbit	Abcam	ab2907	ICC	1:100	10% goat serum in PBS
PD-L1	Rabbit	Cell Signalling	E1L3N	Western Blot	1:1000	TBS/Licor Blocking Buffer

Table 2.2: Primary Antibodies

2.4 Cytotoxicity Assays

Cells were seeded according to densities detailed in Table 2.1 into the central wells (200 μL per well) of 96-well plates (Corning 3596) and treated in the same way for both the sulforhodamine B (SRB) assay and for Celigo confluence scans. PBS was added to all outer wells to prevent evaporation from experimental wells. Cells were seeded on day 0 in complete DMEM and allowed to grow for 48 hours. Any cells intended for hypoxic studies were transferred to the hypoxystation (0.5% O_2) on day 1. Media was aspirated on day 2 and replaced with drug treatments diluted in DMEM to the following concentrations: 0 (control), 0.1, 0.2, 0.5, 1, 2, 5, 10, 20 and 35 μM. Drug treatments were incubated for 24 hours then removed and replaced with complete medium on day 3. Cells were allowed to grow for a further 3 days before the endpoint SRB assay. Each plate included 6 technical replicates for each condition assessed.

2.4.1 Sulforhodamine B Assay

Sulforhodamine B (SRB) assay measures total cellular protein and was used as a surrogate of cell number as an end-point measure. On day 6, 50 μL 25% w/v trichloracetic acid 'TCA' (Sigma Aldrich) was added to each well for 1 hour at 4^{o}C to fix cells. Plates were then washed 10x each under running tap water and left to dry in an oven at 50^{o}C. Once dry, 50 μL SRB dye was added to each well and left for 30 minutes at room temperature, after such time plates were washed 4x each in 1% glacial acetic acid then left to dry in an oven at 50^{o}C. Once dry, 150 μL 10 mM Tris (pH 10.5) was added to each well and placed on a rocker at room temperature to dissolve material for 1 hour. Optical density of wells was measured by scanning plates on the Biohit plate-reader at 540nm. Optical density values for test wells were blanked by subtracting the average of the values for the outer wells. Values were then normalised to the untreated control response and GraphPad Prism software (Version 6.0, San Diego, CA) was used to determine the half maximal inhibitory

concentration (IC_{50}) values using a linear regression, variable slope, dose-response curve analysis.

2.4.2 Celigo Confluence Scans

Plates were scanned using the Celigo Scanner on days 2, 3, 4, 5 and 6 then an algorithm appropriate for each cell line's morphology was applied to determine confluence of cells for each individual well. This data was exported to Excel and growth curves constructed using the average of 6 technical replicate values for each drug concentration, normalised to control. Normalised values were used to calculate IC_{50} values using GraphPad Prism software as described previously.

2.5 Western Blot

2.5.1 Whole cell lysis

Lysis Buffer supplementation

Note that for data detailed in Chapter 3, cells were lysed using RIPA buffer. Data detailed in Chapters 4 and 5 used cell lysis buffer purchased from Cell Signalling as it was found to yield a higher protein concentration.

Pre-prepared standard RIPA or cell signalling lysis buffer (6.5 mL) was supplemented with the following:

1x Mini protease inhibitor tablet (Roche)

50 μL Aprotinin (Sigma Aldrich)

100 μL Phosphatase inhibitor cocktail 2 (Sigma Aldrich)

100 μL Phosphatase inhibitor cocktail 3 (Sigma Aldrich)

100 μL Triton X-100 (Sigma Aldrich)

After supplementing, buffer was referred to as 'complete lysis buffer'.

Cells were lysed at the appropriate time points. Media was removed and cells rinsed 2x in PBS then left to sit at an angle on ice. PBS collected at the bottom of dishes was removed with a pipette. Complete lysis buffer (200 μL) was added to each dish, cells scraped to bottom with cell scrapers then left to lyse on ice for 5-10 minutes. Lysed cell suspension was passed 3 times through a 20-gauge needle (BD) and added to a 1.5 mL tube and centrifuged for 6 minutes at 14.8 gsm at 4^{o}C. Supernatant was transferred to a 0.6 mL tube and stored at -80^{o}C until use.

2.5.2 Bicinchoninic Acid (BCA) Assay

Using the Thermo Fisher Pierce BCA assay kit, protein standards were prepared in borosilicate glass tubes (Thermo Fisher) as described in Table 2.3.

Final Protein Concentration (μg/mL)	**Volume 2mg/mL protein standard (μL)**	**Volume dH_2O (μL)**
0	0	150
100	2.5	47.5
150	3.75	46.25
200	5	45
500	12.5	37.5
1000	25	25
1500	37.5	12.5
2000	50	0

Table 2.3: BCA protein standard components

Protein lysates (5 μL per sample) were diluted in 1:10 in dH_2O (45 μL per sample) in separate borosilicate glass tubes. Working reagent was prepared by combining 1 part copper sulphate solution to 50 parts BCA solution. Prepared working reagent was added to all tubes (1 mL each). Tubes were vortexed and incubated in a water

bath for 15 minutes at 60^{o}C. Tubes were allowed to cool then 200 μL per standard and sample was added to a 96-well plate in triplicate. The plate was read at 540 nm using the Biohit Plate reader and optical density values used to determine protein concentration of each sample from the constructed standard curve. Samples were then diluted in complete lysis buffer to provide 60 μg protein in 60 μL. 5x loading buffer (see recipe in Table 2.4) was then added to samples (15 μL each), giving a total volume of 75 μL. This provided sufficient amounts of each sample to carry out 3 Western blots (20 μg protein in 25 μL for each).

5x Loading Buffer Recipe
12.5 mL 2M Tris pH 6.8
5 g SDS
50 mL glycerol
2.5 mL beta-mercaptoethanol
2.5 mL bromophenol-blue (saturated solution in dH_2O)
Up to 100 mL with dH_2O

Table 2.4: 5x Loading Buffer Recipe

Samples were placed on a heat block for 60 minutes at 60^{o}C to denature proteins before being stored at -80^{o}C until use.

2.5.3 SDS-PAGE

Glass plates were cleaned with 70% EtOH and assembled in casting racks. Tetramethylethylenediamine 'TEMED' (Sigma) and ammonium persulfate 'APS' (Sigma Aldrich) were added to the resolving gel mixture (see Table 2.5) and poured between plates. A little isopropanol was added to the top of the resolving gel to remove any bubbles then these were left to set. Once set, the isopropanol was washed out with dH_2O. TEMED and APS were added to the stacking gel mixture (see Table 2.6) which was poured on top of the resolving gel, with a comb being inserted immediately afterwards. Bubbles were removed by tapping the top of the

comb then gel was left to polymerise. Once set, the comb was removed gently and wells washed with distilled water, ensuring no bubbles.

10% Resolving Gel	**Volume (mL)**
Acrylamide	13.5
1M Tris pH 8.85	15.0
10 % SDS	0.4
dH_2O	11.1
TEMED	0.1
10 % APS	0.1

Table 2.5: Resolving Gel Recipe, sufficient for 1 gel

3.6% Stacking Gel	**Volume (mL)**
Acrylamide	3.6
0.375M Tris pH 6.8	10.0
10 % SDS	0.3
dH_2O	16.0
TEMED	0.1
10 % APS	0.1

Table 2.6: Stacking Gel Recipe, sufficient for 2 gels

Gels were assembled in the running tank and running buffer, prepared as detailed in Table 2.7, was added. Using gel loading tips, 10 μL Chameleon Duo Pre-stained Protein Ladder (Licor) was added to the first lane of each gel. Thawed samples were vortexed then 25 μL added per well. The tank was connected to a cold water supply and a power pack which was set to run at a constant current of 120 mA. Once samples reached the border of the resolving gel, the current was set to 60 mA and samples electrophorised until sufficient separation was achieved, indicated by the pre-stained ladder marker.

Component	Running Buffer	Transfer Buffer
Trizma Base (Sigma)	9.09 g	12.12 g
Glycine (Sigma)	43.26 g	57.68 g
10 % SDS	30 mL	——-
dH_2O	up to 3 L	up to 4 L

Table 2.7: Running and Transfer buffer recipes

2.5.4 Transfer

Transfer Buffer was prepared as described in Table 2.7. Polyvinylidene difluoride (PVDF) membranes (Millipore) were cut to 13x16 cm and activated by placing in methanol for 2 minutes at room temperature followed by dH_2O. Filter paper (Whatman) was cut to 17x15 cm (4 pieces per gel to be transferred). Stacking gel was trimmed from gel and transfer cassettes assembled as detailed in Table 2.8.

Wet pad (soaked in transfer buffer)
2 pieces filter paper (soaked in transfer buffer)
Gel
PVDF Membrane
2 pieces filter paper (soaked in transfer buffer)
Wet pad (soaked in transfer buffer)

Table 2.8: Transfer cassette assembly

Once the second pair of filter papers were placed on the membrane, a pipette was used to gently roll the surface to ensure no bubbles were present between the gel and the membrane. Prepared cassettes were placed in a transfer tank, connected to a power pack and set to transfer overnight at 4^oC at a constant pressure of 30 V.

2.5.5 Antibody Probing

Membranes were transferred to a 50 % Licor Blocking buffer in PBS or Triz-buffered saline (TBS) solution to block for 1 hour at room temperature on the rocker in the dark.

Primary antibody cocktail was prepared. Blocking buffer was removed and primary antibodies incubated on membranes overnight at 4^oC in the dark on a slow oscillating rocker.

Primary antibodies were removed and membranes washed 3x5 minutes in 0.1% PBS- or TBS-Tween20

Secondary antibody cocktail was prepared and incubated for 45 minutes at room temperature in the dark on a slow oscillating rocker.

Secondary antibodies were removed and membranes washed 3x5 minutes in 0.1% PBS- or TBS-Tween20 followed by 3x 5 minutes in PBS or TBS. Membranes were then transferred to an oven to dry.

2.5.6 Detection and Analysis with Licor Odyssey

Membranes were scanned on the Licor Odyssey scanner using the 700 and 800 nm channels. Licor Image Studio software was used to quantify protein expression by detecting the intensity of fluorescent bands. Background was subtracted from signal values then protein of interest values were divided by the corresponding β-actin signal to determine relative protein expression.

2.6 Immunocytochemistry

2.6.1 Cytospin Preparation of Cells on slides

Cells were cultured and treated as appropriate then trypsinised, centrifuged and resuspended in complete DMEM. Cells were diluted to 1,000,000 cells/mL complete DMEM and 75 μL added to each slide assembled in a chamber cassette. Slides were spun at 72.26 g for 5 minutes then cassettes removed and cells fixed in 4% paraformaldehyde (PFA) in 0.1 % PBS-Tween20 for 20 minutes at room temperature. Slides were then washed 3x5 minutes in PBS before being stored in fresh PBS at 4^{o}C until use.

2.6.2 Cleaning and sterilisation of cover slips

Glass cover slips (22x22 mm) were placed in a beaker of 2M NaOH for 2 hours at room temperature, with occasional stirring, then removed and rinsed thoroughly with dH_2O before being dipped in 100% EtOH and dried. Once dry, cover slips were autoclaved.

2.6.3 Poly-l-lysine coating of cover slips

Clean 22x22 mm sterile glass cover slips were placed in a Petri dish and covered with 0.01% Poly-l-lysine (Sigma). Dishes were covered and placed in a 37^{o}C incubator for 5 minutes before removing cover slips and leaving to dry on racks.

2.6.4 Poly-d-lysine coating of cover slips

Poly-d-lysine (5 mg) was diluted in 50 mL sterile cell culture-grade dH_2O to produce a stock concentration of 0.1 mg/mL then stored in aliquots at -20^{o}C between uses. This stock was diluted 1:2 in sterile cell culture-grade dH_2O immediately prior to

use, producing a working concentration of 50 μg/mL. Clean sterile cover slips were rinsed 2x in sterile dH_2O then distributed to 6-well plates. Poly-d-lysine (400 μL) was added to each well and swirled to ensure adequate coating of cover slips before being incubated for 1 hour at 37^{o}C. Poly-d-lysine was then aspirated and cover-slips rinsed 2x in sterile dH_2O. Cell suspension was added immediately.

2.6.5 Culturing and treating cells on cover slips

Cells were trypsinised and counted before being diluted to the appropriate cell density in complete media. Cell suspension (4 mL) was added to each cover slip-containing well of 6 well plates.

2.6.6 Fixation of cells on cover slips

Formaldehyde

Methanol-free Formaldehyde, 16%, (Fisher Scientific) was diluted 1:4 in PBS. Media was aspirated from cover slips and replaced with 500 μL 4 % formaldehyde and cells left to fix for 20 minutes before being rinsed 3x 5 minutes in PBS. Fixed cells on cover slips were then stored in fresh PBS at 4 ^{o}C for no longer than 4 weeks if not being used immediately.

Paraformaldehyde

Paraformaldehyde (16%) in PBS was prepared and frozen in aliquots. This was diluted 1:4 in PBS immediately prior to use then used in the same way as described for 4% formaldehyde. Fixed cells on cover slips were then stored in fresh PBS at 4 ^{o}C for no longer than 4 weeks if not being used immediately.

2.6.7 Immunofluorescence

Cells were permeabilised for 10 minutes in 0.1 % Triton-X-100 (Sigma Aldrich) in PBS at room temperature then washed 3x 5 minutes in PBS. Aldehyde sites were blocked with 0.1M glycine for 5 minutes then washed 3x5 minutes in PBS. Non-specific binding sites were blocked in 10 % goat serum (Sigma Aldrich) in PBS for 10 minutes at room temperature.

Primary antibodies were prepared according to Table 2.2. Parafilm was stretched over a Petri dish and 50 μL primary antibody cocktail added as drops per cover slip. Excess fluid was drained from the corner of each cover slip before being placed cell-side down on antibody droplets and incubated for 1 hour at room temperature. Cover slips were then washed 3x5 minutes in PBS.

Secondary antibodies were prepared according to Table 2.2. The same procedure was followed as for primary antibodies described above with the exceptions that secondary antibodies were incubated in the dark for 45 minutes. From this point on, cells were kept in the dark to avoid any photo bleaching. Cover slips were washed 3x 5 minutes in 0.1 % PBS-Tween20. Hoescht 33342 (Invitrogen) was diluted 1:10,000 in PBS and incubated on cover slips to stain nuclei for 10 minutes at room temperature. This was followed by 3x5 minutes washes in 0.1 % PBS-Tween20, 5 minutes washing in PBS then 2x rinses in dH_2O. Cover slips were then dried and mounted to slides using Prolong Gold antifade mountant (Invitrogen). Slides were stored in the dark until image acquisition using a Leica DM5500 fluorescence microscope. Exposure times were kept constant for each comparative study.

2.6.8 Immunocytochemistry linked with a DAB-Chromogen system

Permeabilisation and blocking of aldehyde sites was the same as described previously.

Non-specific binding sites in cells were blocked in 2 steps. First, slides were incubated

in 3% H_2O_2 for 5 minutes at room temperature in a humidified container. Slides were then washed in 0.1% PBS-Tween20 for 5 minutes. Next, serum-free protein block (Dako X0909) was applied to slides and incubated for 10 minutes. Primary antibody cocktail (100 μL, as described in table 2.2) was applied per slide and incubated for 1 hour at room temperature in a humidified container. Slides were then washed 2x5 minutes in 01.% PBS-Tween20. Anti-rabbit HRP labelled polymer (Dako K4003) was applied to slides and incubated for 30 minutes at room temperature in a humidified container. Slides were then washed 2x5 minutes in 0.1% PBS-Tween20.

DAB+Chromogen substrate (Dako), 1:50, was applied to slides for 10 minutes, followed by rinsing in tap water. Slides were then soaked in haematoxylin for 15 seconds followed by a further tap water rinse. Slides were then placed in Scots Tapwater until blue colour was observed. Slides were allowed to air dry in the dark then coverslips applied using DPX.

2.7 Transmission Electron Microscopy

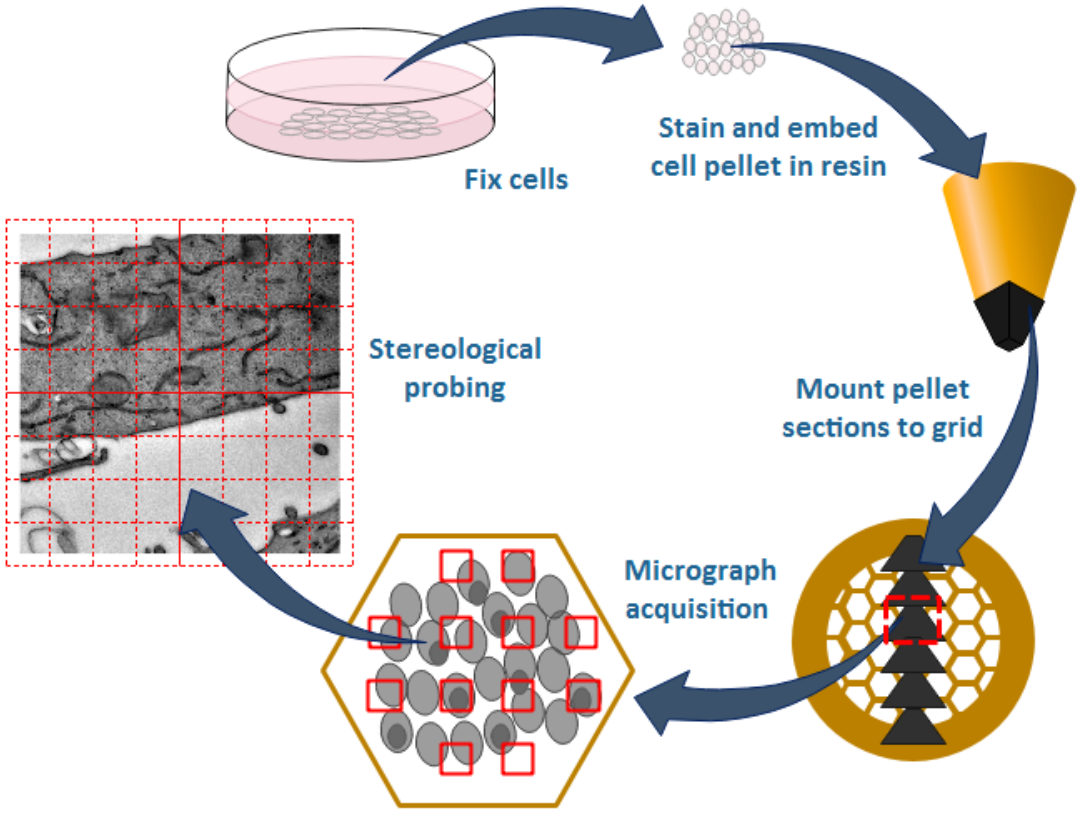

Figure 2.1: Transmission Electron Microscopy Workflow: Cell culture, fixation and preparation of sample for mounting and image acquisition, followed by analysis.

Throughout the entire workflow for Transmission Electron Microscopy (TEM), systematic uniform randomised sampling (SUR) was employed to ensure unbiased stereological estimation of parameters, i.e. every part of the sample has an equal chance of being counted in the final analyses (Howard, C.V., and Reed, M.G., 1998).

2.7.1 Culture, Treatment and Fixation of Cells

Cells were trypsinised, diluted in complete DMEM and seeded in 10 cm petri dishes at the following densities:

HCT116 1x10^5 cells/mL

SW480 1.5x10^5 cells/mL

Cells were allowed to grow for 24 hours then treated as desired with drugs diluted in complete DMEM.

Following appropriate treatment times, media was aspirated from dishes and 10 mL 0.5% glutaraldehyde in 0.2M piperazine-N, N'-bis (PIPES) was added to each dish and left to fix cells for 1 minute. Fixative (9 mL) was removed from each dish and cells scraped and transferred to 1.5 mL tubes. Tubes were centrifuged at 21.1 g for 25 minutes at room temperature before being stored at 4^oC until use.

2.7.2 Osmium Tetroxide Staining

Prior to osmium tetroxide staining, pellets were cut with a sterile scalpel to 1 mm^3 pieces to ensure full and even infiltration of stain and resin.

At this stage, samples were sent to the Electron Microscopy Suite of the Western General Hospital in Edinburgh and kindly processed by Ms Fiona Young as follows:

1. Wash in 0.2M cacodylate buffer 15 minutes
2. Fix in 1% osmium tetroxide 30 minutes
3. Wash in 0.2M cacodylate buffer 10 minutes
4. Dehydrate in 10% alcohol 5 minutes x 3
5. Dehydrate in absolute alcohol 20 minutes x 3
6. Propylene oxide 10 minutes x 2
7. Embed in TAAB resin

2.7.3 Pioloform coating of Grids

Pioloform in chloroform (Agar Scientific) was warmed to room temperature on a magnetic stirrer for 15 minutes prior to use. A clean glass slide was placed inside a flow-through vessel held by a clamp stand and, with the tap closed, pioloform poured to just below the top of the slide. The tap was then opened, slide removed with forceps and held to air dry. Using a fresh razor blade, the slide was scored along the edges on both sides. The slide was breathed on lightly before being placed vertically into a bowl of water, allowing the plastic to peel off the slide and float on the surface. Using forceps, 150 hex-mesh grids were placed shiny side up onto the pioloform with even spacing. Fresh parafilm was gently placed on top then lifted out (grids and pioloform attached) and left to air dry. Grids were stored at 4^{o}C until use.

2.7.4 Sectioning of Samples

Samples were sectioned using an ultramicrotome with a diamond blade to a thickness of 90 nm. Prepared hex-mesh grids were placed under the sample ribbon in milliQ water and lifted out carefully then placed on filter paper to dry.

2.7.5 Lead Citrate Staining

Grids with samples were placed, sample-side down, on a droplet of lead citrate for 5 minutes then dipped 20x in each of 3 glass vials of milli-Q water before being placed on filter paper to dry.

2.7.6 Micrograph Acquisition and Quantification

Micrographs were taken on the Jeol 1200EX Electron Microscope using an 80, 000 V electron beam. SUR sampling was employed throughout with micrographs being

captured every quarter turn where sample was present, starting at the top left corner of a randomly-selected hexagon of the hex-mesh grid. 30 micrographs were acquired for each sample.

2.7.7 Organelle Identification

Organelles and their presentation in TEM were studied extensively prior to measurements. Key features of organelles were identified (Fawcett, D., 1981). Rough endoplasmic reticulum in particular was distinguished by the presence of ribosomes and will henceforth be referred to simply as ER.

2.7.8 Unbiased Stereology: Three-Dimensional Measurement from Micrographs

Accuracy vs. Precision

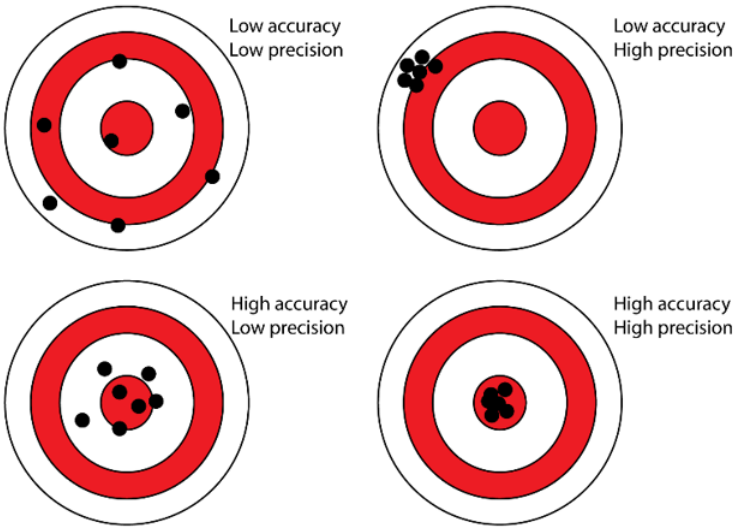

Figure 2.2: Accuracy vs. Precision. Values that are close to the true value are 'accurate'. Values close to each other (small standard deviation) are precise. Self-generated figure.

As depicted in Figure 2.2, accuracy (unbiasedness) and precision (efficiency) are entirely independent of one another. Accuracy refers to experimental values being close to the 'true' value and precision refers to the closeness of a group of values.

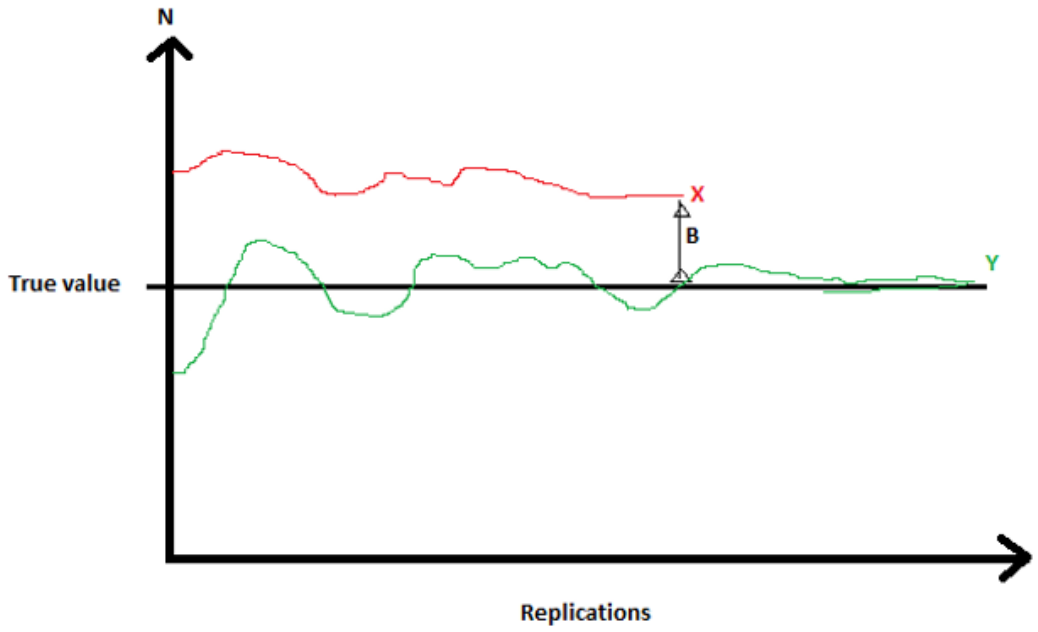

Figure 2.3: As an experiment is replicated, the moving averages of an unbiased and biased estimator of N behave differently. As replications increase, the average will reach a steady value. A biased estimator, X, may reach a steady state more quickly than an unbiased estimator, Y. However, the value estimated may not be close to the true value. The difference between the average of the biased estimator and the true value is referred to as the degree of bias in the estimator (B). Self-generated figure.

An estimator can be efficient, in that it settles to a stable value very quickly with a very small standard deviation (Figure 2.3), however this may be inaccurate. In this study, the true value is unknown but to achieve measurement estimations with as much accuracy as possible, utilisation of unbiased methods was paramount.

Sources of bias in microscopy can be either sampling or systematic. By employing systematic uniform randomised (SUR) sampling, it is ensured that every part of the sample has an equal chance of being selected to contribute to the final measurement. SUR is applied throughout the entire work flow (as shown in Figure 2.1) from cell culture to micrograph acquisition and analysis. Systematic bias refers to the tools being used to make measurements. For example, using a 100 mL

measuring cylinder that was graduated in litres rather than millilitres would incur a 1 million-fold systematic bias. To reduce systematic bias, it is essential that the correct measurement tools are used and that these are properly calibrated. As described in Figure 2.3, the degree of bias in the estimator is not calculable as the true value is unknown. However, by employing SUR and the appropriate measurement tools one can be confident that the estimations of values are as close to the true value as possible.

Stereology

Stereology allows quantitative estimates about the geometrical features of a 3-dimensional object to be made by applying a 2-dimensional geometric probe, in this case a grid, to thin sections of a sample. For stereology to yield accurate measurements, it requires sampling to be unbiased and random (Howard, C.V., and Reed, M.G., 1998).

Estimation of Volume Density (Vv)

Volume density (Vv), also known as volume fraction, is defined as the volume proportion of one phase within a reference volume. Estimation of volume density using a stereological method was first proposed by the French geologist Delesse in 1847. Delesse showed that, on polished rock sections, the areal fraction of a phase of interest was an excellent predictor of volume fraction of the phase of interest in the whole rock, denoted in the following equation:

Vv=Aa

(Volume density is equal to area density)

Glagolev, A.A., (1933), as cited by Cruz-Orive, L.M., (1997), further developed this stereological method by using points as a probe to estimate volume. By placing a grid of fixed points over a cross-section of sample, it is possible to count the points intersecting with the phase of interest (eg. ER) and with the reference space (in

this case the cytoplasm). The sum of these counts on multiple micrographs of the section can then be used to estimate the area fraction of the phase of interest as a surrogate of volume fraction. Therefore, Vv can be defined by the following formula:

Vv (Y, ref) = Sum of points on Y/Sum of points on ref space

Volume density of the phase of interest, Y, in the reference space is equal to the sum of points falling on Y per sum of points falling on the reference space.

Overprojection

Overprojection occurs when a section is too thick, causing the projected image to show a phase of interest larger than the true area of that cross-section due to opaqueness and the phase of interest being darker. This then results in a systematic overestimate of volume fraction. This can be avoided by using the thinnest sections possible.

Estimation of Surface Density (Sv)

Surface density is a valuable measurement in the assessment of surface-limited processes and is defined as the surface area of interface per unit volume of the reference space. Surface density estimation requires linear test probes such as lines. The number of intersections of the test probes (lines) with the surface of the feature of interest increases as the surface area unit per volume of the feature of interest increases, denoted by the following equation:

Sv(Y, ref)= area of interface of Y in ref space/Volume of ref space

Smith, C.S., and Guttman, L., (1953), through a study of geometric probability developed this further. They showed that surface density is equal to twice the number of intersections (I) between the surface and the linear probe, per unit length of test line (l) in the reference space, denoted by the following equation:

Sv= 2Il

This relies on either the object or the probes having isotropy, uniform randomness,

for unbiased estimations. To generate an isotropic direction in 3D, 2 random angles are required. In this study, the nature of the preparation of samples (a cell pellet) ensures random orientation.

Probes and Features

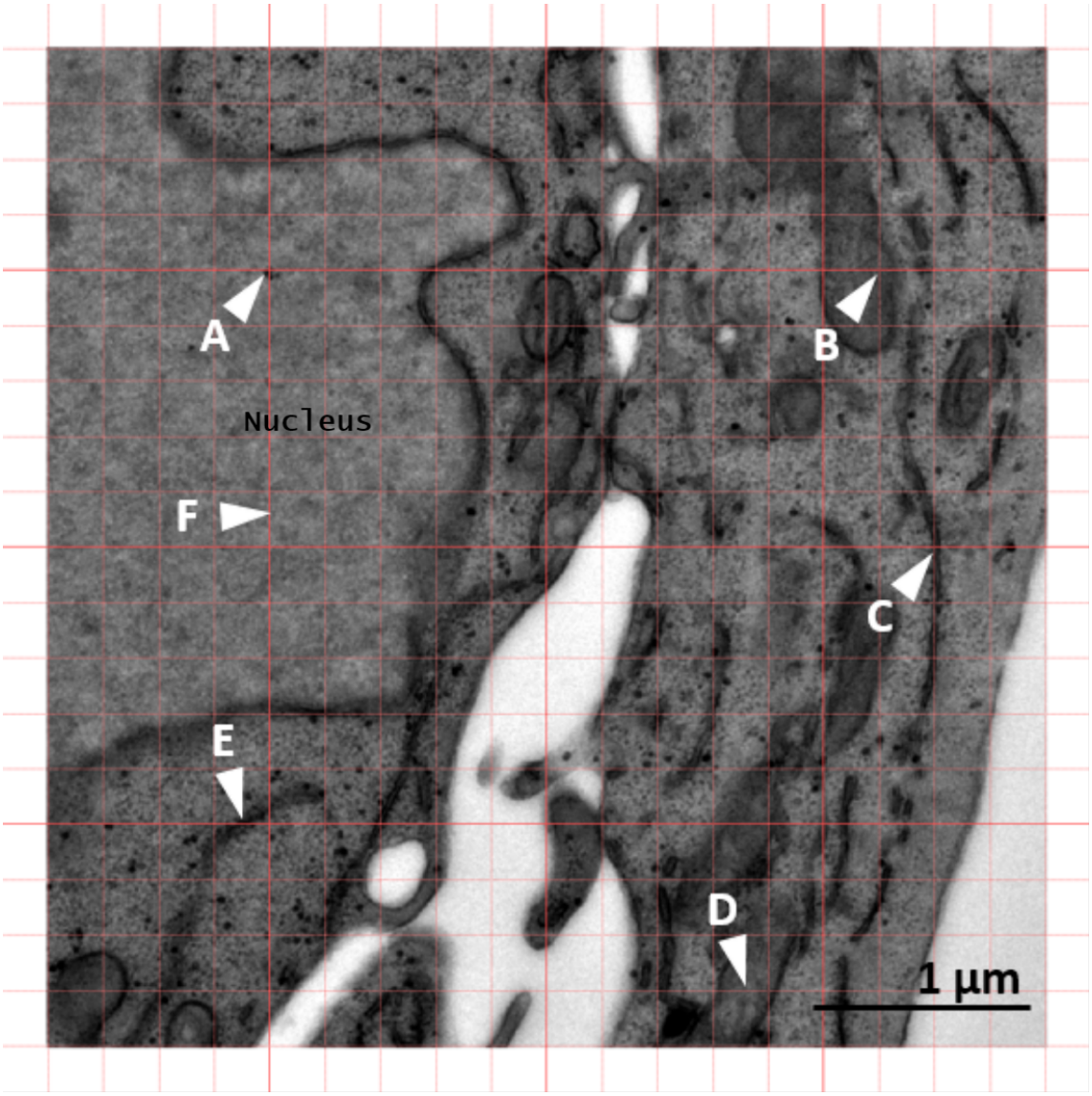

Figure 2.4: Examples of point and line intersections with organelles; A: Nucleus, B: Mitochondrion, C: Endoplasmic Reticulum. Examples of line intersections with organelles; D: Mitochondrion, E: ER, F: Nucleus. Micrograph of HCT116 sample was taken at 3000x magnification.

As in Figure 2.4, point intersections (A, B, C) are defined as the perpendicular crossing of two lines over an organelle. Line intersections are defined as any line

(horizontal or vertical) over an organelle. For membranous structures such as the ER or mitochondria, a single line is counted as '2' because it must pass 2 membranes. In this study the parameters were counted on 30 micrographs per sample as follows:

Cytoplasm points, defined as any points falling on the sample which were not nuclear. For this the 4x4 grid was used and counts multiplied by 25 (each square contains 25 smaller squares).

ER points and lines using the 20x20 grid

Mitochondria points and lines using the 20x20 grid

Contact points and lines, defined as any points or lines intersecting where ER and mitochondria have contact, using the 20x20 grid.

The sums of these counts were then used to estimate volume density of ER in cytoplasm and mitochondria in cytoplasm as well as surface density of ER in cytoplasm, mitochondria in cytoplasm and ER in ER.

2.8 siRNA knockdown of TS

Lyophilised TYMS siRNA (20 nmole, Silencer Select, Ambion) was briefly centrifuged then reconstituted in 400 μL RNase free water to produce a stock concentration of 50 μM. The same was repeated for control (non silencing) siRNA (Quiagen). All reconstituted siRNA was aliquoted and stored at -20^{o}C then brought to room temperature prior to use. Qiagen HiPerfect Transfection reagent (3 μL, lipofectamine-based) was added per 100 μL serum- and antibiotic-free DMEM. Stock siRNA (2 μL of 50 μM stock) was added per 98 μL HiPerfect in DMEM to achieve a siRNA concentration of 1 μM. These were incubated at room temperature for 10 minutes to allow complexes to form. This transfection mix was then added drop-wise to freshly seeded cells to achieve a final concentration of 10 nM, and dishes gently swirled to ensure sufficient mixing. This process was repeated every 24 hours during

all experiments.

2.9 Quantitative reverse transcription polymerase chain reaction (RT-qPCR)

2.9.1 RNA extraction from cells

All RNA work was carried out in a working area that was previously cleaned with RNAse wipes and 70% EtOH. Dishes (60mm) were washed 2x in cold PBS then placed at an angle on ice and excess PBS aspirated. Lysis buffer (300 μL), 1:100 β-mercaptoethanol in Quiagen RLT buffer, was added to all dishes then cells scraped. Cells were left to lyse for 10 minutes then transferred to 1.5 mL tubes and vortexed for 1 minute each. RNA lysates were stored at -20^{o}C until use.

2.9.2 RNA isolation and quantification

Samples were thawed on ice and transferred to spin column tubes. 300 μL 70% EtOH in milliQ dH_2O was added to each sample then centrifuged at 10 g for 15 seconds and flow-through discarded. RW1 wash buffer, 700 μL, (Qiagen) was added to each sample and centrifuged at 10 g for 15 seconds and flow-through discarded. RPE buffer, 500 μL, (EtOH added, Qiagen) was added to each sample, centrifuged for 2 minutes at 10 g and flow-through discarded. Collection tubes were replaced with fresh ones and samples centrifuged for 1 minute at 21.1 g then flow-through discarded. Columns were placed in 1.5 mL tubes and 30 μL RNase-free dH_2O added to the centre of each tube and samples centrifuged at 10 g for 1 minute before being placed on ice.

Nucleic acid concentration was measured using Nanodrop and volumes containing 1 μg RNA were determined for each sample and made up to a total of 12 μL with

RNase free dH_2O in 0.6 mL tubes. gDNA wipeout buffer, 2 μL,(Qiagen) was added to each tube to make a total volume of 14 μL (mix 2) and placed on ice.

2.9.3 Reverse Transcription

Mix 3 was prepared in 0.2 mL tubes as described in Table 2.9.

Component	**Volume/reaction (μL)**
Quantitect Reverse Transcription	1
Quantitect RT Buffer 5x	4
RT Primer Mix	1
Final Volume	**6**

Table 2.9: Reverse Transcription Mix 3. Reagents purchased from Quiagen.

Mix 3 (6 μL per tube) was added to each sample and placed on the heat block at 42 ^{o}C for 15 minutes, then 3 minutes at 95 ^{o}C. Samples were then stored at -20 ^{o}C until use.

2.9.4 SYBR Green qPCR

The reaction components, as detailed in Table 2.10, were mixed thoroughly and appropriate volumes dispensed into PCR tubes. Template cDNA was added last to individual labelled tubes containing the reaction mix.

Component	**Volume/reaction (μL)**	**Final concentration**
2x Rotorgene SYBR Green PCR master mix	12.5	1x
Quantitect primer assay	2.5	1x
Template cDNA (added last)	1	50 ng/reaction
RNase-free dH_2O	9	——
Total reaction volume	25	——

Table 2.10: SYBR Green PCR reaction components. Reagents purchased from Quiagen.

Samples were prepared and run in triplicate using the RotorGene qPCR machine with cycling conditions as described in Table 2.11

Step	**Time**	**Temperature (^{o}C)**
PCR Initial Activation Step	5min	95
Two Step Cycling		
Denaturation	5s	95
Combined Annealing/Extension	10s	60
Number of cycles	40	

Table 2.11: Cycling Conditions

2.9.5 Analysis of qPCR

Cycle Threshold (C_t) values were used to determine fold change in target nucleic acid relative to the untreated control using the formula: fold change = $2^{-\Delta\Delta Ct}$. The difference in C_t values for the gene being tested in experimental samples (TE) and the housekeeping gene in in experimental samples (HE) was calculated as well as between the gene being tested in control samples (TC) and the housekeeping gene in control samples (HC).

TE-HE= ΔCTE

TC-HC= ΔCTC

The difference between ΔCTE and ΔCTC is then calculated to provide the $\Delta\Delta$Ct value. All values are in logarithm base 2, i.e. every time there is twice as much DNA, C_t values decrease by 1. Therefore expression fold change = $2^{-\Delta\Delta Ct}$

In this study the housekeeping gene used was GAPDH and the gene tested was CHOP.

2.9.6 Enzyme-Linked Immunosorbent Assay: ELISA

The Invitrogen Human PD-L1 ELISA kit was used according to the manufacturer instructions.

Preparation of Reagents

All buffer concentrates were equilibrated to room temperature and diluted immediately prior to the test procedure.

Wash buffer Wash buffer concentrate, 50 mL, (20x) was added to 980 mL dH_2O to produce 1000 mL of 1x wash buffer.

Assay buffer Assay buffer concentrate, 5 mL, (20x) was added to 95 mL dH_2O to produce 100 mL of 1x assay buffer.

Biotin-Conjugate A 1:100 dilution of concentrated biotin-conjugate solution was prepared with assay buffer (1x). Diluted biotin-conjugate was then used within 30 minutes of preparation.

Strepdavidin-HRP A 1:200 dilution of concentrated streptavidin-HRP solution was prepared with assay buffer (1x). Diluted streptavidin-HRP was used within 30 minutes of preparation.

Human PD-L1 Standard Human PD-L1 standard was reconstituted in dH_2O according to the vial instructions and mixed gently to ensure complete and homogeneous solubilisation to a concentration of 600 pg/mL. The standard was allowed to reconstitute for 10-30 minutes prior to use but then used immediately. Serial dilutions of the standard were prepared to achieve reference concentrations ranging from 9.4 pg/mL to 600 pg/mL.

Test protocol

Microwell strips were washed twice in 400 μL wash buffer per well then contents thoroughly aspirated. Empty microwell strips were tapped on absorbent paper to remove any excess wash buffer then used immediately. Standard diluent (100 μL) was added in duplicate to all standard wells then 100 μ of each prepared standard was added to wells in duplicate. Final concentration of standards therefore ranged from 4.7 pg/mL to 300 pg/mL. Sample diluent (100 μL) was added in duplicate to blank wells. Sample diluent (50 μL) was added in duplicate to all sample wells followed by 50 μ of sample (40 μg total protein for whole cell lysates) in duplicate. The plate was covered with adhesive film and incubated at room temperature for 2 hours on a microplate shaker.

Adhesive film was removed and wells aspirated. Microwell strips were then washed 4 times in wash buffer. Diluted biotin-conjugate (100 μL) was added to all wells, including blanks. The plate was covered with adhesive film and incubated at room temperature for 1 hour on a microplate shaker.

Adhesive film was removed and wells aspirated. Microwell strips were then washed 4 times in wash buffer. Diluted streptavidin-HRP (100 μL) was added to all wells, including blanks. The plate was covered with adhesive film and incubated at room temperature for 30 minutes on a microplate shaker.

Adhesive film was removed and wells aspirated. Microwell strips were then washed 4 times in wash buffer. 100 μL TMB substrate solution was added to all wells, including blanks. The microwell strips were incubated at room temperature for 30 minutes, avoiding direct exposure to light. During this time, the colour-development of wells was monitored closely so that the reaction could be stopped before positive wells were no longer properly recordable.

Once the highest standard had developed a dark blue colour, the enzyme reaction was stopped by adding 100 μL of Stop solution to each well in quick succession to ensure uniformity and complete inactivation of the enzyme. The absorbance of wells

was then read immediately at 620 nm on an Optima plate reader.

Calculation of Results

The average of the duplicate blank wells was calculated and subtracted from the absorbance values for all standards and samples. The average absorbances for each set of duplicate standard and sample were calculated. A standard curve was created by plotting the mean absorbance value for each standard concentration against the known human PD-L1 concentration. A 5-parameter best fit curve was applied through the points and PD-L1 concentrations of samples extrapolated by substituting the mean absorbance values into the equation of the line. As samples were diluted 1:2, the concentrations read from the standard curve were multiplied by 2.

2.10 Statistics

Unless otherwise stated, 3 biological replicates were undertaken for each experiment, with varying numbers of technical replicates for each biological replicate. Values presented are the mean of replicate values.

Chapter 3

Thymidylate Synthase

3.1 Introduction

TS is a key enzyme in the *de novo* synthesis of dTMP from dUMP, in which 5,10-methylenetetrahydrofolate (CH_2THF) is the methyl donor (Carreras, C.W., and Santi, D.V., 1995). In its active state, TS usually exists as a dimer of two identical subunits of 30-35 kDa each.

As described in Chapter 1, the majority of CRC patients have either innate or acquired resistance to 5-FU-based adjuvant therapy. Amongst the plethora of reported resistance mechanisms associated with 5-FU is TS protein expression, but the literature with regards to TS being a predictive and prognostic biomarker is very mixed. For example, some studies utilising immunohistochemical (IHC) detection or RT-PCR for mRNA detection found that high TS tumour expression is predictive of a patient benefiting from 5FU-based adjuvant therapy (Edler, D., *et al.*, 2002; Inoue, T., *et al.*, 2005). Another study utilising IHC and automated quantitative analysis (AQUA) found that high tumour TS is prognostic of better overall survival in stage II and III patients but was not predictive of benefit from a 5-FU-based therapeutic regimen (Niedzwiecki, D., *et al.*, 2017). Conversely, Johnston, P.G., *et al.* (1995) found that low tumoral TS gene expression was predictive of better

response to 5-FU. TS is a vital component of both cancer cell proliferation and 5-FU-based chemotherapy regimens, but downstream effects of TS inhibition have yet to be fully elucidated.

3.1.1 Aims and Objectives

Due to the vital role of TS in the mechanism of action of 5-FU and NUC-3373, its implication in resistance to treatment and the mixed literature on its value as a predictive or prognostic marker, it was decided that initial studies would address this dynamic protein. Firstly, cell line profiles in response to NUC-3373 should be investigated and cell lines for future studies selected. This chapter will then assess the value of TS protein expression as a predictive biomarker in an *in vitro* setting as well as the dynamics of TS and TS complexes by utilising time-course studies. To date, there have been very few studies of TS cellular localisation so this too will be investigated in the hope that this could be informative of the downstream effects of inhibiting TS protein expression through interaction with the active metabolite of both 5-FU and NUC-3373; FdUMP.

3.2 Results

Initial studies sought to establish appropriate CRC cell lines in which to further study the action of NUC-3373. A panel of nine CRC cell lines were selected based on their IC_{50}s to 5-FU from previous chemosensitivity studies by Dr R. Briffa during her PhD studies at the University of Edinburgh. The panel included cell lines with a wide variation of sensitivities to 5-FU, varied MMR status and TP53 mutation types. Initial experiments conducted were to optimise the starting cell densities for use with the intended assays. These experiments determined the seeding densities for all future experiments (see Appendices).

3.2.1 Characterisation of cell line sensitivity to NUC-3373

Nine adherent CRC cell lines were selected and their sensitivity to NUC-3373 and 5-FU (not shown) under normoxic and hypoxic conditions assessed. Cell survival was assessed using both SRB assay and Celigo cell confluence scans.

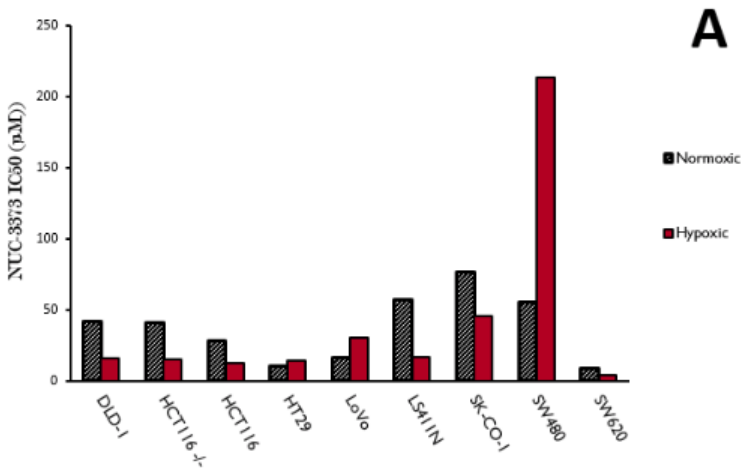

NORMOXIC									
Cell Line	DLD-1	HCT116 -/-	HCT116	HT29	LoVo	LS411N	SK-CO-1	SW480	SW620
IC50 (μM)	41.98	41.46	28.58	10.98	16.57	57.5	76.44	55.59	9.062

HYPOXIC									
Cell Line	DLD-1	HCT116 -/-	HCT116	HT29	LoVo	LS411N	SK-CO-1	SW480	SW620
IC50 (μM)	16.11	15.52	12.49	14.36	30.14	16.85	45.97	213.5	4.063

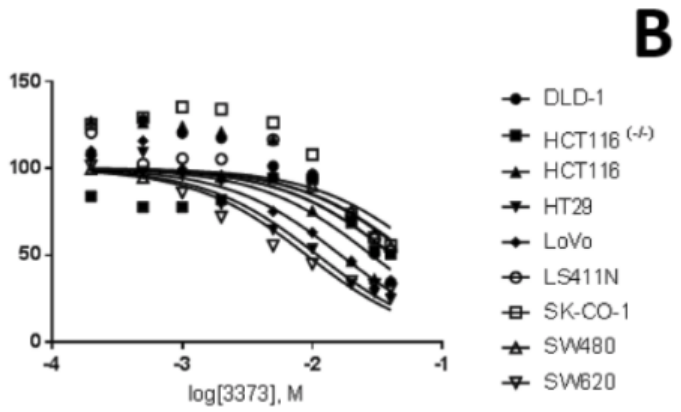

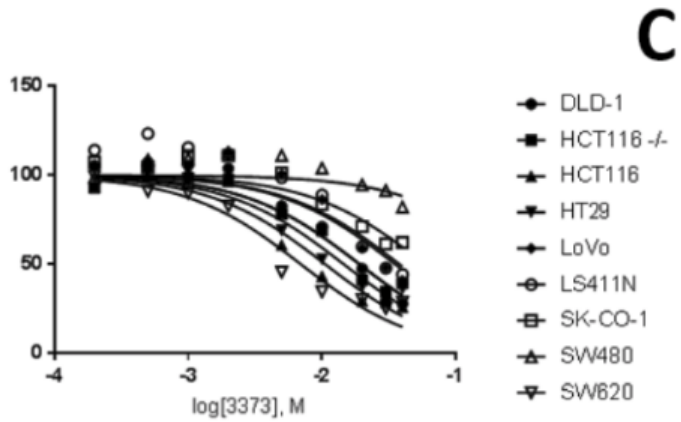

Figure 3.1: Sensitivity of a panel of 9 CRC cell lines to NUC-3373. A: IC_{50} concentrations (μM) for NUC-3373 under normoxic and hypoxic conditions. B: Log-dose response curve for NUC-3373 under normoxia. C: Log dose response curve for NUC-3373 under hypoxia (0.5% O_2. $N_{biological}$=3, 6 technical replicates for each biological.

As detailed in Figure 3.1, IC_{50}s for NUC-3373 in the panel of nine CRC cell lines under normoxic conditions ranged from 9.062 μM to 76.44 μM, whilst those subjected to hypoxia ranged from 4.063 μM to 213.5 μM. Interestingly, only three of the cell lines were more resistant to NUC-3373 treatment under hypoxic conditions. MMR status of cell lines did not appear to have any bearing on sensitivity to NUC-3373. It was decided that two cell lines should be selected for further study- one less sensitive (SW480) and one more sensitive (HCT116).

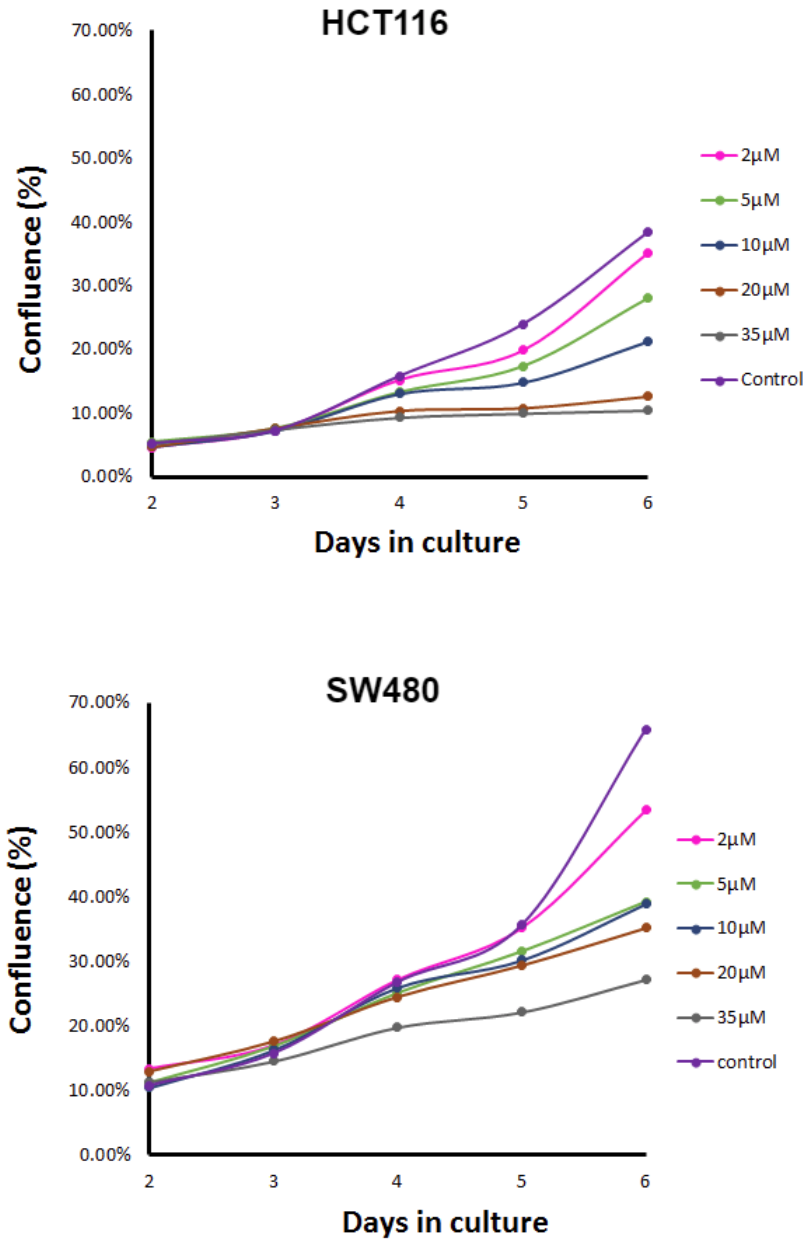

Figure 3.2: Effect of NUC-3373 on the growth of HCT116 and SW480 cells. Treatment concentrations range from 2-35 μM. Growth was measured as cell confluence over 4 days. Cells were seeded on day 0 and drug added on day 2, then washed out on day 3, followed by 72 hours growth in culture medium). $N_{biological}$=3, 6 technical replicates for each biological.

In HCT116 cells, inhibition of growth was not observed until 24 hours post-drug removal. This was also the case for SW480 cells, but with only the top concentration of 35 μM having a minor inhibitory effect at this early time point. Although NUC-3373 caused a net inhibition of growth in both cell lines, growth of SW480

cells was much less susceptible to inhibition than that of HCT116 cells, requiring much higher concentration of drug to produce a noticeable difference.

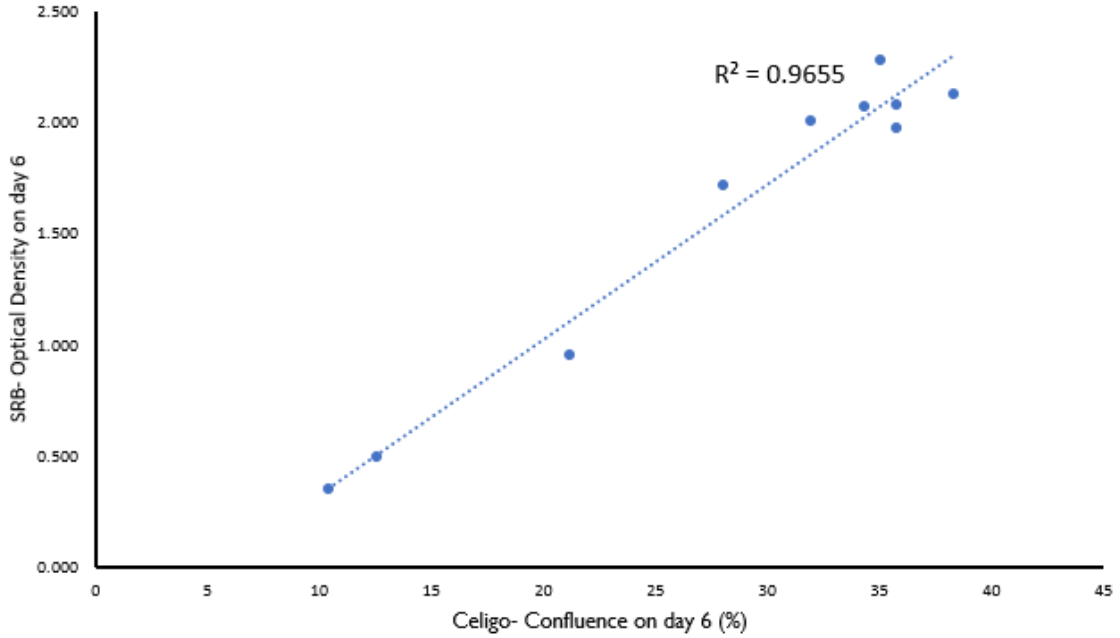

Figure 3.3: Relationship between Celigo cell confluence (%) and optical density derived from SRB colorimetric assay in HCT116 cells treated with various concentrations of NUC-3373.

The survival of HCT116 cells treated with a range of concentrations of NUC-3373 was assessed by both SRB assay (optical density) and by Celigo cell confluence (%). When these two sets of values were plotted against each other as in Figure 3.3 they were found to have a strong linear relationship indicating that data achieved from both assays were reliable.

3.2.2 Thymidine Rescue

Cells were treated with a range of NUC-3373 concentrations plus or minus 8 μg/mL thymidine to assess whether cells could be rescued from a thymine-depleted death. Cell survival was assessed using SRB assay.

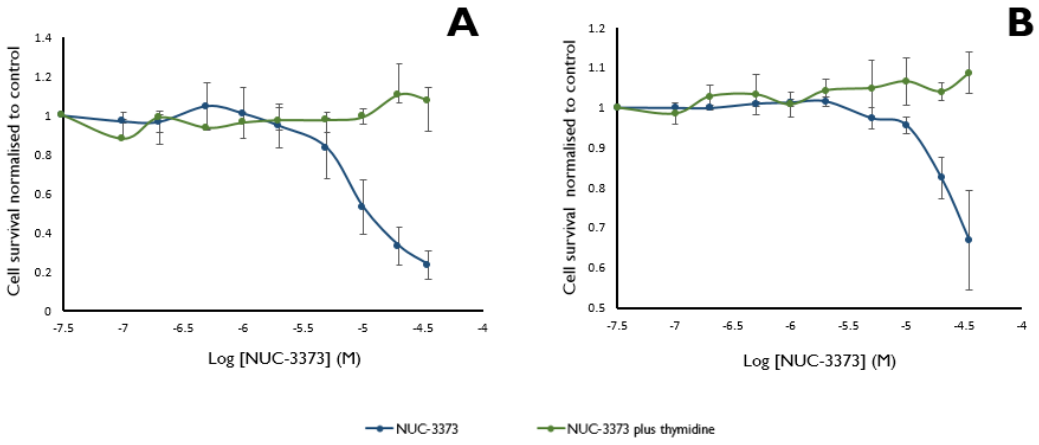

Figure 3.4: The effect of 8 μg/mL Thymidine supplementation on NUC-3373-induced cell death, measured by SRB assay. A: HCT116, B: SW480. $N_{biological}$=3, 6 technical replicates for each biological. Error bars are plotted as plus and minus the standard deviation of 3 biological replicate means.

Thymidine rescued both HCT116 and SW480 cells from NUC-3373-induced death in all treatment concentrations (Figure 3.4).

3.2.3 TS expression and sensitivity to NUC-3373

To explore the role of TS protein as a predictive biomarker for NUC-3373 treatment, TS protein expression was measured in whole cell lysates from the panel of 9 CRC cell lines by Western blot and assessed against each IC_{50} for NUC-3373 as detected by SRB assay.

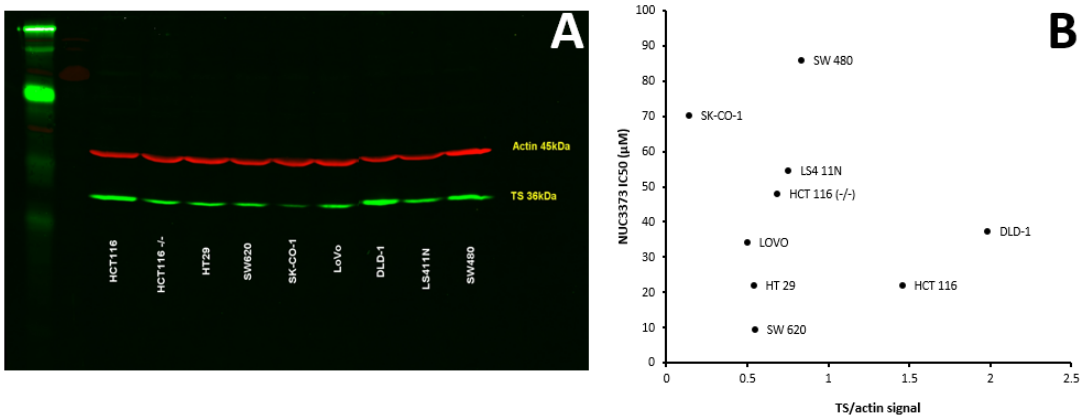

Figure 3.5: Endogenous TS expression vs. sensitivity to NUC-3373 in a panel of 9 CRC cell lines. A: Representative Western blot of TS protein expression (36 kDa), with β-actin (45 kDa) as loading control, in whole cell lysates. B: TS expression (as TS signal/actin signal) vs. NUC-3373 IC_{50} (μM).

TS protein expression varied greatly amongst the 9 cell lines studied, with SK-CO-1 having lowest expression and DLD-1 having the highest. When plotted against their individual IC_{50}s for NUC-3373, no correlation between TS protein expression and sensitivity was found, indicated by the wide scatter of points with no linear relationship.

3.2.4 Dynamics of TS in response to 5-FU and NUC-3373 treatment

Due to no correlation being found between basal TS protein expression and sensitivity to NUC-3373 in cell lines, it was decided that the dynamics of TS and TS ternary complex expression should be explored in response to NUC-3373 and 5-FU treatment, with the hypothesis that sensitivity to NUC-3373 may be determined by the ability to inhibit TS. Cells were treated with 5-FU and NUC-3373 for 6, 12, 24, 48 and 72 hours. Whole cell protein lysates were harvested and Western blot used to assess TS and TS ternary complex protein expression. The antibody used, Abcam 108995, detects both free and ternary complex TS, with lower bands corresponding to free TS and upper bands to ternary complex TS. As can be seen in Figures 3.6 and 3.7, the antibody to TS was highly specific with no additional

unexpected bands observed. Values for total TS protein expression are the sum of the signal detected of both upper and lower TS bands. The average of 3 biological replicates was plotted as a bar with individual replicates plotted as scatter points for full transparency. Although there was significant inter-replicate variability, the expression trend remained similar over the time course.

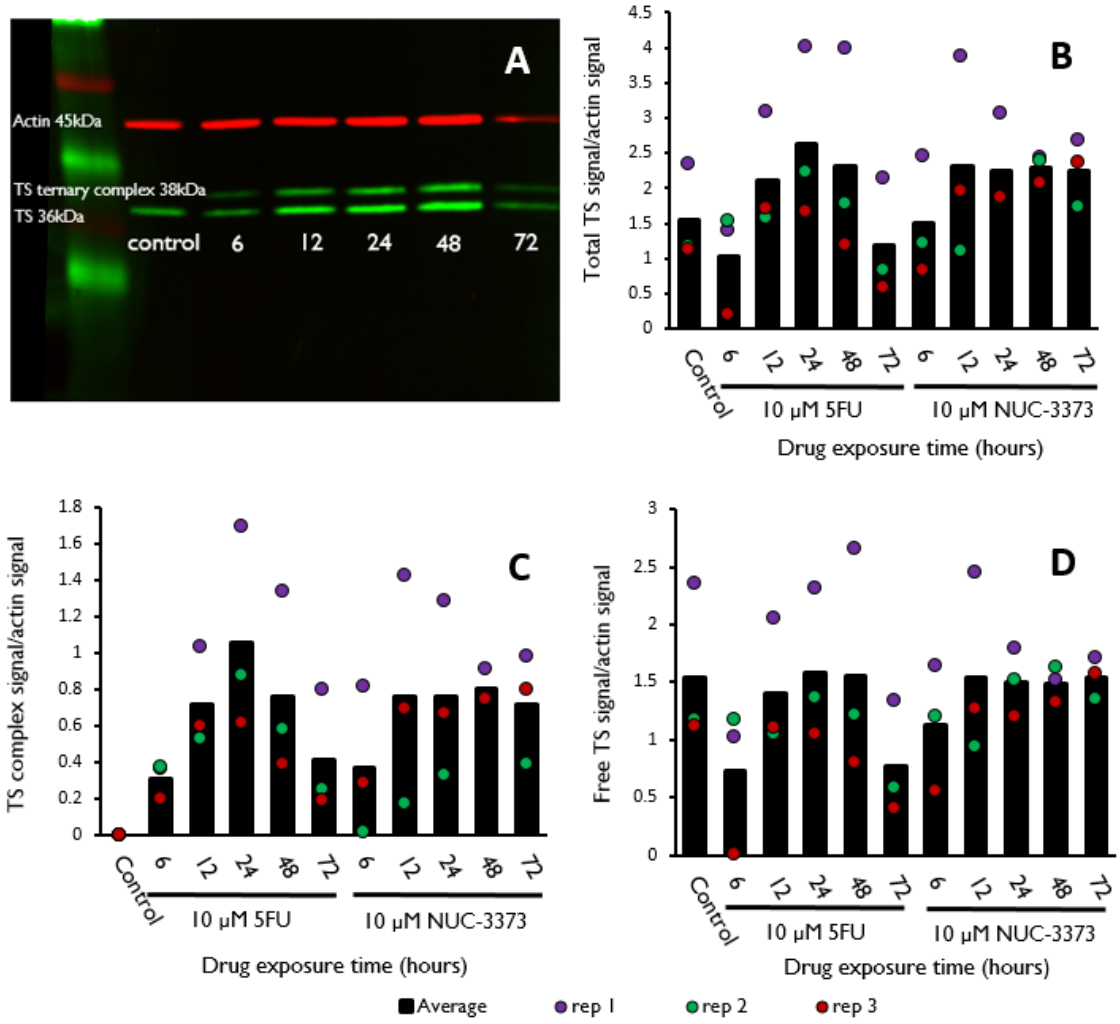

Figure 3.6: TS expression in protein lysates from HCT116 cells treated with either 10 μM 5-FU or 10 μM NUC-3373 for 6, 12, 24, 48 and 72 hours, with control being untreated. A: Representative Western Blot of TS expression. Lower green bands: Free TS (36 kDa), Upper green bands: TS ternary complex ($\sim$38 kDa), Red bands: β-actin (45 kDa) as loading control. B: Total TS expression (Sum of free TS signal and TS ternary complex signal). C: TS ternary complex expression. D: Free TS expression. In B-D quantified protein expression is expressed as signal/actin signal. Values are plotted as the average of 3 biological replicates and each individual replicate is plotted as a scatter point.

In 5-FU-treated HCT116 cells (Figure 3.6, total TS protein decreased after 6 hours then was quickly recovered after 12 hours. Total TS reached a peak after 24 hours,

followed by a decline over the next 48 hours to achieve a signal that was less than that detected in the untreated control. In NUC-3373-treated cells, there was no change in total TS expression at the 6 hour time point but a clear increase after 12 hours which was sustained through to the 72 hour time point. TS ternary complexes (observed at 38 kDa) could be detected after 6 hours of 5-FU and NUC-3373 treatments in HCT116 cells and remained for 72 hours. No upper TS band was detected in the control sample, confirming that the upper band corresponds to TS only when in a ternary complex with FdUMP. Free TS was quantified by detecting the fluorescence intensity of lower TS bands. A decrease in free TS protein expression was observed after 6 hours in both 5-FU- and NUC-3373-treated cells but this was quickly recovered after 12 hours. Under both drug treatments, free TS remained consistent, with the signal detected comparable to that of the control sample for the full 72 hours following treatment, with the exception of 5-FU-treated cells, in which TS expression decreased to approximately 50% of the untreated control. Values were not normalised to the untreated control because for TS ternary complex expression the untreated control was equal to 0.

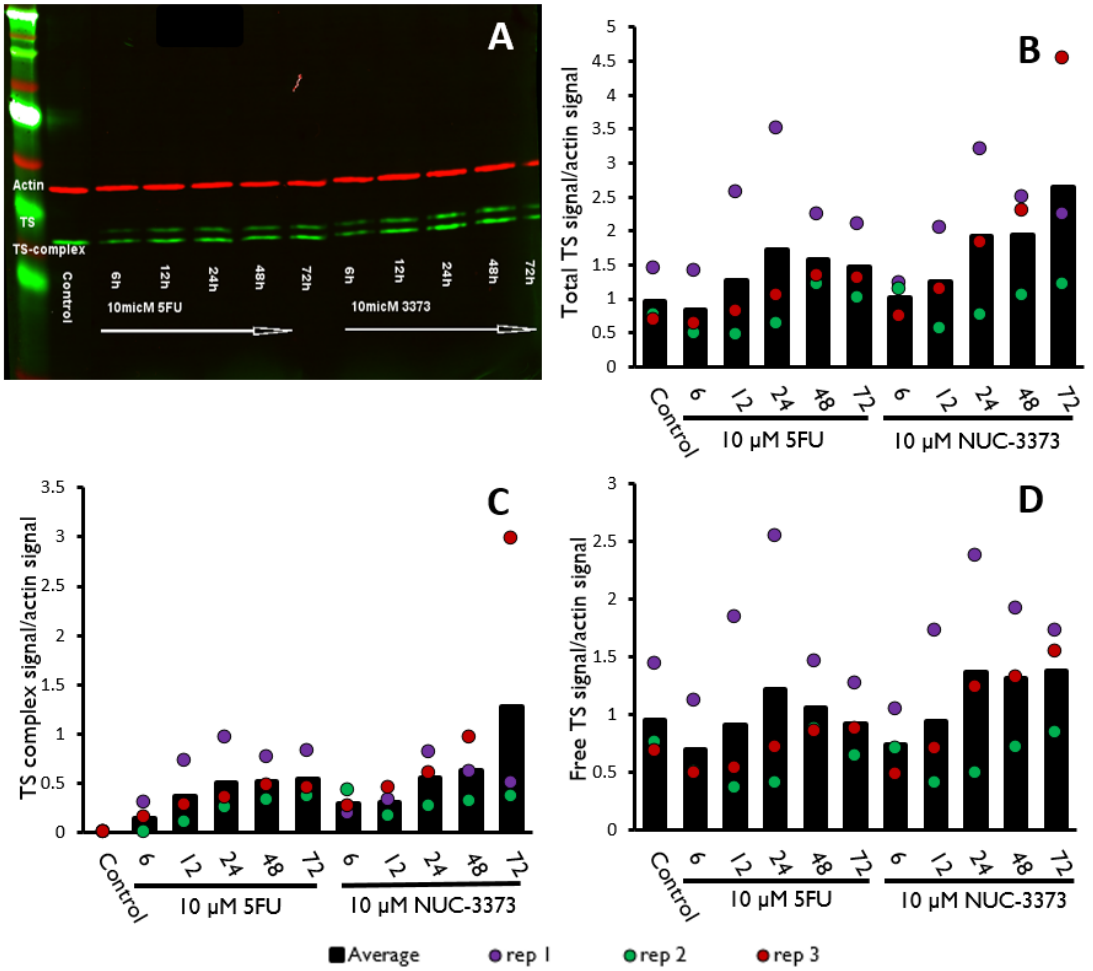

Figure 3.7: TS expression in protein lysates from SW480 cells treated with either 10 μM 5-FU or 10 μM NUC-3373 for 6, 12, 24, 48 and 72 hours, with control being untreated. A: Representative Western Blot of TS expression. Lower green bands: Free TS (36 kDa), Upper green bands: TS ternary complex ($\sim$38 kDa), Red bands: β-actin (45 kDa) as loading control. B: Total TS expression (Sum of free TS signal and TS ternary complex signal). C: TS ternary complex expression. D: Free TS expression. In B-D quantified protein expression is expressed as signal/actin signal. Values are plotted as the average of 3 biological replicates and each individual replicate is plotted as a scatter point.

In SW480 cells treated with 5-FU (Figure 3.7), total TS protein expression increased after 12 hours, reaching a peak at 24 hours at almost double the expression measured in the untreated control. Total TS expression decreased after 48 and 72 hours but still remained higher than that detected in the control sample. A similar pattern was observed in SW480 cells treated with NUC-3373 but TS expression did not decrease after 48 hours, instead there was a marked increase in expression at 72 hours. However, this may be due to the third biological replicate at 72 hours skewing the average. TS ternary complexes were detectable by 6 hours following

both 5-FU and NUC-3373 treatment and continued to increase, reaching a plateau between 24 and 48 hours. In 5-FU-treated SW480 cells, TS ternary complexes remained consistent after 72 hours treatment but in NUC-3373-treated cells there was a considerable increase. As mentioned for total TS levels, this third biological replicate may have distorted the average. Free TS expression, in both 5-FU- and NUC-3373-treated SW480 cells, decreased after 6 hours but was recovered after 12 hours to expression comparable to that of the control. In 5-FU-treated cells, free TS expression continued to rise reaching a peak after 24 hours then fell back to control-level expression by 72 hours. In NUC-3373-treated cells free TS expression was marginally higher than that of 5-FU-treated cells after 24 hours but was consistent for the duration of treatment thereafter.

These data indicate that both 5-FU and NUC-3373 treatment result in the formation of TS ternary complexes from as little as 6 hours, however the time taken for these to form may be shorter and would require an earlier lysis time point to be detected. The complexes formed by NUC-3373 treatment are more sustained than those formed by 5-FU treatment. Interestingly, inhibition of free TS by both drugs is neither long-lasting nor complete, contradictory to their believed mechanism of action.

3.2.5 TS Cellular Localisation

Due to the induction of TS ternary complexes and the finding that free TS expression is recovered quickly following the initial drug insult, the cellular localisation of TS was assessed by ICC and IF (using the same anti-TS antibody).

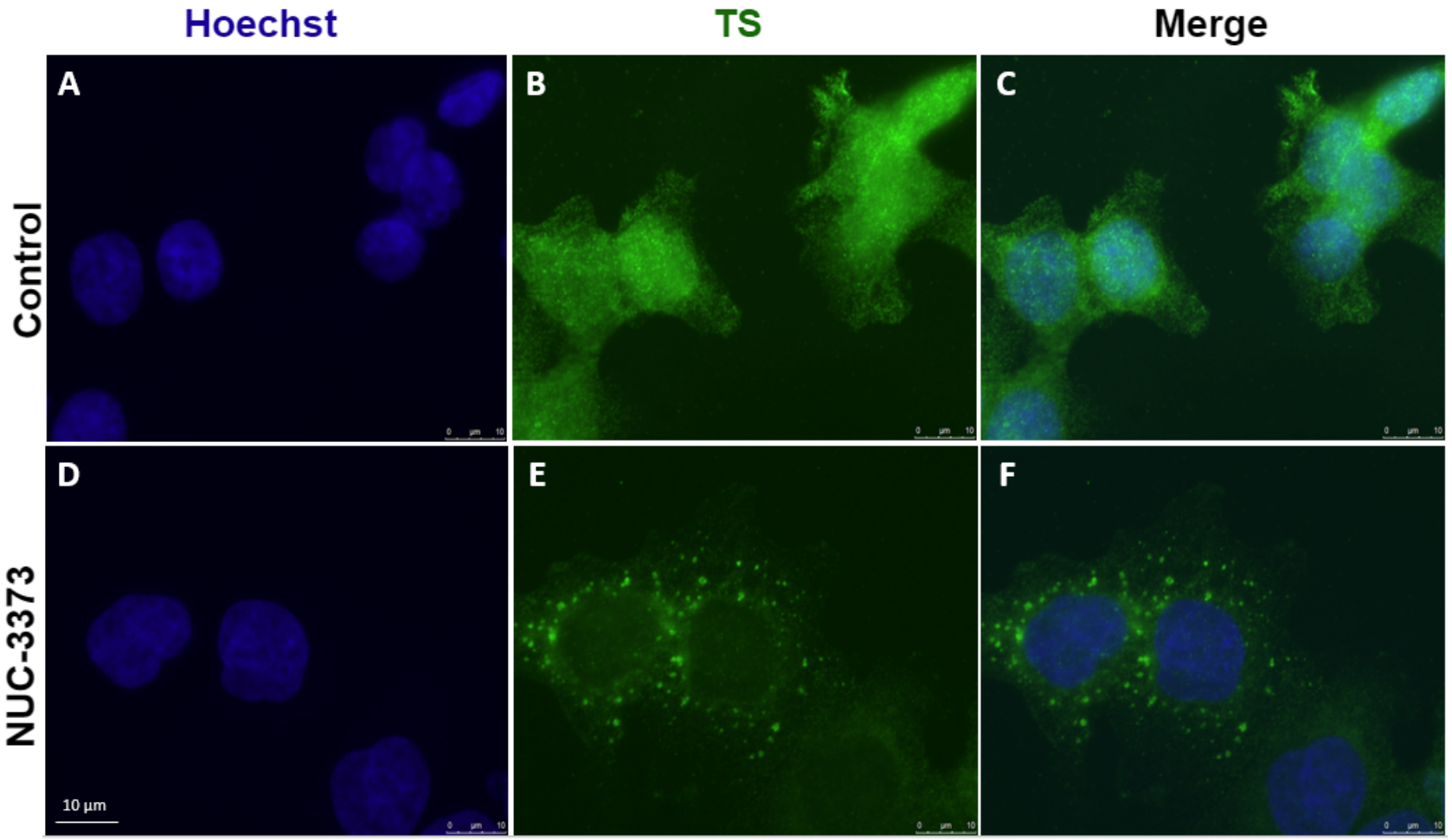

Figure 3.8: The effect of NUC-3373 on TS cellular localisation in HCT116 cells. Representative photomicrograph of cells with punctate cytoplasmic TS expression following NUC-3373 treatment. A-C: untreated HCT116 cells. D-F: HCT116 cells treated with 10 μM NUC-3373 for 24 hours. Blue: Hoechst (nuclear stain), Green: TS, 100x magnification.

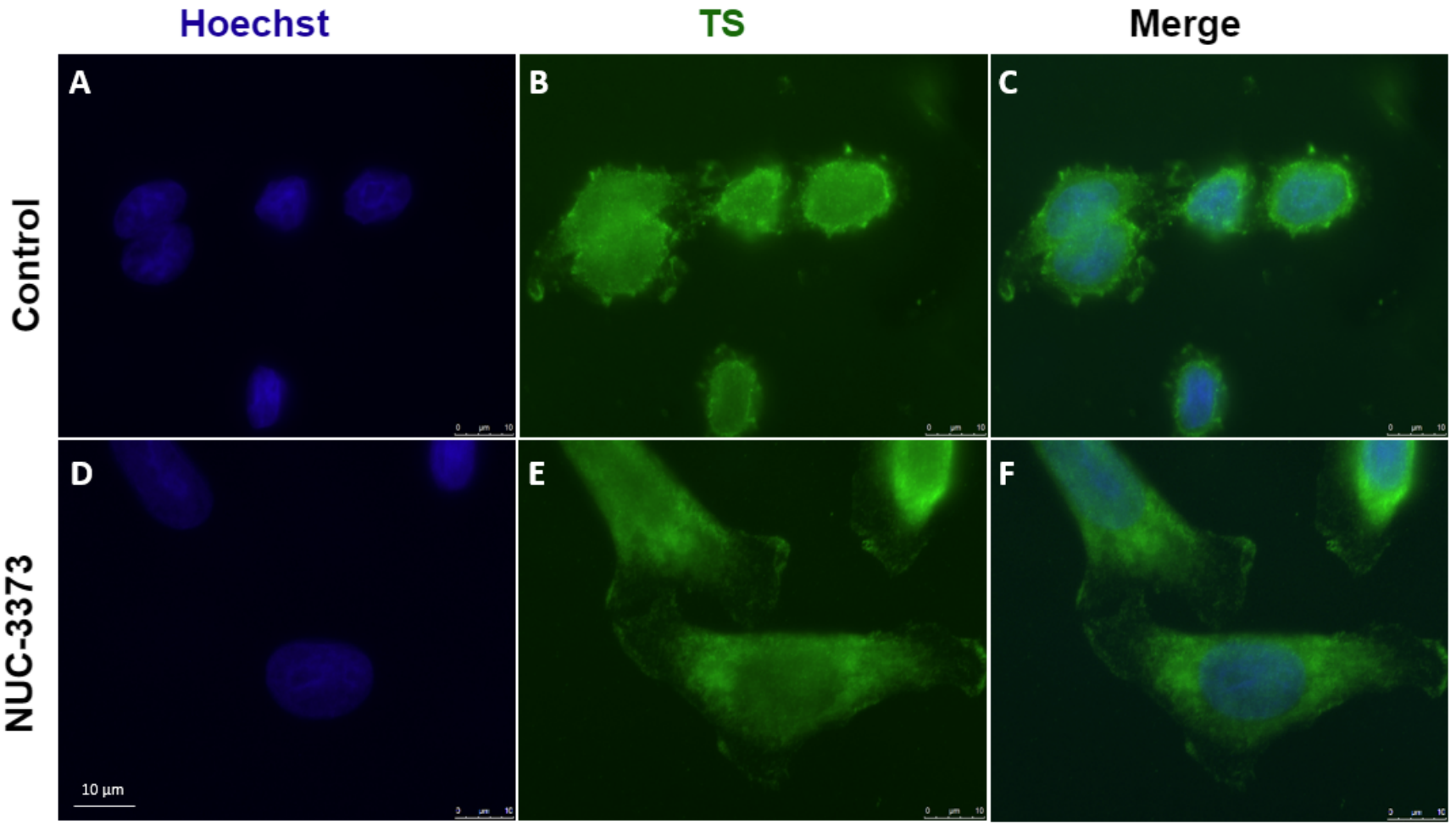

Figure 3.9: The effect of NUC-3373 on TS cellular localisation in SW480 cells. Representative photomicrograph. A-C: untreated SW480 cells. D-F: SW480 cells treated with 10 μM NUC-3373 for 24 hours. Blue: Hoechst (nuclear stain), Green: TS, 100x magnification.

As observed in Figure 3.8, TS expression is predominantly nuclear in untreated HCT116 cells with some diffuse cytoplasmic presence. NUC-3373 treatment resulted in an increased cytoplasmic and decreased nuclear expression of TS. In some cells, this cytoplasmic expression was granular and punctate in nature. The degree of loss of TS from the nuclear compartment was highly varied in this cell line.

Untreated SW480 cells had both nuclear and cytoplasmic expression of TS (Figure 3.9). When treated with NUC-3373, there was some loss of nuclear expression but not as pronounced as that observed in HCT116 cells. NUC-3373 treatment did not result in the punctate cytoplasmic TS expression that was found in some HCT116 cells.

In HCT116 cells especially, there was a high degree of inter-cellular heterogeneity of TS expression therefore it was necessary to assess a larger population of cells in an unbiased manner. Cells were prepared on slides by cytospinning following treatment in order to flatten them and make TS localisation clearer. TS was detected using immunocytochemsitry linked to DAB-chromogen, then slides scanned and 800 cells from each condition (untreated control and NUC-3337) selected for assessment using systematic uniform randomised sampling.

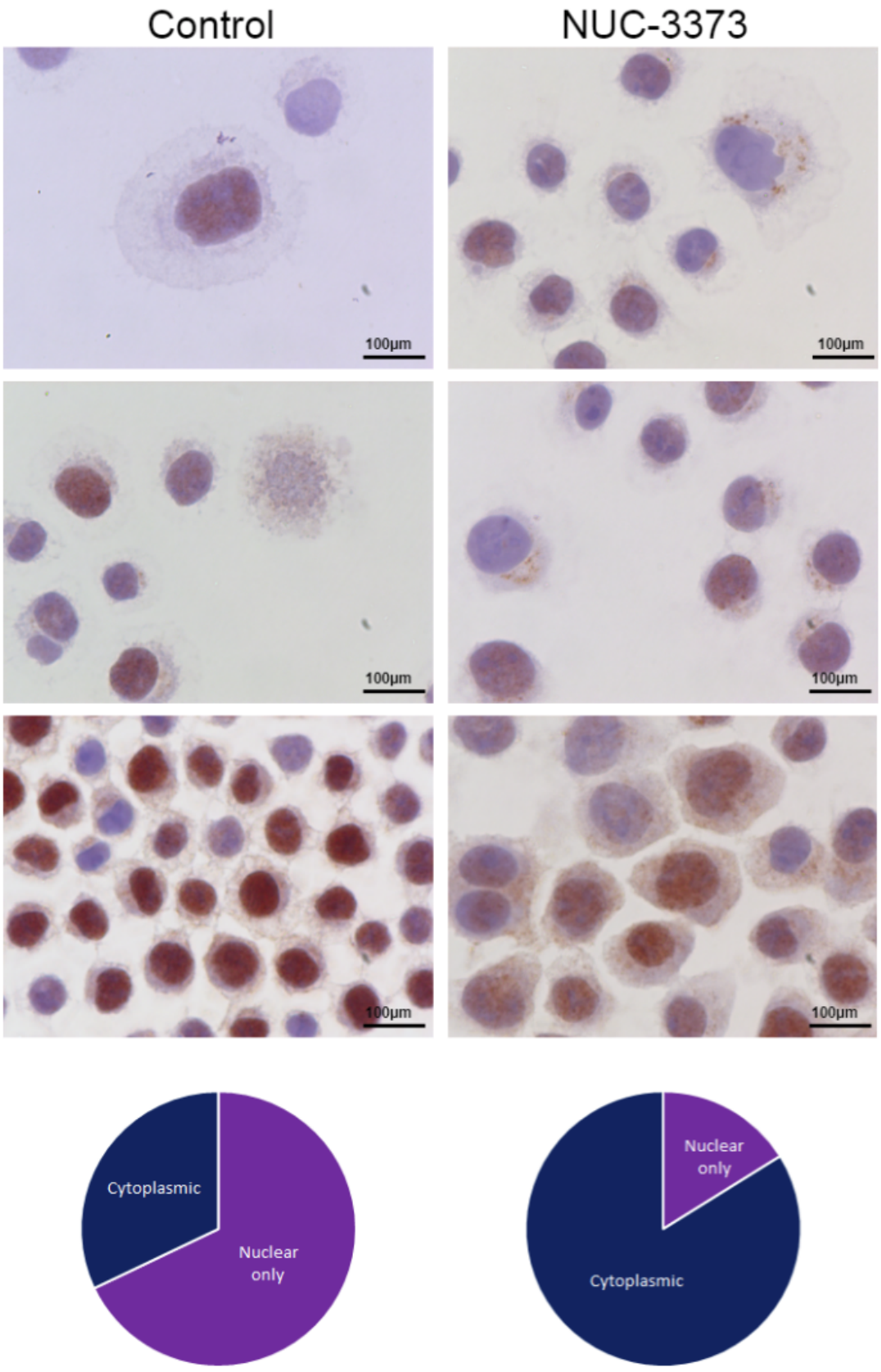

Figure 3.10: Representative images of TS expression and quantified TS expression in cytospinned HCT116 cells either untreated (control) or treated with 10 μM NUC-3373 for 24 hours.

Cells were studied and TS location classified as either nuclear only, or having cytoplasmic presence (Figure 3.10). It was confirmed that the majority of untreated HCT116 cells express nuclear TS, with a clear loss in those cells treated with NUC-3373 in which it appeared to translocate to the cytoplasm.

Candidates proposed for localisation of cytoplasmic TS included, but were not limited to, lysosomes as well as processing bodies. Lysosomes were detected using anti-lysosomal associated membrane protein 1 (LAMP1) antibody and processing bodies were detected using anti-Decapping mRNA protein 1a (Dcp1a) antibody.

Lysosomes

Lysosomes are membrane bound vesicles containing enzymes capable of degrading proteins, DNA, RNA, polysaccharides and lipids. Lysosomes also fuse with autophagosomes to degrade internal organelles (Cooper, G.M., 2000). Integral to lysosomes are the lysosomal associated membrane proteins or 'LAMPs'. These are heavily glycosylated lysosomal membrane proteins and are involved in preventing intracellular proteolysis of the lysosomal membrane (Wang, Q., *et al.*, 2017). LAMP1 has found to be abundantly expressed in colorectal neoplastic tissues (adenoma or cancer) compared with non-neoplastic tissues (Furuta, K., *et al.*, 2001) in addition to being implicated in the metastatic potential of CRC (Saitoh, O., *et al.*, 1992).

HCT116 and SW480 cells were treated with NUC-3373 for 24 hours, fixed in 4% paraformaldehyde and probed with both anti-LAMP1 antibody and anti-TS antibody to assess whether TS was localising with lysosomes for degradation following treatment.

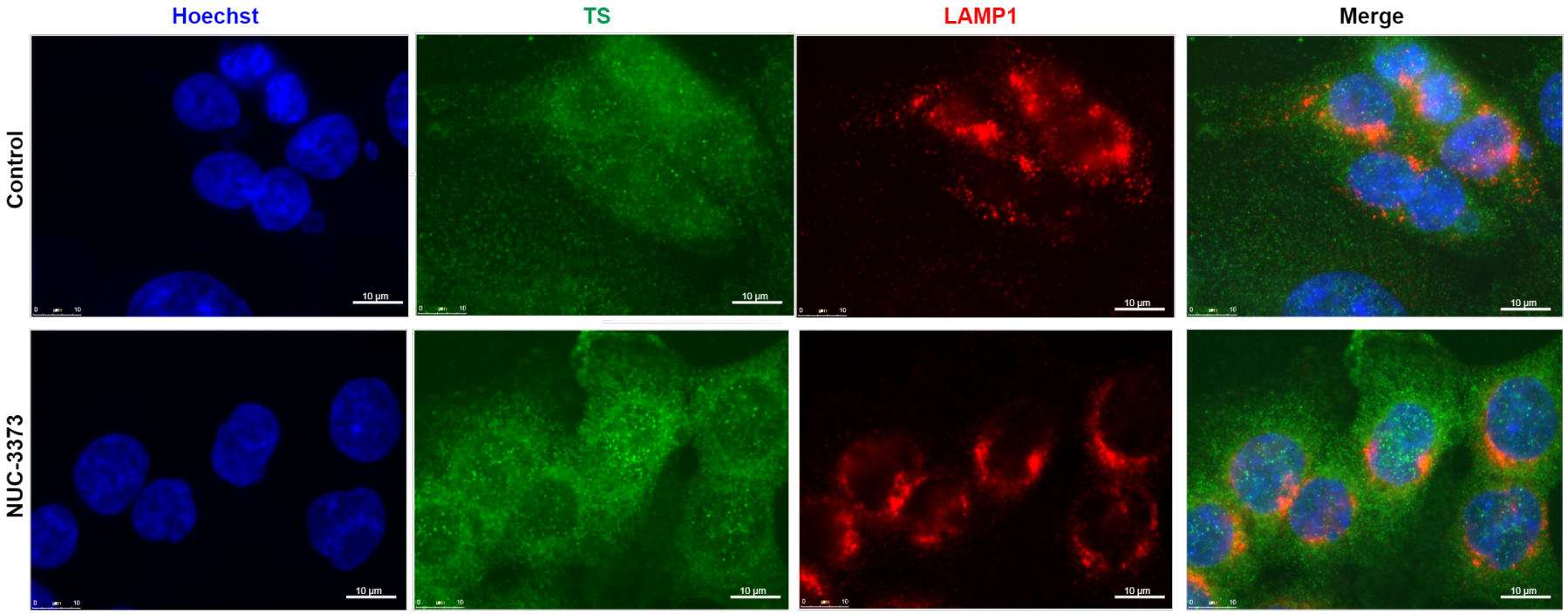

Figure 3.11: LAMP1 and TS expression in HCT116 cells either untreated (control) or treated with 10 μM NUC-3373 for 24 hours. Blue: Hoechst (nuclear stain), Green: TS, Red: LAMP1. 100x magnification.

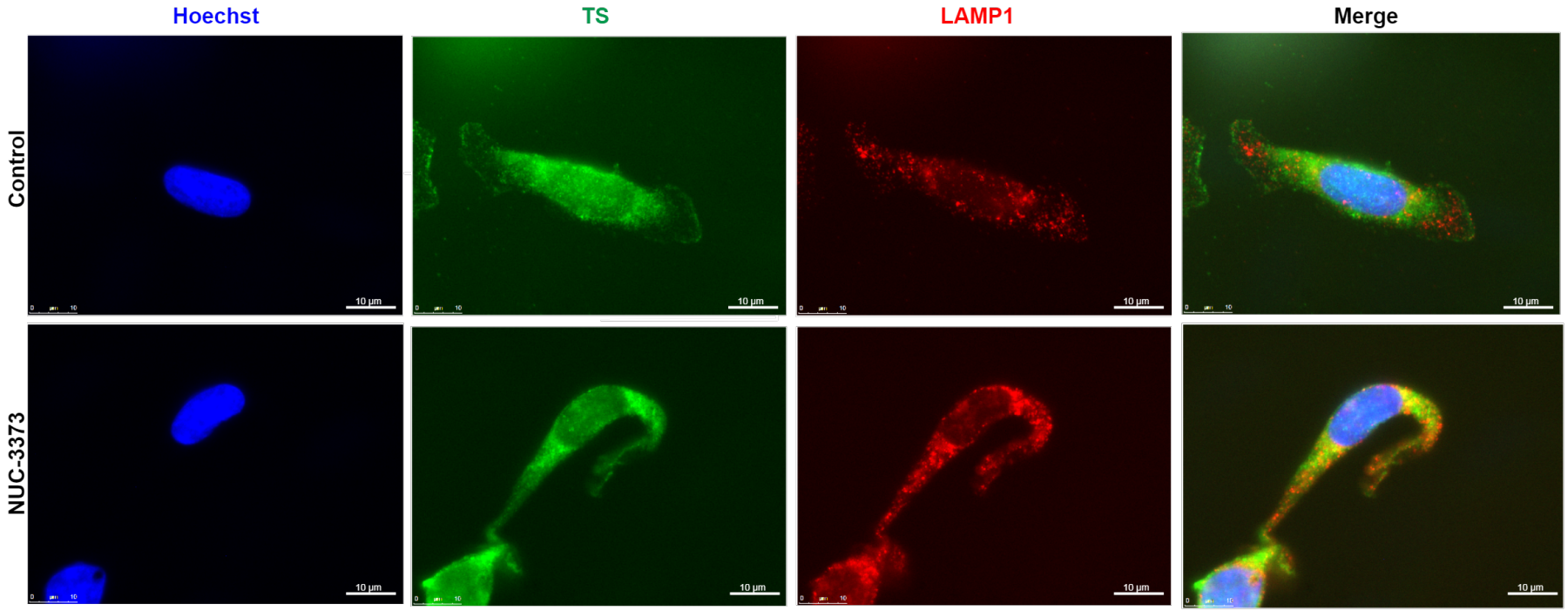

Figure 3.12: LAMP1 and TS expression in SW480 cells either untreated (control) or treated with 10 μM NUC-3373 for 24 hours. Blue: Hoechst (nuclear stain), Green: TS, Red: LAMP1. 100x magnification.

In untreated HCT116 cells, LAMP1 expression was cytoplasmic but not diffuse, localising more prominently to the perinuclear region (Figure 3.11). There was no co-localisation of LAMP1 and TS, indicating that TS is not lysosomal. After 24 hours of treatment with 10 μM NUC-3373 there was no change in the LAMP1 expression pattern compared with untreated HCT116 cells and there was still no co-localisation with TS.

In untreated SW480 cells (Figure 3.12) LAMP1 expression was cytoplasmic, with more diffuse distribution than the peri-nuclear expression observed in HCT116 cells. After 24 hours treatment with 10 μM NUC-3373, SW480 cells had upregulated LAMP1 expression when compared to control and displayed some potential co-localisation with TS, indicated by yellow colour. Lysosomes were also observed to be present in the extended projections of SW480 cells.

Processing Bodies

HCT116 and SW480 cells were treated with 10 μM NUC-3373 for 6, 12 or 24 hours, fixed in 4% formaldehyde and probed with anti-Dcp1a, conjugated to Alexa Fluor 594, as a marker of processing bodies. Due to this ant-Dcp1a being raised in a rabbit, the same species as the previously-mentioned anti-TS antibody, it was not possible to co-probe to determine any co-localisation.

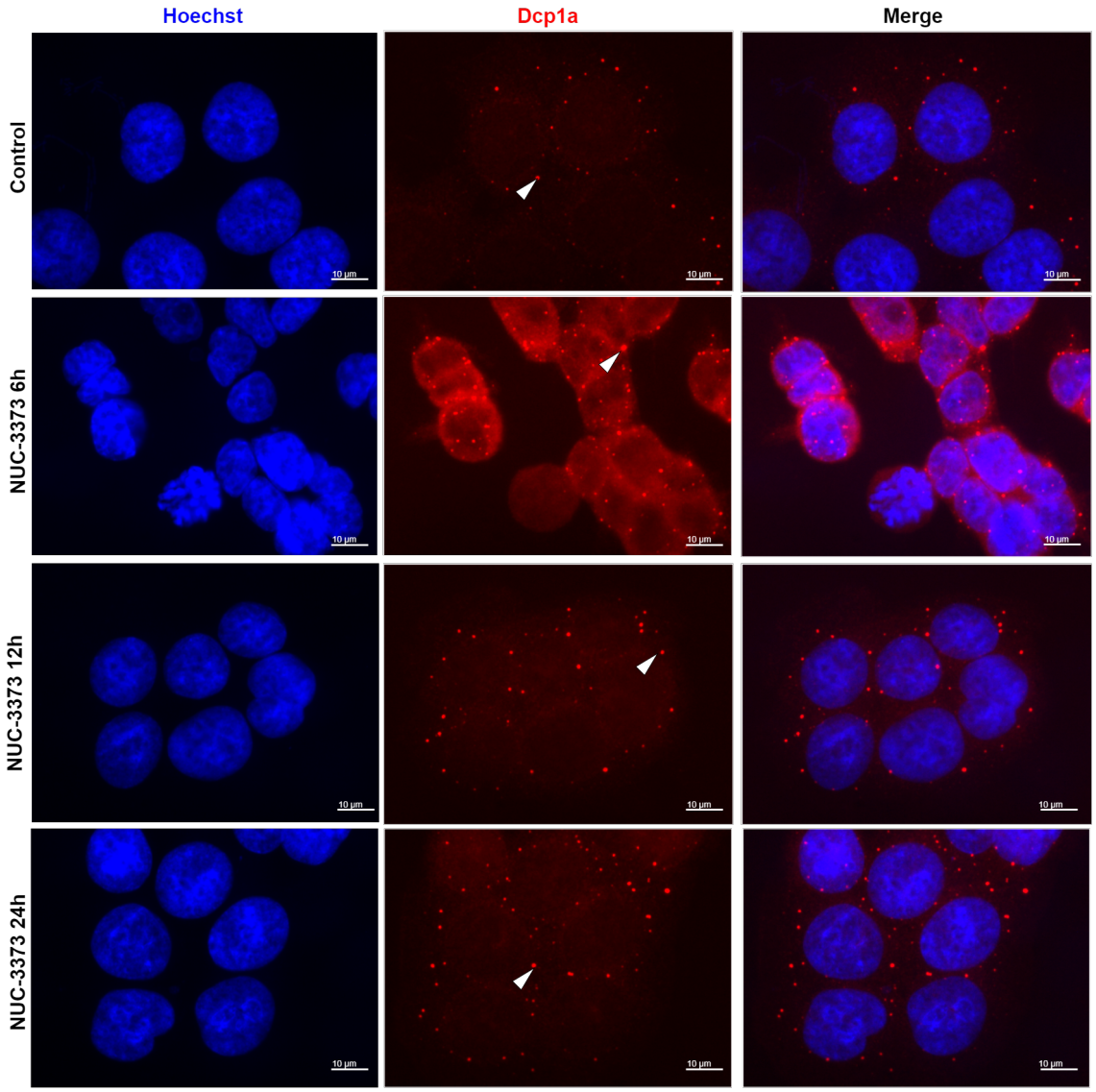

Figure 3.13: Dcp1a expression in HCT116 cells treated with 10 μM NUC-3373 for 6, 12 or 24 hours. Blue: Hoechst (nuclear stain), Red: Dcp1a, Red: LAMP1. Arrows indicate processing bodies. 100x magnification.

In HCT116 cells, there was a very low basal cytoplasmic expression of processing bodies, presenting in a highly punctate manner (Figure 3.13). NUC-3373 treatment resulted in increased Dcp1a expression after 6 hours which presented in both a punctate as well as diffuse manner. By 12 hours and 24 hours treatment, Dcp1a expression was no longer diffuse, but the punctate bodies are larger and more plentiful. It may be that processing bodies undergo disassembly after 6 hours of treatment, indicated by the diffuse expression of Dcp1a at this time point, then are reassembled after 12 hours as Dcp1a is sequestered back to processing bodies.

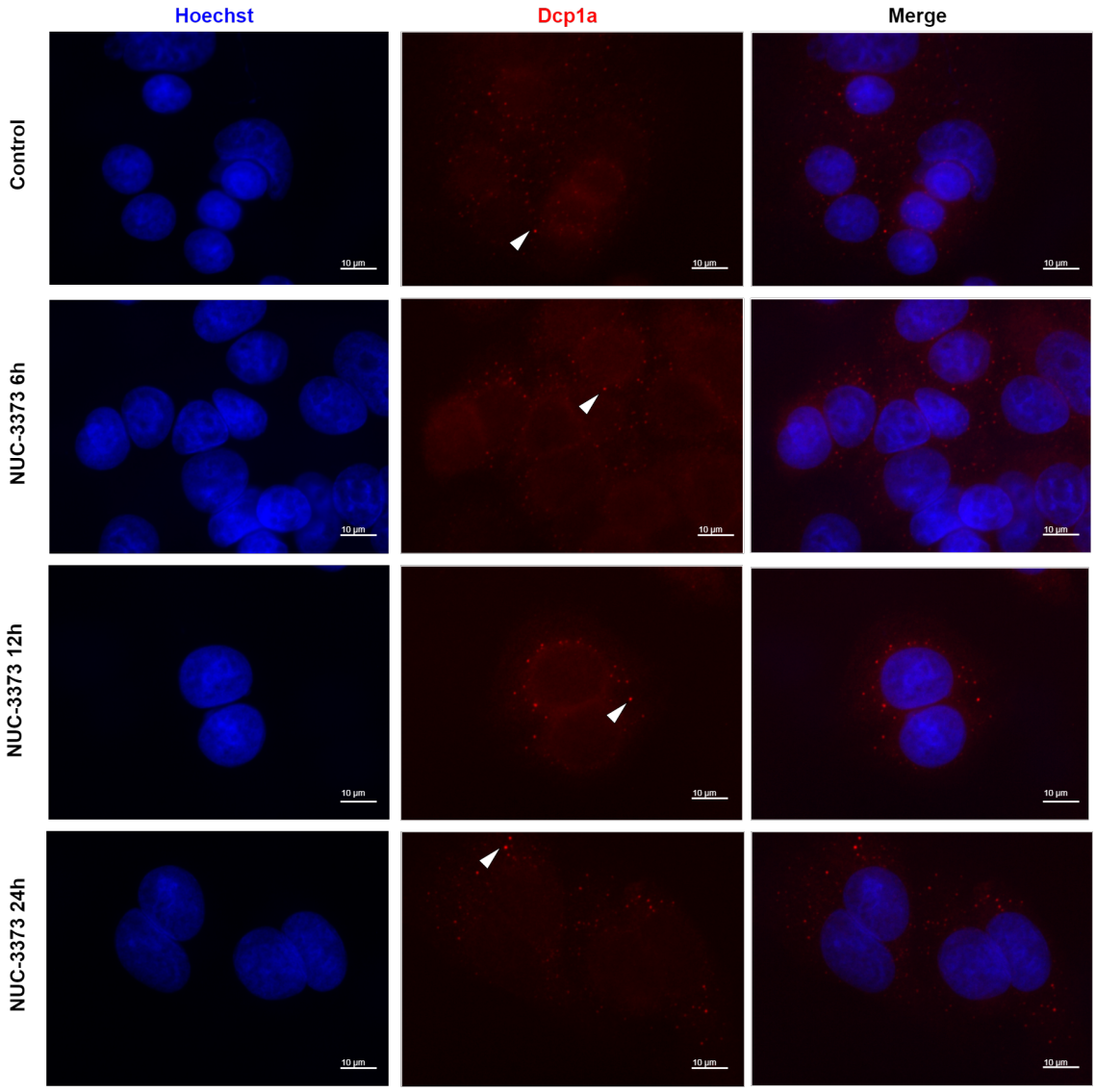

Figure 3.14: Dcp1a expression in SW480 cells treated with 10 μM NUC-3373 for 6, 12 or 24 hours. Blue: Hoechst (nuclear stain), Red: Dcp1a, Red: LAMP1. Arrows indicate processing bodies. 100x magnification.

In SW480 cells, there was much weaker expression of Dcp1a than observed in HCT116 cells, but an increase in punctate bodies was still detected following NUC-3373 treatment (Figure 3.14). This indicates that NUC-3373 also induces processing body formation in SW480 cells.

3.3 Discussion

3.3.1 Sensitivity of Cells to NUC-3373

When assessing the chemo-sensitivity of cell lines to anti-cancer agents, it is pertinent to question the meaning and use of the terms IC_{50}, EC_{50} and LD_{50}. LD_{50} (half maximal lethal dose) refers to the dose of a drug that would result in the direct death of 50% of the original population of cells and thus would be inappropriate to use in this case due to the nature of cells proliferating and it being impossible to identify those from the original population. EC_{50} (half maximal effective concentration) refers to the concentration of a drug that is effective in 50% of the population. IC_{50} is the concentration of a drug required to inhibit 50% of the population, in this case inhibiting the growth of cells as a whole population (Rang, H.P. *et al.*, 2012). From the studies of cell growth using Celigo cell confluence scans it was observed that NUC-3373 treatment results in a net inhibition of cell growth and not a net death of cells. That is to say that some cells may be dying but not necessarily as fast as those proliferating. Alternatively, it could simply be that the rate of proliferation is slowed. Further studies would be required to determine this. It was decided that IC_{50} was the most appropriate term to use for these reasons and that it would be estimated using the SRB assay.

The SRB assay has been used widely in the measurement of IC_{50}s since its development by Skehan, P., *et al.*, (1990). When subjected to mildly acidic conditions, one of the sulfonic groups of SRB dye binds to basic amino acid residues on proteins in TCA-fixed cells. This can then be dissolved by Tris and optical density measured. Whilst this method is inexpensive, quick and reproducible, it is important to note that it is a measure of total cellular protein and not of cellular activity. In this study, the Celigo scanner was used to measure confluence of cells concurrent to the SRB end-point assay. The two methods, as in Figure 3.3, were shown to have a strong linear correlation and therefore SRB was deemed to be reliable, therefore other available assays of cellular viability such as Alamar Blue

and MTT were not considered.

The panel of cell lines tested exhibited a very wide range of sensitivities to NUC-3373 and were varied in terms of their MMR and TP53 status. Of these, HCT116 and SW480 were chosen to study further. This was in part due to their monolayer phenotype allowing for more accurate observations to be made using Celigo. Most importantly was their IC_{50} values being significantly different, with HCT116 chosen to represent tumours more responsive to NUC-3373 and SW480 those less so. The concentration chosen for future studies with these cell lines was 10 μM as, although this is lower than the IC_{50} values, it was sufficient to reduce growth in both cell lines as measured by Celigo cell confluence scans and therefore in theory would bring about some of the pre-apoptotic events that were desired to elucidate further the mechanisms of action of NUC-3373.

3.3.2 Thymidine rescue of cells

By treating cells with NUC-3373 in the presence and absence of thymidine supplementation, it was demonstrated that cells could be saved from a thymine-less death. This is likely due to the utilisation of the salvage pathway for dTMP production (Chu, E., and Allegra, C., 1996) when the *de novo* pathway was inhibited by the formation of TS ternary complexes (Figure 3.15).

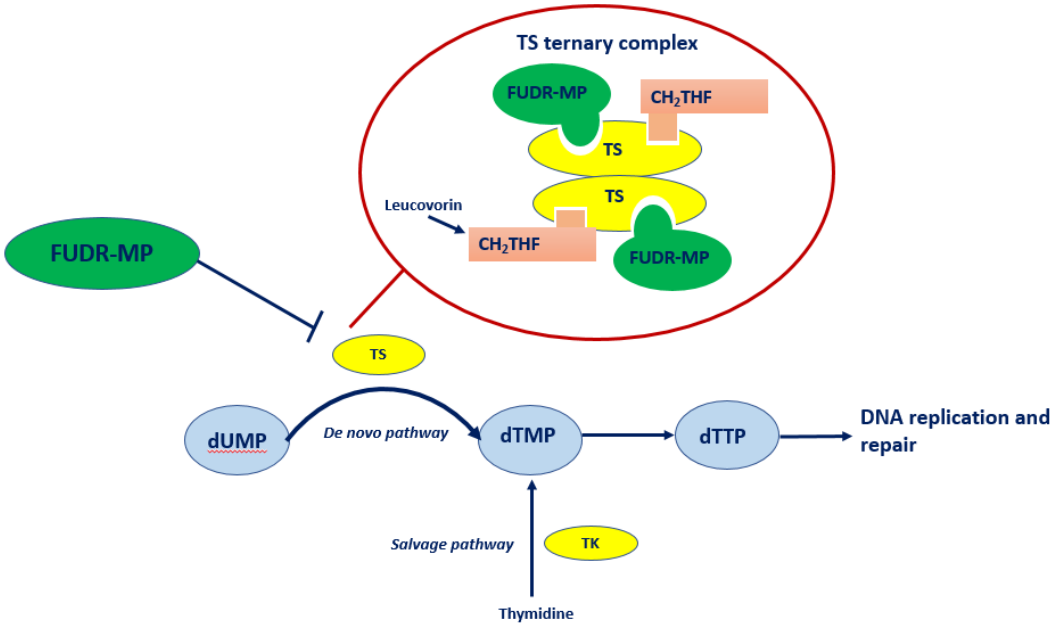

Figure 3.15: Inhibition of *de novo* synthesis of dTMP by TS ternary complexes.

If thymidine can rescue cells from a NUC-3373-induced death, could patient thymidine levels influence treatment outcome or pose a resistance mechanism? Early *in vitro* and animal studies found that inhibition of thymidine salvage potentiates the cytotoxicity of TS inhibitors such as 5-FU and capecitabine (Lehman, N.L., and Danenberg, P.V., 2000; Smith, P.G., *et al.*, 2000). However, it has been found that there is no significant difference in basal plasma thymidine concentration between normal subjects and CRC patients (with thymidine in the 7-15 nmol/L range), in contrast to the 100- and 300-fold higher concentrations in rats and mice (Li. K.M., *et al.*, 2005). Furthermore, it was found that pre- and post-treatment thymidine serum levels demonstrated no correlation between response or toxicity to TS inhibitor treatment (Li, K.M., *et al.*, 2007). However, it must be noted that Li *et al.* did not specify the time course of blood collection for measurement of plasma thymidine levels, which could vary greatly. Despite this, the concentration of thymidine used in these experiments (8 μg/mL) was still much higher than that found in patients so is not representative of the *in vivo* condition. Therefore, these data merely highlight that NUC-3373 is targeting the *de novo* pathway of dTMP synthesis.

3.3.3 Hypoxic studies

In preliminary studies, cells were cultured and treated under both normoxic and hypoxic conditions (0.5% O_2) in order to assess the efficacy of NUC-3373 in oxygen-deprived areas of tumours. 5-FU has previously been reported to be less effective under hypoxic conditions (Li, J., *et al.*, 2017; Yoshiba, S., *et al.*, 2009; Däster, S., *et al.*, 2017). Wang, L. *et al.*, (2016) found that both HCT116 and SW480 cells were less sensitive to growth inhibition by 5-FU when subjected to hypoxia (1% O_2) compared with normoxia, with SW480 being the more resistant of the two. The main mechanism of action of 5-FU is thought to be the inhibition of DNA replication in S phase. When Wang *et al.* sorted HCT116 and SW480 cells by flow cytometry, it was discovered that there was a higher proportion of cells in G1 phase and fewer in S phase when under hypoxic conditions compared with normoxic. This indicates that hypoxic stress may cause G1/S arrest in CRC cells, thus inducing chemo-resistance to 5-FU. In the preliminary studies of the effect of hypoxia on NUC-3373 chemo-sensitivity in this chapter, there was a mixed response throughout the cell line panel. Like the afore-mentioned study by Wang *et al.* utilising 5-FU, SW480 cells exhibited increased resistance to NUC-3373 (3.8-fold) under hypoxic conditions. However, it was found that HCT116 cells were more sensitive to NUC-3373 under hypoxic conditions, contradictory to studies by Wang *et al.* These data were interesting to inform but further hypoxic studies did not lead to any data of functional significance so were excluded from future experiments. Additionally, studying hypoxia in cancer cell culture is not representative of the heterogeneity of O_2 deprivation in cells within tumours *in vivo*.

3.3.4 5-FU vs NUC-3373

It was important to be aware that a direct comparison between 5-FU and NUC-3373 made in an *in vitro* setting would not be representative of their efficacies *in vivo*. Although their active metabolites are the same, the *in vitro* model lacks the vital components that elucidate their differences in the clinic, such as the liver. NuCana

plc. have conducted investigations into the difference in the pharmacokinetic (PK) profiles of NUC-3373 and 5-FU (see Figure 3.16) both *in vitro* and *in vivo*. In the CRC cell line HT29, mass spectrometry studies revealed a 366-fold increase in concentration of the active metabolite FdUMP (also known as FUDR-MP) when treated with NUC-3373 compared with 5-FU. In peripheral blood mononuclear cells extracted from patients in the phase I study NuTide:301, NUC-3373 was found to have a much more favourable PK profile than 5-FU. The plasma half -life of NUC-3373 is much longer than that of 5-FU, TS inhibition was stronger (likely due to the greater concentration of FdUMP), dTMP pools were depleted and no toxic metabolite (dhFU) was detected.

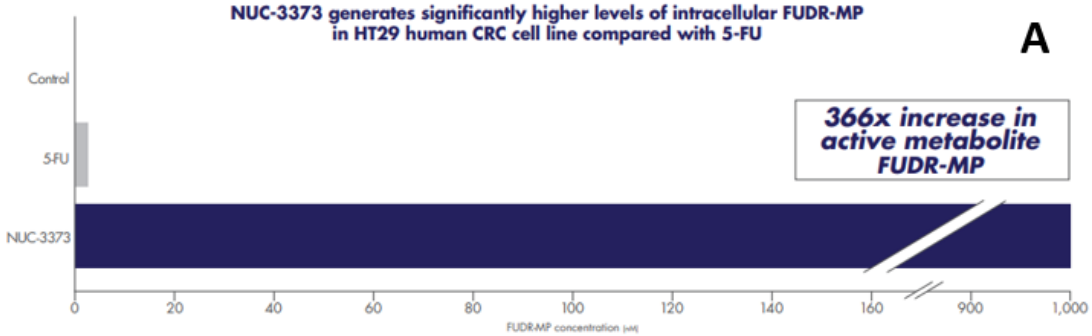

NUC-3373 PK profile comparison with 5-FU B

	NUC-3373	5-FU
Plasma $t_{1/2}$	9.7 hours	8-14 minutes
FUDR-MP (in PBMCs)	Detected (dose proportional)	Undetected[9]
TS inhibition	Strong	Weak
Intracellular levels of dTMP	Depleted	No change
Toxic metabolite (dhFU)	Undetected	High levels

Figure 3.16: Comparison of NUC-3373 and 5FU. A: Active metabolite FdUMP (FUDR-MP) levels in HT29 cells following NUC-3373 or 5FU treatment, detected by mass spectrometry. B: NUC-3373 Pharmacokinetic profile comparison with 5FU in PBMCs derived from phase I clinical trial patients. From Blagden, S., *et al.*, 2018.

3.3.5 Thymidylate Synthase

Due to the vast difference in performances of NUC-3373 and 5-FU *in vivo*, which is in large part due to the degradation by DPD in the liver, this thesis avoided direct

comparisons between the two. Instead, focus was placed on the mechanism of action relating to the active metabolite of both these drugs; FdUMP. Investigations in this chapter focussed on the dynamics of the target of the active metabolite of both 5-FU and NUC-3373; TS. Due to the mixed literature regarding TS expression as a predictive biomarker of response to 5-FU, the chemosensitivity of the cell lines in the panel were first assessed against endogenous (treatment-naïve) TS protein expression, which was found to have no bearing on the chemosensitivity to NUC-3373.

It was then hypothesised that the determining factor in sensitivity of cell lines to NUC-3373 or 5-FU treatment could be the ability to inhibit TS, but this was found not to be the case. The finding that free TS increases with exposure to both 5-FU and NUC-3373 in both cell lines is supported by previous work by Chu, E. and Allegra, C.J., (1996). They presented the first evidence to suggest that a possible resistance mechanism to 5-FU may be its acute induction of TS. In agreement with the data presented in this study they demonstrated that, although a proportion of TS was in its ternary complex form with FdUMP, much of the increase was due to 'free' unbound TS. Their work elucidated the negative autoregulatory mechanism in which translation of TS mRNA is regulated by its own protein product.

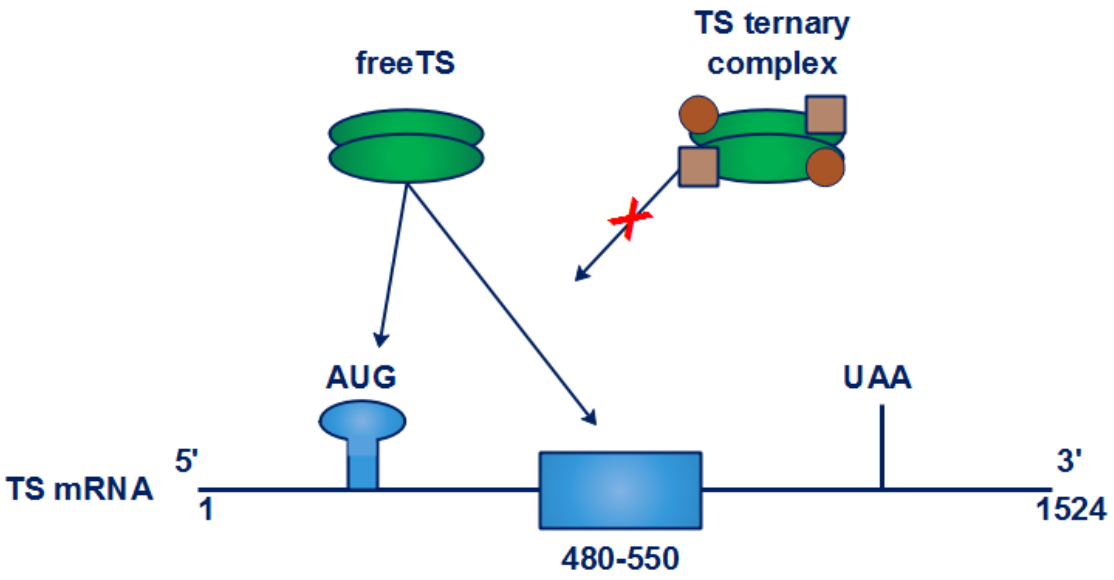

Figure 3.17: The negative self-autoregulatory mechanism of TS mRNA translation. Adapted from Chu, E. and Allegra, C.J., (1996).

TS binds to its own mRNA, resulting in translational inhibition. As demonstrated in Figure 3.17, free TS interacts with high affinity to two cis-elements of TS mRNA. The first is a 30-nt sequence in the 5'UTR which includes the AUG start site. The second site is a 70-nt sequence within the coding region corresponding to nt 480-550. This site transpired to be critical for protein recognition, as a series of mutations that abolished the stem loop resulted in RNA sequences that were unable to interact with TS protein (Liu, J., *et al.*, 2002). This binding activity is dependent on TS being ligand-free so when bound in a ternary complex with FdUMP this translational inhibition is lost, resulting in an increase in TS protein production. This effect was found in several cell lines (see appendices), even those highly sensitive to NUC-3373.

Interestingly, the TS complexes and free TS induced by NUC-3373 treatment appear more sustained than those induced by 5-FU, which decrease after 72 hours. This could be due to either the longer half-life of NUC-3373 or a higher concentration of FdUMP, although mass spectrometry would be required to assess metabolite levels to confirm this.

These data led to the question of where induced TS was located within the cell. It was found that NUC-3373 treatment resulted in a translocation of TS from the nucleus to the cytoplasm. Previous work has found both HCT116 cells *in vitro* (Bissoon-Haqqani, S. *et al.*, 2006) and CRC cells *in vivo* (Wong, N.A.C.S., *et al.*, 2001) to have a strong nuclear TS expression in agreement with this work, but studies have yet to fully elucidate the dynamics of TS intracellular localisation following treatment with 5-FU.

It is unclear whether the TS translocated from nuclei to cytoplasm with NUC-3373 treatment is in its free or ternary complex form. The antibody specific to the TS ternary complex (MABE370) has only been validated for use in western blot. When IF was attempted using this antibody, it could not be validated as a high level of background fluorescence was present in untreated cells. The epitope of this antibody is not detailed so it is unclear what conformation TS protein must present to bind. It was successful in detecting TS ternary complex specifically in

western blot (see appendix), with no detection in untreated lysates under denaturing conditions. TS undergoes a conformational change between its active (free) and inactive (ternary complex) states (Luo, B., *et al.*, 2011). In its ternary complex, TS-FdUMP-CH_2H_4folate, there is a covalent bond between Cys198 and C-6 of the bound nucleotides. Under denaturing conditions, TS ternary complexes retain the covalent bonds with cofactors (agreeing with the weight at which drug-bound TS is detected in western blot). It remains unclear as to why the MABE370 antibody is not specific in IF.

In 2001, Wong, N., *et al.* reported that high nuclear TS predicted poorer response to 5-FU. Similarly, Gustavson, M.D., *et al.*, (2008) reported that a higher nuclear to cytoplasmic ratio of TS expression significantly correlated with poorer 5-year survival in two large cohorts, n=599 and n=447, of CRC patients. The localisation of *de novo* dTMP synthesis may be responsible for these findings. During G1, *de novo* dTMP synthesis takes place in the cytoplasm. Upon S phase, serine hydroxymethyltransferase 1 (SHMT1), TS and dihydrofolate (DHFR) undergo small ubiquitin-like modifier (SUMO)-dependent translocation to the nucleus. MacFarlane, A., *et al.*, (2011) demonstrated that uracil incorporation into DNA was heightened when *de novo* dTMP synthesis was restricted to the cytoplasm. 5-FU causes G1 arrest of cells (Tokunaga, E., *et al.*, 2000), which may provide a basis for the finding that a higher proportion of cells expressed cytoplasmic TS when treated with NUC-3373. When considering the data here in this study, the high levels of intercellular heterogeneity of TS localisation between nuclei and cytoplasm may be explained by the cell cycle-regulation of dTMP synthesis. Quantitative analysis found an overall translocation of TS to the cytoplasm with NUC-3373 treatment which, according to the findings by MacFarlane's group, encourages elevated uracil incorporation into DNA, possibly contributing to NUC-3373-induced cell death. Further work to synchronise cell cycle by flow sorting prior to treatment with NUC-3373 could further illustrate more precisely the effect on TS localisation.

The sequestration of TS to the punctate cytoplasmic expression observed in some NUC-3373-treated cells was investigated further by immunofluorescence in order to

establish any co-localisation with other organelles or vesicles. None of the candidates investigated showed any co-localisation with TS. Whilst not localising with TS expression, the expression of lysosomes (detected by an antibody against LAMP1) was more pronounced in SW480 cells. Additionally, their intracellular distribution extended to peripheral sites of the cell, unlike in HCT116 cells where lysosomes were localised to the cytoplasmic region to the periphery of the nucleus. Saitoh, O., *et al.*, (1992) reported that highly metastatic cancer cell lines have a higher expression of LAMP proteins. It may be that SW480 cells are less sensitive to NUC-3373 treatment due to their lysosomal degradation ability, presenting as a further mechanism gaining an advantage for SW480 cells over NUC-3373 treatment. However, this would require further investigation including functional studies.

Processing bodies, detected by an antibody against Dcp1a, appeared to be the most promising candidate for TS localisation. In response to environmental stress, such as heat, UV radiation or exposure to some drugs, a signalling cascade is activated within cells to shut down protein translation in order to conserve energy required for repair of stress-induced damage. This results in the formation of cytoplasmic aggregates of stalled translational preinitiation complexes termed stress granules (SGs) and cytoplasmic sites of mRNA degradation termed processing bodies (P-bodies) (Anderson, P., and Kedersha, N., 2007; Kedersha, N., *et al.*, 2005). Stress granule expression was assessed in this study by immunocytochemistry linked with fluorescence using an antibody against eukaryotic initiation factor 3 (eIF3) but no expression was found. This may be due to the very transient nature of SGs and not measuring at the correct time point, so positive controls (such as aresnite-treated cells) would have been useful in this study. However, visualisation of p-bodies was successful. Due to the absence of co-probing with anti-TS antibody, their co-localisation can only be speculated against. If they do co-localise, it could be postulated that p-bodies play the role of storing TS bound to mRNA. The diffuse appearance observed with 6 hours of NUC-3373 treatment in HCT116 cells may be due to p-bodies disassembly. When TS is bound by FdUMP, this necessitates the requirement for TS mRNA to become translationally active again to replenish the

cellular level of TS.

3.3.6 Chapter Summary

To summarise, this data chapter has found that basal TS protein expression does not determine sensitivity to NUC-3373 treatment in an *in vitro* setting. Indeed, NUC-3373 treatment to inhibit TS protein expression results in the formation of TS ternary complexes but also a recovery of TS expression and an apparent translocation to the cytoplasm. Although co-localisation of punctate cytoplasmic TS was not confirmed, it was demonstrated that NUC-3373 increases the appearance of p-bodies. Taken together, these data point towards additional mechanisms of cell death by NUC-3373 that are independent of the DNA damage pathway.

Chapter 4

Endoplasmic Reticulum Stress

4.1 Introduction

The previous chapter found that NUC-3373 treatment results in increased TS protein expression accompanied by a nuclear to cytoplasmic translocation of TS. It was hypothesized that either the increased synthesis of TS protein or presence of TS ternary complexes in cytoplasm may induce endoplasmic reticulum (ER) stress. Furthermore, Yadunandam, A.K., *et al.*, (2012) found evidence that 5-FU can induce ER stress in hepatocellular carcinoma Sk-Hep1 cells, indicated by an increase in CCAAT-enhancer-binding protein homologous protein (CHOP) expression.

4.1.1 The Unfolded Protein Response and ER Stress

Cells communicate with their environment through a variety of signalling proteins which convey crucial information relating to the health of the organism. For example, these signals determine whether a cell should divide, migrate, differentiate or die. The majority of these proteins are assembled in the ER before being translocated to the appropriate cellular location for their function. Only proteins that are correctly folded are permitted to exit the ER, whilst misfolded proteins

are retained in the ER and delivered for proteasomal degradation after retrograde translocation into the cytosol (Walter, P., and Ron, D., 2011).

Ca^{2+} disruption and increased traffic of unfolded or misfolded proteins places stress on the ER. In order to restore homeostasis and ensure the survival of the cell, the unfolded protein response (UPR) is induced. The UPR acts to both reduce the load of proteins entering the ER and activate genes to increase the folding capacity of the ER. Accumulation of misfolded proteins in the ER lumen causes dissociation of the master regulator of the UPR, immunoglobulin binding protein (BiP), from ER-resident transmembrane components which are linked to three mechanistically distinct arms of the UPR. Dissociation of BiP from protein kinase RNA-like ER kinase (PERK), inositol-requiring enzyme 1 (IRE1) and activating transcription factor 6 (ATF6), activates a signalling cascade which attempts to regain proteostasis in the ER (see Figure 4.1). Proteostasis is achieved by increasing ER volume, increasing the production of ER chaperones as well as transient attenuation of global protein translation (Ron, D., and Walter, P., 2007). However, if ER stress is prolonged and unmitigated, cells respond by increasing transcription of proteins such as CHOP (Nishitoh, H., 2012) which promote apoptosis. The fine balance of expression between pro-survival and pro-apoptotic determines the fate of cells when subjected to ER stress conditions.

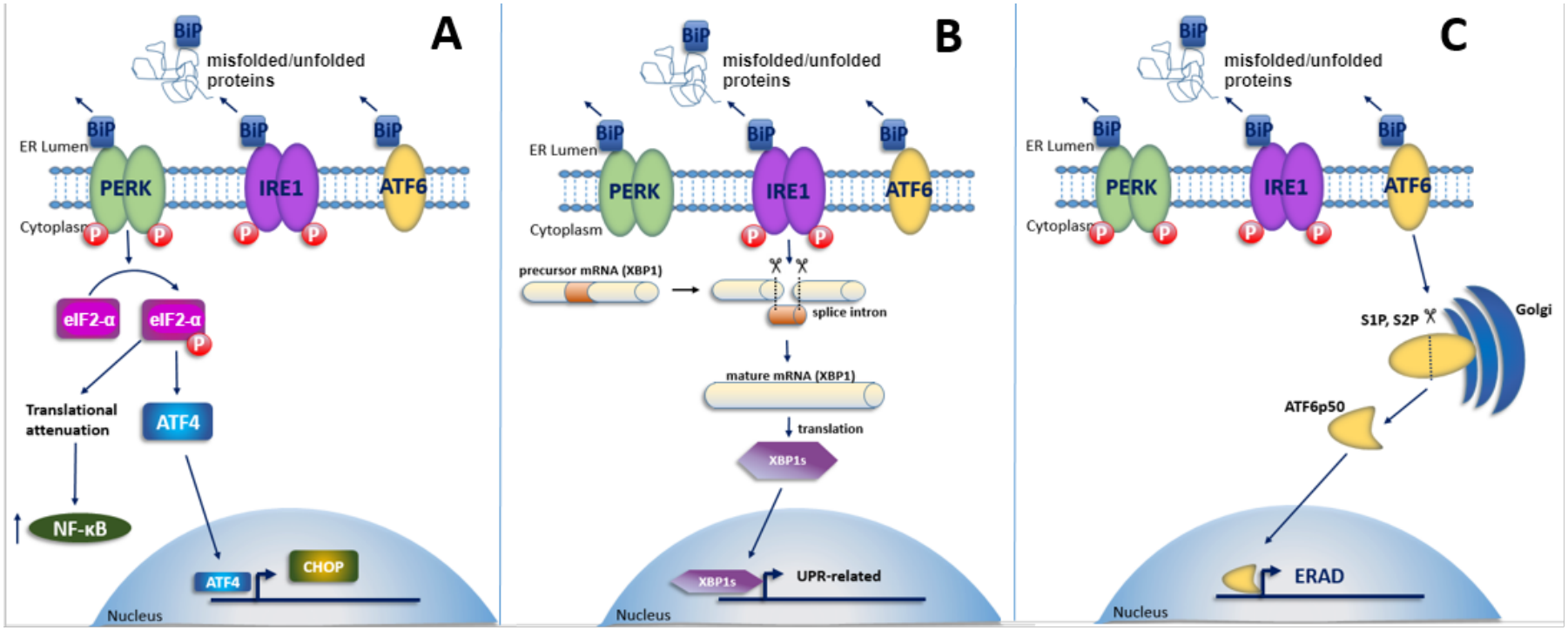

Figure 4.1: The unfolded protein resposne. A: Activation of PERK. B: Activation of IRE1. C: Activation of ATF6. Dissociation of BiP causes autophorylation of PERK. Activated Phospho-PERK then selectively phosphorylates the alpha subunit of eukaryotic initiation factor 2 alpha (eIF2-α), leading to transient translational attenuation but specific increased translational efficiency of stress-responsive activation transcription factor 4 (ATF4) in order to reduce the protein traffic in the ER until proteostasis is recovered (Lebeau, J., *et al.*, 2018). ER stress causes autophosphorylation and activation of IRE1, which splices a 26 nt intron from X-box binding protein 1 (XBP1) mRNA to create the mature and active form the mRNA which will then translate XBP1(S). XBP1(S) protein is a transcription factor that induces expression of pro-survival genes. Upon ER stress, activating transcription factor 6 (ATF6)-α and -β translocate to the golgi and are cleaved by site 1(SP1) and site 2 (SP2) proteases, creating a cytosolic fragment, allowing the free ATF6p50 fragment to translocate to the nucleus where it upregulates expression of genes encoding endoplasmic-associated degradation proteins (Liu, C.Y., and Kaufman, R.J., 2003).

Experimentally, ER stress can be induced using a number of agents. Two classical inducers of ER stress, thapsigargin and tunicamycin, cause accumulation of mis- or unfolded proteins in the ER. Thapsigargin acts by increasing the concentration of cytosolic free Ca^{2+} due to inhibition of the Ca^{2+}-dependent ATPase pump in the ER (Thastrup, O., *et al.*, 1990). This results in a decrease in Ca^{2+} storage and thus decreased activity of Ca^{2+}-dependent chaperones and consequently an accumulation of unfolded proteins in the ER lumen (Backer, M.V., *et al.*, 2011). Tunicamycin, a naturally occurring antibiotic (Guha, P., *et al.*, 2017), induces ER stress by inhibiting the initial step required for biosynthesis of *N*-linked glycans; lipid-linked oligosaccharide synthesis in the ER (Banerjee, A., *et al.*, 2011). This impedes the protein-folding activity of the ER resulting in the accumulation of mis- or unfolded proteins in the ER and subsequent ER stress. If ER stress is prolonged or unmitigated, pro-apoptotic CHOP is upregulated.

4.1.2 Aims and Objectives

This chapter will seek to underpin the impact of NUC-3373 treatment on ER stress-related pathways. The ER is a very dynamic and plastic organelle that is often observed to be dilated under under stress conditions (Oslowski, C., and Urano, F., 2011). Like ER, mitochondria are very responsive to cellular stress and plays a role in the coordinated response to recover from ER stress and achieve proteostasis (Kornmann, B., *et al.*, 2009). ER distension can be detected in cells undergoing ER stress by TEM, having been extensively studied in pancreatic beta cells (Akiyama, M., *et al.*, 2009; Riggs, A.C., *et al.*, 2005; Wang, J., *et al.*, 1999). Therefore, ER stress will be assessed both by ultrastructure using TEM and stereological analysis of ER and mitochondria, as well as biochemical markers of unfolded protein response activation. Direct measurement of the master regulators of the UPR (IRE1, PERK and ATF6) is particularly challenging due to their low endogenous expression being difficult to detect using commercially available antibodies (Oslowski, C.M. and Urano, F., 2011), therefore downstream markers such as phospho-eIF2-α, ATF6 cleavage, and CHOP will be measured as surrogates of their activation.

4.2 Results

4.2.1 Effect of ER stress on cell growth

HCT116 and SW480 cell lines were subjected to treatment with classical ER stress inducers, thapsigargin and tunicamycin and growth assessed daily by Celigo confluence scans.

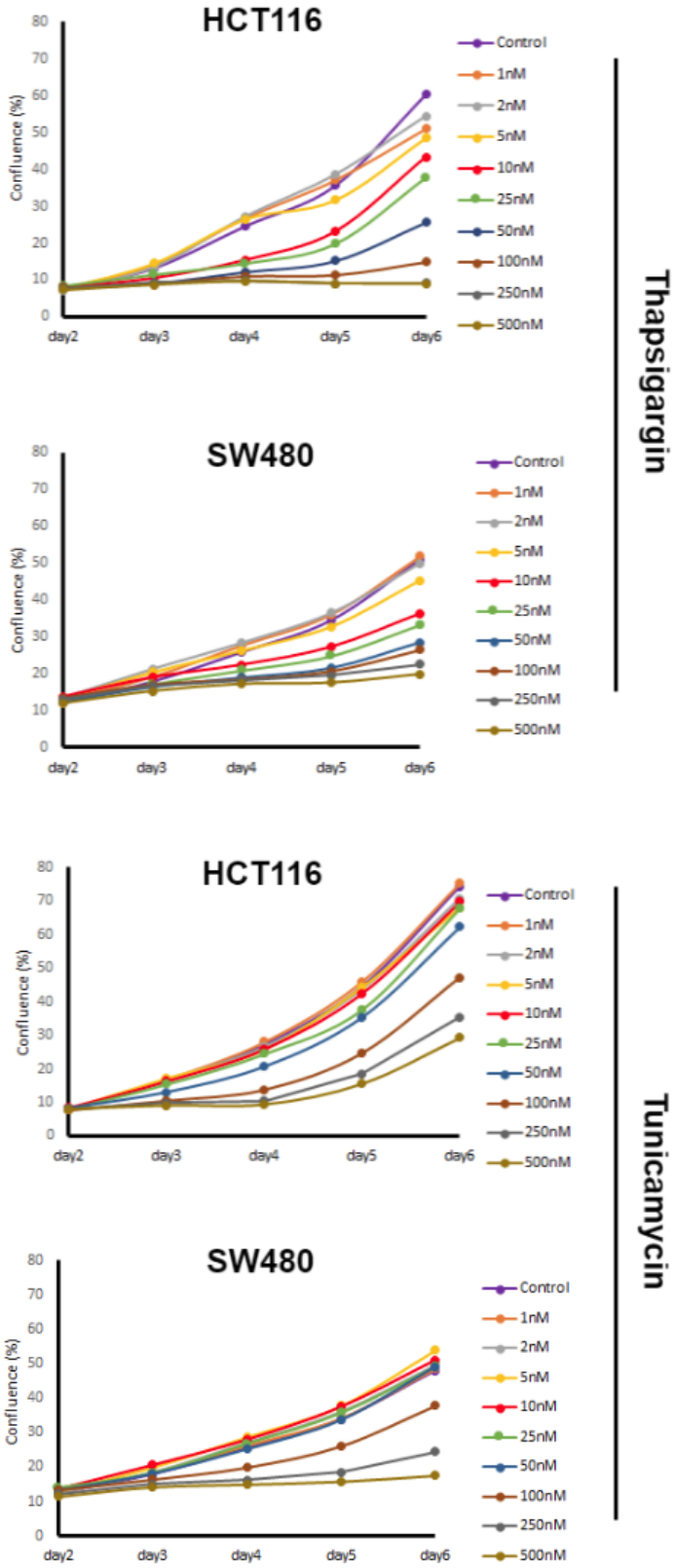

Figure 4.2: Sensitivity of HCT116 and SW480 cells to classical ER stress inducers, Thapsigargin and Tunicamycin. Treatment concentrations range from 1-500 nM. Growth was measured daily as cell confluence, with cells treated on day 2 and drug washed out and replaced with media on day 3. For each drug concentration, $N_{technical}$=6.

In HCT116 cells, thapsigargin has a more pronounced inhibition of cell growth than tunicamycin (see Figure 4.2 A and C). The only concentrations of Thapsigargin sufficient to completely inhibit the growth of HCT116 cells were 250 nM (obscured in graph) and 500 nM. No concentration of tunicamycin was proficient in completely inhibiting growth of HCT116 cells. In SW480 cells treated with thapsigargin, considerable inhibition of growth was achieved at concentrations of 10 nM and above and in those treated with tunicamycin this was achieved at concentrations of 100 nM and above. SW480 cells are more sensitive to the effects of tunicamycin, displaying increased inhibition of growth compared to that observed in HCT116 cells. This indicates that HCT116 cells may be more reliant on calcium-dependent chaperones than SW480 cells and that SW480 cells are more reliant on lipid-linked oligosaccharide synthesis than HCT116 cells.

4.2.2 Ultrastructural Changes

TEM and stereological methods were used to assess ultrastructural changes in ER and mitochondria in response to treatment with thapsigargin, tunicamycin as well as 10 μM NUC-3373 for various time points. 30 SUR micrographs were acquired for each condition and quantified. It is important to note that this study focussed on the quantification of rough ER, identifiable by the presence of ribosomes, which henceforth shall just be referred to as 'ER'. Figures 4.3, 4.4 and 4.5 show representative photo micrographs for cells under different treatments and timepoints.

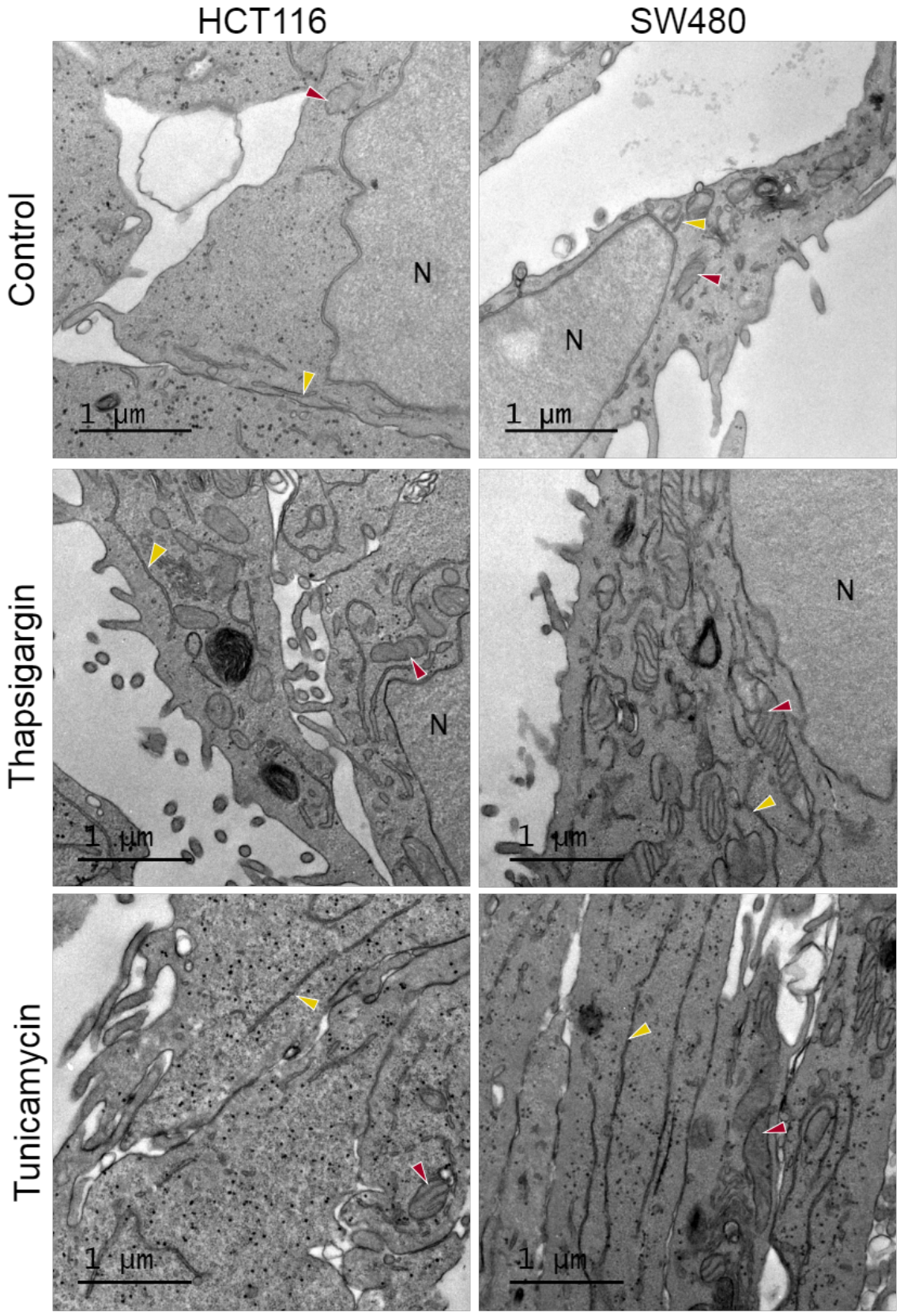

Figure 4.3: Representative micrographs of the effect of ER stress inducers on ultrastructure in HCT116 and SW480 cells. Cells were treated with either 1 μM Thapsigargin or 5 μg/mL Tunicamycin for 5 hours. Red arrows: mitochondria, yellow arrows: ER. Images taken at 3000x magnification on TEM.

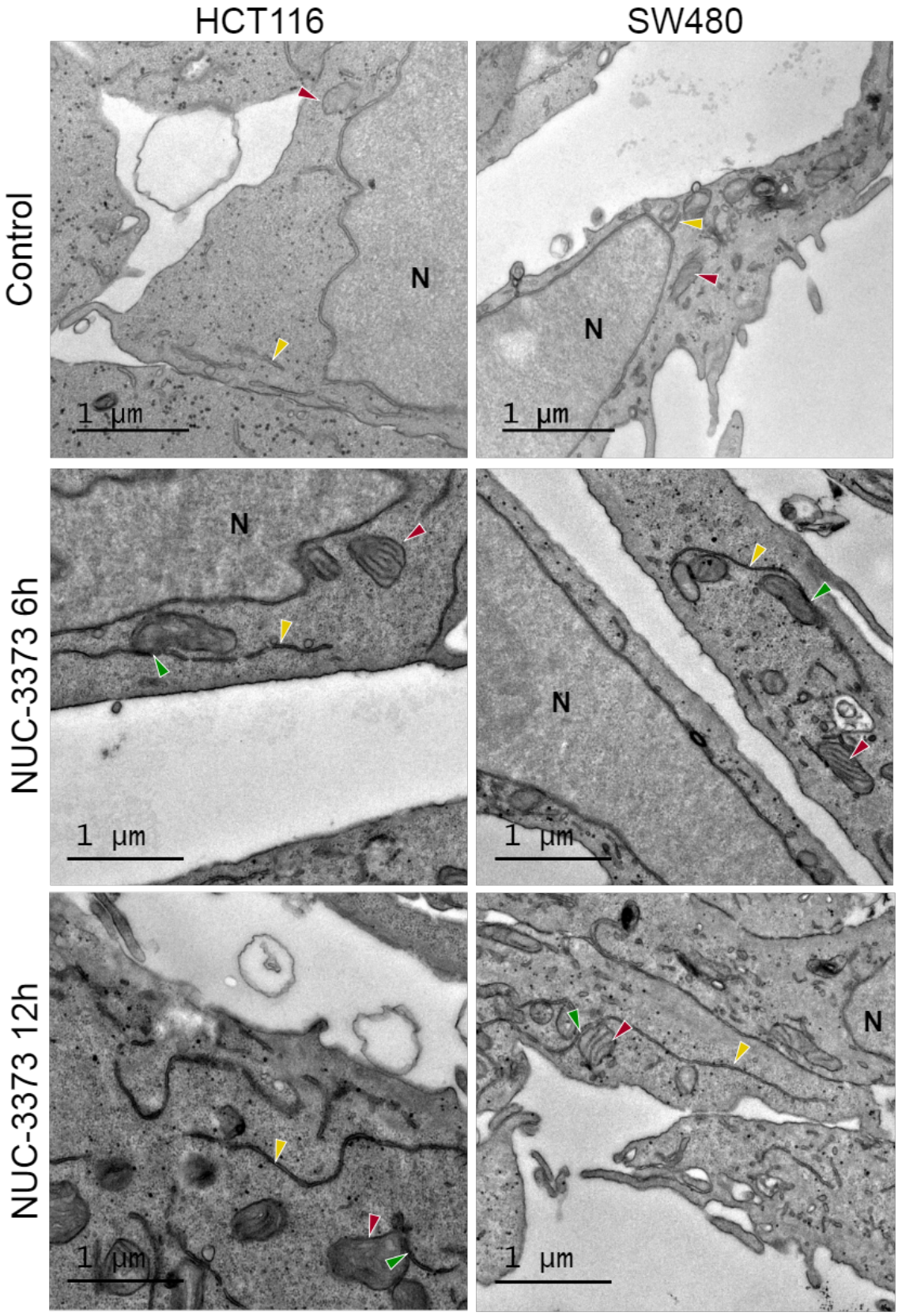

Figure 4.4: Representative micrographs of the effect of NUC-3373 on ultrastructure in HCT116 and SW480 cells. Cells were treated with either 10 μM NUC-3373 for 6 or 12 hours. Red arrows: mitochondria, yellow arrows: ER, green arrows: contact points between ER and mitochondria. Images taken at 3000x magnification on TEM.

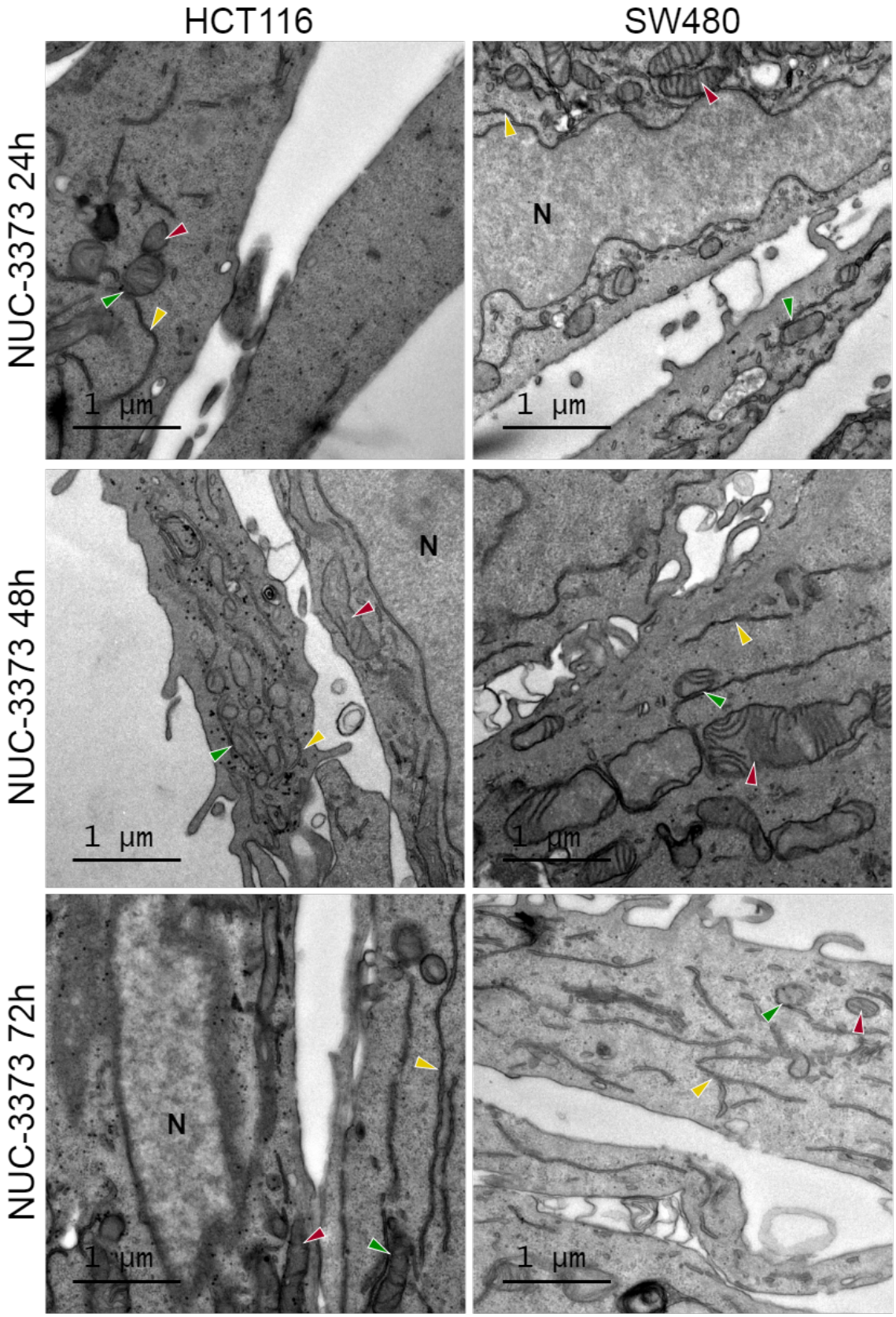

Figure 4.5: Representative micrographs of the effect of NUC-3373 on ultrastructure in HCT116 and SW480 cells. Cells were treated with either 10 μM NUC-3373 for 24, 48 or 72 hours. Red arrows: mitochondria, yellow arrows: ER, green arrows: contact points between ER and mitochondria. Images taken at 3000x magnification on TEM.

Observations of micrographs were not made until after stereological assessment of parameters was complete. Thapsigargin treatment induced an increase in the appearance of mitochondria as well as ER in both HCT116 and SW480 cells (Figure 4.3. Tunicamycin-treated cells had an increase in ER but not as much of an effect on mitochondria as observed with thapsigargin treatment. In NUC-3373-treated HCT116 cells, the ER is visibly increased in diameter, whereas in SW480 cells there is more ER present.

Endoplasmic Reticulum

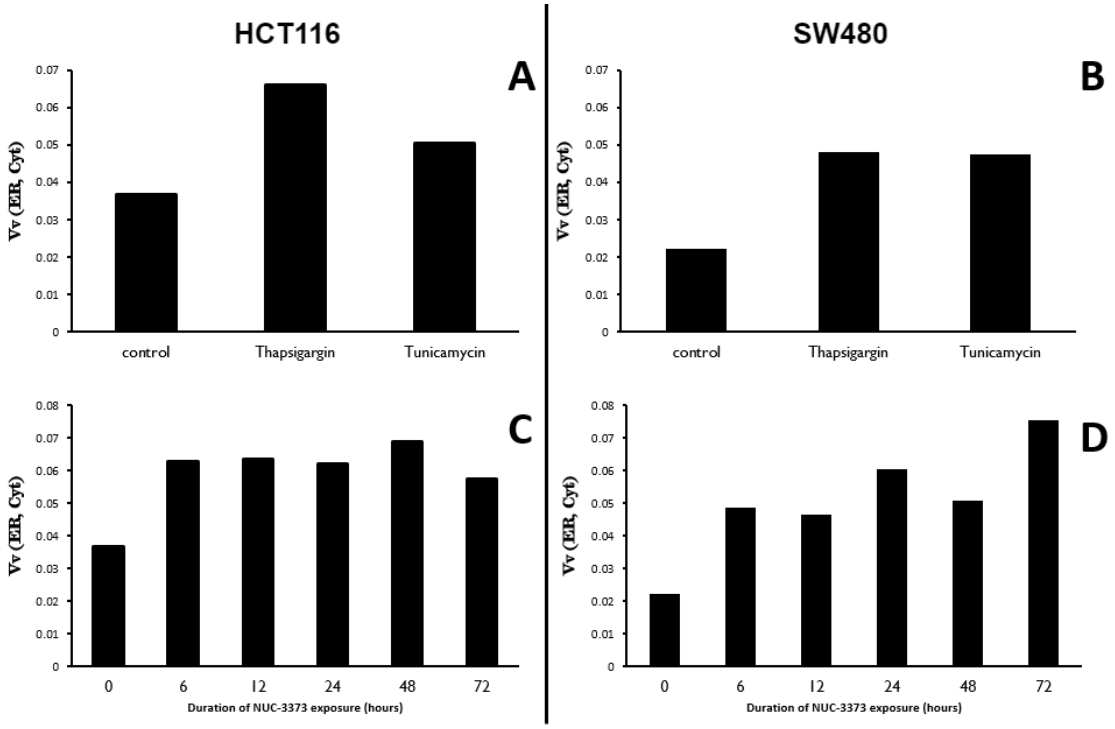

Figure 4.6: Effect of ER stress inducers and NUC-3373 on the volume density of ER in cytoplasm in HCT116 (A and C) and SW480 (B and D) cells. Cells were treated with either 1 μM Thapsigargin or 5 μg/mL Tunicamycin for 5 hours (A and B), or 10 μM NUC-3373 for 6, 12, 24, 48 or 72 hours. Values are the average of two biological replicates for all treatments with the exception of 6, 12 and 72 hour time points for which only one biological sample was assessed. Raw counts for individual photomicrographs can be found in the appendix.

In untreated cells, the volume density of ER in cytoplasm was higher in HCT116 then SW480 cells (Figure 4.6). Treatment with ER stress inducers, thapsigargin and tunicamycin, caused an increase in ER volume density in cytoplasm in both

cell lines but was more marked in SW480 cells. Thapsigargin caused a more potent increase in ER volume density in HCT116 cells than tunicamycin whilst there was very little difference between the effects of thapsigargin and tunicamycin in SW480 cells. SW480 cells experienced almost a two fold increase in ER volume density in response to tunicamycin, compared to only a 20% increase induced in HCT116 cells.

10 μM NUC-3373 was capable of producing changes in ER volume density equalling those of the classical ER stress inducers; thapsigargin and tunicamycin. Treatment of cells with 10 μM NUC-3373 causes a rapid increase in ER volume density in cytoplasm, detectable after only 6 hours (see Figure 4.6). In HCT116 cells this increased volume density remains stable for 48 hours then decreases after 72 hours, although still increased compared to that of the untreated time 0 sample. In SW480 cells, the increase in ER volume density in cytoplasm is more marked, reaching more than double the volume density of the time 0 untreated sample after 6 hours. Unlike HCT116 cells, there is a further increase in volume density after 72 hours.

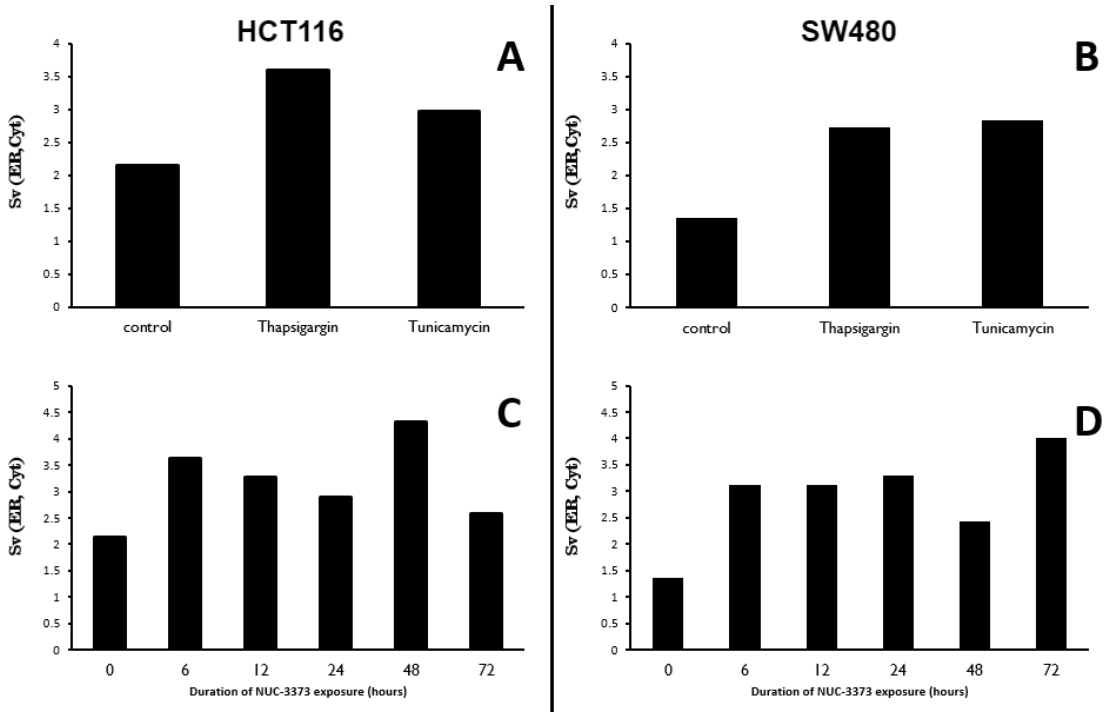

Figure 4.7: Effect of ER stress inducers and NUC-3373 on the surface density of ER in cytoplasm in HCT116 (A and C) and SW480 (B and D) cells. Cells were treated with either 1 μM Thapsigargin or 5 μg/mL Tunicamycin for 5 hours (A and B), or 10 μM NUC-3373 for 6, 12, 24, 48 or 72 hours. Values are the average of two biological replicates for all treatments with the exception of 6, 12 and 72 hour time points for which only one biological sample was assessed. Raw counts for individual photomicrographs can be found in the appendix.

In untreated cells, the surface density of ER in cytoplasm is higher in HCT116 than SW480 cells. Positive inducers of ER stress, thapsigargin and tunicamycin, caused an increase in ER surface density in cytoplasm in both cell lines with HCT116 being more sensitive to the effects of thapsigargin than tunicamycin (Figure 4.7). However, the increase in surface density of ER in response to ER stress inducers was more pronounced in SW480 cells than in HCT116 cells with thapsigargin producing a 2-fold increase in SW480 cells compared with only a 50% increase in HCT116 cells.

Treatment with 10 μM NUC-3373 increased the surface density of ER in cytoplasm after 6 hours in both HCT116 and SW480 cells (Figure 4.7). In HCT116 cells this decreased over the next 18 hours, followed by a sharp increase at 48 hours, returning to the surface density similar to control (time 0) after 72 hours treatment. In SW480 cells, the increase in surface density of ER was not recovered. It remained over 2-fold increased with a small decrease at 48 hours, followed by a sharp increase at 72 hours.

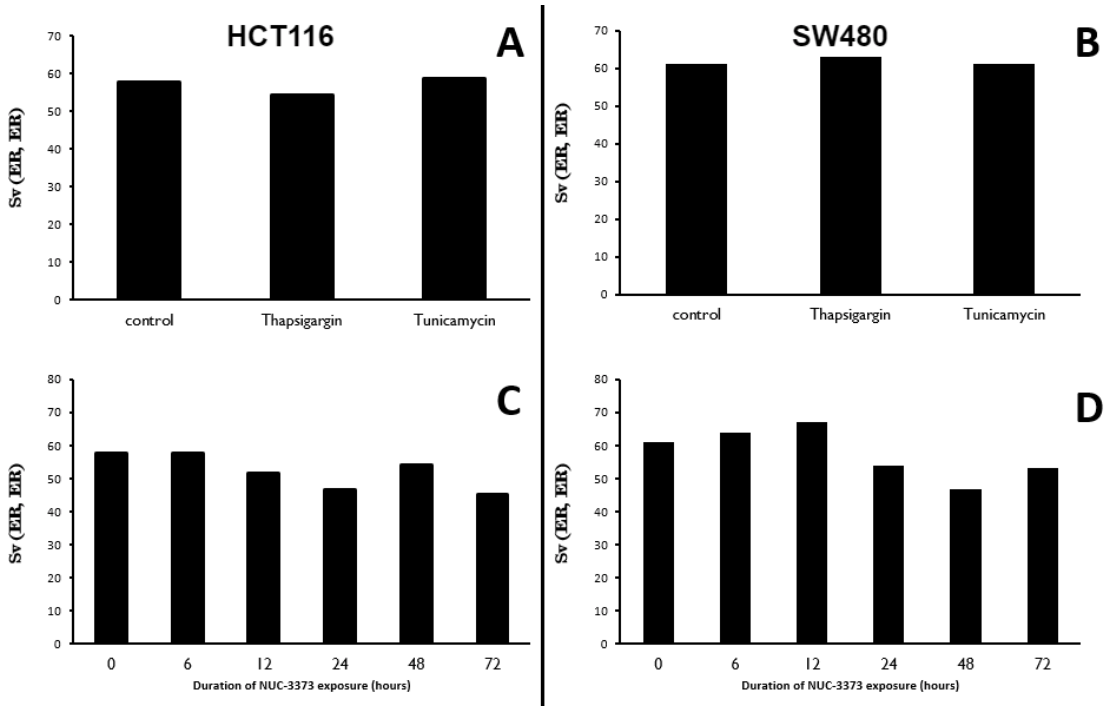

Figure 4.8: Effect of ER stress inducers and NUC-3373 on the surface density of ER in ER in HCT116 (A and C) and SW480 (B and D) cells. Cells were treated with either 1 μM Thapsigargin or 5 μg/mL Tunicamycin for 5 hours (A and B), or 10 μM NUC-3373 for 6, 12, 24, 48 or 72 hours. Values are the average of two biological replicates for all treatments with the exception of 6, 12 and 72 hour time points for which only one biological sample was assessed. Raw counts for individual photomicrographs can be found in the appendix.

In untreated cells, the surface density of ER in ER is very similar in both cell lines (Figure 4.8. Treatment with ER stress inducers had no significant effect on surface density of ER in ER in either cell line.

NUC-3373 treatment caused a small decrease in ER surface density in ER between 6 and 72 hours in HCT116 cells (Figure 4.8). In SW480 cells there was an initial increase over the first 12 hours, which then decreased and plateaued between 24 and 72 hours to less than that of time point 0.

Mitochondria

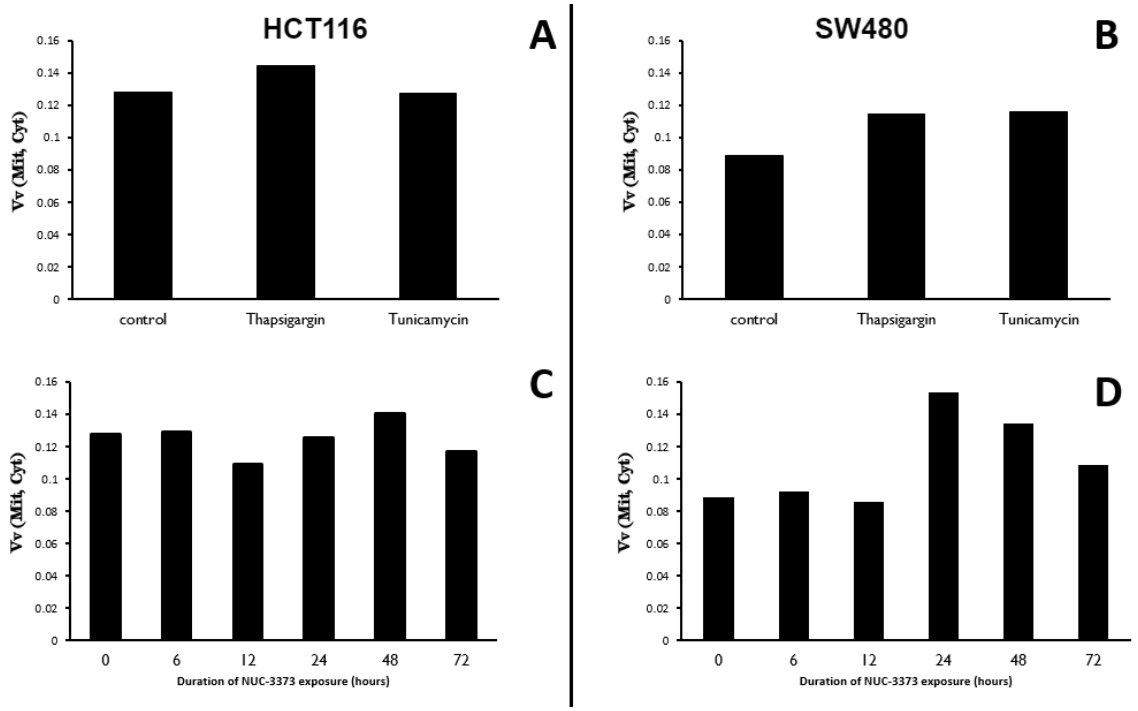

Figure 4.9: Effect of ER stress inducers and NUC-3373 on the volume density of mitochondria in cytoplasm in HCT116 (A and C) and SW480 (B and D) cells. Cells were treated with either 1 μM Thapsigargin or 5 μg/mL Tunicamycin for 5 hours (A and B), or 10 μM NUC-3373 for 6, 12, 24, 48 or 72 hours. Values are the average of two biological replicates for all treatments with the exception of 6, 12 and 72 hour time points for which only one biological sample was assessed. Raw counts for individual photomicrographs can be found in the appendix.

Untreated HCT116 cells have a higher volume density of mitochondria in cytoplasm than SW480 cells. ER stress induction had very minor effects on mitochondria volume. In HCT116 cells only thapsigargin increased mitochondrial volume density,

whilst in SW480 cells the increase evoked by thapsigargin and tunicamycin were both were small.

NUC-3373 had very little influence on the volume density of mitochondria in HCT116 cells, with a small decrease after 12 hours treatment that was recovered by 48 hours. Conversely, in SW480 cells mitochondria volume was constant for the first 12 hours of treatment then increased considerably after 24 hours. Mitochondria volume then recovered to similar to that of time 0 by 72 hours.

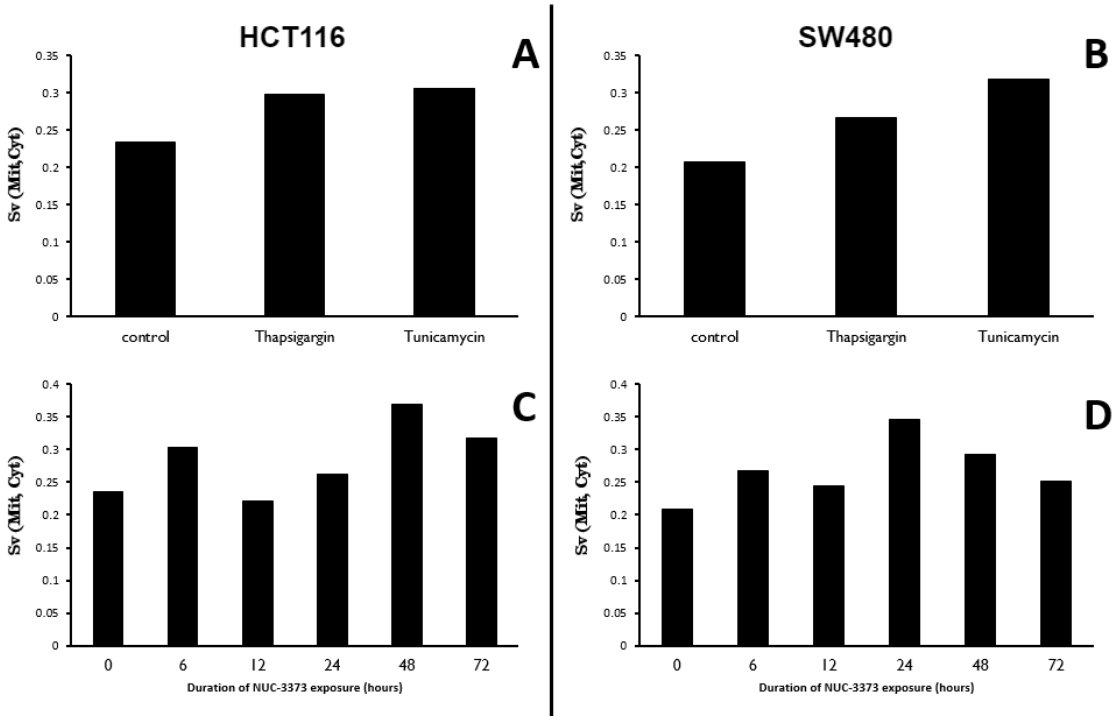

Figure 4.10: Effect of ER stress inducers and NUC-3373 on the surface density of mitochondria in cytoplasm in HCT116 (A and C) and SW480 (B and D) cells. Cells were treated with either 1 μM Thapsigargin or 5 μg/mL Tunicamycin for 5 hours (A and B), or 10 μM NUC-3373 for 6, 12, 24, 48 or 72 hours. Values are the average of two biological replicates for all treatments with the exception of 6, 12 and 72 hour time points for which only one biological sample was assessed. Raw counts for individual photomicrographs can be found in the appendix.

Untreated, the surface density of mitochondria in cytoplasm is marginally higher in HCT116 than SW480 cells. Application of thapsigargin and tunicamycin caused a small increase in HCT116 cells, with no distinction between the two ER stress inducers, whilst SW480 cells were more sensitive to treatment with tunicamycin indicated by a larger magnitude of increase in mitochondrial surface area.

In both cell lines, NUC-3373 appeared to produce a response pattern consisting of two peaks in mitochondria surface density, with the second being larger than the first. The first peak in both cell lines occurred at 6 hours. The second peak occurred at 48 hours in HCT116 cells and 24 hours in SW480 cells. After the second peak, mitochondria surface density decreased in both cell lines.

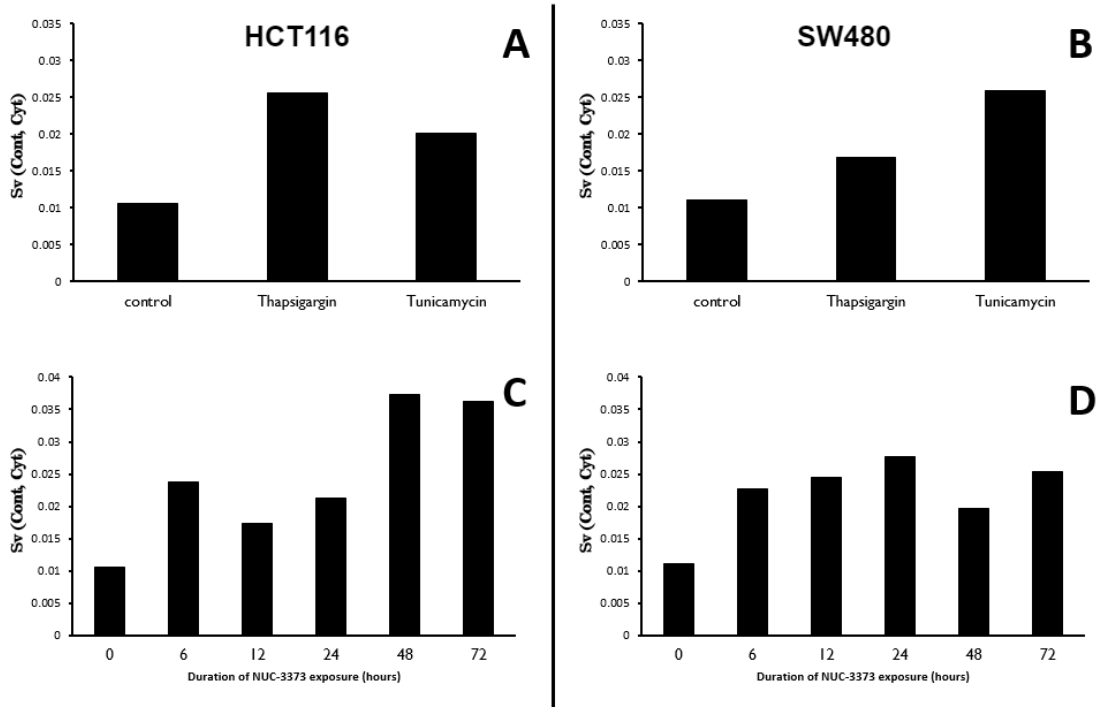

Figure 4.11: Effect of ER stress inducers and NUC-3373 on the surface density of mitochondria contact points with ER in cytoplasm in HCT116 (A and C) and SW480 (B and D) cells. Cells were treated with either 1 μM Thapsigargin or 5 μg/mL Tunicamycin for 5 hours (A and B), or 10 μM NUC-3373 for 6, 12, 24, 48 or 72 hours. Values are the average of two biological replicates for all treatments with the exception of 6, 12 and 72 hour time points for which only one biological sample was assessed. Raw counts for individual photomicrographs can be found in the appendix.

When untreated, the surface density of contact points between mitochondria and ER is similar in both HCT116 and SW480 cells. ER stress inducers cause a marked increase in both cell lines but with HCT116 cells being more sensitive to thapsigargin and SW480 cells being more sensitive to tunicamycin.

NUC-3373 treatment causes a considerable increase in the surface density of contact points with ER in both cell lines. The most pronounced change was in HCT116 cells which experienced a three-fold increase after 48 hours which was maintained at 72

hours. In SW480 cells there was over two-fold increase after 24 hours which then decreased slightly but remained double that observed under control conditions.

4.2.3 Biochemical Changes in Markers of UPR

Activation of the unfolded protein response as a whole was measured by BiP protein expression in whole cell lysates by Western blot. Thapsigargin (Tg) and Tunicamycin (Tu) were used as positive inducers of ER stress (not shown).

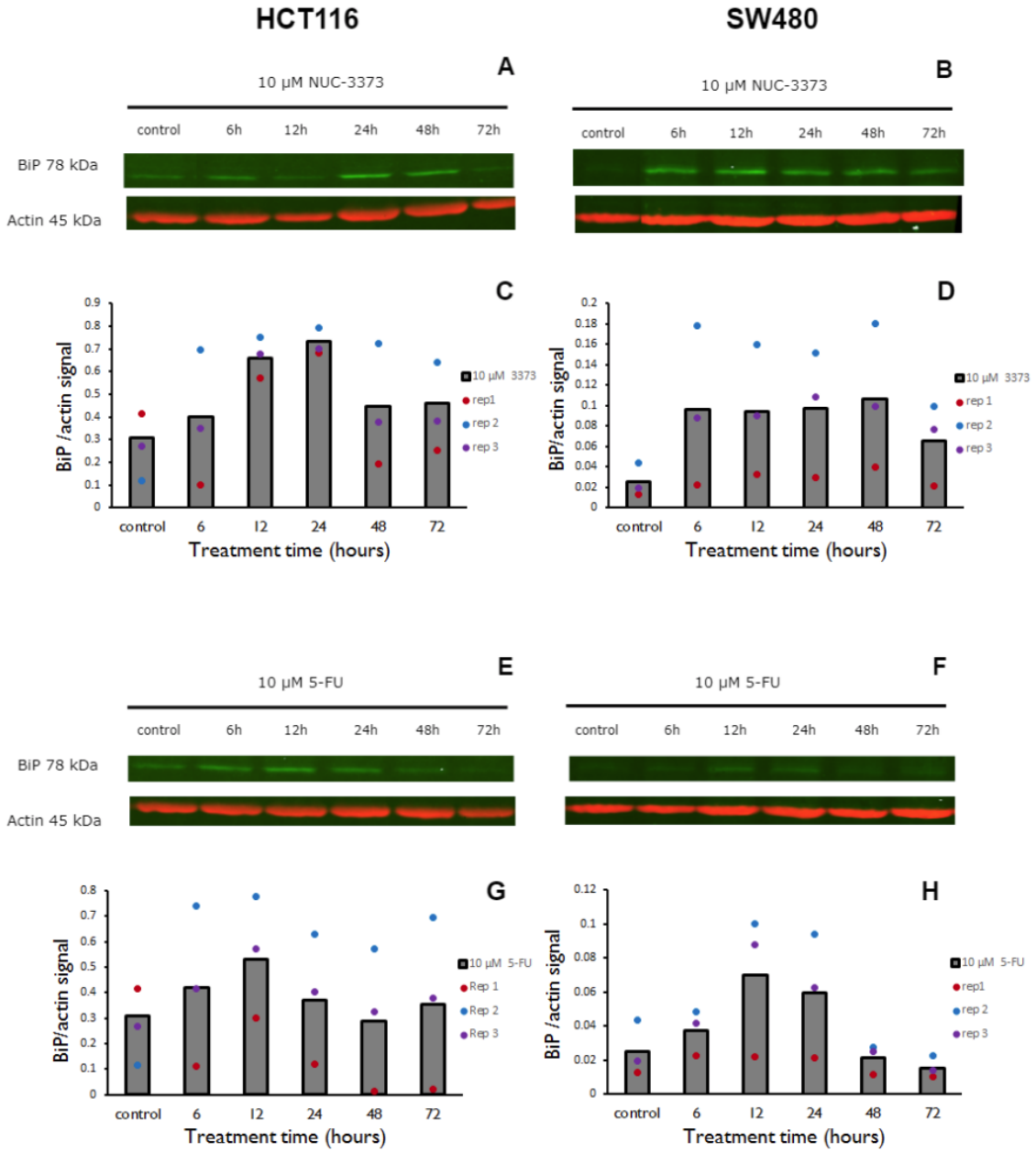

Figure 4.12: BiP expression in whole HCT116 AND SW480 cell lysates. Representative Western blots and quantification of BiP expression in cells treated with 10 μM 5-FU or NUC-3373 for 6, 12, 24, 48 or 72 hours. Red: β-actin loading control, Green: BiP. A and C: NUC-3373-treated HCT116 cells, B and D: NUC-3373-treated SW480 cells, E and G: 5-FU-treated HCT116 cells, F and H: 5-FU-treated SW480 cells. Data presented is representative with the average of 3 biological replicates plotted as a bar whilst each biological replicate is displayed as a scatter point.

Basal BiP expression in HCT116 is very low but still detectable by western blot (Figure 4.12). Treatment with 10 μM 5-FU results in a small increase in BiP protein expression after 12 hours (less than 20% increase from control) which then decreases until 48 hours with a small increase at 72 hours. Treatment with 10 μM NUC-3373

causes more pronounced induction of BiP protein compared with 5-FU. After 12 hours there is a sharp increase, which peaks at 24 hours to almost double that expressed in the control. BiP expression then falls to levels comparable to the untreated control for the rest of the treatment duration.

Similar to HCT116 cells, there is a very low basal expression of BiP in SW480 cells. Treatment with 10 μM 5-FU causes a small decrease in BiP expression after 6 hours which is then recovered, reaching peak expression after 12 hours. This small but detectable induction of BiP is maintained until 24 hours then decreases to expression levels less than 50% of that observed in untreated cells by 48 and 72 hours. NUC-3373 causes a much larger induction of BiP compared with 5FU. After 6 of hours treatment, BiP expression is double that detected in the control. This is maintained for 48 hours them falls to expression levels comparable to control at 72 hours.

The UPR induced by NUC-3373 is much more potent than that of 5-FU. In HCT116 cells, the UPR is not as sustained for as long as it is in SW480 cells.

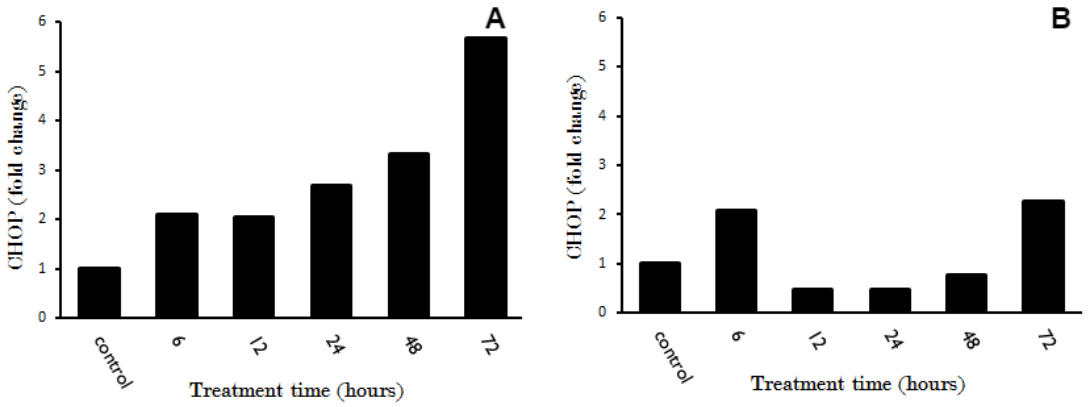

Figure 4.13: CHOP gene expression in (A)HCT116 cells and (B) SW480 cells treated with 10 μM NUC-3373 for 6, 12, 24, 48 and 72 hours. CHOP expression was measured as fold change relative to untreated control, derived from Ct values. Housekeeping gene used was GAPDH. $N_{biological}$=1, $N_{technical}$=3

In HCT116 cells, treatment with 10 μM NUC-3373 causes a prominent increase in CHOP gene expression over the duration of 72 hours treatment (Figure 4.13). After 6 hours, CHOP gene expression is doubled then rises between 12 and 48 hours

before reaching over 5x the expression observed in control by 72 hours treatment. In contrast, NUC-3373 treatment has very minor effects on CHOP gene expression in SW480 cells. There is doubling in expression after 6 hours, after which point expression is suppressed until the 72-hour time point at which it increases. These data would suggest that the ER stress induced by NUC-3373 in HCT116 cells drives cells further towards apoptosis whilst in SW480 cells there is a pro-survival response. This can also be reflected in the BiP expression described previously, with a more prolonged UPR in SW480 cells.

4.3 Discussion

The volume of ER in comparison to cytoplasm increases in both cell lines but the effect is more profound in SW480 cells. In HCT116 cells this is not accompanied by the vast increase in surface area of ER in cytoplasm observed in SW480 cells. By combining these parameters to measure ER packing density (the surface density of ER in ER) it is evident that SW480 cells undergo initial swelling of the ER which is followed by a sharp decrease in packing density indicative of proliferation of ER. These changes in HCT116 are not so pronounced, indicating that they adapt to ER stress by distension of the ER (Figure 4.14). Proliferation of the ER membrane in SW480 cells may be serving to accommodate more protein folding machinery, thus increase protein folding capacity, allowing recovery from ER stress. This may account for their lesser sensitivity to NUC-3373 and could present as a potential resistance mechanism for future drug insult.

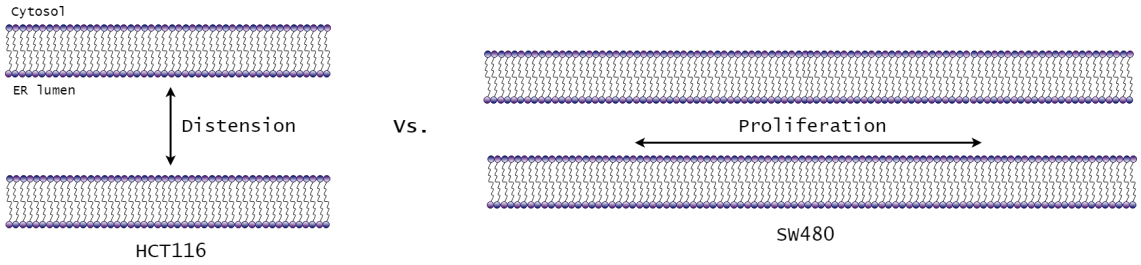

Figure 4.14: Distension in HCT116 cells versus proliferation in SW480 cells of the ER membrane in response to ER stress.

4.3.1 Ultrastructural Changes

To date, the mechanism by which the ER lumen distends remains elusive. Ueda, M., *et al.*, (2016) found evidence for polyglutamine expansion protein being embedded in the ER membrane. In these cells there was ER distension as well as lengthening of the mitochondrial contact points with ER, however it remains unclear whether there is a direct relationship between these distortions and embedding of polyglutamine expansion protein. Prevalence of cancers has been reported to be lower in patients with polyglutamine diseases (Coarelli, G., *et al.*, 2017) but skin cancer was an exception to this finding where instance was higher.

Like distension, there is not an abundance of literature available regarding proliferation of rough endoplasmic reticulum (RER). Ultrastructural studies have instead focussed on hypertrophy of the smooth endoplasmic reticulum (SER) membrane in liver cells in response to drug administration, the most classic inducer being phenobarbital. TEM has been used to detect these changes from as early as 1966 (Meldolesi, J., *et al.*). It has been found that SER in hepatocytes is dynamic in nature and proliferates in response to various drugs to meet demands with excess then being degraded by autophagy upon removal of the drug and recovery of the cell (Pavelka, M. and Roth, J., 2010).

It is yet to be established whether distension or proliferation of ER membrane precedes UPR or vice versa. The ER membrane is composed of a phospholipid

bilayer, with the most abundant phospholipid being phosphatidylchoine (Lykidis, A., and Jackowski, S., 2000). The UPR controls transcription of many enzymes involved in phospholipid synthesis, including phosphatidylcholine. Sriburi, R., *et al.* (2004) found that overexpression of the spliced variant of XBP-1 (XBP-1(s)) in NIH-3T3 fibroblasts induces synthesis of phosphatidylcholine (see Figure 4.15). In cells overexpressing XBP-1(s) an increased surface area and volume of RER was detected, as well as enhanced activity of the cytidine diphosphocholine pathway of phosphatidylcholine biosynthesis, suggesting that XBP1(S) is the link between UPR and ER biogenesis.

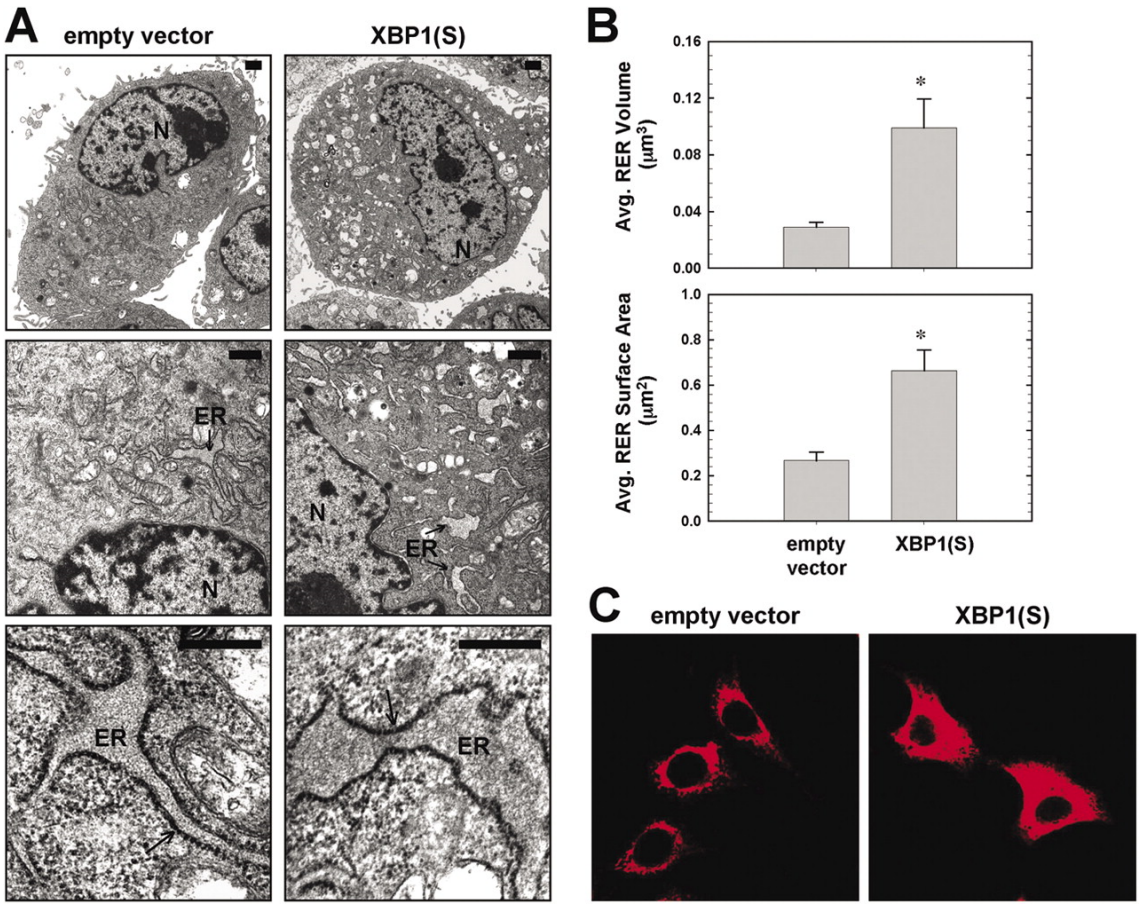

Figure 4.15: Overexpression of XBP-1(s) induces synthesis of phosphatidylcholine and increases RER content in fibroblasts. TEM analysis of ER. Taken from Sriburi et al., 2004.

Activation of the IRE-1 branch of the UPR results in the splicing of a 26-nucleotide intron from XBP-1 mRNA in the cytosol which encodes a functionally active protein: XBP-1(s) (Yoshida, H., *et al.*, 2001). XBP-1(s) acts as a potent transcriptional

activator of UPR-related genes (Calfon, M., *et al.*, 2002; Lee, K., 2002) by translocating to the nucleus and binding to target sequences in regulatory regions of the chaperone genes (Shen, X., *et al.*, 2001). Lee, A., *et al.* (2003) reported that XBP1 regulates the expression of only a subset of UPR target genes such as ERdj4, p58IPK, EDEM, RAMP-4, PD1-P5 and HEDJ. It is therefore not surprising that XBP-1(s) has been reported to be implicated in tumorigenicity, tumour invasion, as well as evading cancer from the immune system.

Mhaidat, N.M., *et al.*, (2015) assessed the expression of vascular endothelial growth factor (VEGF)-R2 and XBP-1(s) expression in relation to invasiveness. Knockdown of XBP-1(s) using siRNA down-regulated invasiveness of HCT116 and SW480 cells. In addition, knockdown of XBP-1(s) was accompanied by down-regulated protein expression of VEGF-R2, suggesting a role for XBP-1(s) in the transcriptional regulation of VEGF-R2 and therefore angiogenesis. However, this is contrary to the conclusions drawn by Romero-Ramirez, L., *et al.* (2004), who reported that loss of XBP1 had little effect on the secretion of VEGF and therefore is not a determinant of the angiogenic capability of cancer. The comparison of these two studies does not make either redundant, however, as one reported whole cell lysate expression of VEGF-R2 and the other secretion of VEGF by ELISA on cell supernatant samples. Linking the methodologies used in both studies would hopefully prove informative in elucidating this debate. Interestingly, in the selection of CRC cell lines studied by Mhaidat *et al.*, HCT116 was found to have the lowest XBP-1(s) protein expression and SW480 the highest. Taking this into account, alongside the finding by Sriburi (2004) that XBP-1(s) may be responsible for RER proliferation, compliments the ultrastructural data obtained in this thesis regarding the proliferation of SW480 ER and not HCT116. This may indicate that a cell's phospholipid synthesis capability and the consequences this has for proliferation of ER may be a determinant of its invasiveness, metastatic potential and sensitivity to drugs that elicit an ER stress response.

Due to the major roles of ER in the cell including (but not limited to) protein folding, phospholipid biosynthesis and Ca^{2+} storage and buffering, it requires the ability

to communicate with other organelles, especially during a coordinated response to stress (van Vilet, A., and Agostinis, P., 2017). Through the action of non-vesicular specific lipid-transfer-proteins 'LTPs', shuttling of phospholipids over the 10 nm cytosolic gap between the ER and an acceptor compartment can occur. It is believed that these LTPs may have specific targeting determinants that interact with other membrane components on the donor and acceptor compartments.

It has been long-known that there is a connection between the membranes of mitochondrial and ER membranes. In 1969, Ruby, J.R. *et al.*, described instances of continuity between mitochondrial and ER membranes, establishing an open channel between these two organelles. Since, the functional significance of this connection has been extensively studied. By 1990, so-called mitochondria-associated membranes or 'MAMs' had been fully discovered as a biochemical entity after being isolated through cell fractionation (Vance, J.E., 1990). In this study, the most notable ultrastructural change observed and quantified in mitochondria was the increase in surface density of mitochondria contact points with ER, which could be described as MAMs. The observation by Sriburi (2004) that overexpression of XBP1(s) induces synthesis of PtdCho and increases RER would implicate MAMs. The majority of phospholipid biosynthesis takes place on ER membranes (Vance, J.E., and Vance, D.E., 1988; van Golde, L.M.G., *et al.*, 1971; van Golde, L.M.G., *et al.*, 1974; Jelsema, C.L. and Morré, D.J., 1978), however there are a number of phospholipid-biosynthetic enzymes that are expressed exclusively in the mitochondria (van Meer, G., 1989; Daum, G., 1985; van de Bosch, H., 1974). This indicates that some cross-talk is required between ER and mitochondria in order to synthesise phospholipids. Depicted in Figure 4.16, Phosphatidylserine 'PtdSer' is formed in the ER then transported to mitochondria. It is then transported to the inner mitochondrial membrane (IMM) where it becomes the substrate for PtdSer-decarboxylase to produce Phosphatidylethanolamine 'PtdEth'. PtdEth is shuttled back to the ER where the synthesis of Phosphatidylcholine 'PtdCho' can be completed by the action of PtdEth-methyltransferases 1 and 2 (Voelker, D.R., 1989).

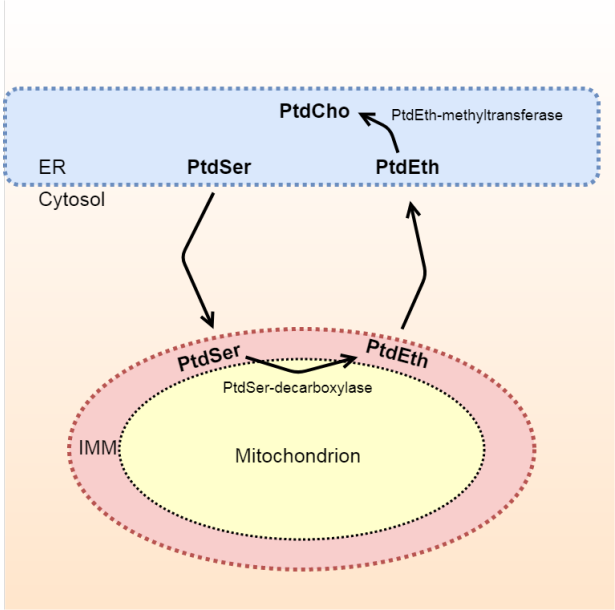

Figure 4.16: Phospholipid Biosynthesis takes place in the ER and mitochondria.

The most widely known role of mitochondria is probably as the 'powerhouse' of the cell. Adequate folding of proteins in the ER demands high energy in the form of ATP. It has been shown that tunicamycin-induced ER stress results in mitochondria relocating to associate with rough ER (Bravo, R., *et al.*, 2011). This complements the data shown in this thesis, with tunicamycin-treated cells exhibiting a potent increase in mitochondrial contact points with ER. Interestingly, NUC-3373 induced an increase in contact points comparable to that of the classical ER stress inducer. Whether increased mitochondrial contact points with ER is pro-survival or pro-apoptosis may depend on which arm of the UPR is predominant. Although increased ATP provision may allow the demands of the stressed ER to be met, it has been shown that activation of the PERK-ATF4 axis of the UPR may favour apoptosis. Chami, M., *et al.*, (2008) showed that a truncated variant of the sarco/endoplasmic reticulum Ca^{2+} ATPase 1 (S1T) localises to MAMs during ER stress, causing mitochondrial Ca^{2+} overload and inhibition of mitochondrial movement and eventual apoptosis. This induction of S1T required activation of the PERK-ATF4 arm of the UPR. Further confirming the involvement of PERK-ATF4 in mitochondrial contact site-mediated apoptosis, Verfaillie, T., *et al.*, (2012) found

that genetic ablation of PERK in MEF cells interrupted ER MAMs and provided protection from apoptosis induced by ER stress-causing agents.

4.3.2 Biochemical changes complement ultrastructure

In NUC-3373-treated HCT116 cells, mitochondria and ER contact points are dramatically increased at 48 and 72 hours. It has been said that increase in MAMs is a response during the early adaptive phases of ER stress but, considering the findings of Chami *et al.* and Verfaillie *et al.*, it may be that this adaptation is in response to the PERK-ATF4 axis. ATF4 expression would need to be assessed to confirm this. Indeed, when considering data for BiP expression at these time points, in which there is a decrease, it supports mitochondrial contact sites with ER being pro-apoptotic. Further corroborating this is the rich expression of CHOP, the pro-apoptotic marker downstream of ATF4. Additional studies would be required to confirm this, but the evidence is quite compelling.

The expression of BiP and CHOP in both cell lines in response to NUC-3373 treatment appeared to have a complementary relationship, mirroring each other's expression. This suggests a fine balance between pro-survival activities, such as ER proliferation in SW480 cells, and apoptosis. As this study only measured the UPR activation (by BiP protein expression) and terminal ER stress (by CHOP gene expression), little can be said regarding the arms of the UPR that are predominant and mediating the cellular response to NUC-3373-induced ER stress. Therefore, downstream molecular targets for combination therapy to potentiate these effects could not be addressed at present. However, phospho-eIF2α and ATF6 expression were studied by Western blot (data not shown), but with no success. It is unclear whether no signal was detected due to the expression being too low or it being a methodological problem such as failure of antibodies, therefore positive controls should be used to validate these antibodies prior to probing samples.

Future studies should investigate the individual axes downstream of the UPR

activation, in order to complement and underpin the mechanisms which may harness ultrastructural changes. Unveiling these factors could lead to the possibility of identification of targets for combination therapy to potentiate ER stress induced by NUC-3373. Targeting the UPR in cancer is problematic due to the dual roles of the signalling axes in preventing or potentiating apoptosis (Ojha, R., *et al.*, 2017). Further complicating matters is the apparent context-dependent nature of their actions, meaning that treatment would require to be highly personalised and targeted in order to achieve any therapeutic benefit.

4.3.3 Chapter Summary

The response of ER to stress conditions has been frequently studied by TEM, however very few studies utilise unbiased stereology in their assessments. This lends the possibility to biased and inaccurate reporting of results. Here, it has been shown that robust, extensive and unbiased sampling can be used to reliably identify changes in ultrastructure. It must, however, be noted that this study is only based on two biological replicates with 30 micrographs for each condition. It would be prudent to carry out more biological replicates in order to ensure parameter measurements are as close as possible to the (unknown) true value, which could also be established by the study of serial sections. In addition, assessment of features relies on the ability of the observer to accurately identify organelles which in some micrographs can be more obscure. This could potentially lead to inter observer variability so future studies could utilise a second observer. Also, it would be beneficial to design an algorithm in automated image analysis software to recognise organelles, however this would require rigorous testing due to the heterogeneity of morphology/angles/sections etc. Manual counting of line and point intersections with organelles is laborious and time-consuming so this could save valuable time, allowing more replicates to be conducted and therefore more robust and reliable measurements.

A previously mentioned, study by Yadunandam, K., *et al.*, (2012) demonstrated ER stress induced by 5-FU in Sk-Hep1 Hepatocellular carcinoma cells. However, the

concentration of 5-FU used was 50 μg/mL (384 μM). This study has shown that ER stress is inducible by NUC-3373 at clinically translatable concentrations which releases the potential for a host immune response to cancer cells, to be explored in the next chapter.

Chapter 5

The Distressed Cancer Cell

5.1 Introduction

The previous chapters have established that NUC-3373 treatment results in an induction of TS protein that appears to translocate to the cytoplasm, as well as a profound induction of the UPR in response to ER stress which differs between the sensitive (HCT116) and less sensitive (SW480) cell lines. This chapter will set out to address these aspects to further elucidate the apparent additional mechanism of action of NUC-3373 and the possibilities this may lend itself to, particularly an immune response.

5.1.1 Damage Associated Molecular Patterns and Immunogenic Cell Death

Activation of the UPR has been linked to inflammatory pathways by activation of NF-κB through PERK-eIF2α-mediated translational attenuation (Cubillos-Ruiz., J.R., *et al.*, 2017) as well as the culmination of secreted pro-inflammatory cytokines such as the Interleukin family and tumour necrosis factor (Grivennikov, S.I., *et al.*, 2010).

The type of cell death induced by agents has consequences for the outcome of therapy. For example, apoptosis is deemed to be an immunologically disparate process thus termed 'physiological apoptosis'. Conversely, a necrotic death implicates a pro-inflammatory pathway which facilitates pro-tumorigenic processes (Poon, I.K., *et al.*, 2014). Some chemotherapeutic agents, such as oxaliplatin, have now been reported to heighten the immunogenic potential of dying cancer cells by a so-called 'immunogenic cell death', with induction of ER stress being a prerequisite (Tesniere, A., *et al.*, 2008).

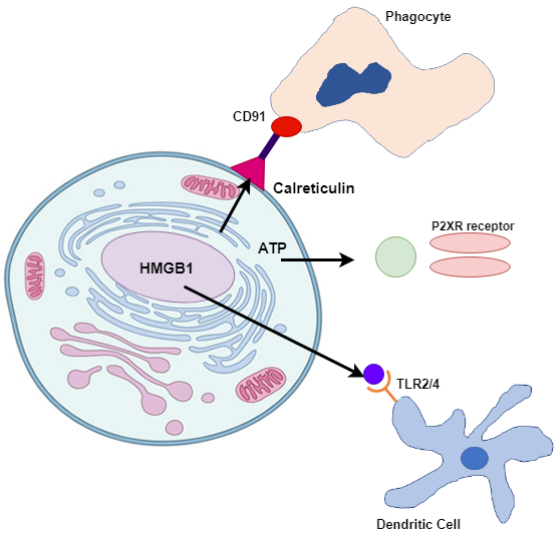

Figure 5.1: The release of DAMPs to induce ICD. Self-generated figure.

Damage-associated molecular patterns 'DAMPs' are distinct molecules, usually with housekeeping roles, that are released or expressed on the cell surface to act as a danger signal (see Figure 5.1). They elicit an immune response by binding to pattern recognition receptors, often on dendritic cells. DAMPs are spatiotemporally sensitive during cell death. During the early apoptotic phase, cell surface exposure of the ER chaperone calreticulin presents as an 'eat-me' signal to Alpha-2-macroglobulin (CD91) receptors on phagocytes thus inducing engulfment of dying cancer cells. Heat shock proteins-70 and -90 can also act in this manner (Garg, A.D., *et al.*, 2014). During pre-apoptotic or early/mid-apoptotic phases, active or passive secretion of ATP has a two-pronged role. It can either be perceived as a

'find-me' signal for monocytes or it can act as a pro-inflammatory molecule through binding to purinoceptor 7 (P2X7) receptors on immune cells (Ghiringhelli, F., *et al.*, 2009). During late apoptosis, high mobility group box protein 1 'HMGB1' is passively released and binds to toll-like receptors 'TLR'-2 and -4 on dendritic cells, resulting in the production of pro-inflammatory cytokines as well as antigen presentation (Apetoh, L., *et al.*, 2007).

The establishment of this juxtaposition between the dying cancer cells and the immune system creates a milieu ideal for the invocation of T-cell-mediated immune responses which are capable of eliminating residual cancer cells and endowing an immunological memory (Krysko, D.V., *et al.*, 2012).

5.1.2 PD-L1

Tumours must adapt to their hostile micro-environment to survive. This includes mechanisms to avoid immune surveillance, such as exploitation of immune checkpoint pathways. One mechanism in which cancer cells can evade an immune-mediated death is by expressing programmed death ligand 'PD-L1' on their surface which binds to PD-1 receptors on T cells. PD-L1 normally acts as an 'off switch' to protect healthy cells from attack by the immune system. Interaction of PD-1 with PD-L1 on tumour cells causes T-cell dysfunction and exhaustion and subsequent weakened cytotoxic activity (Sun, Z., *et al.*, 2015). Over-expression of PD-L1 by cancer cells therefore functions to protect against cytotoxic T-cell (CD8+)- mediated cell killing (Zou, W., and Chen, L., 2008). Monoclonal antibody therapies have been developed to target either PD-1 or PD-L1 in order to prevent this mechanism of evasion of the immune system by cancer cells. Nivolumab and Pembrolizumab were approved by the FDA in 2014 (Gong, J., *et al.*, 2018) with research and development into anti-PD-1/PD-L1 therapies gaining interest since. If NUC-3373 is capable of inducing an immunogenic cell death, then this effect could be abolished by the expression of PDL-1 on the cancer cell surface. Therefore, it is pertinent to investigate this and to consider combination with PDL-1 checkpoint

inhibitors if this is the case.

5.1.3 Aims and Objectives

This chapter will seek to establish whether free TS or TS ternary complexes are responsible for NUC-3373-induced ER stress. This will be investigated by using short interfering RNA against TYMS, the gene that encodes for TS protein. In order to ensure that the thymine-depleted state is not responsible for ER stress induction, cells will be supplemented with thymidine to allow dTMP to be synthesized via the salvage pathway.

To investigate the release of DAMPs, the expression of HMGB1 will be assessed by immunocytochemistry linked to fluorescence to determine whether there is a nuclear loss of the protein. Calreticulin and HSP70/90 surface expression on cells will also be investigated in the same way.

PDL-1 expression will be assessed both by ICC and IF as well as by Western blot and ELISA on whole cell lysates and conditioned medium from NUC-3373-treated cells.

5.2 Results

5.2.1 Effect of TS knock-down on ER stress

siRNA against TYMS, the gene encoding TS protein, was used to knock down TS in order to assess whether it, or its ternary complexes, play a role in the ER stress induced by NUC-3373 treatment. Cells were supplemented with 8 μg/mL thymidine in order to prevent death and to assess ER stress independently of a thymineless state and DNA damage. Non-silencing 'scrambled' siRNA was used as a transfection control. The transfection protocol was adapted from a single transfection on day

0 to transfection every 24 hours to accommodate for the proliferation of cells and resultant transient knock-down.

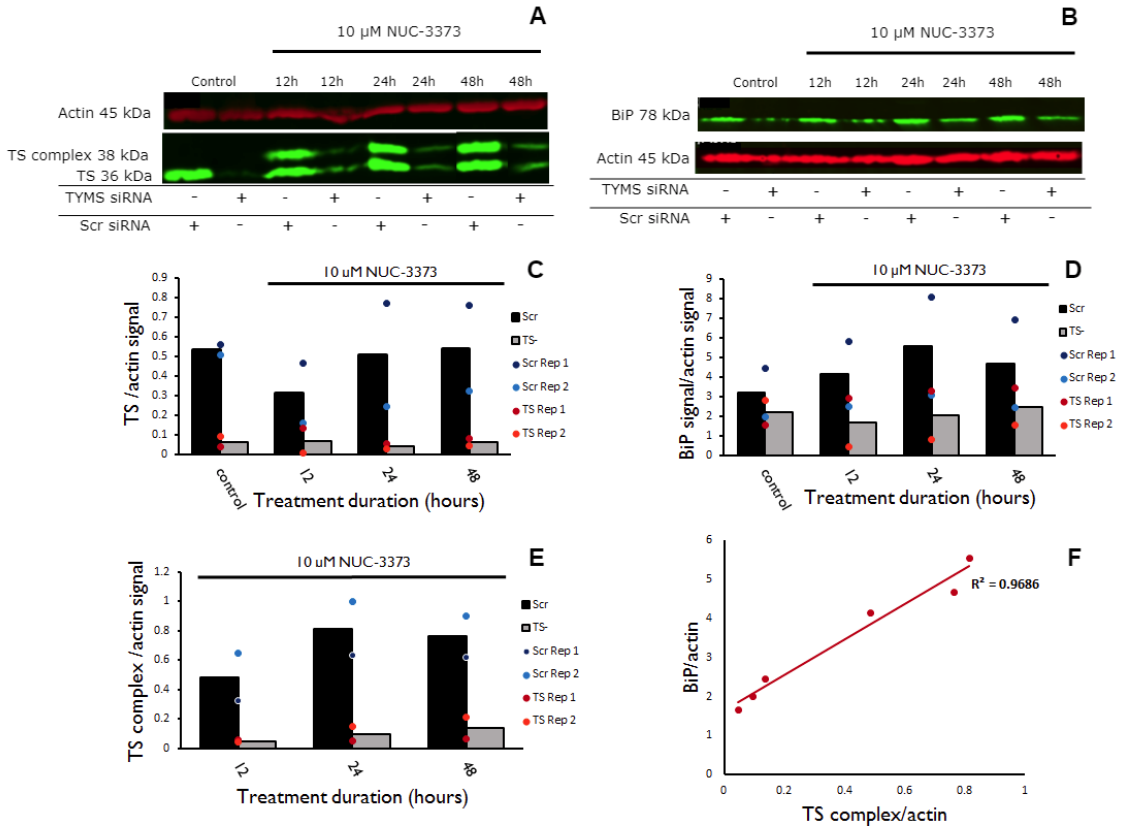

Figure 5.2: BiP in HCT116 cells subjected to siRNA knock-down of TS. A: Representative Western blot of TS protein expression in cells treated with 10 μM NUC-3373 for 12, 24, or 48 hours in the presence and absence of TS knock-down. Red: β-actin loading control, Green: TS. B: Representative western blot of BiP protein expression in cells treated with 10 μM NUC-3373 for 12, 24, or 48 hours in the presence and absence of TS knock-down. C: quantified free TS expression, D: quantified BiP expression, E: quantified TS complex expression, F: BiP vs. TS and TS complex expression. Averages of biological replicates are displayed as bars. Individual biological replicates are plotted as individual scatter points. $N_{biological}$=2, $N_{technical}$=2

Considerable knock-down of TS was achieved in HCT116 cells (Figure 5.2). Re-transfection every 24 hours achieved sufficient knock-down of TS for the duration of the longest NUC-3373 treatment time of 48 hours. BiP protein expression is considerably down-regulated in HCT116 cells subjected to TS knock-down, when compared with scrambled siRNA controls. When quantified BiP was plotted against TS ternary complex expression, a positive linear relationship was found, indicated by an R^2 value of 0.9686. There was a positive relationship between BiP and TS

expression, however the correlation was very weak. This suggests that TS complexes may play a role in the induction of UPR by NUC-3373 in HCT116 cells. An additional observation was that BiP expression was up-regulated in untreated cells in the presence of non-targeting siRNA, indicating that the transfection procedure may have induced an unfolded protein response. Furthermore, TS knock-down abolished the UPR in response to NUC-3373-induced ER stress instead of reducing it, as indicated by the lack of BiP induction with NUC-3373 treatment of these cells. This proposes that, regardless of treatment with NUC-3373, TS may play a role in BiP regulation.

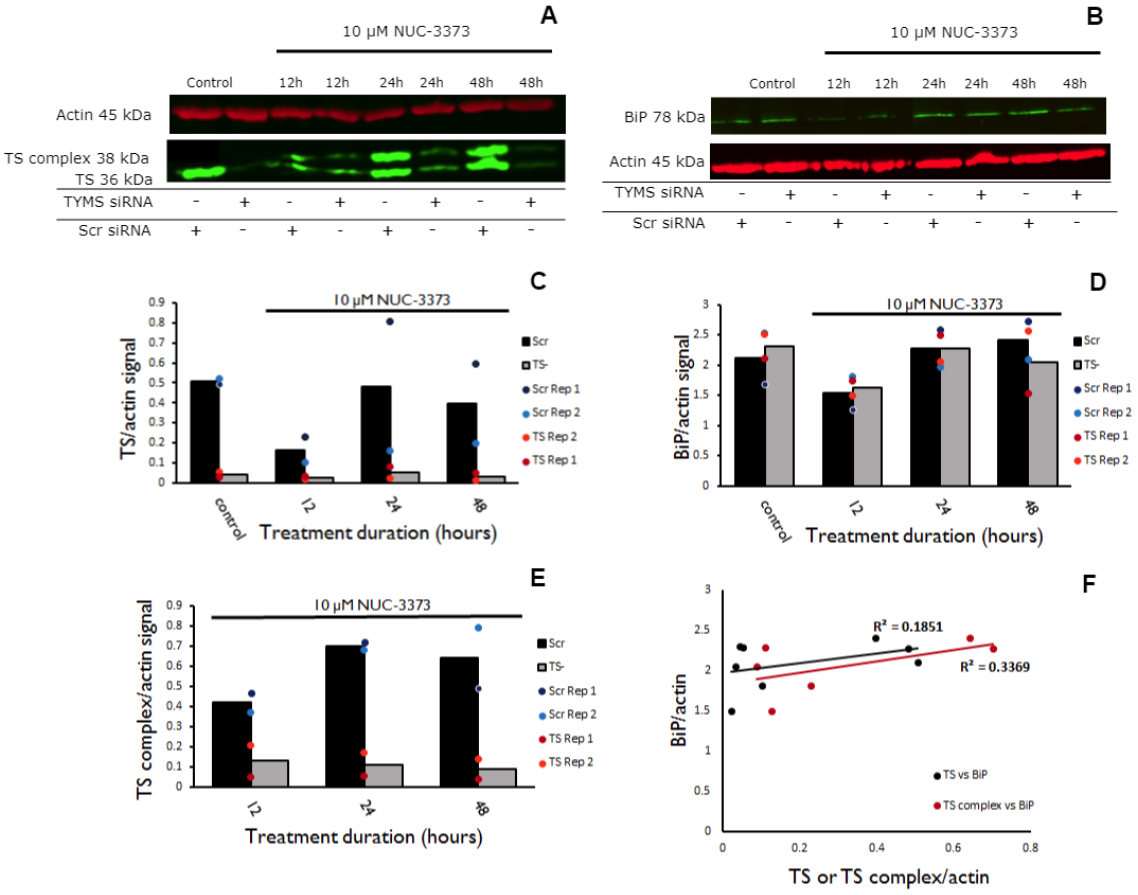

Figure 5.3: BiP in SW480 cells subjected to siRNA knock-down of TS. A: Representative Western blot of TS protein expression in cells treated with 10 μM NUC-3373 for 12, 24, or 48 hours in the presence and absence of TS knock-down. Red: β-actin loading control, Green: TS. B: Representative western blot of BiP protein expression in cells treated with 10 μM NUC-3373 for 12, 24, or 48 hours in the presence and absence of TS knock-down. C: quantified free TS expression, D: quantified BiP expression, E: quantified TS complex expression.F: BiP vs. TS and TS complex expression. Averages of biological replicates are displayed as bars. Individual biological replicates are plotted as individual scatter points. $N_{biological}$=2, $N_{technical}$=2

In SW480 cells, knock-down of TS was also successful (Figure 5.3). However, in contrast to HCT116, BiP did not appear to be affected by loss of TS or TS ternary complexes, with there being very little linear correlation between the two sets of values. It is important to note that the pattern of BiP protein expression in the scrambled control samples here is different to that observed in non-siRNA experiments of Chapter 4. This indicates that the transfection itself may have an effect on the unfolded protein response. In future studies, non-siRNA samples should be prepared in tandem to ensure trasnfection is not producing any unintended modifications to cells. Regardless, the UPR of cells to NUC-3373 is not altered by depleting TS and TS complexes, pointing to other factors relating to NUC-3373 treatment contributing to ER stress in these less sensitive cells.

5.2.2 Damage Associated Molecular Patterns

High mobility group box protein 1

HMGB1 protein can be passively released from cells in the late stages of apoptosis so was assessed in HCT116 and SW480 cells treated with 10 μM NUC-3373 for 24 or 48 hours by immunofluorescence. All images are representative of the cell population studied.

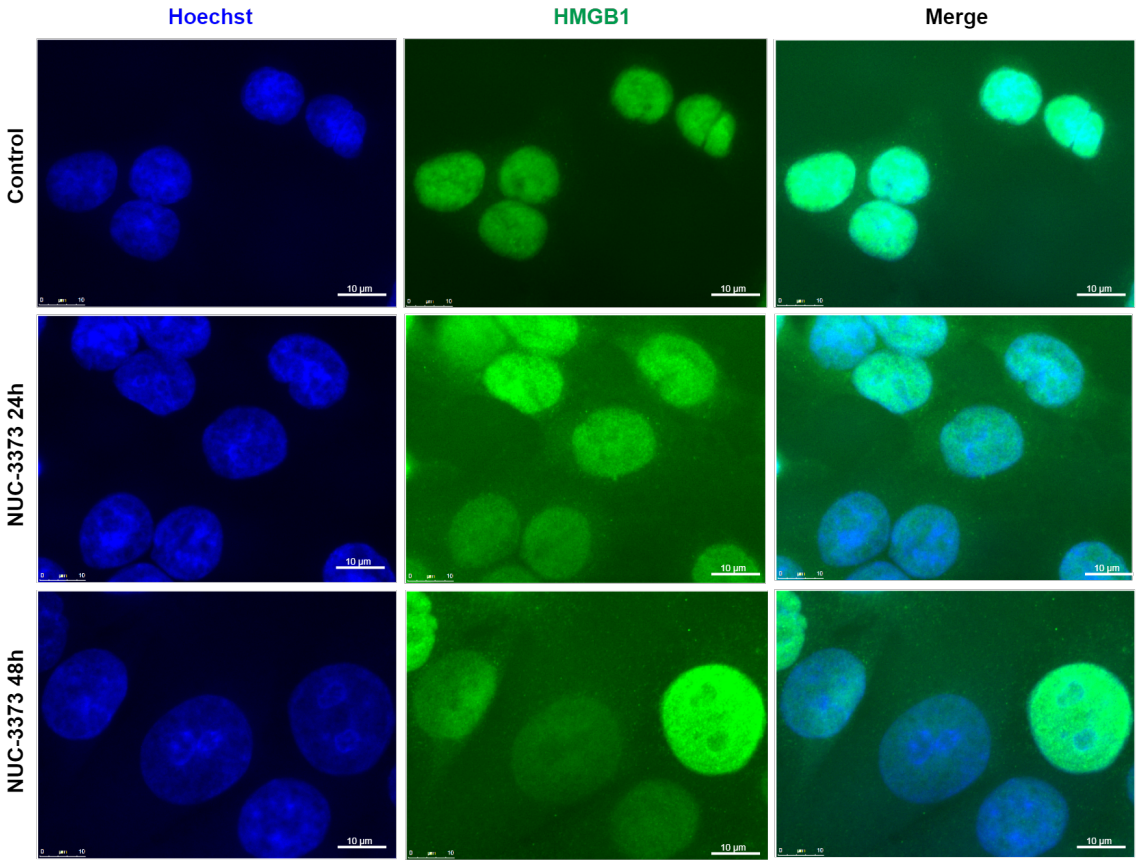

Figure 5.4: HMGB1 expression in HCT116 cells treated with 10 μM NUC-3373 for 24 or 48 hours. Green: HMGB1, Blue: Hoechst (nuclear stain). 100x magnification. Photomicrographs are representative.

HMGB1 has an intense nuclear expression in untreated HCT116 cells (detected by co-localisation with hoechst stain), which is noticeably weaker after 24 hours of treatment with NUC-3373 (Figure 5.4). After 24 and 48 hours NUC-3373 treatment there is also a diffuse cytoplasmic expression of HMGB1. Loss of nuclear HMGB1 continues after 48 hours. However, this loss is not conserved amongst all cells, with inter-cellular expression being fairly heterogeneous. Additionally, nuclei were observed to be significantly enlarged, which was most evident after 48 hours of NUC-3373 treatment.

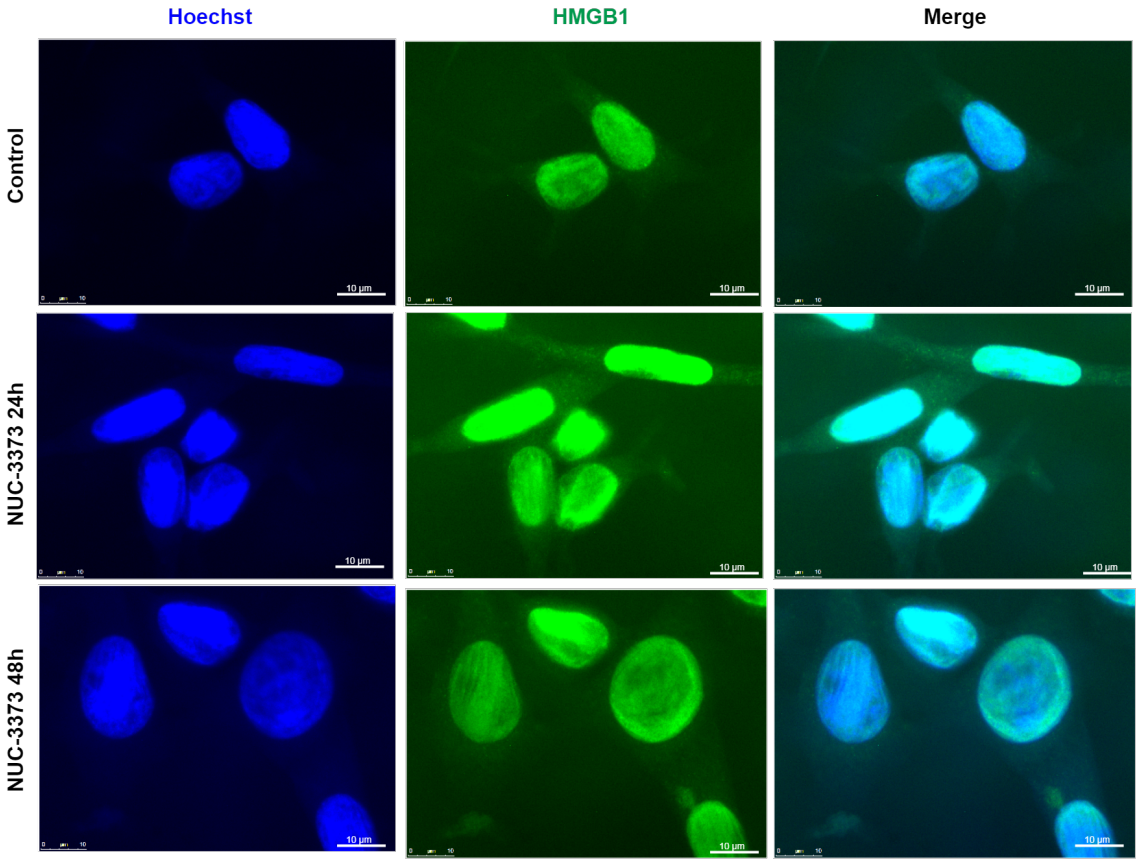

Figure 5.5: HMGB1 expression in SW480 cells treated with 10 μM NUC-3373 for 24 or 48 hours. Green: HMGB1, Blue: Hoechst (nuclear stain). 100x magnification. Photomicrographs are representative.

Like HCT116 cells, HMGB1 also has a strong nuclear expression in SW480 cells under basal conditions (Figure 5.5). Conversely, HMGB1 expression appears stronger in some cells after 24 hours of NUC-3373 treatment with some cytoplasmic localisation also evident. By 48 hours of NUC-3373 treatment, HMGB1 expression was similar to that in control cells. Overall, there was no significant loss of HMGB1 in SW480 cells but nuclear enlargement was again present after 48 hours.

Calreticulin

As described earlier, calreticulin is an ER chaperone protein that is said to present on the cell surface as an 'eat me' signal during early apoptosis. Therefore, its cellular localisation was examined by immunofluorescence in cells treated with 10 μM NUC-3373. All images are representative of the cell population studied.

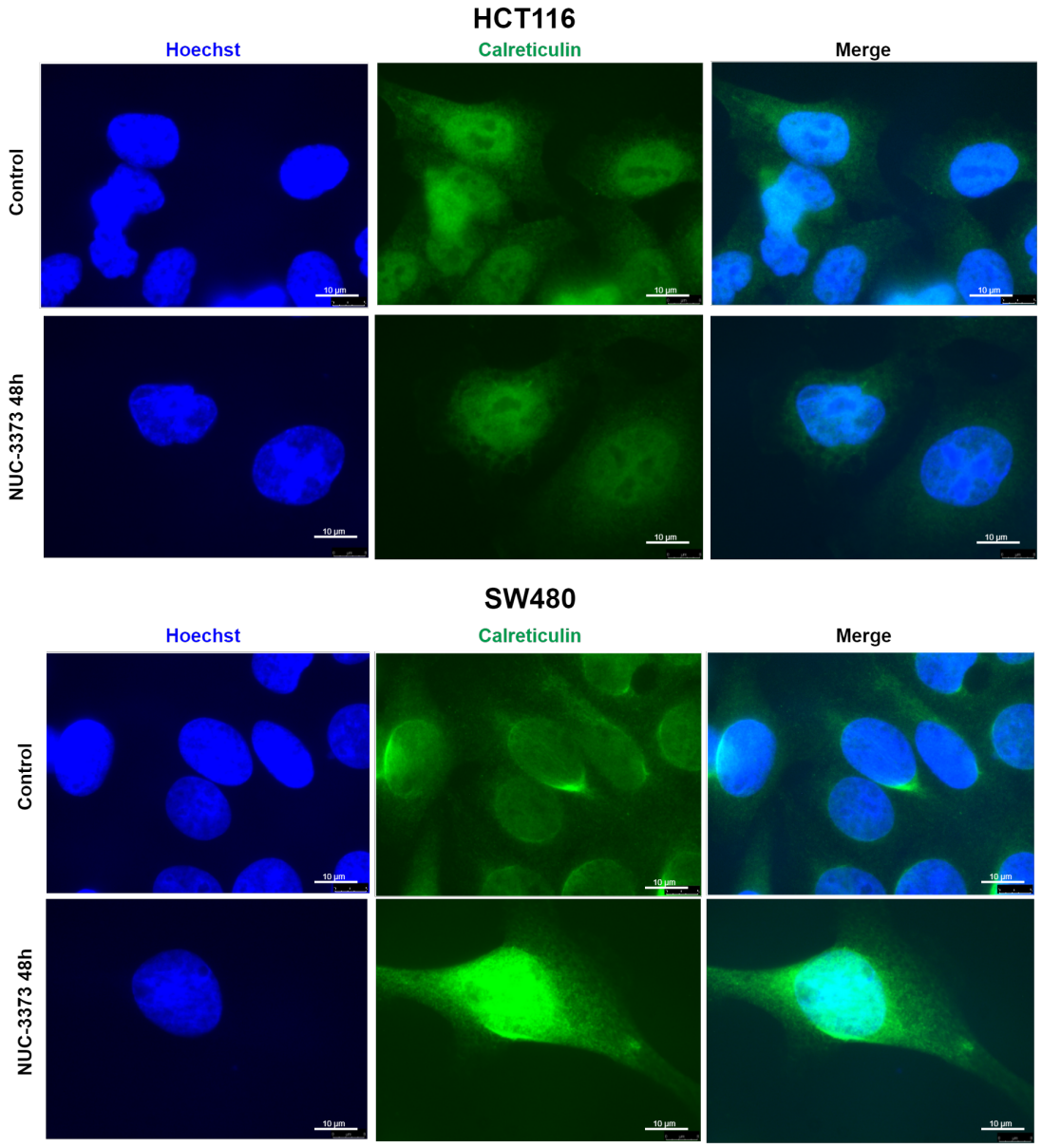

Figure 5.6: Calreticulin expresion in HCT116 and SW480 cells treated with 10 μM NUC-3373 for 48 hours. Green: Calreticulin, Blue: Hoechst (nuclear stain). 100x magnification. Photomicrographs are representative.

In HCT116 cells, calreticulin expression was relatively weak when compared to that of SW480 cells (Figure 5.6). The difference following NUC-3373 treatment was negligible in HCT116 cells, with calreticulin appearing to localise to nuclei and weakly to cytoplasm. In SW480 cells, the expression of calreticulin was strong in the perinuclear region, most likely to be rough endoplasmic reticulum. NUC-3373 treatment caused an increase in calreticulin expression with the same localisation pattern. This finding complements the ER ulstrastructural changes in Chapter 4,

with SW480 having proliferated rough ER. In both cell lines there was no apparent cell surface expression of calreticulin but this may be due to the methodology used. It may be that permeabilisation prevents the detection of this protein when cell surface bound. In addition, surface exposed calreticulin is an early apoptosis DAMP so it may be that the time of detection (48 hours) was too late.

5.2.3 Programmed death-ligand 1

PDL-1 protein expression was initially investigated by Western blot on whole cell lysates from HCT116 and SW480 cells. However, PDL-1 was not detectable in these lysates. In order to assess whether this was a true finding or due to experimental protocol, a positive control was required. Breast cancer cell line MDA-MB-231 has been reported in a previous study to express PDL-1 abundantly (Rom-Jurek, E., *et al.*, 2018), thus it was selected for use in these PDL-1 studies as a positive control.

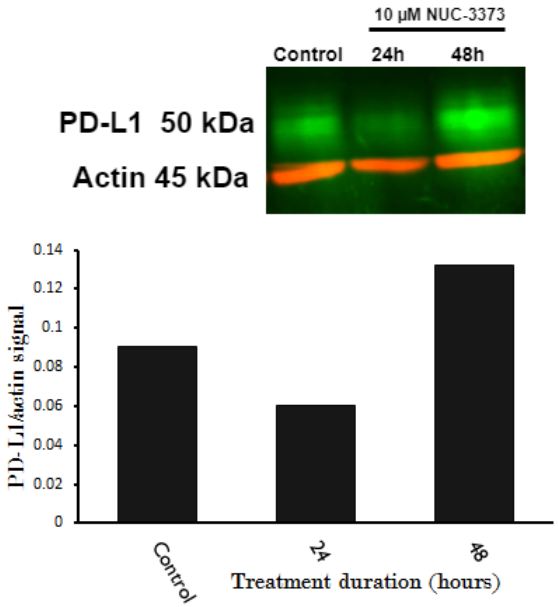

Figure 5.7: Representative Western blot of PD-L1 expression in MDA-MB-231 cells treated with 10 μM NUC-3373 for 24 or 48 hours. Green bands: PD-L1, Red bands: actin as loading control. $N_{Biological}$=1.

In MDA-MB-231 whole cell lysates, PD-L1 protein expression decreased after 24

hours of 10 μM NUC-3373 treatment then increased after 48 hours (Figure 5.7). Since PD-L1 protein could not be detected in HCT116 or SW480 cells by Western blot, enzyme-linked immuno-assay (ELISA) was utilised as it may be that expression was either too low in these cells or that it was released to cell supernatant. Whole cell lysates as well as cultured medium from NUC-3373-treated cells was assessed by ELISA. Interferon-gamma (INF-γ) is known to induce PD-L1 expression (Mandai, M., *et al.*, 2016) so was used to induce expression in HCT116 and SW480 cells.

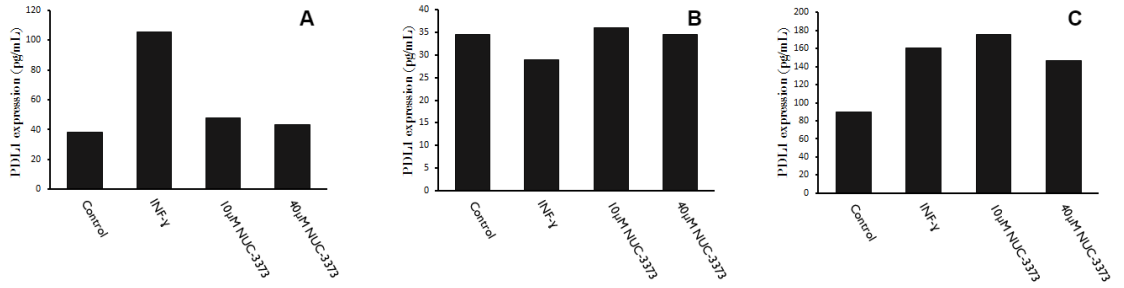

Figure 5.8: PDL-1 expression in A: HCT116, B: SW480 and C: MDA-MB-231 whole cells treated with either INF-γ, 10 μM or 40 μM NUC-3373 for 48 hours. PDL-1 protein was detected by ELISA with values expressed as the average of 2 technical replicates. $N_{Biological}$=1.

In conditioned media from treated cells, PD-L1 was not detected (data not shown). ELISA was able to detect PD-L1 protein in both SW480 and HCT116 whole cell lysates in the picogram range (Figure 5.8). In HCT116 cells, INF-γ caused an almost three-fold increase in PD-L1 protein expression, whilst NUC-3373 did not cause any considerable change in expression. In SW480 cells, INF-γ treatment resulted in a small decrease in PDL-1 expression, whilst NUC-3373 had no effect. MDA-MB-231 cells had double the basal expression of PD-L1 detected in the other cell lines. Interestingly, 10 μM NUC-3373 caused a potent increase in PD-L1 protein expression in MDA-MD-231 cells that was comparable to that produced by INF-γ treatment.

These data obtained for PD-L1 detection by Western blot and ELISA are preliminary as only one biological sample was assessed.

5.3 Discussion

5.3.1 ER Stress: TS or ternary complexes?

Knocking down TS protein expression abolished the UPR in NUC-3373-treated HCT116 cells but not in SW480 cells, suggestive of TS being responsible for activation of the UPR in these cells. Previous studies have explored the relationship between TS and BiP. Powell, C.M.H., *et al.*, (2000) demonstrated that inhibition of the transcription factor Late SV40 factor (LSF) resulted in downregulation of TS expression and S-phase-dependent apoptosis with 5-FU treatment. Gu, Y., *et al.* (2015) reported that overexpression of BiP activates phosphorylation of c-Src, resulting in an elevated LSF/TS axis in hepatocellular carcinoma cells. These studies demonstrate the potential link between TS and BiP proteins. However, this thesis suggests a bidirectional relationship between TS and BiP, whereby TS can also regulate BiP expression. There may be more dynamic interplay between these two proteins than once thought. The unfolded protein response may also provide more arsenal in the battle of the cancer cell against a NUC-3373-induced death by using BiP upregulation to elevate depleted TS levels. Furthermore, BiP overexpression has been known to cause resistance of tumours to various chemotherapies, including 5-FU. Further exploration of this relationship should include functional studies of BiP knockdown to establish whether this can potentiate NUC-3373-induced apoptosis by inhibiting TS production further, as well as more extensive study of timepoints to establish early events.

5.3.2 HMGB1

As previously mentioned, the additional mechanism of action of NUC-3373 to induce ER stress in CRC cells demonstrates a potential for an immune-mediated host response by the release of DAMPs from stressed cells. One such DAMP is HMGB1; a small (22 kDa) chromatin-associated protein consisting of three distinct

domains with both intranuclear as well as extracellular functions (Tang, D., *et al.*, 2010). In this study, the more sensitive HCT116 cells had a very strong nuclear expression of HMGB1 under basal conditions with NUC-3373 inducing a nuclear loss and appearance of cytoplasmic HMGB1. In unstressed conditions, HMGB1 has been reported to have nuclear localisation, where it can bind to and bend DNA to modulate gene transcription, DNA repair and chromatin remodelling (Lotze, M.T., and Tracey, K.J., 2005). Interestingly, the less sensitive SW480 cell line presented an increase in nuclear HMGB1 expression along with some weaker cytoplasmic expression in response to NUC-3373 treatment. A previous study found that HMGB1 contributes to a nuclear protein complex with p53, HMGB2, Hsp70, ERp60 and GAPDH which can recognise DNA damage induced by nucleoside analogues such as 5-FU (Achanta, G.,*et al.*, 2001) and provide a link to genotoxic stress-induced apoptosis signalling (Krynetskaia, N., *et al.*, 2007). It may be that in SW480 cells, HMGB1 plays a protective role against NUC-3373-induced DNA damage.

The role of HMGB1 in cancer is multifaceted, with its cytoplasmic expression being implicated in protective autophagy, as well as regulation of mitochondrial function (Tang, D., *et al.*, 2010; White, E., 2012). The appearance of cytoplasmic HMGB1 in both cell lines indicates that it may mediate autophagy or mitochondrial function in these cells. However, further studies would be required to determine this, such as immunofluorescent detection of autophagosomes using markers such as ATG5 or ATG7 or investigation of co-localisation with mitochondria.

The diffuse expression of HMGB1 in the cytoplasm of HCT116 cells does not appear strong enough to account for all HMGB1 loss from the nucleus, pointing to possible release from the cell. When released from cells, HMGB1 can act as a DAMP by initiating a pro-inflammatory cytokine and immune response through binding to TLRs on dendrites (Kang, R., *et al.*, 2013).

A meta-analysis found overexpression of HMGB1 to be associated with poorer overall survival and shorter progression free survival, which was significant regardless of tumour type (Wu, T., *et al.*, 2016). The paradoxical roles of HMGB1 appear to

be pro-survival or pro-death depending on its location. Taken together, it could be hypothesised that NUC-3373 treatment causes HMGB1 to act as a DAMP in HCT116 cells but not in SW480 cells, where its nuclear expression could be protective from DNA damage-induced apoptosis.

5.3.3 Calreticulin

Another well-characterised DAMP is calreticulin; a Ca^{2+}-binding chaperone protein which is mostly found in the ER but can be present in other cellular compartments as well as on the cell surface. Its main function is to bind to, buffer and maintain intracellular Ca^{2+} homeostasis (Wang, W.A., *et al.*, 2012). In fact, the C-domain binds to more than 50% of the Ca^{2+} present in the ER, making it the main site of Ca^{2+} storage (Nakamura, K., *et al.*, 2001).

It has been established that surface exposed calreticulin (ecto-CRT) is required for the engulfment of apoptotic cells by phagocytes (Gardai, S., *et al.*, 2005), acting as an 'eat me signal', with knockdown of calreticulin by siRNA in cancer cells suppressing this immunogenic cell death (Obeid, M., *et al.*, 2007). The aim of investigating calreticulin expression and localisation in this study was to determine if it was induced as a DAMP with NUC-3373 treatment. However, in both cell lines no ecto-CRT was detected. It is unclear as to whether this is a true finding, however, as any ecto-CRT may have been lost due to the permeabilization of cells. Ecto-CRT would be better detected by flow-cytometry should it be pursued in future studies.

Despite this, the finding that calreticulin was mainly nuclear in HCT116 cells and that it increased in cytoplasmic expression in SW480 cells was surprising. Calreticulin, through its N- and P-domains, acts as a 'folding checking unit' to ensure the proper folding of newly synthesised glycoproteins. By interaction with calnexin and ERp57 in the calreticulin/calnexin cycle, calreticulin guides inappropriately folded glycoproteins to the degradation pathway (Michalak, *et al.*, 2009). It would be reasonable to hypothesise that SW480 cells cope better with ER stress by

accompanying their proliferated rough ER with an increase in the expression of calreticulin to effectively fold proteins and regain proteostasis. Furthermore, it has recently been shown that calreticulin expression is required to overcome ER stress. Yang, Y., *et al.*, (2018) showed that knockdown of calreticulin prevented recovery from ER stress and that the increase in calreticulin expression with induction of ER stress was accompanied by an increase in expression of and punctate appearance of autophagy marker LC3. This suggests that overexpression of calreticulin may ameliorate ER stress by promoting an autophagic flux through association with LC3. With this in mind, future studies of ER stress in SW480 cells would benefit from the addition of the study of autophagy by immunofluorescence detection of LC3 as well as the study of calreticulin protein expression in subcellular fractions by Western blot. If calreticulin-dependent autophagy is a potential resistance mechanism to NUC-3373 treatment, then it would be useful to investigate combination with inhibitors of autophagy, such as chloroquine.

In HCT116 cells there was very little cytoplasmic expression of calreticulin, with the majority being nuclear. Nuclear localisation of calreticulin has been a subject of controversy, with some arguing that there is no reasonable mechanism for it to relocate to the cytosol (Johnson, S., *et al.*, 2001), and suggesting its nuclear expression is an artefact of immunostaining (Michalak, M., *et al.*, 1996). Roderick, H., *et al.* (1997) provided evidence alluding to calreticulin having nuclear expression due to interaction of its N-domain with glucocorticoid receptors, despite its possession of ER targeting and retention signals. However, the immunofluorescence they present is very weak and may simply represent calreticulin present in the outer membrane of the nuclear envelope, which is continuous with the rough ER (Pavelka, M., and Roth, J., 2010). It is difficult to ascertain the true localisation of calreticulin in HCT116 cells in this study, but what can be gleaned is that NUC-3373 does not have any apparent effect on its intracellular localisation or expression.

When considering the increase in calreticulin expression in SW480 cells alongside the ultrastructural findings, calreticulin overexpression seems a probable mechanism of recovery from NUC-3373-induced ER stress and should be investigated further.

When considering calreticulin as a DAMP, these data have been inconclusive and would require detection by flow cytometry to investigate further.

5.3.4 PD-L1

It cannot yet be concluded whether NUC-3373 has the potential to induce an ICD. With only one molecule, HMGB1, found to act in a DAMP-like manner this may not be enough to induce an immune response. However, as explained previously it is necessary to employ other techniques such as flow-cytometry to assess the surface expression of molecules such as calreticulin as well as perhaps Hsp70. For the moment, ICD induction by NUC-3373 will not be ruled out. Therefore, it is important to consider the impact of PD-L1 in evading immunosurveillance.

The only cell line in which NUC-3373 induced an induction of PD-L1 expression in was MDA-MB-231 cells. The decreased expression detected at 24 hours in Western blot could be explained by PD-L1 being released from cells then upregulated to replenish intracellular expression, detected by the increase at 48 hours. However, no PD-L1 was detected in the conditioned medium from treated cells. Alternatively, PD-L1 may be expressed on the surface of cells and require flow cytometry detection. The studies of PD-L1 in this thesis are considered preliminary and should be approached with caution until further biological replicates have been carried out. At this stage, it cannot be confirmed whether the combination of NUC-3373 with PD-1 or PD-L1 inhibitors may have clinical benefit.

5.3.5 Chapter Summary

Whilst the data in this chapter strongly suggest TS complexes may be responsible for activation of the UPR in HCT116 cells, it remains unclear whether this is a direct relationship. With there being no correlation between the two in SW480 cells, it would indicate that it is not the TS or TS complexes that are responsible but perhaps a downstream event of their formation. Further work is needed to ascertain

this. The pathways involved in ER stress are complex as well as context- and location-dependent so investigations must consider this, especially in experimental design with regard to time points. Whilst much of the data generated in this chapter was preliminary, it provided the groundwork and indications of where to focus future studies and the techniques which should be employed, such as flow cytometry. Loss of HMGB1 strongly suggests that NUC-3373 confers a distressed cancer cell and this could be exploited to achieve maximal efficacy of treatment. Additionally, this study highlights the necessity for a better pre-clinical screening tool for anti-cancer drugs, due to the lack of immune system to assess any immune-mediated processes.

Chapter 6

Final Discussion

Cancer cells possess an impressive repertoire of mechanisms which permit them to evade the immune system and adapt to hostile environments, including insult by chemotherapeutic agents. Subsequently, much research has focussed on identifying predictive biomarkers to inform the potential response of tumours to anti-cancer agents and identify markers of resistance. NUC-3373 has been shown, *in vivo*, to bypass a major resistance mechanism faced by 5-FU; degradation by DPD in the liver to produce higher levels of the active metabolite FdUMP in cells to inhibit TS. Currently, it would appear that the difference in efficacy between 5-FU and NUC-3373 is due to the elevated level of active metabolite reaching cells for the same given dose. However, the downstream events of TS inhibition and TS ternary complex formation by FdUMP are not fully understood.

There are mixed findings of other studies with regard to the value of TS as a predictive biomarker of response. Therefore, the initial studies of this thesis sought to explore this in an *in vitro* setting. The data from this body of work suggest that TS is not predictive of response to NUC-3373 treatment and that there is instead a complex and dynamic cellular response to inhibition of this protein by FdUMP. One cell line more sensitive to death induced by NUC-3373 was selected; HCT116, and another less so; SW480. These cell lines were selected with the aim to expose differences in less sensitive cells, which may confer their survival advantage. By

identifying these, it can provide the rationale for future combination therapies that would enhance the efficacy of NUC-3373 (and indeed 5-FU). The inhibition of TS by NUC-3373 was not sustained in either cell line, yet NUC-3373 was still effective in killing cells. This necessitated the presence of further downstream events that could contribute to apoptosis of cells, indicating an additional mechanism of action.

6.0.1 An additional mechanism of action

The recovery of TS as well as its cytoplasmic translocation provided the basis for the hypothesis that NUC-3373 may be inducing ER stress. Indeed, it was found that the UPR was profoundly invoked in both cell lines in response to NUC-3373. However, the UPR in HCT116 cells was not as sustained as that of SW480 cells. When coupling this with the dynamic of apoptotic marker CHOP, it revealed that cells more sensitive to NUC-3373 were unable to surmount ER stress, whereas less sensitive cells elicited a pro-survival response. Previous studies have implicated 5-FU in the induction of ER stress but have lacked the ability to be clinically translated due to the supra-pharmacologically high concentrations of drug used. This study demonstrated that NUC-3373 was proficient in ER stress induction at much lower doses and thus had the potential to execute this in a clinical setting. This study, through ultrastructural analysis, also elucidated a potential mechanism by which some cells can overcome this ER stress, by proliferation of the RER membrane. Upregulation of the spliced and therefore active XBP1(S) protein has been found to be necessary to produce phospholipids required to proliferate RER (Sriburi, R., *et al.*, 2004). Previous studies have shown that XBP1(S) promotes CRC cell proliferation (Ji, H., *et al.*, 2019) as well as invasiveness (Jin, C., *et et al.*, 2016). Considering the findings of this study with the current literature, further study of XBP1(S) as a potential drug target is warranted. Targeting the UPR in cancer can pose as a double-edged sword due to its complexity and context-dependence as well as the ability of cancer to adapt to a hostile environment. Therefore, UPR-inhibiting drugs could benefit from being administered concomitantly with other cytotoxic drugs such as NUC-3373 which are able to overcome other hallmarks of cancer.

6.0.2 Implications for clinical utility

This study revealed an expression pattern of HMGB1 in NUC-3373-treated HCT116 cells that was consistent with it acting as a DAMP, which could have the ability to invoke an immune response. Further work is required to determine the potential of NUC-3373 as an ICD-inducing agent. If NUC-3373 were confirmed to induce an immune response, the dosing of patients would need to be considered. A key objective of phase I oncology clinical trials is to establish the maximum tolerated dose (MTD) with acceptable side effects in patients (Sachs, J., *et al.*, 2015). Whilst the objective of cytotoxic drugs is to kill cancer cells, they inevitably result in damage to and death of immune cells (Rébé, C., and Ghiringhelli, F., 2015). Due to the current practice of using MTD to inform recommended dose for phase II (RDP2), any potential for cytotoxic drugs to induce an immune-mediated death of cancer cells is masked. For an ICD-inducing drug to work effectively, it must be administered at a dose sufficient to illicit a response but not impair the immune system. However, challenging the MTD concept would pose an ethical debate with concern that the patient may be under-treated. NUC-3373 generates a higher level of FdUMP in cells for an equimolar dose of 5-FU, therefore would be the superior fluoropyrimidine for use in the context of ICD. Oxaliplatin has already been shown to improve the outcome of 5-FU in the chemotherapy regimen 'FOLFOX'. In addition, Tesniere, A., *et al.* (2010) demonstrated the ability of oxaliplatin to induce ICD, making it a promising candidate for combination therapy with NUC-3373.

6.0.3 Caveats and Limitations

Cell Line Selection

One sensitive and one less sensitive cell line were selected from a screen of nine CRC cell lines for further study. This model, whilst providing a basis for the mechanism of action of NUC-3373 to be studied in, fails to represent the heterogeneous nature of real tumours. This study could have benefitted from using a wider range of cell lines

with differing genetic mutations and MMR statuses, as well as cell lines with different sensitivities to NUC-3373. The use of explant culture to create patient-derived organoids could have provided an *in vitro* environment closer mirroring the *in vivo* reality.

Dose-response

In the assessment of biological responses of cells to chemotherapy agents, events are typically both time- and dose-dependent. Whilst this study utilised time points, these could have been more extensive. For example, had a 6-hour time point not been incorporated into this study, the initial inhibition of TS would not have been detected. The inconclusive results from the study of both calreticulin expression and PD-L1 may be due to time-dependent events. Similarly, using 10 μM NUC-3373 may have masked some important processes that could have been identified by using a wider range of concentrations.

DNA damage

This study identified some new areas of importance in the mechanism of action of fluoropyrimidines but failed to capture and investigate the wider range of cellular events in response to NUC-3373. The main mechanism of action of 5-FU is believed to be its ability to induce DNA damage. Whilst this body of work does not discount DNA damage as a vital component of NUC-3373's anticancer effects, it suggests that additional mechanisms of action are present which serve to support the dynamic interplay of events culminating in cell death.

The Cell Culture Model

Pre-clinical screening of drug candidates relies heavily on data acquired through *in vitro* cell culture models. This model is cheap, convenient and allows for high

through-put screens but it lacks the vital components that affect the activity of a drug *in vivo*, such as the immune system and blood supply. The inability of the cell culture model to predict the response of different tissues and organs to new compounds often leads to withdrawal of drugs from the clinic due to side effects such as liver and cardiotoxicity (Astashkina, A., *et al.*, 2012). Of specific significance to this study is the inability to assess the interaction with the immune system. Rodent models are routinely used in the pre-clinical assessment of anti-cancer drugs. When considering rodent models in the study of NUC-3373, it is important to note the disparities in enzymatic activity between humans and rodents. Rodents have extremely high carboxylesterase activity compared to humans, in which it is minimal (Rudakova, E.V., *et al.*, 2011), so would hydrolyse the ester group of the phosphoramidate moiety of NUC-3373 thus abolishing its prime *in vivo* advantage over 5-FU. In addition, rodents have a 10-fold higher plasma thymidine concentration than humans (Nottebrock, H., and Then, R., 1977) so would not be as effective in inducing DNA damage by creating a thymineless state.

6.0.4 Future Work

As well as ER stress, the main mechanism of action for FdUMP is to induce DNA damage. Investigation of intracellular metabolites using mass spectrometry as well as nucleotide misincorporation into RNA and DNA by qPCR should be undertaken. In addition, DNA damage could be measured using the gel electrophoresis-based comet assay.

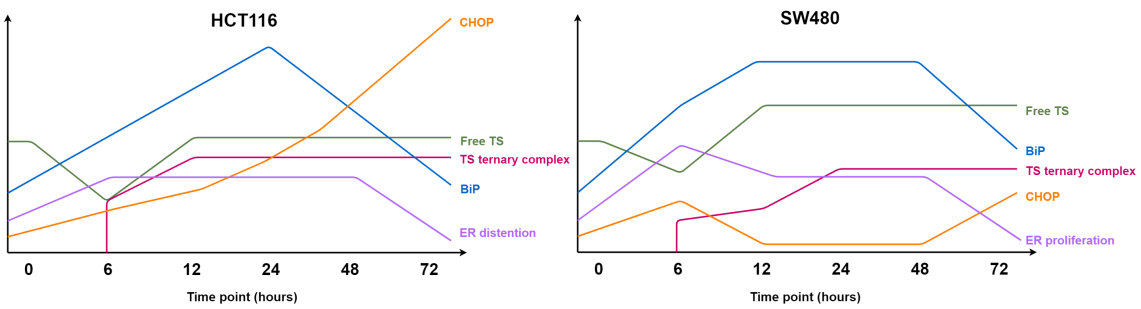

Figure 6.1: Cellular events over a time-course of NUC-3373 treatment in HCT116 vs SW480 cells.

Figure 6.1 illustrates the dynamic nature of elements of the UPR and ER stress in response to NUC-3373 inhibition of TS and formation of TS ternary complexes in sensitive and less sensitive cells. This further highlights the need for studies to consider the time-sensitive nature of cellular events. These data would benefit from the inclusion of more functional studies such as knockdown of key players in the UPR eg. BiP because there is currently no causative link established between TS complex formation and ER stress. As discussed in chapter 4, XBP1(S) is a requirement for the ER proliferation in SW480 cells and studies suggest its overexpression to be pro-tumorigenic. Therefore, future studies should assess its expression, with a view to down-regulating its expression in order to induce sensitivity by preventing the protective proliferation of ER membrane.

This study has only incorporated preliminary studies of DAMP release. It became evident that cell-surface expressing DAMPs such as calreticulin and HSP70/90 required detection by flow cytometry. Further exploring the realms of ICD, combination of NUC-3373 with known ICD-inducer oxaliplatin could prove beneficial. If there is sufficient evidence for DAMP release using a cell model, there may be a basis for *in vivo* studies to validate the effect. Whilst assessing the direct effect of NUC-3373 in rodents would not be representative of its action in humans (described earlier), mouse models can be used to effectively validate ICD induction, as detailed by Humeau, J., *et al.*, (2019). In their experimental protocol, syngenic murine tumour cells are treated with the cytotoxic agent *in vitro* until 50 to 70% of the cells are dead, at such point any non-dead cells should be dying. Cytotoxicant-treated tumour cells are then injected to a mouse, with control mice receiving tumour cells that have been treated with a non-ICD-inducing cytotoxic. Mice are rechallenged with living tumour cells one week later, with mice that were vaccinated by tumour cells treated with an ICD-inducing drug demonstrating increased tumour-free survival in contrast to control mice. If NUC-3373 is confirmed as a *bona fide* ICD-inducer, PD-L1 surface expression or release need to be investigated to establish whether PD-L1 or PD-1 inhibitors would enhance treatment outcome.

6.0.5 Conclusion

To conclude, this thesis provides strong evidence for ER stress induction being an additional mechanism of action, independent of the DNA damage pathway, for novel ProTide NUC-3373. The use of ultrastructural studies identified proliferation of ER as a potential resistance mechanism which could be exploited. Further work is required to fully elucidate this complex story and its implications for NUC-3373 in the clinic.

References

Achanta, G., Pelicano, H., Feng, L. Plunkett, W., and Huang, P. (2001). Interaction of p53 and DNA-PK in response to nucleoside analogues: potential role as a sensor complex for DNA damage. *Cancer Research.* **61**:8723-8729.

Aherne, G.W., and Brown, S. *Antifolate Drugs in Cancer Therapy: The Role of Uracil Misincorporation in Thymineless Death.* (Human Press, Totowa NJ, 1999).

Alcindor, T. and Beauger, N. (2011). Oxaliplatin: a review in the era of molecularly targeted therapy. *Current oncology.* **18**:18-25.

Apetoh, L., Ghiringhelli, F., Tesniere, A., Criollo, A., Ortiz, C., Lidereau, R., Mariette, C., Chaput, N., Mira, J., Delaloge, S. Andre, F., Tursz, T., Kroemer, G., and Zitvogel, L. (2007). The interaction between HMGB1 and TLR4 dictates the outcome of anticancer chemotherapy and radiotherapy. *Immunological reviews.* **220**:47-59.

Astashkina, A., Mann, B., Grainger, D.W.(2012). A critical evaluation of in vitro cell culture models for high-throughput drug screening and toxicity. *Pharmacology & Therapeutics.* **134**: 82-106.

Attene-Ramos, M.S., Wagner, E.D., Plewa, M.J., Gaskins, H.R. (2006). Evidence that hydrogen sulfide is a genotoxic agent. *Molecular Cancer Research.* **4(1)**:9-14.

Aune, D., Chan, D.S.M., Lau, R., Vieira, R., Greenwood, D.C., Kampman, E., and Norat, T. (2011). Dietary fibre, whole grains, and risk of colorectal cancer:

systematic review and dose-response meta-analysis of prospective studies. *Clinical research ed.*. **343**:d6617.

Backer, M.V., Backer, J.M., and Chinnaiyan, P. Targeting the Unfolded Protein Response in Cancer Therapy. *Methods in Enzymology*. **491**:37-56.

Banerjee, A., Lang, J., Hung, M., Sengupta, K., Banerjee, S.K., Baksi, K., and Banerjee, D.K. (2011). Unfolded protein response is required in nu/nu mice microvasculature for treating breast tumor with tunicamycin. *The Journal of biological chemistry*. **286**:29127-29138.

Bassotti, G., and Battaglia, E. *Coloproctology: Physiology of the Colon*. (Springer International Publishing, 2015). booktitle = Coloproctology,

Bissoon-Haqqani, S., Moyana, T., Jonker, D., Maroun, J.A., Birnboim, H.C. (2006). Nuclear Expression of Thymidylate Synthase in Colorectal Cancer Cell Lines and Clinical Samples. *Journal of Histochemistry & Cytochemistry*. **54**:19-29.

Blagden, S.P., Slusarczyk, M., Serpi, M., McGuigan, C., and Ghazaly, S. (2016). First-in-human phase I study of the nucleotide analogue NUC-3373 designed to overcome fluoropyrimidine drug resistance mechanisms. Poster presented at: AACR 107th Annual Meeting 2016.

Blagden, S.P., Evans, T.R.J., Ghazaly, E., Gnanaranjan, C., De Gramont, A., Tabernero, J., Berlin, J.D. (2018). A Phase Ib open label study to asses the safety and pharmacokinetics of NUC-3373, a nucleotide analog, given in combination with standard agents used in colorectal cancer treatment (NuTide:302). Poster presented at: ASCO annual meeting 2018.

Boardman, L.A., Morlan, B.W., Rabe, K.G., Petersen, G.M., Lindor, N.M., Nigon, S.K., Goldberg, J., and Gallinger, S. (2007). Colorectal cancer risks in relatives of young-onset cases: is risk the same across all first-degree relatives? *Clinical gastroenterology and hepatology*. **5**:1195-1198.

Bokemeyer, C., Van Cutsem, E., Rougier, P., Ciardiello, F., Heeger, S., Schlichting,

M., Celik, I., Köhne, C.H. (2012) Addition of cetuximab to chemotherapy as first-line treatment for KRAS wild-type metastatic colorectal cancer: pooled analysis of the CRYSTAL and OPUS randomised clinical trials. *European Journal of Cancer*. **48(10)**:1466-1475.

Botteri, E., Iodice, S., Bagnardi, S., Raimondi, A.B., Lowenfels, M., and Maisonneuve, P. (2008). Smoking and Colorectal Cancer. *Jama*. **300**:2765-2778.

Bravo, R., Vicencio, J.M., Parra, V., Troncoso, R., Munoz, J.P., Bui, M., Quiroga, C., Rodriguez, A.E., Verdejo, H.E., Ferreira, J., Iglewski, M., Chiong, M., Simmen, T., Zorzano, A., Hill, J.A., Rothermel, B.A., Szabadkai, G., and Lavandero, S. (2011). Increased ER-mitochondrial coupling promotes mitochondrial respiration and bioenergetics during early phases of ER stress. *Journal of Cell Science*. **124**:2143-2152.

Briffa, R. *Towards Functional Multiscale Analysis of Colorectal Cancer*. (The University of Edinburgh, 2014).

Calfon, M., Zeng, H., Urano, F., Till, J.H., Hubbard, S., Harding, H.P., Clark, S.G., and Ron, D. (2002). IRE1 couples endoplasmic reticulum load to secretory capacity by processing the XBP-1 mRNA. *Nature*. **415**:92-96.

Cancer Research UK. Bowel cancer statistics(2016). Available at https://www.cancerresearchuk.org/health-professional/cancer-statistics/statistics-by-cancer-type/bowel-cancer. [ACCESSED AT 31.03.19].

Carreras, C.W., and Santi, D.V. (1995). The Catalytic Mechanism and Structure of Thymidylate Synthase. *Annual Review of Biochemistry*. **64**:721-762.

Carter, P., Alifrangis, C., Cereser, B., Chandrasinghe, P., Belluz, L., Herzog, T., Levitan, J., Moderau, N., Schwartzberg, L., Tabassum, N., Wen, J., Krell, J., Stebbing, J. (2018). Does molecular profiling of tumors using the Caris molecular intelligence platform improve outcomes for cancer patients? *Oncotarget*. **9**:9456-9467.

Cavaliere, A., Probst, K.C., Westwell, A.D., and Slusarczyk, M. (2017). Fluorinated nucleosides as an important class of anticancer and antiviral agents. *Future Medicinal Chemistry.* **9**:1809-1833.

Chami, M., Oulès, B., Szabadkai, G., Tacine, R., Rizzuto, R., and Paterlini-Bréchot, P. (2008). Role of SERCA1 Truncated Isoform in the Proapoptotic Calcium Transfer from ER to Mitochondria during ER Stress. *Molecular Cell.* **32**: 641-652.

Chan, D.S.M., Lau, R., Aune, D., Vieira, R., Greenwood, D.C., Kampman, E., and Norat, T. (2011). Red and processed meat and colorectal cancer incidence: meta-analysis of prospective studies. *PloS one.* **6**:e20456.

Chu, E., and Allegra, C.J. (1996). The role of thymidylate synthase in cellular regulation. *Advances in Enzyme Regulation.* **36**:143-163.

Coarelli, G., Diallo, A., Thion, M.S., Rinaldi, D, Calvas, F., Boukbiza, O.L., Tataru, A., Charles, P., Tranchant, C., Marelli, C., Ewenczyk, C., Tchikviladzé, M., Monin, M., Carlander, B., Anheim, M., Brice, A., Mochel, F., Tezenas du Montcel, S., Humbert, S., and Durr, A. Low cancer prevalence in polyglutamine expansion diseases. *Neurology.* **88**:1114-1119.

Colussi, D., Brandi, G., Bazzoli, F., Ricciardiello, L. (2013). Molecular Pathways Involved in Colorectal Cancer: Implications for Disease Behavior and Prevention. *International Journal of Molecular Science.* **14**:16365-16385.

Cooper, G.M. *The Cell: A Molecular Approach. Lysosomes.* (Sinaier Associates Sunderland MA, 2000).

Cruz-Orive, L. M. (1997). Stereology of single objects. *Journal of Microscopy.* **186**:93-107.

Cubillos-Ruiz, J.R., Bettigole, S.E., and Glimcher, L.H. (2017). Tumorigenic and Immunosuppressive Effects of Endoplasmic Reticulum Stress in Cancer. *Cell.* **168**:692-706.

Dahmus, J.D., Kotler, D.L., Kastenberg, D.M., Kistle, C.A. (2018). The gut microbiome and colorectal cancer: a review of bacterial pathogenesis. *Journal of Gastrointestinal Oncology.* **9(4)**: 769–777.

Dancey, J., and Eisenhauer, E.A. (1996). Current perspectives on camptothecins in cancer treatment. *British Journal of Cancer.* **74**:327-338.

Däster, S., Amatruda, N., Calabrese, D., Ivanek, R., Turrini, E., Droeser, R.A., Zajac, P., Fimognari, C., Spagnoli, G.C., Iezzi, G., Mele, V., and Muraro, M. (2017). Induction of hypoxia and necrosis in multicellular tumor spheroids is associated with resistance to chemotherapy treatment. *Oncotarget.* **8**:1725-1736.

Daum, G. (1985). Lipids of mitochondria. *Biochimica et biophysica acta.* **822**:1-42.

de Gramont, A., Figer, A., Seymour, M., Homerin, M., Hmissi, A., Cassidy, J., Boni, C., Cortes-Funes, H., Cervantes, A., Freyer, G., Papamichael, D., Le Bail, N., Louvet, C., Hendler, D., de Braud, F., Wilson, C., Morvan, F. and Bonetti, A. (2000). Leucovorin and Fluorouracil With or Without Oxaliplatin as First-Line Treatment in Advanced Colorectal Cancer. *Journal of Clinical Oncology.* **18**:2938-2947.

de Jong, A.E., Morreau, H., Nagengast, F.M., Mathus-Vliegen, E.M.H., Kleibeuker, J.H., Griffioen, G., Cats, A., and Vasen, H.F.A. (2005). Prevalence of adenomas among young individuals at average risk for colorectal cancer. *The American journal of gastroenterology.* **100**:139-143.

Delesse, M.A. (1847). Procede mecanique pour determiner la composition des roche. *Compte-Rendus d' Academie des Sciences.* **25**:544-545.

Dolnick, B.J., and Cheng, Y.C. (1978). Human thymidylate synthetase. II. Derivatives of pteroylmono- and -polyglutamates as substrates and inhibitors. *The Journal of biological chemistry.* **253**:3563-3567.

Douillard, J.Y., Cunningham, D., Roth, A.D., Navarro, M., James, R.D., Karasek, P., Jandik, P., Iveson, T., Carmichael, J., Alakl, M., Gruia, G., Awad, L.

and Rougier, P. (2000). Irinotecan combined with fluorouracil compared with fluorouracil alone. as first-line treatment for metastatic colorectal cancer: a multicentre randomised trial. *Lancet.* **255**:1041-1047.

Edler, D., Glimelius, B., Hallström, M., Jakobsen, A., Johnston, P.G., Magnusson, I., Ragnhammar, P., and Blomgren, H. (2002). Thymidylate synthase expression in colorectal cancer: a prognostic and predictive marker of benefit from adjuvant fluorouracil-based chemotherapy. *Journal of clinical oncology.* **20**:1721-1728.

Egner, J.R. (2010). AJCC Cancer Staging Manual. *JAMA.* **304**:1726.

Fawcett, D.W. *The Cell.* (W.B. Saunders Co Philadelphia, 1981).

Fearon, E.R., and Vogelstein, B. (1990). A genetic model for colorectal tumorigenesis. *Cell.* **61**:759-767.

Fedirko, V., Tramacere, I., Bagnardi, V., Rota, M., Scotti, L., Islami, F., Negri, E., Straif, K., Romieu, I., La Vecchia, C., Boffetta, P., and Jenab, M. (2011). Alcohol drinking and colorectal cancer risk: An overall and dose-Response meta-analysis of published studies. *Ann Oncol.* **22**:1958-1972.

Fischel, J.L., Formento, P., Ciccolini, J., Rostagno, P., Etienne, M.C., Catalin, J., and Milano, G. (2002). Impact of the oxaliplatin-5 fluorouracil-folinic acid combination on respective intracellular determinants of drug activity. *British journal of cancer.* **86**:1162-1168.

French, S.W., and DiSibio, G. (2008). Metastatic Patterns of Cancers: results from a large autopsy study. *Arch Pathol Lab Med.* **132**:931-939.

Furuta, K., Ikeda, M., Nakayama, Y., Nakamura, K., Tanaka, M., Hamasaki, N., Himeno, M., Hamilton, S.R., and August, J.T. (2001). Expression of Lysosome-Associated Membrane Proteins in Human Colorectal Neoplasms and Inflammatory Diseases. *The American Journal of Pathology.* **159**:449-455.

Gardai, S.J., McPhillips, K.A., Frasch, S.C., Janssen, W.J., Starefeldt, A.,

Murphy-Ullrich, J.E., Bratton, D.L., Oldenborg, P., Michalak, M., and Henson, P.M. (2005). Cell-Surface Calreticulin Initiates Clearance of Viable or Apoptotic Cells through trans-Activation of LRP on the Phagocyte *Cell.* **123**:321-334.

Garg, A.D., Maes, H., van Vliet, A.R., and Agostinis, P. (2014). Targeting the hallmarks of cancer with therapy-induced endoplasmic reticulum (ER) stress. *Mol Cell Concol.* **2**:e975089.

Ghiringhelli, F., Apetoh, L., Tesniere, A., Aymeric, L., Ma, Y., Ortiz, C., Vermaelen, K., Panaretakis, T., Mignot, G., Ullrich, E., Perfettini, J., Schlemmer, F., Tasdemir, E., Uhl, M., Génin, P., Civas, A., Ryffel, B., Kanellopoulos, J., Tschopp, J., André, F., Lidereau, R., McLaughlin, N., Haynes, N.M., Smyth, M.J., Kroemer, G., and Zitvogel, L. (2009). Activation of the NLRP3 inflammasome in dendritic cells induces IL-1beta-dependent adaptive immunity against tumors. *Nature medicine.* **15**:1170-1178.

Giacchetti, S, Perpoint, B., Zidani, R., Le Bail, N., Faggiuolo, R., Focan, C., Chollet, P., Llory, J.F., Letourneau, Y., Coudert, B., Le Rol, A., Walter, S., Adam, R., Misset, J.L., and Levi, F. (2000). Phase III multicenter randomized trial of oxaliplatin added to chronomodulated fluorouracil – leucovorin as first-Line treatment of metastatic colorectal cancer. *Journal of Clinical Oncology.* **18**:136-147.

Gillen, C.D., Walmsley, R.S., Prior, P., Andrews, H.A., and Allan, R.N. (1994). Ulcerative colitis and Crohn's disease: a comparison of the colorectal cancer risk in extensive colitis. *Gut.* **35**:1590-1592.

Glagolev, A.A.(1933). n the geometrical methods of quantitative mineralogic analysis of rocks. *Trans. Inst. Econ. Min.* **59**:1-47.

Gong, J., Chehrazi-Raffle, A., Reddi, S., and Salgia, R. (2018). Development of PD-1 and PD-L1 inhibitors as a form of cancer immunotherapy: a comprehensive review of registration trials and future considerations. *Journal for ImmunoTherapy of Cancer.* **6**:8.

Gottesman, M.M., Fojo, T., and Bates, S.E. (2002). Multidrug resistance in cancer: role of ATP-dependent transporters. *Nature reviews. Cancer.* **2**:48-58.

Gu, Y., Li, H., Zhao, L., Zhao, S., He, W., Rui, L., Su, C., Zheng, H., and Su, R. (2015). GRP78 confers the resistance to 5-FU by activating the c-Src/LSF/TS axis in hepatocellular carcinoma. *Oncotarget.* **6**:33658-33674.

Guha, P., Kaptan, E., Gade, P., Kalvakolanu, D.V., and Ahmed, H. (2017). Tunicamycin induced endoplasmic reticulum stress promotes apoptosis of prostate cancer cells by activating mTORC1. *Oncotarget.* **8**:68192-68207.

Gullick, W.J. (1991). Prevalence of aberrant expression of the epidermal growth factor receptor in human cancers. *British medical bulletin.* **47**:87-98.

Gustavson, M.D., Molinaro, A.M., Tedeschi, G., Camp, R.L., and Rimm, D.L. (2008). AQUA Analysis of Thymidylate Synthase Reveals Localization to be a Key Prognostic Biomarker in 2 Large Cohorts of Colorectal Carcinoma. *Arch Pathol Lab Med.* **132**:1746-1752.

Guthrie, B., Makubate, B., Hernandez-Santiago, V., Dreischulte, T. (2015). The rising tide of polypharmacy and drug-drug interactions: population database analysis 1995–2010. *BMC Medicine.* **13**:74.

Haggar, F. and Boushey, R.P. (2009). Colorectal Cancer Epidemiology : Incidence , Mortality , Survival , and Risk Factors. *Clinics in colon and rectal surgery.* **6**:191-197.

Hardcastle, J.D., Chamberlain, J.O., Robinson, M.H., Moss, S.M., Amar, S.S., Balfour, T.W., James, P.D., and Mangham, C.M. (1996). Randomised controlled trial of faecal-occult-blood screening for colorectal cancer. *Lancet.* **348**:1472-1477.

Heidelberger, C., Chaudhuri, N.K., Denneberg, P., Mooren, D., Griesbach, L., Dusginsky, R., Schnitzer, R.J., Pleven, E., and Scheiner, J. (1957). Fluorinated Pyrimidines, A New Class of Tumour-Inhibitory Compounds. *Nature.* **179**:663-666.

Herbst, R.S., and Shin, D.M. (2002). Monoclonal antibodies to target epidermal growth factor receptor-positive tumors: a new paradigm for cancer therapy. *Cancer.* **94**:1593-1611.

Hewitson, P., Glasziou, P., Irwig, L., Towler, B., and Watson, E. (2007). Screening for colorectal cancer using the faecal occult blood test, Hemoccult. *The Cochrane database of systematic reviews.* **24**:CD001216.

Houghton, J.A., Tillman, D.M., and Harwood, F.G. (1995). Ratio of 2'-deoxyadenosine-5'-triphosphate/thymidine-5'-triphosphate influences the commitment of human colon carcinoma cells to thymineless death. *Clinical cancer research.* **1**:723-730.

Howard, C.V. and Reed, M.G. *Unbiased Stereology: Three-Dimensional Measurement in Microscopy.* (BIOS Scientific Publishers Oxford, 1998).

Hughes, R., Cross, J., Pollock, J.R., and Bingham, S. (2001). Dose-dependent effect of dietary meat on endogenous colonic N-nitrosation. *Carcinogenesis.* **22**:199-202.

Humeau, J., Lévesque, S., Kroemer, G., and Pol, J.G. Gold Standard Assessment of Immunogenic Cell Death in Oncological Mouse Models. *Methods in molecular biology.* **1884**:297-315. booktitle = Methods in molecular biology (Clifton, N.J.),

Inoue, T., Hibi, K., Nakayama, G., Komatsu, Y., Fukuoka, T., Kodera, Y., Ito, K., Akiyama, S., and Nakao, A. Expression level of thymidylate synthase is a good predictor of chemosensitivity to 5-fluorouracil in colorectal cancer. *Journal of Gastroenterology.* **40**:143-147.

Jackson-Thompson, J., Ahmed, F., German, R.R., Lai, S., and Friedman, C. (2006). Descriptive epidemiology of colorectal cancer in the United States, 1998–2001. *Cancer.* **107**:1103-1111.

Jelsema, C.L., and Morré, D.J. (1978). Distribution of phospholipid biosynthetic enzymes among cell components of rat liver. *J. Biol. Chem.* **253**:7960-7971.

Jemal, A., Siegel, R., Ward, E., Hao, Y., Xu, J., and Thun, M.J. (2009). Cancer Statistics, 2009. *CA: A Cancer Journal for Clinicians.* **59**:225-249.

Jemal, A., Tiwari, R.C., Murray, T., Ghafoor, A., Samuels, A., Ward, E., Feuer, E.J., and Thun, M.J. Cancer statistics, 2004. *CA: a cancer journal for clinicians.* **54**:8-29.

Ji, H., Huang, C., Wu, S., and Kasim, V. (2019). XBP1-s promotes colorectal cancer cell proliferation by inhibiting TAp73 transcriptional activity. *Biochemical and Biophysical Research Communications.* **508**:203-209.

Jin, C., Jin, Z., Chen, N., Lu, M., Liu, C., Hu, W., and Zheng, C. (2016). Activation of IRE1α-XBP1 pathway induces cell proliferation and invasion in colorectal carcinoma. *Biochemical and Biophysical Research Communications.* **470**:75-81.

Johnson, S., Michalak, M., Opas, M., and Eggleton, P. (2001). The ins and outs of calreticulin: from the ER lumen to the extracellular space. *Trends in Cell Biology.* **11**:122-129.

Johnston, P.G., Lenz, H., Leichman, C.G., Danenberg, K.D., Allegra, C.J., Danenberg, P.V., and Leichman, L. (1995). Thymidylate Synthase Gene and Protein Expression Correlate and Are Associated with Response to 5-Fluorouracil in Human Colorectal and Gastric Tumors. *Cancer Research.* **55**:1407-1412.

Jones, S., Chen, W., Parmigiani, G., Diehl, F., Beerenwinkel, N., Antal, T., Traulsen, A., Nowak, M.A., Siegel, C., Velculescu, V.E., Kinzler, K.W., Vogelstein, B., Willis, J., Markowitz, S.D. (2008). Comparative lesion sequencing provides insights into tumor evolution. *Prodeedings of the National Academy of Sciences.* **105(11)**:4283-4288.

Kang, R., Zhang, Q., Zeh, H.J., Lotze, M.T., Tang, D., and Tang, D. (2013). HMGB1 in cancer: good, bad, or both? *Clinical cancer research.* **19**:4046-4057.

Kawato, Y., Aonuma, M., Hirota, Y., Kuga, H. and Sato, K. (1991). Intracellular roles of SN-38, a metabolite of the camptothecin derivative CPT-11, in the antitumor

effect of CPT-11. *Cancer research.* **51**:4187-4191.

Kedersha, N., Stoecklin, G., Ayodele, M., Yacono, P., Lykke-Andersen, J., Fritzler, M.J., Scheuner, D., Kaufman, R.J., Golan, D.E., and Anderson, P. (2005). Stress granules and processing bodies are dynamically linked sites of mRNP remodeling. *The Journal of cell biology.* **169**:871-884.

Kedersha, N., and Anderson, P. (2007). Mammalian Stress Granules and Processing Bodies. *Methods in Enzymology.* **431**:61-81.

Koopman, M., Venderbosch, S., van Tinteren, H., Ligtenberg, M.J., Nagtegaal, I., Van Krieken, J.H., and Punt, C.J. (2009). Predictive and prognostic markers for the outcome of chemotherapy in advanced colorectal cancer, a retrospective analysis of the phase III randomised CAIRO study. *European Journal of Cancer.* **45**:1999-2006.

Kornmann, B., Nunnari, J., Weissman, J.S., Schuldiner, M., Collins, S.R., Currie, E. and Walter, P. (2009). An ER-Mitochondria Tethering Complex Revealed by a Synthetic Biology Screen. *Science.* **325**:477-481.

Kronborg, O., Fenger, C., Olsen, J., Jørgensen, O.D., and Søndergaard, O. (1996). Randomised study of screening for colorectal cancer with faecal-occult-blood test. *Lancet.* **348**:1467-1471.

Krynetskaia, N., Xie, H., Vucetic, S., Obradovic, Z., and Krynetskiy, E. (2007). High Mobility Group Protein B1 Is an Activator of Apoptotic Response to Antimetabolite Drugs. *Molecular Pharmacology.* **73**:260-269.

Krysko, D.V., Garg, A.D., Kaczmarek, A., Krysko, O., Agostinis, P., and Vandenabeele, P. (2012). Immunogenic cell death and DAMPs in cancer therapy. *Nature Reviews Cancer.* **12**:860-875.

Lee, A., Iwakoshi, N.N., and Glimcher, L.H. (2003). XBP-1 Regulates a Subset of Endoplasmic Reticulum Resident Chaperone Genes in the Unfolded Protein Response. *Molecular and Cellular Biology.* **23**:7448-7459.

Lee, K., Tirasophon, W., Shen, X., Michalak, M., Prywes, R., Okada, T., Yoshida, H., Mori, K., and Kaufman, R.J. (2002). IRE1-mediated unconventional mRNA splicing and S2P-mediated ATF6 cleavage merge to regulate XBP1 in signaling the unfolded protein response. *Genes & development.* **16**:452-466.

Lehman, N.L., and Danenberg, P.V. (2000). Modulation of RTX cytotoxicity by thymidine and dipyridamole in vitro: implications for chemotherapy. *Cancer Chemotherapy and Pharmacology.* **45**:142-148.

Li, J., Wu, X., Gan, L., Yang, X., and Miao, Z. (2017). Hypoxia induces universal but differential drug resistance and impairs anticancer mechanisms of 5-fluorouracil in hepatoma cells. *Acta Pharmacologica Sinica.* **38**:1642-1654.

Li, K.M., Rivory, L., and Clarke, S. (2005). Rapid quantitation of plasma 2'-deoxyuridine by high-performance liquid chromatography/atmospheric pressure chemical ionization mass spectrometry and its application to pharmacodynamic studies in cancer patients. *Journal of Chromatography B.* **820**:121-130.

Li, K.M., Rivory, L.P., Hoskins, J., Sharma, R., and Clarke, S.J. (2007). Altered deoxyuridine and thymidine in plasma following capecitabine treatment in colorectal cancer patients. *British journal of clinical pharmacology.* **63**:67-74.

Liu, C., and Kaufman, R.J. (2003). The unfolded protein response. *Journal of cell science.* **116**:1861-1862.

Liu, J., Schmitz, J.C., Lin, X., Tai, N., Yan, W., Farrell, M., Bailly, M., min Chen, T. and Chu, E. (2002). Thymidylate synthase as a translational regulator of cellular gene expression. *Biochimica et biophysica acta.* **1587**:174-182.

Longley, D.B. and Johnston, P.G. (2005). Molecular mechanisms of drug resistance. *Journal of Pathology.* **205**:275-292.

Longley, D., Harkin, D., and Johnston, P. (2003). 5-Fluorouracil: Mechanisms of Action and Clinical Strategies. *Nature reviews. Cancer.* **3**:330-338.

Lotze, M.T. and Tracey, K.J. (2003). High-mobility group box 1 protein (HMGB1): nuclear weapon in the immune arsenal. *Nature Reviews Immunology.* **5**:331-342.

Lu, K., McGuire, J.J., Slocum, H.K., and Rustum, Y.M. (1997). Mechanisms of acquired resistance to modulation of 5-fluorouracil by leucovorin in HCT-8 human ileocecal carcinoma cells. *Biochemical Pharmacology.* **53**:689-696.

Luo, B., Repalli, J., Yousef, A., Johnson, S.R., Lebioda, L., and Berger, S.H. uman thymidylate synthase with loop 181-197 stabilized in an inactive conformation: ligand interactions, phosphorylation, and inhibition profiles. *Protein science.* **20**:87-94.

Lykidis, A., and Jackowski, S. (2000). Regulation of mammalian cell membrane biosynthesis. *Progress in Nucleic Acid Research and Molecular Biology.* **65**:361-393.

Ma, M.K., and McLeod, H.L. (2003). Lessons learned from the irinotecan metabolic pathway. *Current medicinal chemistry.* **10**:41-49.

MacFarlane, A.J., Anderson, D.D., Flodby, P., Perry, C.A., Allen, R.H., Stabler, S.P., and Stover, P.J. (2011). Nuclear localization of de novo thymidylate biosynthesis pathway is required to prevent uracil accumulation in DNA. *The Journal of biological chemistry.* **286**:44015-44022.

Mandai, M., Hamanishi, J., Abiko, K., Matsumura, N., Baba, T., and Konishi, I. (2016). Dual Faces of IFN in Cancer Progression: A Role of PD-L1 Induction in the Determination of Pro- and Antitumor Immunity. *Clinical Cancer Research.* **22**:2329-2334.

Mandel, J.S., Bond, J.H., Church, T.R., Snover, D.C., Bradley, G.M., Schuman, L.M., and Ederer, F. (1993). Reducing Mortality from Colorectal Cancer by Screening for Fecal Occult Blood. *New England Journal of Medicine.* **328**:1365-1371.

Mann, B., Gelos, M., Siedow, A., Hanski, M.L., Gratchev, A., Bodmer, W.F., Moyer, M.P., Riecken, E.O., Buhr, H.J., and Hanski, C. (1999). Target genes of

beta-catenin-T cell-factor/lymphoid-enhancer-factor signaling in human colorectal carcinomas. *Medical Sciences.* **96**:1603-1608.

Marques, R.P., Duarte, G.S., Sterrantino, C., Pais, H.L., Quintela, A., Martins, A.P., and Costa, J. (2017). Triplet (FOLFOXIRI) versus doublet (FOLFOX or FOLFIRI) backbone chemotherapy as first-line treatment of metastatic colorectal cancer: A systematic review and meta-analysis. *Critical Reviews in Oncology/Hematology.* **118**:54-62.

McGuigan, C., Murziani, P., Slusarczyk, M., Gonczy, B., Vande Voorde, J., Liekens, S., and Balzarini, J. (2011). Phosphoramidate protides of the anticancer agent FUDR successfully deliver the preformed bioactive monophosphate in cells and confer advantage over the parent nucleoside. *Journal of Medicinal Chemistry.* **54**:7247-7258.

Meldolesi, J. (1967). On the significance of the hypertrophy of the smooth endoplasmic reticulum in liver cells after administration of drugs. *Biochemical Pharmacology.* **16**:125-129.

Meyers, M., Wagner, M.W., Mazurek, A., Schmutte, C., Fishel, R., Boothman, D.A. (2005).DNA mismatch repair-dependent response to fluoropyrimidine-generated damage. *The Journal of biological chemistry.* **280**:5516-5526.

Mhaidat, N.M., Alzoubi, K.H., and Abushbak, A. (2015). X-box binding protein 1 (XBP-1) enhances colorectal cancer cell invasion. *Journal of Chemotherapy.* **27**:167-173.

Michalak, M., Burns, K., Andrin, C., Mesaeli, N., Jass, G.H., Busaan, J.L., and Opas, M. (1996). Endoplasmic reticulum form of calreticulin modulates glucocorticoid-sensitive gene expression. *The Journal of biological chemistry.* **271**:29436-29335.

Michalak, M., Groenendyk, J., Szabo, E., Gold, L.I. and Opas, M. (2009). Calreticulin, a multi-process calcium-buffering chaperone of the endoplasmic

reticulum. *Biochemical Journal.* **417**:651-666.

Nakamura, K., Zuppini, A., Arnaudeau, S., Lynch, J., Ahsan, I., Krause, R., Papp, S., De Smedt, H., Parys, J.B., Müller-Esterl, W., Daniel, P., Krause, K., Demaurex, N., Opas, M., and Michalak, M. Functional specialization of calreticulin domains. *The Journal of Cell Biology.* **154**:961-972.

National Institute for HeaLth and Care Excellence. *Colorectal cancer: diagnosis and management (2014).* Available at https://www.nice.org.uk/guidance/cg131. [ACCESSED ON 21/03/19].

Niedzwiecki, D., Hasson, R.M., Lenz, H., Ye, C., Redston, M., Ogino, S., Fuchs, C.S., Compton, C.C., Mayer, R.J., Goldberg, R.M., Colacchio, T.A., Saltz, L.B., Warren, R.S., and Bertagnolli, M.M. (2017). A Study of Thymidylate Synthase Expression as a Biomarker for Resectable Colon Cancer: Alliance (Cancer and Leukemia Group B) 9581 and 89803. *The Oncologist.* **22**:107-114.

Nishitoh, H. (2012). CHOP is a multifunctional transcription factor in the ER stress response. *J. Biochem.* **151**:217-219.

Nottebrock, H., and Then, R. (1977). Thymidine concentrations in serum and urine of different animal species and man. *Biochemical Pharmacology.* **26**:2175-2179.

Obeid, M., Tesniere, A., Ghiringhelli, F., Fimia, G., Apetoh, L., Perfettini, J., Castedo, M., Mignot, G., Panaretakis, T., Casares, N., Métivier, D., Larochette, N., van Endert, P., Ciccosanti, F., Piacentini, M., Zitvogel, L., and Kroemer, G. (2007). Calreticulin exposure dictates the immunogenicity of cancer cell death. *Nature Medicine.* **13**:54-61.

Ojha, R. and Amaravadi, R.K. (2017). Targeting the unfolded protein response in cancer. *Pharmacological research.* **120**:258-266.

Oldenhuis, C.N.A.M., Oosting, S.F., Gietema, J.A. and de Vries, E.G.E. (2008). Prognostic versus predictive value of biomarkers in oncology. *European Journal of Cancer.* **44**:946-953.

Omura, K. (2008). Advances in Chemotherapy against Advanced or Metastatic Colorectal Cancer. *Digestion.* **77**:13-22.

Oslowski, C.M., and Urano, F. (2011). Measuring ER stress and the unfolded protein response using mammalian tissue culture system. *Methods in enzymology.* **490**:71-92.

Pavelka, M., and Roth, J. *Functional Ultrastructure: Nuclear Envelope and Rough Endoplasmic Reticulum.* (Springer Vienna, 2010).

Peters, G.J., van der Wilt, C.L., van Groeningen, C.J., Smid, K., Meijer, S., and Pinedo, H.M. (1994). Thymidylate synthase inhibition after administration of fluorouracil with or without leucovorin in colon cancer patients: implications for treatment with fluorouracil. *Journal of Clinical Oncology.* **12**:2035-2042.

Pettersen, H.S., and Visnes, T., Vågbø, C.B., and Svaasand, E.K., Doseth, B., Slupphaug, G., Kavli, B., and Krokan, H.E. (2011). UNG-initiated base excision repair is the major repair route for 5-fluorouracil in DNA, but 5-fluorouracil cytotoxicity depends mainly on RNA incorporation. *Nucleic Acids Research.* **39**:8430-8444.

Pino, Ma.S., and Chung, D.C. (2010). The chromosomal instability pathway in colon cancer. *Gastroenterology.* **138**:2059-2072.

Polk, A., Vaage-Nilsen, M., Vistisen, K., and Nielsen, D.L. (2013). Cardiotoxicity in cancer patients treated with 5-fluorouracil or capecitabine: A systematic review of incidence, manifestations and predisposing factors. *Cancer Treatment Reviews.* **39**:974-984.

Poon, I.K.H., Lucas, C.D., Rossi, A.G., and Ravichandran, K.S. (2014). Apoptotic cell clearance: basic biology and therapeutic potential. *Nature Reviews Immunology.* **14**:166-180.

Potten, C.S., Kellett, M., Rew, D.A., and Roberts, S.A. (1992). Proliferation in human gastrointestinal epithelium using bromodeoxyuridine in vivo: data for

different sites, proximity to a tumour, and polyposis coli. *Gut.* **33**:524-529.

Powell, C.M., Rudge, T.L., Zhu, Q., Johnson, L.F., and Hansen, U. (2000). Inhibition of the mammalian transcription factor LSF induces S-phase-dependent apoptosis by downregulating thymidylate synthase expression. *The EMBO journal.* **19**:4665-4675.

Powell, S.M., Zilz, N., Beazer-Barclay, Y., Bryan, T.M., Hamilton, S.R., Thibodeau, S.N., Vogelstein, B., and Kinzler, K.W. (1992). APC mutations occur early during colorectal tumorigenesis. *Nature.* **359**:235-237.

Radparvar, S., Houghton, P.J., and Houghton, J.A. (1989). Effect of polyglutamylation of 5,10-methylenetetrahydrofolate on the binding of 5-fluoro-2'-deoxyuridylate to thymidylate synthase purified from a human colon adenocarcinoma xenograft. *Biochemical Pharmacology.* **38**:335-342.

Rang, H., Ritter, J., Flower, R., Henderson, G., and Dale, M. *Rang and Dale's pharmacology.* (Churchhill Livingstone Edinburgh, 2012).

Rébé, C., and Ghiringhelli, F. (2015). Cytotoxic effects of chemotherapy on cancer and immune cells: how can it be modulated to generate novel therapeutic strategies? *Future Oncology.* **11**:2645-2654.

Riggs, A.C., Bernal-Mizrachi, E., Ohsugi, M., Wasson, J., Fatrai, S., Welling, C., Murray, J., Schmidt, R.E., Herrera, P.L., and Permutt, M.A. (2005). Mice conditionally lacking the Wolfram gene in pancreatic islet beta cells exhibit diabetes as a result of enhanced endoplasmic reticulum stress and apoptosis. *Diabetologia.* **48**:2313-2321.

Roderick, H.L., Campbell, A.K., and Llewellyn, D.H. (1997). Nuclear localisation of calreticulin in vivo is enhanced by its interaction with glucocorticoid receptors. *FEBS Letters.* **405**:181-185.

Romero-Ramirez, L., Cao, H., Nelson, D., Hammond, E., Lee, A., Yoshida, H., Mori, K., Glimcher, L.H., Denko, N.C., Giaccia, A.J., Le, Q., and Koong, A.C. (2004).

XBP1 Is Essential for Survival under Hypoxic Conditions and Is Required for Tumor Growth. *Cancer Research.* **64**:5943-5947.

Rom-Jurek, E., Kirchhammer, N., Ugocsai, P., Ortmann, O., Wege, A.K., and Brockhoff, G. (2018). Regulation of Programmed Death Ligand 1 (PD-L1) Expression in Breast Cancer Cell Lines In Vitro and in Immunodeficient and Humanized Tumor Mice. *International journal of molecular sciences.* **19**:563.

Ron, D., and Walter, P. (2007). Signal integration in the endoplasmic reticulum unfolded protein response. *Nature Reviews Molecular Cell Biology.* **8**:519-529.

Roper, J., and Hung, K. (2013). *Molecular Mechanisms of Colorectal Carcinogenesis.* (Springer New York, 2013).

Rubinfeld, B., Albert, I., Porfiri, E., Fiol, C., Munemitsu, S., and Polakis, P. (1996). Binding of GSK3β to the APC-β-catenin complex and regulation of complex assembly. *Science.* **272**:1023-1026.

Ruby, J.R., Dyer, R.F., and Skalko, R.G. (1969). Continuities between mitochondria and endoplasmic reticulum in the mammalian ovary. *Zeitschrift fur Zellforschung und Mikroskopische Anatomie.* **97**:30-37.

Rudakova, E.V., Boltneva, N.P., and Makhaeva, G.F. (2011). Comparative analysis of esterase activities of human, mouse, and rat blood. (2011). *Bulletin of experimental biology and medicine.* **152**:73-75.

Sachs, J.R., Mayawala, K., Gadamsetty, S., Kang, S.P., and De Alwis, D.P. (2016). Optimal Dosing for Targeted Therapies in Oncology: Drug Development Cases Leading by Example. *Clinical Cancer Research.* **22**:1318-1324.

Saif, M.W., and Diasio, R. (2006). Is Capecitabine Safe in Patients with Gastrointestinal Cancer and Dihydropyrimidine Dehydrogenase Deficiency? *Clinical Colorectal Cancer.* **5**:359-362.

Saitoh, O., Wang, W.C., Lotan, R., and Fukuda, M. (1992). Differential

glycosylation and cell surface expression of lysosomal membrane glycoproteins in sublines of a human colon cancer exhibiting distinct metastatic potentials. *The Journal of biological chemistry.* **267**:5700-5711.

Shen, X., Ellis, R.E., Lee, K., Liu, C., Yang, K., Solomon, A., Yoshida, H., Morimoto, R., Kurnit, D.M., Mori, K., and Kaufman, R.J. (2001). Complementary Signaling Pathways Regulate the Unfolded Protein Response and Are Required for C. elegans Development. *Cell.* **107**:893-903.

Shia, J. (2008). Immunohistochemistry versus Microsatellite Instability Testing For Screening Colorectal Cancer Patients at Risk For Hereditary Nonpolyposis Colorectal Cancer Syndrome. *The Journal of Molecular Diagnostics.* **10**:293-300.

Skehan, P., Storeng, R., Scudiero, D., Monks, A., McMahon, J., Vistica, D., Warren, J.T., Bokesch, H., Kenney, S., and Boyd, M.R. (1990). New Colorimetric Cytotoxicity Assay for Anticancer-Drug Screening. *Journal of the National Cancer Institute.* **82**:1107-1112.

Smith, C.S., and Guttman, L. (1953). Measurement of internal boundaries in three-dimensional structures by random sectioning. *Trans. AIME.* **197**:81.

Smith, P.G., Marshman, E., Newell, D.R., and Curtin, N.J. (2000). Dipyridamole potentiates the in vitro activity of MTA (LY231514) by inhibition of thymidine transport. *British journal of cancer.* **82**:924-930.

Soeda, H., Shimodaira, H., Gamoh, M., Ando, H., Isobe, H., Suto, T., Takahashi, S., Kakudo, Y., Amagai, K., Mori, T., Watanabe, M., Yamaguchi, T., Kato, S., Ishioka, C. (2014). Phase II trial of cetuximab plus irinotecan for oxaliplatin- and irinotecan-based chemotherapy-refractory patients with advanced and/or metastatic colorectal cancer: evaluation of efficacy and safety based on KRAS mutation status (T-CORE0801). *Oncology.* **87(1)**:7-20.

Sottoriva, A., Kang, H., Ma, Z., Graham, T., Salomon, M.P., Zhao, J., Marjoram, P., Siegmund, K., Press, M., Shibata, D., and Curtis, C. (2015). A Big Bang model

of human colorectal tumor growth. *Nature Genetics.* **47**:209-216.

Sriburi, R., Jackowski, S., Mori, K., and Brewer, J.W. (2004). XBP1: a link between the unfolded protein response, lipid biosynthesis, and biogenesis of the endoplasmic reticulum. *The Journal of cell biology.* **167**:35-41.

Steele, S.R., Park, G.E., Johnson, E.K., Martin, M.J., Stojadinovic, A., Maykel, J.A., Causey, M.W. (2014). The impact of age on colorectal cancer incidence, treatment, and outcomes in an equal-access health care system. *Diseases of the colon and rectum.* **57(3)**:303-10.

Strese, S., Fryknäs, M., Larsson, R., and Gullbo, J. (2013). Effects of hypoxia on human cancer cell line chemosensitivity. *BMC cancer.* **13**:331.

Sun, Z., Fourcade, J., Pagliano, O., Chauvin, J.M., Sander, C., Kirkwood, J.M., and Zarour, H.M. (2015). IL10 and PD-1 Cooperate to Limit the Activity of Tumor-Specific CD8+ T Cells. *Cancer Research.* **75**:1635-1644.

Tajima, A., Hess, M.T., Cabrera, B.L., Kolodner, R.D., and Carethers, J.M. (2004). The mismatch repair complex hMutS alpha recognizes 5-fluorouracil-modified DNA: implications for chemosensitivity and resistance. *Gastroenterology.* **127**:1678-1684. journal = Gastroenterology,

Takebayashi, Y., Yamada, K., Miyadera, K., Sumizawa, T., Furukawa, T., Kinoshita, F., Aoki, D., Okumura, H., Yamada, Y., Akiyama, S., and Aikou, T. (1990). The activity and expression of thymidine phosphorylase in human solid tumours. *European journal of cancer.* **32A**:1227-1232.

Tang, D., Kang, R., Zeh, H.J., Lotze, M.T., and Lotze, M.T. (2010). High-mobility group box 1 and cancer. *Biochimica et biophysica acta.* **1799**:131-140.

Terzić, J., Grivennikov, S., Karin, E., and Karin, M. (2010). Inflammation and Colon Cancer. *Gastroenterology.* **138**:2101-2114.

Tesniere, A., Apetoh, L., Ghiringhelli, F., Joza, N., Panaretakis, T., Kepp, O.,

Schlemmer, F., Zitvogel, L., and Kroemer, G. (2008). Immunogenic cancer cell death: a key-lock paradigm. *Current Opinion in Immunology.* **20**:504-511.

Tesniere, A., Schlemmer, F., Boige, V., Kepp, O., Martins, I., Ghiringhelli, F., Aymeric, L., Michaud, M., Apetoh, L., Barault, L., Mendiboure, J., Pignon, J., Jooste, V., van Endert, P., Ducreux, M., Zitvogel, L., Piard, F., and Kroemer, G. (2010). Immunogenic death of colon cancer cells treated with oxaliplatin. *Oncogene.* **29**:482-491.

Thastrup, O., Cullen, P.J., Drøbak, B.K., Hanley, M.R., and Dawson, A.P. (1990). Thapsigargin, a tumor promoter, discharges intracellular Ca2+ stores by specific inhibition of the endoplasmic reticulum Ca2+ -ATPase. *Proceedings of the National Academy of Sciences of the United States of America.* **87**:2466-2470.

Thirion, P., Michiels, S., Pignon, J.P., Buyse, M., Braud, A.C., Carlson, R.W., O'Connell, M., Sargent, P., Piedbois, P.; Meta-Analysis Group in Cancer. (2004). Modulation of Fluorouracil by Leucovorin in Patients With Advanced Colorectal Cancer: An Updated Meta-Analysis. *Journal of Clinical Oncology.* **18**:3766-3775.

Timmers, L., Boons, C., Mangnus, D., Van de Ven, P.M., Van den Berg, P.H., Beeker, A., Swart, E.L., Honeywell, R.J., Peters, G.J., Boven, E., and Hugtenburg, J.G. (2016). Adherence and Patients' Experiences with the Use of Capecitabine in Daily Practice. *Frontiers in pharmacology.* **7**:310.

Tsujie, M., Nakamori, S., Nakahira, S., Takahashi, Y., Hayashi, N., Okami, J., Nagano, H., Dono, K., Umeshita, K., Sakon, M., and Monden, M. Human equilibrative nucleoside transporter 1, as a predictor of 5-fluorouracil resistance in human pancreatic cancer.*Anticancer research.* **27**:2241-2249.

Twelves, C., Gollins, S., Grieve, R., and Samuel, L. (2004). A randomised cross-over trial comparing patient preference for oral capecitabine and 5-fluorouracil/leucovorin regimens in patients with advanced colorectal cancer. *Annals of Oncology.* **17**:239-245.

Ueda, M., Li, S., Itoh, M., Wang, M., Hayakawa, Miki and Islam, S., Tana, Nakagawa, K., Chen, H., and Nakagawa, T. (2016). Expanded polyglutamine embedded in the endoplasmic reticulum causes membrane distortion and coincides with Bax insertion. *Biochemical and Biophysical Research Communications.* **474**:259-263.

Ullman, B., Lee, M., Martin, D.W., and Santi, D.V. (1978). Cytotoxicity of 5-fluoro-2'-deoxyuridine: Requirement for reduced folate cofactors and antagonism by methotrexate (thymidylate synthase/irreversible inhibition/folinic acid. *Medical Sciences.* textbf75:980-983.

Van den Bosch, H. (1974). Phosphoglyceride Metabolism. *Annual Review of Biochemistry.* **43**:243-277.

Van Golde, L.M.G., Fleischer, B., and Fleischer, S. (1971). Some studies on the metabolism of phospholipids in Golgi complex from bovine and rat liver in comparison to other subcellular fractions. *Biochimica et Biophysica Acta.* **249**:318-330.

van Golde, L.M.G., Raben, J., Batenburg, J.J., Fleischer, B., Zambrano, F., and Fleischer, S. (1974). Biosynthesis of lipids in golgi complex and other subcellular fractions from rat liver. *Biochimica et Biophysica Acta.* **360**:179-192.

van Meer, G. (1989). Lipid Traffic in Animal Cells. *Annual Review of Cell Biology.* **5**:247-275.

van Vliet, A.R., and Agostinis, P. (2017). Mitochondria-Associated Membranes and ER Stress. *Current Topics in Microbiology and Immunology.* **414**:73-102.

Vance, J.E., and Vance, D.E. (1988). Does rat liver golgi have the capacity to synthesize phospholipids for lipoprotein secretion. *J. Biochem.* **263**:5898-5909.

Vance, J.E. (1990). Phospholipid Synthesis in a Membrane Fraction Associated with Mitochondria. *The Journal of Biological Chemsitry.* **265**:1.

Verfaillie, T., Rubio, N., Garg, A.D., Bultynck, G., Rizzuto, R., Decuypere, J.P., Piette, J., Linehan, C., Gupta, S., Samali, A., and Agostinis, P. (2012). PERK is required at the ER-mitochondrial contact sites to convey apoptosis after ROS-based ER stress. *Cell Death & Differentiation.* **19**:1880-1891.

Voelker, D.R. (1989). Reconstitution of phosphatidylserine import into rat liver mitochondria. *J. Biol. Chem.* **264**:8019-8025.

Wagstaff, A.J., Ibbotson, T., and Goa, K.L. (2003). Capecitabine. *Drugs.* **63**:217-236.

Walko, C.M., and Lindley, C. (2005). Capecitabine: A review. *Clinical Therapeutics.* **27**:23-44.

Walter, P., and Ron, D. (2011). The Unfolded Protein Response: From Stress Pathway to Homeostatic Regulation. *Science.* **334**:1081-1086.

Wang, J., Takeuchi, T., Tanaka, S., Kubo, S., Kayo, T., Lu, D., Takata, K., Koizumi, A., and Izumi, T. (1999). A mutation in the insulin 2 gene induces diabetes with severe pancreatic β-cell dysfunction in the Mody mouse. *Journal of Clinical Investigation.* **103**:27-37.

Wang, L., Xue, M., and Chung, D.C. (2016). c-Myc is regulated by HIF-2α in chronic hypoxia and influences sensitivity to 5-FU in colon cancer. *Oncotarget.* **7**:78910-78917.

Wang, Q., Yao, J., Jin, Q., Wang, X., Zhu, H., Huang, F., Wang, W., Qiang, J., and Ni, Q. (2017). LAMP1 expression is associated with poor prognosis in breast cancer. *Oncology letters.* **14**:4729-4735.

Wang, W., Groenendyk, J., and Michalak, M. (2012). Calreticulin signaling in health and disease. *The International Journal of Biochemistry & Cell Biology.* textbf44:842-846.

Watson, J. and Crick, F. (1953). Molecular Structure of Nucleic Acids: A Structure

for Deoxyribose Nucleic Acid. *Nature*. **171**:737-738.

White, E. (2012). Deconvoluting the context-dependent role for autophagy in cancer. *Nature Reviews Cancer*. **12**:401-410.

Willett, W.C., Stampfer, M.J., Colditz, G.A., Rosner, B.A., and Speizer, F.E. (1990). Relation of Meat, Fat, and Fiber Intake to the Risk of Colon Cancer in a Prospective Study among Women. *New England Journal of Medicine*. **323**:1664-1672.

Winawer, S.J., Zauber, A.G., Ho, M.N., O'Brien, M.J., Gottlieb, L.S., Sternberg, S.S., Waye, J.D., Schapiro, M., Bond, J.H., Panish, J.F., Ackroyd, F., Shike, M., Kurtz, R.C., Hornsby-Lewis, L., Gerdes, H., and Stewart, E.T. (1993). Prevention of Colorectal Cancer by Colonoscopic Polypectomy. *New England Journal of Medicine*. **329**:1977-1981.

Wong, N.A.C.S., Brett, L., Stewart, M., Leitch, A., Longley, D.B., Dunlop, M.G., Johnston, P.G., Lessells, A.M., and Jodrell, D.I. (2001). Nuclear thymidylate synthase expression, p53 expression and 5FU response in colorectal carcinoma. *British Journal of Cancer*. **85**:1937-1943.

Wu, T., Zhang, W., Yang, G., Li, H., Chen, Q., Song, R., Zhao, L. (2016). HGB1 overexpression as a prognostic factor for survival in cancer: a meta-analysis and systematic review. *Oncotarget*. **7**:50417-50427.

Wyatt, M.D., and Wilson, D.M. (2009). Participation of DNA repair in the response to 5-fluorouracil. *Cellular and molecular life sciences*. **66**:788-799.

Yadunandam, A.K., Yoon, J., Seong, Y., Oh, C., and Kim, G. (2012). Prospective impact of 5-FU in the induction of endoplasmic reticulum stress, modulation of GRP78 expression and autophagy in Sk-Hep1 cells. *International Journal of Oncology*. **41**:1036-1042.

Yen-Revollo, J.L., Goldberg, R.M., and McLeod, H.L. (2008). Can Inhibiting Dihydropyrimidine Dehydrogenase Limit Hand-Foot Syndrome Caused

by Fluoropyrimidines? *Clinical Cancer Research.* **14**:8-13.

Yoshiba, S., Ito, D., Nagumo, T., Shirota, T., Hatori, M., and Shintani, S. (2009). Hypoxia induces resistance to 5-fluorouracil in oral cancer cells via G1 phase cell cycle arrest. *Oral Oncology.* **45**:109-115.

Yoshida, H., Matsui, T., Yamamoto, A., Okada, T., and Mori, K. (2001). XBP1 mRNA Is Induced by ATF6 and Spliced by IRE1 in Response to ER Stress to Produce a Highly Active Transcription Factor. *Cell.* **107**:881-891.

Yoshioka, A., Yanaka, S., Hiraoka, O., Koyama, Y., Hirota, Y., Ayusawa, D., Seno, T., Garrett, C., and Wataya, Y. (1987). Deoxyribonucleoside triphosphate imbalance. 5-Fluorodeoxyuridine-induced DNA double strand breaks in mouse FM3A cells and the mechanism of cell death. *The Journal of biological chemistry.* **262**:8235-8241.

Zackular, J.P., Baxter, N.T., Iverson, K.D., Sadler, B., Petrosino, J.F., Chen, G.Y., and Schloss. P.D. (2013). The Gut Microbiome Modulates Colon Tumorigenesis. *mBio.* **4**:1-9.

Zarkavelis, G., Boussios, S., Papadaki, A., Katsanos, K.H., Christodoulou, D.K., and Pentheroudakis, G. (2017). Current and future biomarkers in colorectal cancer. *Ann Gastroenterol.* **30**:613-621.

Zou, W., and Chen, L. (2008). Inhibitory B7-family molecules in the tumour microenvironment. *Nature Reviews Immunology. 8*:467-477.

Appendix

6.1 Micoplasma Testing

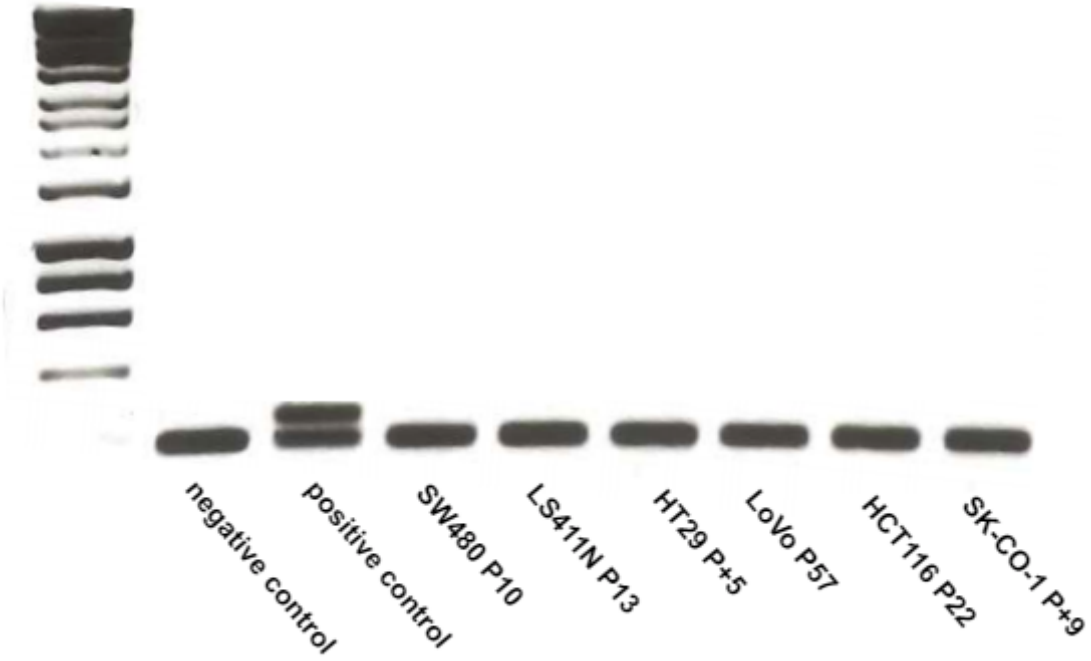

Figure 6.2: Mycoplasma test of cell lines.

As previously mentioned, cell lines were regularly tested for mycoplasma infection, an example of which is shown in Figure 6.2.

6.2 Cell Line information

Cell Line	Stage	Disease	Patient	Derived from	MMR status	TP53 status
DLD-1	Dukes' C	Colorectal adenocarcinoma	Male	Primary tumour	MSI	wt
HCT116 $p53^{-/-}$	Dukes' D	Colorectal carcinoma	48 year-old male	Primary tumour	MSI	-/-
HCT116	Dukes' D	Colorectal carcinoma	48 year-old male	Primary tumour	MSI	wt
HT29	Dukes' C	Colorectal adenocarcinoma	44 year-old female	Primary tumour	MSS	mt
LoVo	Dukes' C	Colorectal adenocarcinoma	56 year-old male	Left supraclavicular region	MSI	wt
LS411N	Dukes' B	Colorectal carcinoma	32-year-old male	Primary tumour	MSS	mt
SK-CO-1	unknown	Colorectal adenocarcinoma	65-year-old male	Ascites	MSS	wt
SW480	Dukes' B	Colorectal adenocarcinoma	50 year-old male	Primary tumour	MSS	wt
SW620	Dukes' C	Colorectal adenocarcinoma	51 year-old male	Lymph node metastasis	MSS	wt

Table 6.1: Cell Line information

6.3 TS and TS-complex in other cell lines

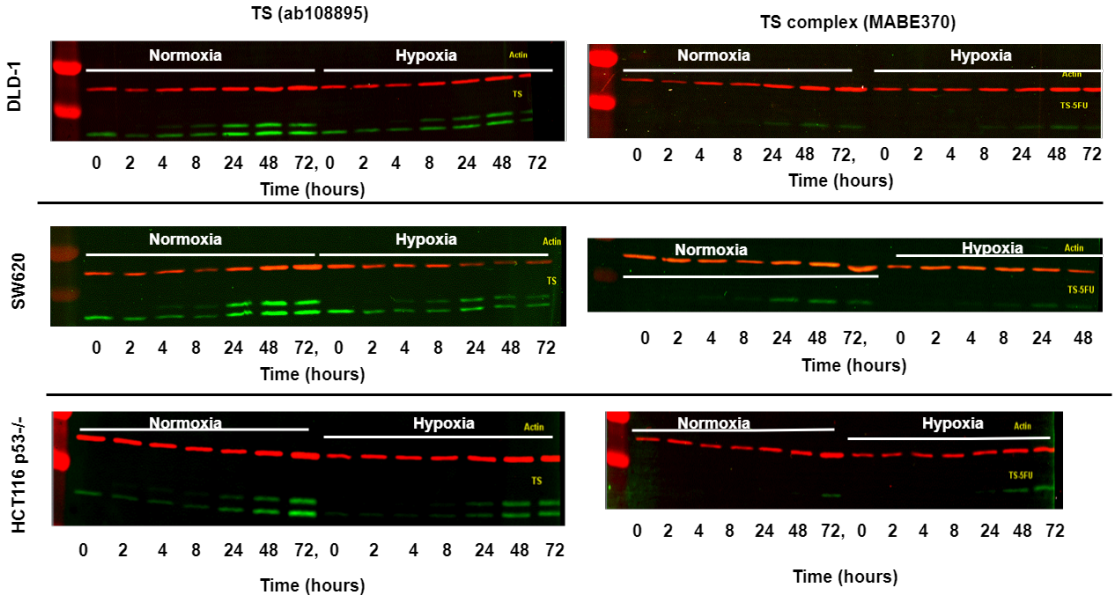

Figure 6.3: TS and TS-complex protein expression in other cell lines. Whole lysates of DLD-1, SW620 and HCT116 p53-/- cells treated with 10 μM 5-FU.

Figure 6.3 displays representative western blots of other cell lines that TS dynamics were studied in. Also shown in western blots utilising the antibody specific to TS-ternary complexes (MABE370), confirming the correspondence of the upper TS bands (using antibody ab108995) to the ternary complex.

HCT116 control rep. 1							
Micrograph	**Cytoplasm points**	**ER points**	**ER lines**	**Contact points**	**Contact lines**	**Mitochondria lines**	**Mitochondria points**
1	1	2	10	0	0	0	0
2	5	2	8	0	0	18	7
3	7	2	60	0	1	50	21
4	9	5	68	0	1	100	64
5	3	1	8	0	0	0	0
6	5	2	22	0	0	58	26
7	1	2	54	0	0	18	10
8	4	7	40	0	0	0	0
9	1	1	30	0	0	8	4
10	7	7	98	0	5	70	32
11	0	3	26	0	0	0	0
12	2	4	50	0	0	8	2
13	5	4	50	0	0	12	8
14	5	9	102	1	5	26	11
15	8	7	80	2	4	100	46
16	1	4	60	0	2	32	9
17	2	4	32	0	0	0	0
18	3	6	54	0	0	10	4
19	2	4	30	0	0	0	0
20	4	1	12	0	0	0	0
21	1	2	44	0	0	0	0
22	0	1	14	0	0	0	0
23	3	2	34	0	0	20	8
24	6	5	96	2	5	50	22
25	7	10	118	1	2	48	26
26	3	2	30	0	0	0	0
27	1	3	52	0	0	0	0
28	2	1	28	0	0	34	14
29	5	3	46	0	1	64	24
31	7	2	70	0	1	56	27
TOTAL	110	108	1426	6	27	782	365
(adjusted for grid)	2750						

Volume density/fraction (Vv)				
Vv ER, Cyt	0.03927273		1 micron	9.7
Vv Mit, Cyt	0.13272727		1 division	10.02
Surface density (Sv)				
Sv ER, Cyt	2.5099256		real L 1 div	1.032989691
Mit, Cyt	0.23499576			
Contacts, Cyt	0.00811366			
ER, ER	63.9101427	2/Sv	31.2939373	Average spacing of ER membrane
Surface Ratio (Sr)				
Sr Contacts, Mit	0.03452685			

HCT116 Thapsigargin rep. 1							
Micrograph	**Cytoplasm points**	**ER points**	**ER lines**	**Contact points**	**Contact lines**	**Mitochondria lines**	**Mitochondria points**
1	5	11	112	2	4	42	17
3	5	0	0	0	0	52	27
4	8	6	68	2	5	104	97
6	0	1	24	0	0	18	7
7	1	3	22	0	4	24	7
9	3	9	52	0	0	14	8
10	1	8	50	0	0	16	8
11	0	5	42	0	0	30	10
12	3	13	110	3	9	34	11
13	1	3	26	0	6	18	12
15	3	0	0	0	0	0	0
16	0	0	2	0	0	0	0
17	1	3	28	1	2	4	0
18	5	7	110	0	0	0	0
19	4	6	102	4	13	78	37
20	1	3	26	0	0	0	0
21	2	3	42	1	3	22	10
22	1	7	42	1	6	24	7
23	3	4	44	1	3	10	4
24	9	12	150	0	0	14	3
25	6	19	190	2	7	42	17
27	0	5	54	0	0	0	0
28	5	5	66	0	0	0	0
29	7	6	44	1	4	20	7
30	6	13	90	0	0	20	6

31	9	1	32	0	0	72	31
32	5	2	30	0	0	50	19
33	9	14	132	1	6	90	44
34	2	0	4	0	0	0	0
TOTAL	105	169	1694	19	72	798	389
(adjusted for grid)	2625						

Volume density/fraction (Vv)	
Vv ER, Cyt	0.064381
Vv Mit, Cyt	0.1481905
Surface density (Sv)	
Sv ER, Cyt	3.1236194
Mit, Cyt	0.2512231
Contacts, Cyt	0.0226667
ER, ER	48.517757
Surface Ratio (Sr)	
Sr Contacts, Mit	0.0902256

1 micron	9.7		
1 division	10.02		
real L 1 div	1.032989691		
2/Sv	41.22202072	Average spacing of ER membrane	

HCT116 Tunicamycin rep. 1							
Micrograph	**Cytoplasm points**	**ER points**	**ER lines**	**Contact points**	**Contact lines**	**Mitochondria lines**	**Mitochondria points**
1	9	14	234	3	14	130	49
2	6	7	68	0	0	20	7
3	2	4	12	1	2	26	10
4	4	16	104	0	2	30	10
5	7	17	214	0	0	102	35
6	8	5	76	1	6	48	19
7	4	2	60	0	0	24	7
8	5	10	108	3	8	52	20
10	0	2	16	0	1	22	8
11	0	4	26	0	0	4	1
12	4	7	78	0	2	22	5
13	1	3	28	0	0	28	10
14	9	15	102	0	0	10	3
15	7	9	158	1	2	18	6
16	8	9	102	1	4	38	18
17	2	1	14	2	8	44	15

18	8	5	126	5	10	48	22
19	4	6	68	0	0	0	0
20	6	0	42	0	3	90	38
21	1	3	30	1	2	14	4
22	4	2	48	1	3	44	13
23	4	0	14	0	1	10	2
24	3	1	22	0	2	70	25
25	0	0	8	0	0	0	0
26	4	7	50	0	2	86	27
27	9	3	130	0	0	12	4
28	5	3	20	0	0	0	0
30	8	4	84	1	4	36	16
31	9	13	132	2	16	190	62
TOTAL	141	172	2174	22	92	1218	436
Adjusted for grid	3525						

Volume density/fraction (Vv)				
Vv ER, Cyt	0.0487943		1 micron	9.7
Vv Mit, Cyt	0.1236879		1 division	10.02
Surface density (Sv)				
Sv ER, Cyt	2.9852069		real L 1 div	1.032989691
Mit, Cyt	0.2855447			
Contacts, Cyt	0.0215682			
ER, ER	61.179385	2/Sv	32.6907501	Average spacing of ER membrane
Surface Ratio (Sr)				
Sr Contacts, Mit	0.0755337			

HCT116 NUC-3373 6 hours rep. 1							
Micrograph	**Cytoplasm points**	**ER points**	**ER lines**	**Contact points**	**Contact lines**	**Mitochondria lines**	**Mitochondria points**
1	8	13	94	0	0	28	15
2	7	21	112	1	4	32	12
3	3	5	64	2	6	16	5
4	6	5	68	2	6	96	31
5	5	4	66	1	4	26	11
6	0	0	0	0	0	0	0
7	0	0	0	0	0	0	0
8	3	6	66	2	9	56	21
9	6	10	86	3	6	60	21

10	5	14	114	1	2	38	16
11	7	4	80	0	1	72	26
12	1	6	62	0	0	4	1
13	4	8	160	1	2	52	16
14	6	9	110	0	7	56	19
15	6	6	92	1	4	28	7
16	4	12	134	1	5	56	13
17	2	5	90	0	0	14	5
18	3	3	60	0	0	22	7
19	1	0	28	0	0	0	0
20	3	2	60	1	4	54	13
21	2	0	16	0	1	30	13
23	1	0	10	0	0	0	0
24	0	2	20	0	0	0	0
25	3	3	64	0	2	26	7
26	1	0	10	0	0	0	0
27	4	10	66	0	1	36	16
28	5	2	30	1	4	48	23
29	0	1	8	0	0	0	0
30	1	1	42	0	2	42	14
TOTAL	97	152	1812	17	70	892	312
Adjusted for grid	2425						

Volume density/fraction (Vv)					
Vv ER, Cyt	0.062680412		1 micron		9.7
Vv Mit, Cyt	0.128659794		1 division		10.02
Surface density (Sv)					
Sv ER, Cyt	3.616766467		real L 1 div		1.032989691
Mit, Cyt	0.303975853				
Contacts, Cyt	0.023854607				
ER, ER	57.70170186	2/Sv	34.66102	Average spacing of ER membrane	
Surface Ratio (Sr)					
Sr Contacts, Mit	0.078475336				

HCT116 NUC-3373 12 hours rep. 1							
Micrograph	**Cytoplasm points**	**ER points**	**ER lines**	**Contact lines**	**Contact lines**	**Mitochondria lines**	**Mitochondria points**
1	7	15	172	0	1	52	20
2	5	19	142	1	4	44	13
3	7	14	162	0	4	58	26
4	3	7	78	0	1	4	1
5	0	4	34	0	1	8	3
6	3	3	24	0	1	36	11
7	9	7	50	0	0	58	30
8	6	14	168	1	2	30	10
9	3	6	70	1	2	24	14
10	2	3	54	0	0	4	1
15	6	6	108	2	4	72	24
16	0	5	38	0	1	14	5
17	0	0	0	0	0	0	0
18	8	8	66	1	4	22	10
19	5	4	50	1	5	60	29
20	2	9	62	0	1	4	1
21	6	3	38	0	2	22	13
22	7	11	112	5	10	102	42
23	6	10	136	1	9	66	24
24	0	0	0	0	0	0	0
25	2	4	24	0	0	0	0
26	9	17	208	1	6	56	25
27	3	8	82	0	1	6	2
28	8	2	56	0	1	14	4
29	9	10	88	2	4	50	22
30	6	4	36	0	0	8	3
TOTAL	122	193	2058	16	64	814	333
Adjusted for grid	3050						

Volume density/fraction (Vv)					
Vv ER, Cyt	0.063278689		1 micron		9.7
Vv Mit, Cyt	0.109180328		1 division		10.02
Surface density (Sv)					
Sv ER, Cyt	3.266025326		real L 1 div		1.032989691
Mit, Cyt	0.220551766				
Contacts, Cyt	0.017340679				
ER, ER	51.6133536	2/Sv	38.749662	Average spacing of ER membrane	
Surface Ratio (Sr)					
Sr Contacts, Mit	0.078624079				

HCT116 NUC-3373 24 hours rep. 1							
Micrograph	**Cytoplasm points**	**ER points**	**ER lines**	**Contact points**	**Contact lines**	**Mitochondria lines**	**Mitochondria points**
1	7	8	66	1	4	110	50
2	2	5	34	0	0	0	0
3	3	7	58	0	0	12	4
4	6	8	94	3	7	58	25
5	6	14	78	0	0	0	0
6	9	10	88	0	0	0	0
7	4	4	84	1	2	26	7
8	8	6	40	0	0	12	4
9	6	11	126	0	6	68	25
10	0	3	26	0	0	8	4
11	8	8	122	0	3	30	8
12	2	3	38	0	1	24	7
13	1	4	34	0	0	0	0
14	7	14	96	3	7	40	13
15	6	12	112	2	9	68	30
16	6	6	60	2	8	8	4
17	7	11	184	2	11	104	39
18	5	8	120	0	4	30	11
19	0	1	18	0	0	0	0
20	4	13	108	1	6	38	12
21	4	9	72	0	0	0	0
22	3	3	22	2	7	38	13
23	7	5	72	1	3	34	11

24	3	10	84	2	4	26	8
25	3	6	72	2	7	62	24
26	4	3	42	1	6	68	23
27	4	6	50	0	0	16	2
29	7	11	138	0	0	0	0
30	2	2	40	0	0	0	0
31	3	4	62	0	4	76	23
TOTAL	137	215	2240	23	99	956	347
Adjusted for grid	3425						

Volume density/fraction (Vv)					
Vv ER, Cyt	0.062773723		1 micron	9.7	
Vv Mit, Cyt	0.101313869		1 division	10.02	
Surface density (Sv)					
Sv ER, Cyt	3.165639524		real L 1 div	1.03299	
Mit, Cyt	0.230665844				
Contacts, Cyt	0.023886944				
ER, ER	50.42937381	2/Sv	39.659426	Average spacing of ER membrane	
Surface Ratio (Sr)					
Sr Contacts, Mit	0.103556485				

HCT116 NUC-3373 48 hours rep. 1							
Micrograph	**Cytoplasm points**	**ER points**	**ER lines**	**Contact points**	**Contact lines**	**Mitochondria lines**	**Mitochondria points**
1	8	12	72	1	16	130	46
2	5	6	96	2	6	52	11
3	2	4	40	0	0	14	2
4	1	2	44	0	1	4	1
5	5	10	110	2	12	60	12
6	4	14	116	0	0	0	0
7	0	4	50	1	8	20	4
8	3	6	52	2	15	92	22
9	2	1	28	0	0	16	5
10	0	1	12	0	0	0	0
11	5	6	58	1	3	38	13
12	3	3	42	2	4	16	5
13	5	8	92	1	6	56	18

14	0	1	34	0	0	0	0
15	6	8	174	1	7	76	32
16	4	10	116	2	10	72	23
17	2	2	32	0	0	12	7
18	9	13	208	1	3	48	17
19	2	1	34	1	3	32	9
20	1	1	12	0	0	0	0
21	5	5	68	0	4	38	11
22	2	2	8	0	0	22	5
23	4	5	72	1	3	32	8
24	1	7	52	0	2	20	6
25	1	1	16	0	0	14	3
26	7	4	50	2	5	22	9
27	2	1	26	0	0	58	10
28	6	16	150	2	10	80	23
29	1	2	12	0	0	0	0
30	7	20	170	1	4	24	8
TOTAL	103	176	2046	23	122	1048	310
Adjusted for grid	2575						

Volume density/fraction (Vv)				
Vv ER, Cyt	0.06834951			
Vv Mit, Cyt	0.12038835			
Surface density (Sv)				
Sv ER, Cyt	3.84593919			
Mit, Cyt	0.33633342			
Contacts, Cyt	0.03915332			
ER, ER	56.2687126	2/Sv	35.54373	Average spacing of ER membrane
Surface Ratio (Sr)				
Sr Contacts, Mit	0.11641221			

1 micron	9.7		
1 division	10.02		
real L 1 div	1.032989691		

HCT116 NUC-3373 72 hours rep. 1							
Micrograph	**Cytoplasm points**	**ER points**	**ER lines**	**Contact points**	**Contact lines**	**Mitochondria lines**	**Mitochondria points**
1	6	8	160	0	3	60	17
2	1	0	0	0	0	0	0
3	3	0	16	0	0	34	8
4	9	5	66	1	10	154	52
12	6	3	18	0	0	44	12
13	9	2	12	0	2	72	20
14	1	9	82	1	6	28	6
15	3	4	32	1	8	64	17
16	3	7	36	0	0	0	0
17	5	5	78	0	4	74	23
18	8	9	94	3	9	130	32
19	9	26	146	2	7	66	27
20	3	8	26	0	0	0	0
21	2	2	18	0	0	0	0
22	6	12	110	0	2	38	10
23	3	6	32	0	0	6	2
24	9	16	130	1	5	26	7
25	5	7	66	1	4	74	28
26	1	8	50	1	2	34	13
27	4	5	84	0	0	14	5
28	0	5	38	0	0	0	0
29	0	1	18	0	3	18	4
31	9	4	68	1	2	44	18
32	9	14	104	0	0	0	0
33	7	16	136	2	6	80	26
34	3	0	0	0	0	6	1
35	4	1	44	0	2	116	33
36	7	16	156	0	1	40	13
37	5	4	60	4	7	96	30
38	4	3	40	1	8	64	17
TOTAL	144	206	1920	19	91	1382	421
Adjusted for grid	3600						

Volume density/fraction (Vv)				
Vv ER, Cyt	0.05722222		1 micron	9.7
Vv Mit, Cyt	0.11694444		1 division	10.02
Surface density (Sv)				
Sv ER, Cyt	2.58150366		real L 1 div	1.0329897
Mit, Cyt	0.31724261			
Contacts, Cyt	0.02088935			
ER, ER	45.1136562	2/Sv	44.3324742	Average spacing of ER membrane
Surface Ratio (Sr)				
Sr Contacts, Mit	0.0658466			

SW480 control rep. 1							
Micrograph	**Cytoplasm points**	**ER points**	**ER lines**	**Contact points**	**Contact lines**	**Mitochondria lines**	**Mitochondria points**
1	4	1	18	0	2	8	2
2	5	2	14	0	0	2	0
4	3	0	14	0	3	8	3
5	8	3	32	0	3	72	23
6	3	1	4	0	0	26	13
7	5	2	18	1	2	30	12
9	7	6	66	0	5	46	15
10	4	2	36	1	2	26	8
11	4	5	32	2	5	32	10
14	6	2	26	0	0	36	21
15	8	6	54	0	2	86	38
17	9	6	102	0	2	26	6
18	7	3	22	0	0	0	0
20	6	1	30	0	0	36	16
21	6	3	38	2	4	28	12
22	0	0	0	0	0	0	0
23	6	6	64	0	0	34	13
24	2	1	18	0	0	0	0
25	4	4	34	1	4	54	23
26	7	1	4	0	0	72	39
27	5	0	20	0	0	42	12
28	2	0	10	0	2	56	25
29	2	0	4	0	0	12	5
30	2	2	28	0	3	14	5
31	8	4	16	0	2	60	19

32	4	7	26	2	4	18	9
33	2	1	8	0	0	0	0
34	9	4	44	1	3	30	12
35	6	9	88	2	6	34	13
36	1	1	10	0	0	0	0
TOTAL	145	83	880	12	54	888	354
Adjusted for grid	3625						

Volume density/fraction (Vv)					
Vv ER, Cyt	0.0228966		1 micron		9.7
Vv Mit, Cyt	0.0976552		1 division		10.02
Surface density (Sv)					
Sv ER, Cyt	1.1750293		real L 1 div		1.032989691
Mit, Cyt	0.2024375				
Contacts, Cyt	0.0123104				
ER, ER	51.319049	2/Sv	38.97188379	Average spacing of ER membrane	
Surface Ratio (Sr)					
Sr Contacts, Mit	0.0608108				

SW480 Thapsigargin rep. 1							
Micrograph	**Cytoplasm points**	**ER points**	**ER lines**	**Contact points**	**Contact lines**	**Mitochondria lines**	**Mitochondria points**
2	3	1	14	0	0	18	7
3	7	7	102	0	0	16	4
4	8	0	0	0	0	0	0
5	1	0	0	0	0	0	0
6	3	1	72	0	0	18	3
7	2	0	0	0	0	0	0
9	1	0	8	0	0	0	0
10	0	1	12	0	0	0	0
11	5	1	36	0	0	10	4
12	2	2	32	0	0	16	1
14	0	0	0	0	0	0	0
16	9	7	94	1	9	118	40
17	4	4	58	0	4	22	10
18	2	0	0	0	0	0	0
19	2	2	18	0	0	0	0
20	0	1	6	0	0	0	0

21	4	3	26	0	5	54	21
22	0	0	8	0	0	8	2
23	6	0	18	0	0	16	7
24	4	0	0	0	0	0	0
25	2	2	26	0	0	0	0
26	2	3	70	0	2	10	4
27	1	5	48	0	0	0	0
28	1	0	0	0	0	0	0
29	3	0	24	0	0	0	0
31	4	3	46	0	6	48	20
33	0	1	20	0	0	0	0
34	3	2	22	0	1	10	1
35	0	2	10	0	0	0	0
36	2	3	28	0	2	8	3
TOTAL	81	51	798	1	29	372	127
Adjusted for grid	2025						

Volume density/fraction (Vv)				
Vv ER, Cyt	0.02518519			
Vv Mit, Cyt	0.06271605			
Surface density (Sv)				
Sv ER, Cyt	1.90744437			
Mit, Cyt	0.15181123			
Contacts, Cyt	0.01183475			
ER, ER	75.7367618	2/Sv	26.407255	Average spacing of ER membrane
Surface Ratio (Sr)				
Sr Contacts, Mit	0.07795699			

1 micron	9.7
1 division	10.02
real L 1 div	1.03299

SW480 Tunicamycin rep. 1							
Micrograph	**Cytoplasm points**	**ER points**	**ER lines**	**Contact points**	**Contact lines**	**Mitochondria lines**	**Mitochondria points**
2	4	4	44	0	2	48	16
4	2	2	74	0	4	58	19
5	3	2	44	0	0	0	0
6	6	7	116	1	10	48	15
8	9	6	70	4	7	74	28
9	4	7	86	2	9	72	18
10	6	2	20	0	2	10	2

11	1	3	46	0	1	14	2
12	7	6	110	0	0	0	0
13	1	2	46	1	5	42	12
14	3	4	24	0	0	0	0
15	2	6	78	0	0	0	0
17	1	4	32	0	2	22	3
18	3	4	66	0	0	12	4
19	2	2	24	0	0	4	1
20	0	0	0	0	0	22	9
22	8	5	72	0	1	72	21
23	1	1	26	0	2	12	4
24	1	3	30	0	3	18	6
25	5	11	130	0	0	16	5
26	1	0	0	0	0	16	3
28	4	8	92	0	0	8	1
29	1	3	42	0	0	60	12
30	4	5	74	3	13	104	29
31	5	1	18	0	0	0	0
32	6	1	30	0	0	22	4
33	3	1	26	1	3	12	3
34	6	2	72	1	2	30	9
35	1	1	18	0	1	16	6
36	3	2	48	0	0	10	3
TOTAL	103	105	1558	13	67	822	235
Adjusted for grid	2575						

Volume density/fraction (Vv)					
Vv ER, Cyt	0.0407767		1 micron		9.7
Vv Mit, Cyt	0.09126214		1 division		10.02
Surface density (Sv)					
Sv ER, Cyt	2.92862818		real L 1 div		1.032989691
Mit, Cyt	0.2638035				
Contacts, Cyt	0.02150223				
ER, ER	71.8211197	2/Sv	27.84696	Average spacing of ER membrane	
Surface Ratio (Sr)					
Sr Contacts, Mit	0.08150852				

SW480 NUC-3373 6 hours rep. 1							
Micrograph	**Cytoplasm points**	**ER points**	**ER lines**	**Contact points**	**Contact lines**	**Mitochondria lines**	**Mitochondria points**
2	4	10	78	0	2	74	20
3	2	7	68	2	6	18	3
4	1	8	88	0	0	0	0
5	2	4	30	0	2	6	0
6	5	8	94	0	6	34	8
7	1	2	24	0	0	0	0
8	3	7	106	0	0	4	0
10	5	2	84	2	5	68	18
11	0	2	24	0	2	30	15
12	4	3	44	0	2	14	3
13	7	10	114	0	0	0	0
14	3	2	20	0	0	12	0
15	1	3	26	0	0	8	2
16	7	7	144	0	2	18	5
17	3	3	36	0	1	18	4
18	2	6	50	1	2	10	1
19	8	7	64	0	0	26	6
20	6	7	106	0	3	38	12
22	1	0	0	0	0	0	0
23	9	5	68	2	6	148	54
25	2	0	0	0	0	0	0
27	3	4	98	0	4	76	25
28	1	4	30	0	0	20	5
29	2	1	12	0	2	10	3
30	4	6	82	2	8	36	10
31	4	0	50	0	0	0	0
32	6	6	88	2	10	96	24
34	6	2	28	0	4	52	16
35	1	0	8	0	1	14	4
36	3	3	40	2	5	28	7
TOTAL	106	129	1704	13	73	858	245
Adjusted for grid	2650						

Volume density/fraction (Vv)				
Vv ER, Cyt	0.04867925		1 micron	9.7
Vv Mit, Cyt	0.09245283		1 division	10.02
Surface density (Sv)				
Sv ER, Cyt	3.11241668		real L 1 div	1.032989691
Mit, Cyt	0.26756382			
Contacts, Cyt	0.02276475			
ER, ER	63.9372418	2/Sv	31.2806737	Average spacing of ER membrane
Surface Ratio (Sr)				
Sr Contacts, Mit	0.08508159			

SW480 NUC-3373 12 hours rep.1							
Micrograph	**Cytoplasm points**	**ER points**	**ER lines**	**Contact points**	**Contact lines**	**Mitochondria lines**	**Mitochondria points**
2	2	3	32	1	3	10	2
3	4	7	112	4	8	38	11
4	1	1	40	0	0	12	3
6	8	11	164	4	16	120	49
7	7	4	48	0	0	12	2
8	3	3	58	1	7	52	16
9	5	4	64	0	0	0	0
10	2	2	8	0	2	22	5
11	3	9	86	0	0	6	1
12	7	17	236	0	5	50	14
13	4	1	62	2	7	26	8
14	4	6	70	1	2	56	18
15	4	1	26	0	0	28	5
16	3	2	34	0	0	0	0
17	9	9	198	0	9	36	10
18	4	5	62	1	5	118	32
20	8	9	68	0	0	18	9
21	5	9	78	1	4	52	12
22	5	6	96	1	4	42	10
23	6	7	68	0	0	6	2
24	6	9	104	0	0	28	8
25	1	0	0	0	0	14	5
26	4	4	36	0	0	18	4
28	1	1	34	0	1	6	3
29	4	5	64	0	3	12	3

30	7	4	58	2	9	120	32
31	6	5	62	0	0	12	3
32	0	3	22	1	5	8	2
33	3	2	58	0	3	12	2
34	6	4	78	0	5	42	11
TOTAL	132	153	2126	19	98	976	282
Adjusted for grid	3300						

Volume density/fraction (Vv)				
Vv ER, Cyt	0.04636364		1 micron	9.7
Vv Mit, Cyt	0.08545455		1 division	10.02
Surface density (Sv)				
Sv ER, Cyt	3.11833908		real L 1 div	1.0329897
Mit, Cyt	0.24441162			
Contacts, Cyt	0.02454133			
ER, ER	67.2582939	2/Sv	29.7361096	Average spacing of ER membrane
Surface Ratio (Sr)				
Sr Contacts, Mit	0.10040984			

SW480 NUC-3373 24 hours rep. 1							
Micrograph	**Cytoplasm points**	**ER points**	**ER lines**	**Contact points**	**Contact lines**	**Mitochondria lines**	**Mitochondria points**
2	3	6	60	0	0	0	0
3	0	4	46	0	0	12	3
4	5	6	154	1	6	28	9
5	7	11	110	1	3	20	8
6	3	9	114	3	14	66	22
7	3	6	46	0	0	0	0
8	2	1	28	0	0	32	10
9	3	13	130	1	8	100	28
10	0	0	12	0	0	6	2
11	4	5	56	1	11	108	36
12	7	29	156	0	0	16	5
13	1	3	28	0	0	20	6
14	5	7	94	2	5	86	28
15	1	4	40	0	5	30	12
16	3	4	64	0	0	6	2
17	2	5	72	0	2	14	3
18	2	3	48	0	3	72	20

19	5	14	138	2	5	50	10
20	0	1	16	0	1	8	3
21	4	7	92	0	1	68	20
22	3	0	26	0	0	10	3
23	3	8	90	2	13	56	24
24	3	1	28	0	0	0	0
25	1	1	28	0	0	0	0
26	1	4	62	0	0	20	5
28	2	1	30	0	1	54	12
29	3	6	82	2	6	32	10
30	3	13	110	2	9	34	17
31	5	4	68	0	0	0	0
32	2	1	14	0	0	0	0
TOTAL	86	177	2042	17	93	948	298
Adjusted for control	2150						

Volume density/fraction (Vv)				
Vv ER, Cyt	0.08232558		1 micron	9.7
Vv Mit, Cyt	0.13860465		1 division	10.02
Surface density (Sv)				
Sv ER, Cyt	4.59717774		real L 1 div	1.0329897
Mit, Cyt	0.36438111			
Contacts, Cyt	0.03574625			
ER, ER	55.8414245	2/Sv	35.8157052	Average spacing of ER membrane
Surface Ratio (Sr)				
Sr Contacts, Mit	0.09810127			

SW480 NUC-3373 48 hours rep. 1							
Micrograph	**Cytoplasm points**	**ER points**	**ER lines**	**Contact points**	**Contact lines**	**Mitochondria lines**	**Mitochondria points**
1	6	17	108	0	1	54	25
2	5	3	90	1	7	116	42
3	3	7	64	0	0	0	0
4	4	8	96	1	3	30	10
5	7	2	42	1	7	148	49
6	9	3	44	0	0	38	15
7	6	5	72	1	5	60	24

8	5	8	62	2	3	20	5
9	1	1	16	0	1	10	3
10	1	3	38	1	2	4	1
11	6	3	52	0	0	0	0
12	7	5	164	0	4	48	17
13	9	17	128	0	2	112	33
14	6	6	50	1	6	54	30
15	0	3	18	0	0	0	0
16	9	21	198	8	18	62	25
17	6	23	188	1	8	122	38
18	9	19	224	1	4	52	19
19	4	9	90	2	8	70	29
20	9	9	130	2	6	44	15
21	3	8	70	1	3	30	8
22	2	2	22	0	0	24	7
23	8	19	208	0	1	36	9
24	4	2	22	0	0	4	0
25	3	0	0	0	0	6	2
26	7	3	46	0	0	60	15
27	9	21	182	1	6	60	22
28	3	6	52	0	0	6	1
29	0	1	16	0	1	10	3
30	9	35	266	6	19	138	56
TOTAL	160	269	2758	30	115	1418	503
Adjusted for grid	4000						

Volume density/fraction (Vv)					
Vv ER, Cyt	0.06725		1 micron		9.7
Vv Mit, Cyt	0.12575		1 division		10.02
Surface density (Sv)					
Sv ER, Cyt	3.3374002		real L 1 div		1.03299
Mit, Cyt	0.29295588				
Contacts, Cyt	0.02375876				
ER, ER	49.6267688	2/Sv	40.300831	Average spacing of ER membrane	
Surface Ratio (Sr)					
Sr Contacts, Mit	0.08110014				

SW480 NUC-3373 72 hours rep. 1							
Micrograph	**Cytoplasm points**	**ER points**	**ER lines**	**Contact points**	**Contact lines**	**Mitochondria lines**	**Mitochondria points**
1	5	11	34	0	0	0	0
2	1	0	16	0	0	0	0
3	9	25	290	0	1	14	9
4	7	24	292	3	8	32	12
5	2	4	50	2	7	28	8
6	2	7	74	0	3	52	14
7	3	9	98	1	6	34	14
8	4	6	70	0	3	48	15
9	8	12	154	0	4	62	15
10	8	12	190	0	2	22	5
11	6	0	54	0	13	148	53
13	0	1	28	0	2	10	3
14	4	6	52	2	8	52	13
15	5	1	28	0	1	52	22
16	5	0	4	0	0	0	0
17	0	2	34	0	0	0	0
18	1	10	52	0	0	4	1
19	6	8	102	1	5	62	28
20	8	5	60	2	9	86	42
21	1	0	14	0	0	18	5
23	5	14	120	3	8	56	16
24	3	9	40	1	4	48	24
26	7	15	170	0	2	22	8
27	2	2	20	0	1	12	3
28	1	0	12	0	0	0	0
29	3	4	52	0	1	8	3
31	4	17	174	0	0	6	1
32	0	1	14	0	0	0	0
33	2	5	44	1	2	12	3
34	5	11	86	0	0	0	0
TOTAL	117	221	2428	16	90	888	317
Adjusted for grid	2925						

Volume density/fraction (Vv)					
Vv ER, Cyt	0.07555556		1 micron		9.7
Vv Mit, Cyt	0.10837607		1 division		10.02
Surface density (Sv)					
Sv ER, Cyt	4.01787877		real L 1 div		1.03299
Mit, Cyt	0.25088406				
Contacts, Cyt	0.02542744				
ER, ER	53.1778073	2/Sv	37.6096741	Average spacing of ER membrane	
Surface Ratio (Sr)					
Sr Contacts, Mit	0.10135135				

HCT116 control rep. 2							
Micrograph	**Cytoplasm points**	**ER points**	**ER lines**	**Contact points**	**Contact lines**	**Mitochondria lines**	**Mitochondria points**
1	3	2	44	1	4	36	23
2	3	1	36	0	1	48	17
3	2	7	76	0	0	8	2
4	0	0	0	0	0	26	11
5	7	1	4	0	0	32	24
6	5	8	64	1	2	10	3
7	4	3	46	0	0	0	0
8	7	10	136	1	9	74	47
9	2	0	20	1	4	22	14
10	3	0	12	0	1	40	16
11	5	0	0	0	0	16	7
12	6	1	28	0	0	52	21
13	6	9	64	0	2	68	31
14	2	2	24	0	0	0	0
15	2	1	14	1	2	14	4
16	4	4	42	1	2	18	8
17	8	9	74	0	3	88	32
18	6	9	74	2	6	60	20
19	0	0	0	0	0	0	0
20	2	1	20	0	0	0	0
21	4	4	50	1	5	46	20
22	1	3	20	0	0	0	0
23	2	1	6	0	0	0	0
24	8	3	32	0	0	0	0
25	4	5	36	0	1	72	31

26	1	8	42	0	0	0	0
27	1	0	12	0	0	8	3
28	6	2	24	0	2	24	4
29	2	1	22	0	0	6	2
30	9	4	32	0	1	48	13
TOTAL	115	99	1054	9	45	816	353
Adjusted for grid	2875						

Volume density/fraction (Vv)					
Vv ER, Cyt	0.0344348		1 micron		9.7
Vv Mit, Cyt	0.1227826		1 division		10.02
Surface density (Sv)					
Sv ER, Cyt	1.7745032		real L 1 div		1.0329897
Mit, Cyt	0.2345515				
Contacts, Cyt	0.0129348				
ER, ER	51.532289	2/Sv	38.810618	Average spacing of ER membrane	
Surface Ratio (Sr)					
Sr Contacts, Mit	0.0551471				

HCT116 Thapsigargin rep. 2							
Micrograph	**Cytoplasm points**	**ER points**	**ER lines**	**Contact points**	**Contact lines**	**Mitochondria lines**	**Mitochondria points**
1	4	2	38	0	0	16	6
2	5	17	134	1	4	56	16
3	0	2	46	0	0	20	5
4	4	5	44	0	1	28	8
5	3	5	84	1	2	42	14
6	7	8	114	2	11	92	40
7	3	8	120	2	15	42	9
8	1	5	66	0	6	40	14
9	4	5	80	0	0	50	19
10	1	9	74	1	6	22	8
11	1	0	4	0	0	0	0
12	6	5	68	2	6	102	36
13	5	12	158	0	2	60	33
14	3	2	56	1	3	30	8
15	7	13	190	1	5	90	20
16	8	10	116	2	12	66	34

17	6	17	146	1	4	64	17
21	9	13	132	4	9	124	40
22	0	2	18	1	3	6	2
23	4	5	68	0	0	42	12
25	5	2	84	0	1	48	13
26	8	13	152	0	3	48	12
27	4	6	72	0	1	54	20
28	6	5	74	1	3	46	23
29	7	2	16	0	1	72	20
30	8	16	218	4	13	100	32
31	2	8	92	0	2	6	2
32	9	20	230	0	3	36	11
33	1	2	36	0	0	4	1
34	4	9	92	0	0	0	0
TOTAL	135	228	2822	24	116	1406	475
Adjusted for grid	3375						

Volume density/fraction (Vv)					
Vv ER, Cyt	0.06755556		1 micron		9.7
Vv Mit, Cyt	0.14074074		1 division		10.02
Surface density (Sv)					
Sv ER, Cyt	4.04722407		real L 1 div		1.03299
Mit, Cyt	0.34426868				
Contacts, Cyt	0.02840339				
ER, ER	59.9095668	2/Sv	33.38365	Average spacing of ER membrane	
Surface Ratio (Sr)					
Sr Contacts, Mit	0.08250356				

HCT116 Tunicamycin rep. 2							
Micrograph	**Cytoplasm points**	**ER points**	**ER lines**	**Contact points**	**Contact lines**	**Mitochondria lines**	**Mitochondria points**
1	4	0	20	0	1	44	18
2	7	8	120	0	3	66	21
3	1	4	46	0	1	18	4
4	4	1	20	0	1	20	7
5	2	11	84	0	2	46	12
6	4	13	94	0	3	52	15
7	4	5	96	0	2	4	1
8	4	1	24	0	3	48	19
9	0	1	14	0	0	0	0
10	6	6	68	0	0	42	17
11	7	3	82	0	0	58	19
12	4	7	84	0	0	2	0
13	7	5	98	1	5	52	12
14	4	6	86	0	2	56	18
15	0	4	50	0	1	26	11
16	4	1	38	0	0	32	7
17	1	2	8	1	2	8	2
18	3	8	48	1	3	48	11
19	1	1	18	0	0	0	0
20	2	3	30	0	2	14	5
21	5	15	70	2	4	54	24
22	2	5	32	0	0	8	3
23	5	6	46	2	5	64	28
24	3	2	14	0	1	72	22
25	1	3	14	0	0	4	1
26	1	2	28	0	0	12	4
27	9	5	122	0	4	90	26
28	9	11	204	3	17	106	43
29	6	6	50	0	0	50	16
30	4	4	26	1	2	26	8
TOTAL	114	149	1734	11	64	1122	374
Adjusted for grid	2850						

Volume density/fraction (Vv)					
Vv ER, Cyt	0.0522807		1 micron		9.7
Vv Mit, Cyt	0.1312281		1 division		10.02
Surface density (Sv)					
Sv ER, Cyt	2.9449522		real L 1 div		1.03299
Mit, Cyt	0.3253374				
Contacts, Cyt	0.0185576				
ER, ER	56.329623	2/Sv	35.505297	Average spacing of ER membrane	
Surface Ratio (Sr)					
Sr Contacts, Mit	0.057041				

HCT116 NUC-3373 24 hours rep. 2							
Micrograph	**Cytoplasm points**	**ER points**	**ER lines**	**Contact points**	**Contact lines**	**Mitochondria lines**	**Mitochondria points**
1	2	2	28	0	0	30	14
2	1	3	48	1	2	8	2
3	5	10	80	0	0	18	6
4	0	4	22	0	1	16	5
5	9	8	88	0	0	44	18
6	3	1	28	0	0	34	13
7	9	6	36	0	2	176	78
9	5	6	64	0	0	18	7
10	6	12	96	0	3	14	5
11	2	4	40	0	1	38	15
12	9	24	120	3	8	54	28
13	4	6	58	0	3	16	4
14	7	9	76	0	0	14	7
15	3	3	70	1	6	40	17
16	6	4	60	1	7	62	26
17	4	6	56	0	1	28	13
18	4	5	44	1	2	46	18
19	4	6	74	1	4	52	22
20	4	12	88	1	2	28	11
21	2	4	28	1	3	20	9
22	1	5	44	0	0	10	4
23	5	4	48	1	2	20	8
24	3	6	52	2	6	32	13

25	9	7	72	1	7	156	64
26	8	7	66	0	0	32	16
27	8	25	178	2	8	66	30
28	1	6	40	0	0	0	0
29	5	9	66	1	5	76	33
30	1	1	8	0	0	0	0
31	7	4	56	1	5	68	24
TOTAL	137	209	1834	18	78	1216	510
Adjusted for grid	3425						

Volume density/fraction (Vv)					
Vv ER, Cyt	0.0610219		1 micron		9.7
Vv Mit, Cyt	0.1489051		1 division		10.02
Surface density (Sv)					
Sv ER, Cyt	2.5918674		real L 1 div		1.03299
Mit, Cyt	0.2933992				
Contacts, Cyt	0.01882				
ER, ER	42.474381	2/Sv	47.087207	Average spacing of ER membrane	
Surface Ratio (Sr)					
Sr Contacts, Mit	0.0641447				

HCT116 NUC-3373 48 hours rep. 2							
Micrograph	**Cytoplasm points**	**ER points**	**ER lines**	**Contact points**	**Contact lines**	**Mitochondria lines**	**Mitochondria points**
1	4	18	196	0	2	20	8
2	1	7	42	0	0	0	0
3	3	7	104	2	6	26	13
4	2	3	80	0	7	100	25
5	6	9	102	0	4	64	19
6	2	6	50	0	1	4	1
7	5	11	126	2	8	50	16
8	4	7	54	1	6	118	35
9	5	11	144	2	10	50	19
10	1	5	44	1	3	4	1
11	1	5	58	0	0	10	3
12	4	10	118	2	11	94	21
13	4	4	42	0	2	24	5
14	7	10	200	0	1	22	6

15	3	7	78	0	0	0	0
16	3	6	44	0	1	12	4
17	9	28	222	1	3	62	28
18	2	4	34	0	0	0	0
19	0	3	14	0	0	0	0
20	1	1	14	0	0	0	0
21	3	6	44	3	6	68	21
22	6	9	80	3	8	26	9
23	3	4	58	2	4	42	19
24	3	11	122	0	2	32	14
25	3	4	42	1	2	6	1
26	3	8	82	1	5	74	38
27	5	6	136	1	8	90	30
28	5	11	118	2	6	110	26
29	5	14	108	0	4	62	21
30	5	13	114	1	6	140	49
TOTAL	108	248	2670	25	116	1310	432
Adjusted for grid	2700						

Volume density/fraction (Vv)					
Vv ER, Cyt	0.09185		1 micron		9.7
Vv Mit, Cyt	0.16		1 division		10.02
Surface density (Sv)					
Sv ER, Cyt	4.78654		real L 1 div		1.03299
Mit, Cyt	0.40095				
Contacts, Cyt	0.0355				
ER, ER	52.1115	2/Sv	38.379242	Average spacing of ER membrane	
Surface Ratio (Sr)					
Sr Contacts, Mit	0.08855				

SW480 control rep. 2							
Micrograph	**Cytoplasm points**	**ER points**	**ER lines**	**Contact points**	**Contact lines**	**Mitochondria lines**	**Mitochondria points**
1	2	0	6	0	0	0	0
2	5	2	26	0	4	24	10
3	2	0	0	0	0	0	0
4	1	1	4	0	0	6	2
5	2	1	20	0	2	22	8
6	6	2	22	0	1	98	30
7	2	1	10	0	2	8	1
8	3	1	64	1	3	8	3
9	0	4	24	0	0	0	0
10	3	4	94	0	5	38	13
11	7	6	66	0	2	20	8
12	2	3	42	1	2	26	14
13	3	0	24	0	1	14	4
14	2	1	38	0	2	28	7
15	6	1	34	0	0	44	11
16	2	9	40	0	0	0	0
17	3	2	20	1	3	50	12
18	5	2	26	0	0	6	1
19	3	1	20	0	1	24	5
20	8	2	30	0	2	90	25
21	3	0	0	0	0	14	5
22	1	1	10	0	0	30	6
23	3	4	30	0	0	0	0
24	8	4	56	0	1	14	4
25	2	0	10	0	0	0	0
26	6	0	38	0	0	12	3
27	2	1	14	0	0	10	3
28	5	3	30	0	0	46	19
29	3	0	0	0	0	10	2
30	5	1	38	0	0	36	13
TOTAL	105	57	836	3	31	678	209
Adjusted for grid	2625						

Volume density/fraction (Vv)					
Vv ER, Cyt	0.02171429		1 micron		9.7
Vv Mit, Cyt	0.07961905		1 division		10.02
Surface density (Sv)					
Sv ER, Cyt	1.54152647		real L 1 div		1.03299
Mit, Cyt	0.21344518				
Contacts, Cyt	0.00975929				
ER, ER	70.9913506	2/Sv	28.172446	Average spacing of ER membrane	
Surface Ratio (Sr)					
Sr Contacts, Mit	0.04572271				

SW480 Thapsigargin rep. 2							
Micrograph	**Cytoplasm points**	**ER points**	**ER lines**	**Contact points**	**Contact lines**	**Mitochondria lines**	**Mitochondria points**
1	5	3	36	0	0	26	42
2	0	1	10	0	0	16	7
3	3	4	34	0	1	46	17
4	6	16	172	0	2	64	15
5	1	4	50	0	0	18	4
6	1	7	52	1	4	38	18
7	3	8	70	0	1	34	8
8	0	0	0	0	0	0	0
9	6	11	150	1	4	88	29
10	5	4	56	0	2	40	14
11	3	3	34	0	0	16	4
12	1	1	22	0	0	10	5
13	3	7	64	1	5	70	26
14	0	0	30	0	1	34	10
15	2	1	12	0	1	76	36
16	2	6	84	1	6	62	15
17	5	7	104	0	0	0	0
18	1	0	12	0	0	10	6
19	6	3	14	0	1	32	9
20	4	9	84	3	8	32	7
21	5	2	56	0	3	82	21
22	1	2	12	0	0	0	0
23	4	13	76	2	4	18	8
24	3	9	116	0	1	16	6
25	9	7	82	1	5	20	6

26	5	6	36	0	0	60	21
27	0	5	28	0	2	12	3
28	4	9	68	0	1	98	35
29	8	22	184	1	12	88	26
30	3	6	74	0	1	40	12
TOTAL	99	176	1822	11	65	1146	410
Adjusted for grid	2475						

Volume density/fraction (Vv)				
Vv ER, Cyt	0.0711111			
Vv Mit, Cyt	0.1656566			
Surface density (Sv)				
Sv ER, Cyt	3.5632573			
Mit, Cyt	0.3826444			
Contacts, Cyt	0.0217032			
ER, ER	50.108306	2/Sv	39.913542	Average spacing of ER membrane
Surface Ratio (Sr)				
Sr Contacts, Mit	0.056719			

1 micron	9.7
1 division	10.02
real L 1 div	1.03299

SW480 Tunicamycin rep. 2							
Micrograph	**Cytoplasm points**	**ER points**	**ER lines**	**Contact points**	**Contact lines**	**Mitochondria lines**	**Mitochondria points**
1	1	1	30	1	4	22	6
2	3	1	26	0	3	46	11
3	5	9	86	2	10	82	24
4	1	3	18	0	0	4	1
5	3	2	42	1	3	118	35
6	0	5	40	0	0	0	0
7	8	24	190	0	2	76	19
8	8	15	174	5	14	86	28
9	5	16	124	2	9	94	28
10	7	4	12	0	0	58	19
11	3	5	60	0	5	80	21
12	8	5	92	1	5	72	27
13	3	0	8	0	3	26	9
14	3	1	24	1	5	64	23
15	0	2	18	0	0	0	0

17	0	2	30	0	0	28	9
18	4	4	34	0	0	50	15
19	6	8	78	3	6	54	21
20	7	3	60	1	3	46	11
21	3	7	88	1	4	42	15
22	7	12	82	1	13	90	32
23	4	6	44	1	2	18	6
24	3	2	20	0	0	0	0
25	7	5	48	0	3	46	14
26	2	2	20	1	5	68	16
27	6	10	120	0	1	28	10
28	2	1	28	2	5	28	10
30	5	6	88	0	2	24	6
31	5	6	62	2	6	34	13
32	4	0	2	0	0	8	3
TOTAL	123	167	1748	25	113	1392	432
Adjusted for grid	3075						

Volume density/fraction (Vv)			1 micron		9.7
Vv ER, Cyt	0.05430894				
Vv Mit, Cyt	0.1404878		1 division		10.02
Surface density (Sv)					
			real L 1		
Sv ER, Cyt	2.75150512		div		1.03299
Mit, Cyt	0.37409344				
Contacts, Cyt	0.03036822				
				Average spacing of ER	
ER, ER	50.6639416	2/Sv	39.475807	membrane	
Surface Ratio (Sr)					
Sr Contacts, Mit	0.08117816				

SW480 NUC-3373 24 hours rep. 2							
Micrograph	**Cytoplasm points**	**ER points**	**ER lines**	**Contact points**	**Contact lines**	**Mitochondria lines**	**Mitochondria points**
1	6	4	72	2	5	60	29
2	4	6	56	1	4	24	8
3	2	5	18	0	1	16	6
4	2	3	22	0	2	20	6
5	1	4	38	0	0	6	1
6	2	1	10	0	0	28	6
7	1	0	0	0	0	20	6
8	5	2	20	0	0	56	18
10	2	7	38	0	1	38	13
11	3	0	0	0	0	62	39
12	5	4	56	0	1	8	3
13	4	3	22	0	0	18	5
14	5	0	12	0	0	8	3
15	7	4	42	0	3	54	22
16	3	2	20	0	3	26	12
17	2	2	8	0	0	0	0
18	0	1	10	0	0	0	0
19	1	1	20	0	0	8	5
20	2	3	28	0	0	16	6
21	4	5	48	0	4	78	25
22	8	5	88	1	4	48	17
23	5	6	70	0	1	16	3
24	9	7	88	2	18	212	116
25	1	1	8	0	2	10	4
26	1	0	0	0	0	8	4
27	3	1	24	1	3	30	21
28	4	9	56	0	0	0	0
29	0	0	0	0	0	0	0
30	2	3	56	0	3	42	16
31	3	4	66	0	3	54	14
TOTAL	97	93	996	7	58	966	408
Adjusted for grid	2425						

Volume density/fraction (Vv)					
Vv ER, Cyt	0.03835052		1 micron		9.7
Vv Mit, Cyt	0.16824742		1 division		10.02
Surface density (Sv)					
Sv ER, Cyt	1.98802395		real L 1 div		1.03299
Mit, Cyt	0.32919358				
Contacts, Cyt	0.01976525				
ER, ER	51.838259	2/Sv	38.581543	Average spacing of ER membrane	
Surface Ratio (Sr)					
Sr Contacts, Mit	0.06004141				

SW480 NUC-3373 48 hours rep. 2							
Micrograph	**Cytoplasm points**	**ER points**	**ER lines**	**Contact points**	**Contact lines**	**Mitochondria lines**	**Mitochondria points**
1	2	0	2	0	0	36	9
2	4	3	20	1	7	42	20
3	1	0	6	0	0	0	0
4	2	2	30	0	0	0	0
5	9	7	68	0	8	82	31
6	2	0	10	0	0	0	0
7	0	2	8	0	3	28	9
8	4	0	6	0	0	0	0
9	2	0	12	0	0	64	36
10	1	0	8	0	1	44	26
11	6	6	42	1	2	10	4
12	1	0	4	0	0	8	2
13	7	0	24	0	2	138	64
14	5	4	48	0	0	18	3
15	3	7	44	0	1	38	17
16	9	19	102	0	2	92	29
17	2	3	36	0	2	40	10
18	1	0	8	0	1	26	7
19	1	3	26	1	4	46	21
20	1	1	18	0	0	38	15
21	0	1	2	0	0	6	2
22	5	2	12	0	0	0	0
23	6	11	68	1	2	12	3
24	0	1	34	0	2	6	1

25	6	10	72	0	0	0	0
26	3	3	24	0	3	16	3
27	9	0	24	0	1	98	38
28	9	1	4	0	0	0	0
29	9	7	70	0	0	38	14
30	8	9	100	3	14	122	58
TOTAL	118	102	932	7	55	1048	422
Adjusted for grid	2950						

Volume density/fraction (Vv)					
Vv ER, Cyt	0.034576271		1 micron		9.7
Vv Mit, Cyt	0.143050847		1 division		10.02
Surface density (Sv)					
Sv ER, Cyt	1.529212761		real L 1 div		1.03299
Mit, Cyt	0.293579172				
Contacts, Cyt	0.015407304				
ER, ER	44.22723181	2/Sv	45.221008	Average spacing of ER membrane	
Surface Ratio (Sr)					
Sr Contacts, Mit	0.052480916				

University of St Andrews | FOUNDED 1413

University Teaching and Research Ethics Committee

15th January 2018

Professor David Harrison
School of Medicine

Dear Professor Harrison

Thank you for submitting your amendment application which comprised the following documents:

1. Ethical Amendment Application Form

The School of Medicine Ethics Committee is delegated to act on behalf of the University Teaching and Research Ethics Committee (UTREC) and has approved this ethical amendment application. The particulars of this approval are as follows –

Original Approval Code:	MD9202	**Approved on:**	16/10/2012
Amendment 5 Approval Date:	15/01/18	**Approval Expiry Date:**	16/10/2022
Term of Approval	10 YEARS		
Project Title:	Systems pathology of disease		
Researcher(s):	David Harrison, Fiona McKissock, Jennifer Bre, Peter Caie, In Hwa Um, Oliver Read, Ines Nearchou, Christos Gavriel, Neofytos Dimitriou, Hannah Williams, Mustafa Elshani, Raffaele De Filippis, Mary Kudsy, Mark Bates, Romina Briffa, Nourjahan Khafaga, Sophie Rao, Tsz Chan, Matthew Scott, Beth Gwyther	**Supervisor(s):**	David Harrison

Ethical amendment approval does not extend the originally granted approval period, rather it validates the changes you have made to the originally approved ethical application. If you are unable to complete your research within the original validation period, you are required to write to your School Ethics Committee Convener to request a discretionary extension of no greater than 6 months or to re-apply if directed to do so, and you should inform your School Ethics Committee when your project reaches completion.

Any serious adverse events or significant change which occurs in connection with this study and/or which may alter its ethical consideration, must be reported immediately to the School Ethics Committee, and an Ethical Amendment Form submitted where appropriate.

Approval is given on the understanding that you adhere to the 'Guidelines for Ethical Research Practice' (http://www.st-andrews.ac.uk/media/UTRECguidelines%20Feb%2008.pdf).

Yours sincerely

Dr Morven Shearer, Convenor School of Medicine Ethics Committee